

Final report

Validation of the IFDM-model for use in urban applications

Wouter Lefebvre, Stijn Vranckx (Eds.)

Study accomplished in the framework of the ATMOSYS-project
2013/RMA/R/56

May 2013

MANAGEMENT SUMMARY

The Immission Frequency Distribution Model (IFDM) is developed as a Gaussian model for applications in the framework of Environmental Impact Assessments of point sources. During the development of IFDM, and in the years after this period, several validation studies for point sources have been performed. It was shown in these studies that IFDM performs very well in the typical applications for point sources in Flanders. Next to further refinements for point sources, the introduction of line sources into IFDM and an extension of possibilities of coupling the IFDM-model with other models enables the use of IFDM in regional/urban cases, mainly for road sources. Since then, this application has been used in several projects and a web application, IFDM-traffic, has been implemented for use of IFDM in the context of Environmental Impact Assessments. This report aims in presenting the validation studies that have been made during the last years in this new application field, i.e. the use of IFDM in an regional/urban scale, mainly for line sources (road traffic).

First of all, it is shown that there is an added value of IFDM in this type of applications. However, this can only be demonstrated for pollutants for which the major sources are well-known and included in IFDM (in general pollutants strongly influenced by traffic). In particular, close to the traffic sources (both urban and highway traffic sources), an increased modelling skill thanks to the inclusion of IFDM is shown.

Secondly, it is shown that the IFDM model is fit for use for regulatory purposes. The very good spatial validation, which has been shown in different validation studies supports the use of the IFDM model for the several limit values which have long aggregation periods (e.g., yearly averages). Furthermore, it is shown that the model also performs very well at a daily time scale, leading to a good skill in assessing the PM₁₀ daily limit value. Although the hourly validation is somewhat less good than the validation at longer time scales, the influence on the assessment of the exceedences of the NO₂ limit values is shown to be small.

For exposure estimations, IFDM is shown to have an added value both for static (persons are supposed to be at home at all times) and dynamic (persons are moving through the model domain) exposure. Due to the high spatial and temporal resolution, more precise estimations of exposure can be given and distinctions can be made between exposure during different activities. Furthermore, the feasibility of the simulation of dynamic exposure at a regional scale has been demonstrated.

There are still several points where the IFDM modelling can be improved, which have been listed in the full document, such as the underestimation of the spatial variability in several cases. However, next to these changes, it is shown that the quality of the input data provided to the model is very important. First of all, the quality of the emission inputs is of paramount importance. The lack of even a small source close to a measurement location can make the model results deteriorating significantly. In addition, small changes in the time profiles of emissions can also have large

influences. Finally, the quality of the meteorology measurements has also an important influence on the model results.

The uncertainty on the emissions is probably, in many cases, larger than the model uncertainty itself. This should, however, not stop us to further strive to improve the IFDM model.

TECHNICAL SUMMARY

This report presents the results from a series of validation studies that have been performed with IFDM. All these validation studies discuss the use of IFDM at an urban/regional scale, where the major pollution sources is in general road traffic. In some cases IFDM was coupled to a regional model (RIO/AURORA), in some cases IFDM was coupled to a street box model (OSPM). The following studies are presented:

- Case 1: Spatial validation of the EC-concentration in Flanders simulated by the AURORA-IFDM model and the measurements during the ChemKar-campaign (Lefebvre et al., 2011b).
- Case 2: Comparisons of the RIO-IFDM model chain over Flanders and Brussels with the measurements of the telemetric measurement network (Lefebvre et al., 2013a).
- Case 3: Spatial validation of the RIO-IFDM-OSPM model chain over Antwerp for NO₂ and measurements with passive samplers (Lefebvre et al., 2013b).
- Case 4: Sensitivity study of the RIO-IFDM-OSPM model chain over Antwerp for NO₂ (not previously published).
- Case 5: Spatial and temporal validation of the IFDM-model against measurements close to the E40 at Affligem (ATMOSYS highway campaign, not previously published).
- Case 6: Spatial and temporal validation of the RIO-IFDM model chain over Belgium with measurements of the telemetric measurement network (ATMOSYS action 9, not previously published).

A summary is given in Table 1.

Number	Regional Model	Street canyon model	Pollutants	Spatial (S) temporal (T) cyclical (C) validation	Measurement campaign (M) or Telemetric network (T)	Regional (R), Urban (U) or Local (L)
Case 1	AURORA	none	EC	S	M	R
Case 2	RIO	none	NO ₂ , O ₃ , PM ₁₀	S & C	T	R
Case 3	RIO	OSPM	NO ₂	S	M	U
Case 4	RIO	OSPM	NO ₂	Sensitivity study		U
Case 5	none	none	NO ₂ , BC, PM ₁₀ , PM _{2.5}	S, T & C	M	L
Case 6	RIO	none	NO ₂ , O ₃ , PM ₁₀ , PM _{2.5}	S, T	T	R
	AURORA		EC	S, T	M	

Table 1 : Summary table with the different studies used in this report. This table is a copy of Table 4.

Taking into account all this different validation campaigns, we try to answer a series of questions.

1. Does IFDM have an added value over to the RIO- and AURORA-model in an urban region?

Despite difficulties to show the added value of IFDM to RIO on a Belgian/Flemish scale using the current telemetric network for NO₂, O₃, PM₁₀ and PM_{2.5}, there is ample evidence that IFDM does improve on the background concentrations provided to it for pollutants strongly influenced by traffic:

- For the EC study in Flanders (Case 1), there is a significant increase in R² between AURORA (columns AUR07 and AUR10 in Table 2) and AURORA-IFDM (column Combined in Table 2), without strong changes in the bias and the RMSE.
- For the NO₂-study in Antwerp (Case 3), there is a significant increase in model performance between RIO and RIO-IFDM-OSPM (Figure 1).
- In the simulations of the ATMOSYS highway campaign (Case 5), close to the E40, considerable skill is shown by IFDM, both at the spatial (Figure 2) and at the temporal (Figure 3) scale. None of these local effects would be visible in RIO/AURORA.

For pollutants for which the effect of the sources included in IFDM is small compared to the background concentrations, the improvement of IFDM over RIO is insignificant (Figure 5).

Nevertheless, IFDM also takes resources to run. It is thus important, despite its added value compared to RIO/AURORA, to estimate for each purpose if the addition of IFDM is worthwhile.

	Meas	AUR07	AUR10	CK1_comp	CK2_comp	Combined
R²	1.000	0.675	0.680	0.703	0.698	0.739
Mean (µg/m³)	1.09	1.10	0.98	1.19	1.04	1.11
Bias (µg/m³)	0.00	0.01	-0.11	0.10	-0.05	0.02
RMSE (µg/m³)	0.00	0.29	0.30	0.37	0.30	0.32

Table 2 : Comparison of different simulations (Lefebvre et al., 2011b) with the measurements (Case 1). The measurement values are collected in column "Meas". The AUR07 column describes the AURORA run for 2007, while the AUR10 column describes the AURORA run for 2010. The CK1_comp and CK2_comp column respectively denote the IFDM simulations for ChemKar 1 and ChemKar2. The "Combined" column combines the "CK1_comp" and the "CK2_comp" column by taking the value of the CK1_comp column if the measurement is performed during the Chemkar1 campaign and of the CK2_comp column otherwise. This table is part of Table 7.

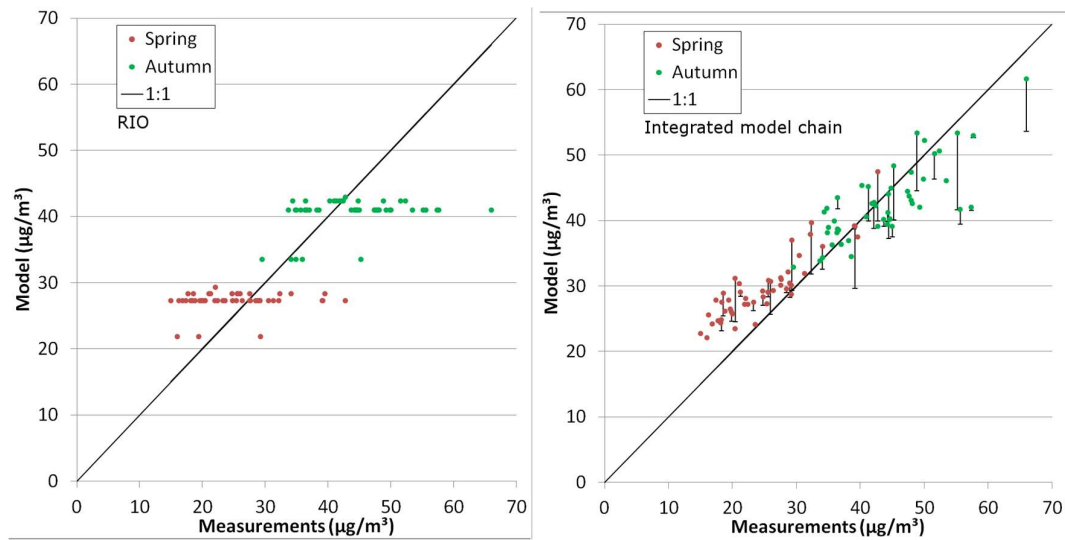


Figure 1 : Validation plots for the Antwerp NO₂-study (Lefebvre et al., 2013b) (Case 3). Left: RIO. Right: RIO-IFDM-OSPM. The black lines represent the differences between RIO-IFDM and RIO-IFDM-OSPM. Every point represents the weekly averaged concentration (in $\mu\text{g}/\text{m}^3$) measured (X-axis) and modelled (Y-axis). This figure is a combination of parts of Figure 32 and Figure 33.

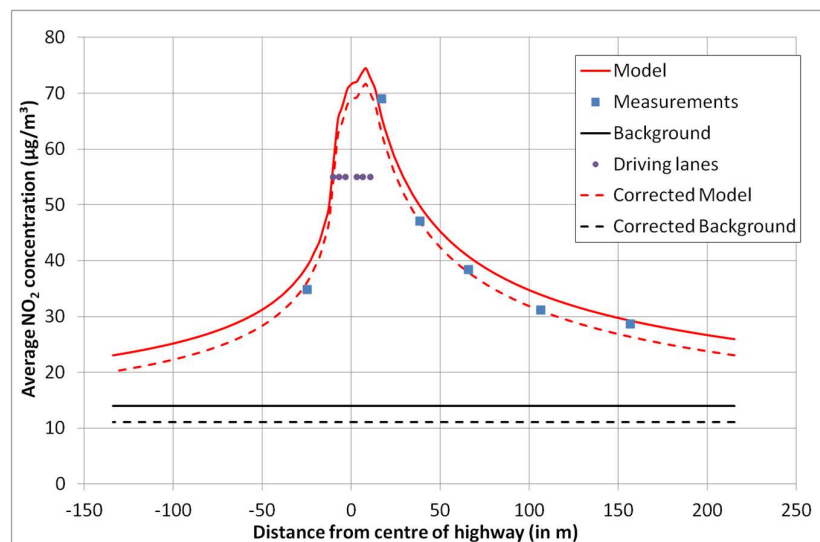


Figure 2 : Model values (red), measurements (blue squares) and background concentrations (black line) (NO_2 , all in $\mu\text{g}/\text{m}^3$) plotted by their distance to the centre of the highway (Case 5). Purple dots represent the different driving lanes. The red dashed lines shows the model values corrected for too high background concentrations, the new background is given in the dashed black line. This figure is a copy of Figure 50. AURORA and RIO models can only reproduce the background lines (black), while IFDM gives the detailed local spatial concentration gradients.

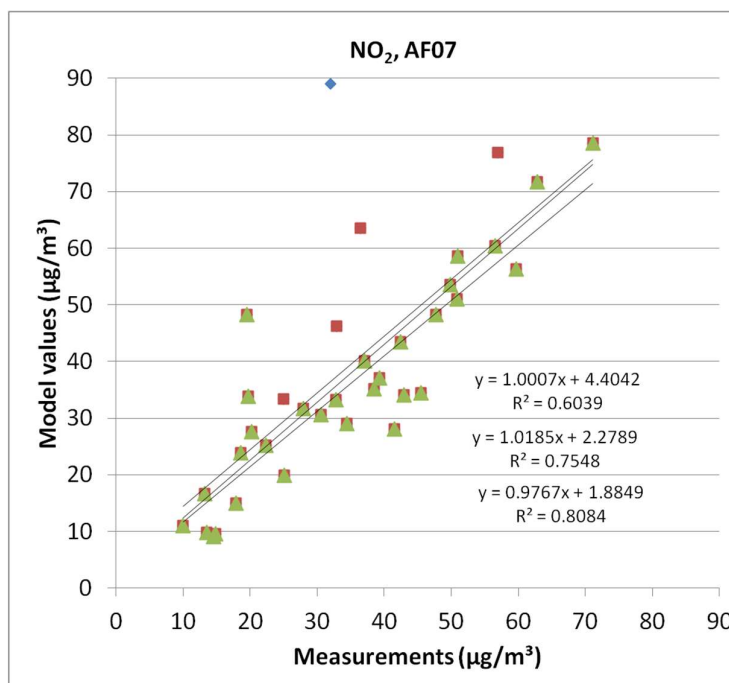


Figure 3 : Example of the temporal variability obtained with IFDM (Case 5). Scatter plot of the modelled NO₂ concentration at AF07 on the measured concentration (both in µg/m³). Every symbol represents one week. The blue symbol represents a week for which the measurement was dubious. The red dots without a triangle represent the weeks at which the background concentrations from Idegem were unavailable, resulting in lower quality of input data to the model. Three trendlines are plotted; one with all data; one without the blue diamond and with only the green triangles. This figure is a copy of Figure 51.

2. Is the IFDM model fit for use for regulatory purposes?

In order to answer this question we have to define the air quality regulations that are important at an urban scale. We'll discuss them one by one:

- The yearly limit value of NO₂ is 40 µg/m³. In order to test for this value, the spatial validation of the model is paramount. As shown for instance in Figure 1 and Figure 2, the spatial validation is excellent. On top of this, the deviation of the regression line in Figure 1 of the measurements onto the model value crosses the 1:1 line close to the limit value of 40 µg/m³ showing only small deviations between measurements and model values close to this critical limit. The deviations may be larger further away from the limit value (overestimations for low concentrations, underestimations for high concentrations), but this will not play a role in determining the adherence to this limit value.
- The hourly limit value for NO₂ of 200 µg/m³ may be exceeded only 18 times per year. It has been shown that, although the model in general is reasonable well in simulating the (half)hourly values, there is a possible model overestimation for low sources and low wind speeds close to the source (Figure 4, which shows half-hourly values for BC, however,

similar results were obtained for NO₂, Table 3). As a result, this would lead to an overestimation of the extent of exceedance of this limit value. However, the extent in which the model estimates this limit value to be exceeded is very small and is completely included in the region with yearly average values much larger than the annual limit value. As a result, the inability of the IFDM model in determining the exact extent of exceedance of this limit value is not very important. Furthermore, there is no official Belgian measurement location where this limit value is exceeded at this moment.

- The yearly limit value of PM₁₀ is 40 µg/m³. As with the yearly limit value of NO₂, the spatial validation will be the most important. As it is shown before, for cases for which the emissions and background concentrations are well known, IFDM simulations are very close to the reality. Therefore, the model will be fit for regulatory purposes provided that the input data is of sufficient quality. The coupling of the IFDM model to RIO shows good skill in determining these concentrations (Table 3).
- The daily limit value of PM₁₀ of 50 µg/m³ may be exceeded only 35 times per year. It has been shown that the model validation at a daily resolution is good (Figure 4, which shows half-hourly values for BC, however, similar results can be assumed for PM₁₀, Table 3). Of course, the same caveat concerning the input data applies.
- The yearly limit value of PM_{2.5} is 25 µg/m³ combined with a three-yearly averaged limit value of PM_{2.5} at urban background locations (different limit values for different regions). As for the yearly limit value for PM₁₀, the spatial validation is the most important, which has been shown to be very good. Therefore, the model will be fit for regulatory purposes provided that the input data is of sufficient quality. The coupling of the IFDM model to RIO shows good skill in determining these concentrations (Figure 5).
- The other existing limit values are less important at an urban scale. It is nevertheless possible that new regulations important at an urban scale will be put into place. Based on the experience with the limit values described above, we can state that they would be probably well represented by the IFDM-model, provided good input for emissions and background concentrations. A possible exception would be limit values for certain pollutants that can only be exceeded during a small number of hours per year, as the temporal validation for traffic sources at an hourly scale is only reasonable. However, this problem will be important only near line sources (due to accumulation effects) and only near those, which are found just above the ground. This has to be taken into account if at certain moment such a new regulation is put in place.

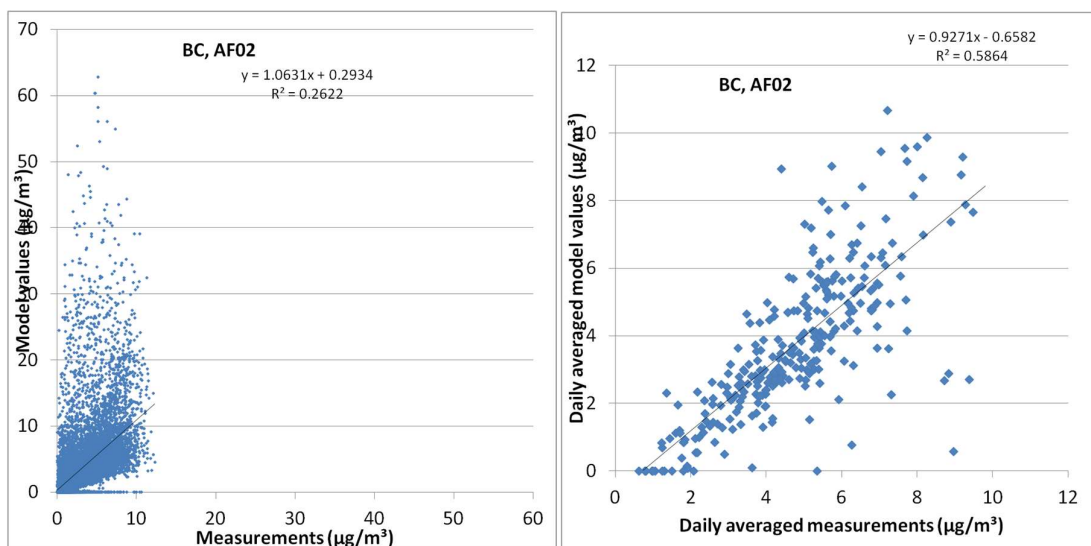


Figure 4 : Scatter plot of the modelled BC concentration (without background) at AF02 (highway campaign, Case 5) on the measured concentrations (both in $\mu\text{g}/\text{m}^3$). Left: Every symbol represents 30 minutes. Right: Every symbol represents 1 day. This figure is a combination of Figure 62 and Figure 66.

		Bias	MAB	RMSE	BCRMSE	R ²
		$\mu\text{g}/\text{m}^3$	$\mu\text{g}/\text{m}^3$	$\mu\text{g}/\text{m}^3$	$\mu\text{g}/\text{m}^3$	
NO ₂	Spatial comparison	-3.08		7.56	6.91	0.68
	Temporal comparison, averaged over all stations		5.08	11.58	9.44	0.76
PM ₁₀	Spatial comparison	-2.84		4.39	3.35	0.45
	Temporal comparison, averaged over all stations		3.59	10.67	9.31	0.84
O ₃	Spatial comparison	1.51		3.25	2.87	0.65
	Temporal comparison, averaged over all stations		2.60	8.03	6.98	0.92

Table 3: Validation parameters of the comparison with the measurement for the SBO-case for different pollutants, for year-long RIO-IFDM simulations within the SBO-Mase project (Case 2). MAB = Mean Absolute Bias; RMSE = Root mean square error; BCRMSE = Bias corrected root mean square error ; Mean = Average of observations. This table is part of Table 8.

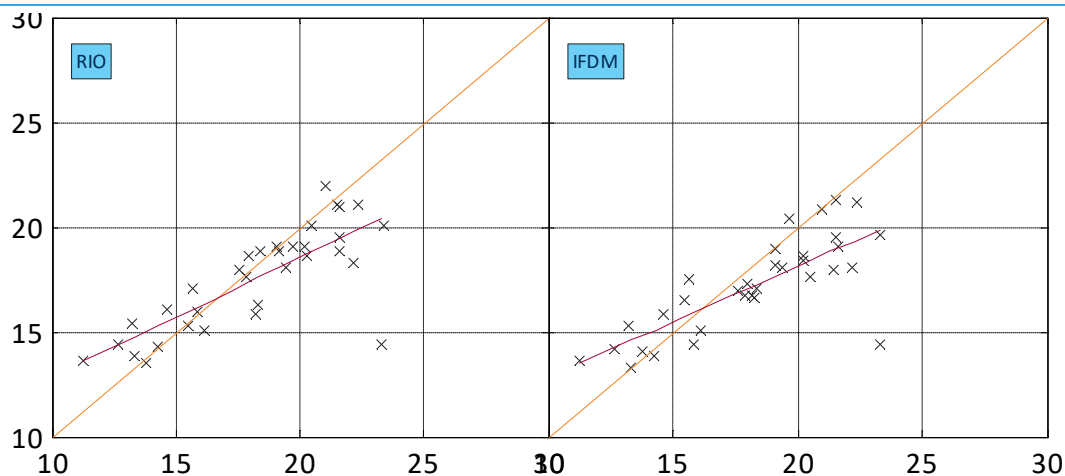


Figure 5 : The scatter spatial validation plot for RIO (left) and IFDM (right) over Belgium in the case of the hindcast-simulations (Case 6) for PM_{2.5}. On the X-axis: the measurements (in $\mu\text{g}/\text{m}^3$); on the Y-axis the model values (in $\mu\text{g}/\text{m}^3$). The difference between both models is deemed to be insignificant. This figure is part of Figure 112.

3. Is the IFDM model fit for use for determining exposure?

For exposure estimations, there is a large difference in what is needed from a model depending if one determines static or dynamic exposure.

- **Static exposure:** In this case, only the spatial validation of the model is important. This validation is previously shown to be very good (Figure 1, Figure 2, Figure 5, Table 2, Table 3), certainly when coupled to a regional model such as RIO or AURORA. The improved spatial resolution due to IFDM will increase the accuracy of the exposure estimations.
- **Dynamic exposure:** In this case, both the spatial validation and the temporal validation of the model is important. As has been seen before, aggregated to daily and weekly averages, the temporal validation of the model is good; however, larger discrepancies between the model and the measurements exist at lower frequencies. However, for dynamic exposure, the presence of the typical cycles (within the day, within the week and within the year) is very important as individual over- and underestimations at an hourly scale will cancel out, but problems with typical cycles will not. The presence of these cycles in the RIO-IFDM model is shown in Figure 6 to be very good, for NO₂, O₃ and PM₁₀. For EC, the capability of the model to reproduce these cycles is not yet proven.

Finally, the feasibility of doing so has to be demonstrated. This has been done within the SBO-Mase project, where dynamic exposure of the Flemish population was determined.

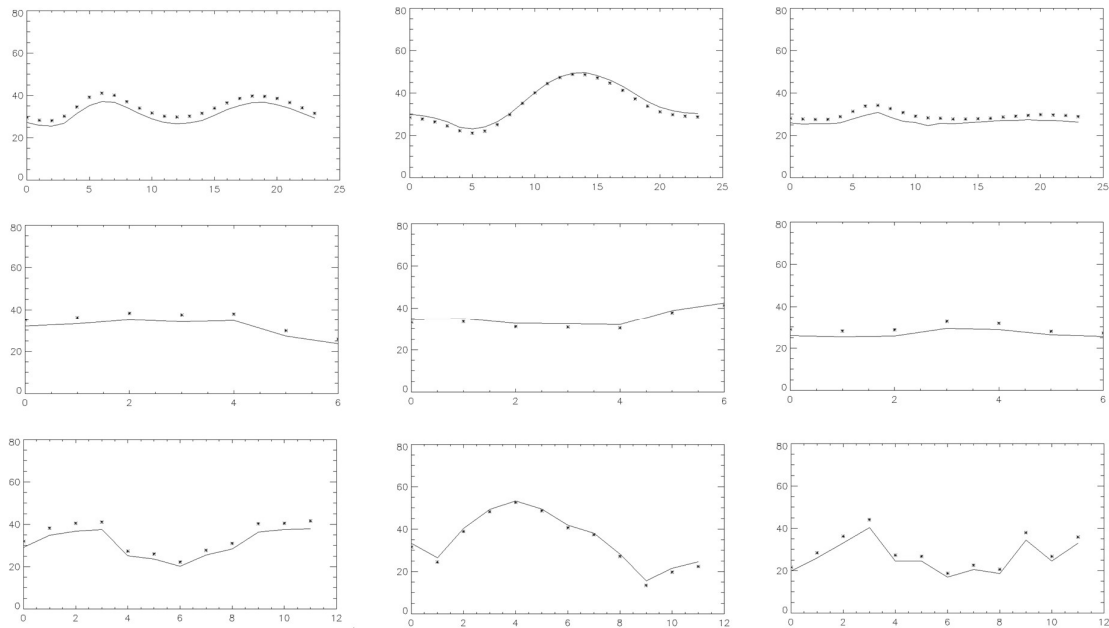


Figure 6: Validation results for NO₂ (left), O₃ (middle) and PM₁₀ (right) for Flanders and Brussels combined (Case 5). Shown are the intra-daily cycle (top figures, x-axis: 0 = first hour of the day, 23 = last hour of the day; GMT), the intra-weekly cycle (middle, x-axis: 0 = Monday, 6 = Sunday) and the intra-annual cycle (bottom, x-axis: 0 = January, 11 = December). Asterisks: measurements, line: model. Shown is the mean over all measurement stations. Y-axis: mean concentration (in µg/m³, ranging from 0 to 80). This figure is a copy of Figure 22.

4. How can modelling using IFDM be further improved for the urban to local scale?

There are several points where the IFDM modelling can be improved. The following list gives an overview of the points that should be addressed in order to improve the IFDM-model.

- The model shows a tendency to overestimate low concentrations and underestimate high concentrations (e.g. Figure 1). More research is needed to find the source of this deviation. This is probably due in part due to the detail of the input data (both emissions and meteorology) which entail a certain degree of averaging.
- The model does not take into account differences in roughness lengths in its simulations.
- Increased wind direction variation at low wind speeds is not modelled yet. An improved model scheme has been presented in this work. However, some deviations between the measurements and the modelling remain.
- The treatment of traffic-induced dispersion should be made wind-dependent, although this is shown to have only a small effect.

However, next to these changes, it is shown that the quality of the input data provided to the model is very important. First of all, the quality of the emission inputs is of paramount importance. The lack of even a small source close to a measurement location can make the model results deteriorating significantly. In addition, small changes in the time profiles of emissions can also have large influences. Finally, the quality of the meteorology measurements has an important influence on the model results.

The uncertainty on the emissions is probably, in many cases, larger than the model uncertainty itself. This should, however, not stop us to further strive to improve the IFDM model.

Conclusion

It has been shown that the IFDM model does provide an added value over RIO and AURORA and that it is fit for use both for regulatory and for determination of exposure. It is our goal to continue to update, refine and improve the IFDM-model in the future.

TABLE OF CONTENTS

Management Summary	I
Technical Summary	III
Table of Contents	XII
List of Figures	XV
List of Tables	XXIII
CHAPTER 1 Introduction	1
CHAPTER 2 Validation using the Chemkar-measurements, on a Flemish scale	3
2.1. <i>Introduction</i>	3
2.2. <i>Model Description</i>	4
2.2.1. Emissions	4
2.2.2. AURORA	5
2.2.3. IFDM	6
2.2.4. AURORA-IFDM coupling	6
2.3. <i>Measurement campaign</i>	7
2.3.1. Sampling sites	7
2.3.2. Sampling and EC/OC analysis	7
2.3.3. Meteorology measurements	8
2.4. <i>Model setup and simulations</i>	8
2.5. <i>Results</i>	9
2.5.1. Comparison to measurements	9
2.5.2. Estimation of the EC carbon concentrations due to Flemish road emissions	10
2.5.3. Further sensitivity tests	10
2.6. <i>Discussion and conclusions</i>	10
2.7. <i>Supplementary Material</i>	20
2.7.1. Effect of meteorology	20
2.7.2. Extra information on the meteorology during the measurement campaigns	22
2.8. <i>Further work on this subject since the publication of the paper</i>	26
CHAPTER 3 Conclusions from the SBO-Mase project, relevant to this validation exercise	28
3.1. <i>Introduction</i>	29
3.2. <i>An activity-based modelling approach for air quality purposes</i>	29
3.3. <i>The ten steps on development and evaluation of environmental models</i>	31
3.4. <i>Model setup</i>	31
3.4.1. FEATHERS and Transcad	32
3.4.2. MIMOSA	32
3.4.3. RIO	32

3.4.4.	IFDM	33
3.4.5.	Coupling of RIO and IFDM	34
3.4.6.	Model setup and simulations	34
3.5.	<i>Results of the model chain</i>	35
3.5.1.	Concentration maps	35
3.5.2.	Evaluation methodology	35
3.5.3.	Evaluation	36
3.5.4.	Comparison of the daily cycle	37
3.6.	<i>Limitations of the integrated model chain and implications for exposure assessment</i>	37
3.7.	<i>Example of use of the model chain: the origin of the daily NO₂-cycle.</i>	38
3.8.	<i>Conclusions and applications of the model chain</i>	39
3.9.	<i>Supplementary material</i>	40
CHAPTER 4	Evaluation of The RIO-IFDM-street canyon model chain	49
4.1.	<i>Introduction</i>	50
4.2.	<i>Measurement campaign</i>	52
4.3.	<i>Model description and setup</i>	53
4.3.1.	Overview and setup	53
4.3.2.	RIO	54
4.3.3.	Local emissions	54
4.3.4.	IFDM	55
4.3.5.	IFDM street canyon	55
4.3.6.	Coupling of different models into one integrated model chain	56
4.3.7.	Post processing	56
4.4.	<i>Results</i>	57
4.4.1.	Correlation, RMSE and bias of the integrated model chain	57
4.4.2.	Impact of different model steps on improvement of modelling results	57
4.5.	<i>Conclusions</i>	59
CHAPTER 5	Sensitivity tests	71
5.1.	<i>Sensitivity to the NO₂/NO_x-ratio</i>	71
5.2.	<i>Sensitivity to the double counting procedure</i>	72
5.3.	<i>Sensitivity to the road network</i>	72
5.4.	<i>Sensitivity to the emissions</i>	73
CHAPTER 6	Highway-campaign	90
6.1.	<i>Introduction</i>	90
6.2.	<i>Measurement campaign</i>	90
6.3.	<i>Model parametrization choices and input data</i>	91
6.4.	<i>NO₂</i>	92
6.4.1.	Spatial validation	92
6.4.2.	Temporal validation	93

6.5.	<i>BC</i>	103
6.5.1.	Spatial validation _____	103
6.5.2.	Temporal validation _____	104
6.5.3.	Sensitivity analysis _____	118
6.6.	<i>PM₁₀ and PM_{2.5}</i>	124
6.7.	<i>NO_x</i>	126
6.8.	<i>Sensitivity to the urban parameterization</i>	131
6.9.	<i>Traffic counts</i>	133
6.9.1.	Time factors _____	134
6.9.2.	Traffic speeds _____	136
6.9.3.	Distribution over the traffic lanes _____	138
6.10.	<i>Model adaptations</i>	138
6.11.	<i>Results with model adaptations for BC</i>	139
6.12.	<i>The influence of results aggregation time on the validation parameters</i>	143
6.13.	<i>Conclusions and some extra remarks</i>	144
CHAPTER 7 ATMOSYS city campaign and the NO₂-measurement campaign using passive samplers in cities _____		146
7.1.	<i>The NO₂-measurement campaign using passive samplers in cities in 2010</i>	146
7.2.	<i>The ATMOSYS city campaign</i>	146
CHAPTER 8 Validation of the ATMOSYS-retrospective simulations for the year 2009 _____		148
8.1.	<i>Methodology</i>	148
8.2.	<i>Validation for NO₂, O₃, PM₁₀ and PM_{2.5}</i>	152
8.2.1.	Methodology _____	152
8.2.2.	RIO-IFDM Temporal Validation _____	154
8.2.3.	RIO-IFDM Spatial Validation _____	157
8.3.	<i>EC-validation</i>	160
8.4.	<i>Conclusions</i>	165
CHAPTER 9 Conclusion _____		167
List of Literature _____		171

LIST OF FIGURES

- Figure 1 : Validation plots for the Antwerp NO₂-study (Lefebvre et al., 2013b) (Case 3). Left: RIO. Right: RIO-IFDM-OSPM. The black lines represent the differences between RIO-IFDM and RIO-IFDM-OSPM. Every point represents the weekly averaged concentration (in $\mu\text{g}/\text{m}^3$) measured (X-axis) and modelled (Y-axis). This figure is a combination of parts of Figure 32 and Figure 33. _____ V
- Figure 2 : Model values (red), measurements (blue squares) and background concentrations (black line) (NO₂, all in $\mu\text{g}/\text{m}^3$) plotted by their distance to the centre of the highway (Case 5). Purple dots represent the different driving lanes. The red dashed lines shows the model values corrected for too high background concentrations, the new background is given in the dashed black line. This figure is a copy of Figure 50. AURORA and RIO models can only reproduce the background lines (black), while IFDM gives the detailed local spatial concentration gradients. _____ V
- Figure 3 : Example of the temporal variability obtained with IFDM (Case 5). Scatter plot of the modelled NO₂ concentration at AF07 on the measured concentration (both in $\mu\text{g}/\text{m}^3$). Every symbol represents one week. The blue symbol represents a week for which the measurement was dubious. The red dots without a triangle represent the weeks at which the background concentrations from Idegem were unavailable, resulting in lower quality of input data to the model. Three trendlines are plotted; one with all data; one without the blue diamond and with only the green triangles. This figure is a copy of Figure 51. _____ VI
- Figure 4 : Scatter plot of the modelled BC concentration (without background) at AF02 (highway campaign, Case 5) on the measured concentrations (both in $\mu\text{g}/\text{m}^3$). Left: Every symbol represents 30 minutes. Right: Every symbol represents 1 day. This figure is a combination of Figure 62 and Figure 66. _____ VIII
- Figure 5 : The scatter spatial validation plot for RIO (left) and IFDM (right) over Belgium in the case of the hindcast-simulations (Case 6) for PM_{2.5}. On the X-axis: the measurements (in $\mu\text{g}/\text{m}^3$); on the Y-axis the model values (in $\mu\text{g}/\text{m}^3$). The difference between both models is deemed to be insignificant. This figure is part of Figure 112. _____ IX
- Figure 6: Validation results for NO₂ (left), O₃ (middle) and PM₁₀ (right) for Flanders and Brussels combined (Case 5). Shown are the intra-daily cycle (top figures, x-axis: 0 = first hour of the day, 23 = last hour of the day; GMT), the intra-weekly cycle (middle, x-axis: 0 = Monday, 6 = Sunday) and the intra-annual cycle (bottom, x-axis: 0 = January, 11 = December). Asterisks: measurements, line: model. Shown is the mean over all measurement stations. Y-axis: mean concentration (in $\mu\text{g}/\text{m}^3$, ranging from 0 to 80). This figure is a copy of Figure 22. _____ X
- Figure 7 : The different steps in the coupling of AURORA and IFDM. Case G denotes the different grids: in black AURORA, in red IFDM. In this example, in order to keep the figure simple, only a regular IFDM grid has been shown. The green line is a road as the major emission source in this example. _____ 12
- Figure 8 : The locations of the Chemkar monitoring sites, superimposed on a population map of Flanders and Brussels (gray = densely populated). In circles, the type of monitoring site is shown (e.g. rural background, suburban, ...). The squares within the circles show the Chemkar-campaign in which the monitoring site was included. _____ 13
- Figure 9 : The different components of the EC concentration (in $\mu\text{g}/\text{m}^3$). Top: the EC concentration as simulated in AUR07. Middle: the concentration as simulated in I07_ARPS_r averaged out over 3x3 km². Bottom: the concentration as simulated in I_CK1_07, the road contribution. The final simulation CK1_comp is calculated as the upper panel minus the middle panel plus the lower panel and is shown in the top part of Figure 4. _____ 14

Figure 10 : The modelled EC concentration (in $\mu\text{g}/\text{m}^3$) in the CK1_comp simulation (top) and in the CK2_comp simulation (bottom). The circles are the monitoring sites and are filled corresponding to the measured concentrations. _____	15
Figure 11 : The validation graph for the campaign-mean EC concentrations. On the X-axis: the measured EC concentrations in $\mu\text{g}/\text{m}^3$. On the Y-axis: the modelled EC concentrations in $\mu\text{g}/\text{m}^3$, using CK1_comp results for Chemkar1-monitoring sites and CK2_comp results for Chemkar2-monitoring sites. Every dot represents one monitoring site during one campaign: green for Chemkar1, red for Chemkar2. The dashed line is the 1-1 line. The black full line shows the regression between the measurements and the model, for which the equation and the R^2 are shown on the right side. _____	16
Figure 12 : The difference in the modelled EC concentration (in $\mu\text{g}/\text{m}^3$) between the CK2_comp and the CK1_comp simulation (top) and the ΔEb term (bottom). _____	23
Figure 13 : The ΔEI (top) and the ΔMI term (bottom) (in $\mu\text{g}/\text{m}^3$). _____	24
Figure 14 : The wind roses for the first Chemkar-campaign (left), the second Chemkar-campaign (right) and the mean over the period 2006-2009 (middle). _____	25
Figure 15 : Meteorological conditions during the first Chemkar-campaign. _____	25
Figure 16 : Meteorological conditions during the second Chemkar-campaign. _____	26
Figure 17 : Update of Figure 5 of Lefebvre et al. (2011b) (Figure 11) to include the Chemkar 3 campaign. _____	27
Figure 18: The model chain. In yellow parallelograms: the input data. In green squares: the model chain components. In orange parallelograms: the output of the models, used as input for the next model in the chain. _____	41
Figure 19: Annual mean PM_{10} concentration (2007). The background map shows the modelled concentrations. In the circles, the annual mean concentrations of the measurements are shown. _____	42
Figure 20 : Annual mean NO_2 concentration (2007). The background map shows the modelled concentrations. In the circles, the annual mean concentrations of the measurements are shown. _____	43
Figure 21 : Annual mean O_3 concentration (2007). The background map shows the modelled concentrations. In the circles, the annual mean concentrations of the measurements are shown. _____	44
Figure 22: Validation results for NO_2 (left), O_3 (middle) and PM_{10} (right). Shown are the intra-daily cycle (top figures, x-axis: 0 = first hour of the day, 23 = last hour of the day; GMT), the intra-weekly cycle (middle, x-axis: 0 = Monday, 6 = Sunday) and the intra-annual cycle (bottom, x-axis: 0 = January, 11 = December). Asterisks: measurements, line: model. Shown is the mean over all measurement stations. Y-axis: mean concentration (in $\mu\text{g}/\text{m}^3$, ranging from 0 to 80). _____	45
Figure 23: The intra-daily cycle (above, x-axis: 0 = first hour of the day, 23 = last hour of the day; GMT), the intra-weekly cycle (middle, x-axis: 0 = Monday, 6 = Sunday) and the intra-annual cycle (below, x-axis: 0 = January, 11 = December) for NO_2 . Asterisks: measurements, line: model with traffic emissions included. Dashed line: model with traffic emissions excluded. Shown is the mean over all measurement stations. Y-axis: mean concentration (in $\mu\text{g}/\text{m}^3$, ranging from 0 to 80). _____	46
Figure 24: Bar-chart of the intra-daily cycle (x-axis: hours in GMT, y-axis: NO_2 -concentration averaged over all days and all measurement locations). In black squares: model results with all traffic emissions included. Blue bars: model results with traffic emissions excluded. Other bars: model results for heavy duty vehicles (red), for person cars going home (green bars), for person cars going to work (purple bars), for person cars in transit through the region (light blue bars) and for person cars with other motives (orange bars). _____	47
Figure 25 : The graphical abstract _____	50

- Figure 26 : The location of the NO₂-measurements. Green dots are measurement locations within street canyons; blue dots are found outside street canyons. In black: roads. The red dot represents the location where the meteorological measurements have been made. Only the area within the city limits of Antwerp is shown. _____ 62
- Figure 27 : The modelling chain. In yellow parallelograms: input data sets. In blue rectangles: the different processes. In green parallelograms: intermediate results. In the salmon-coloured parallelogram: the final result. The red letters A-D denote the model steps shown in Figure 29, Figure 32 and Figure 33. _____ 63
- Figure 28: In red lines: the administrative boundaries of the communities in the region around Antwerp. In black lines: major roads. In blue dots: the measurement stations used by RIO. In the green cadre: the approximate region shown in Figure 29. _____ 64
- Figure 29 : Concentration maps (NO₂, in µg/m³) in different steps of the methodology for the AwAll-week. Upper left: the RIO-map. Upper right: the interpolated RIO-map. Lower left: the concentration map including IFDM. Lower right: the complete map. The red dot is the location of the meteorology measurement. Only concentrations within the city of Antwerp are shown. _____ 65
- Figure 30 : Different steps in the postprocessing of the results, shown for a small region of the city of Antwerp. Part A: postprocessing of the IFDM roof-top results. In crosses: the concentrations at the receptor locations of the IFDM-grid; In black: road segments; Background colors: interpolated concentration results. In white with red border: the street canyon polygon (see §4.3.7). Part B: the initial situation before postprocessing the IFDM street canyon results. In circles: the concentrations given by the IFDM street canyon module at the locations of the street canyons for the limited street canyon receptor points (see end of §4.3.5); In black squares: the receptor points which are part of the full street canyon receptor points (see end of §4.3.5) which are not part of the limited street canyon receptor points; In grey: the buildings; In red line: the border of the street canyon polygon. Part C: the postprocessing of the IFDM street canyon results. In circles: the concentrations given by the IFDM street canyon module at the locations of the street canyons for the limited street canyon receptor points (see end of §4.3.5); In crosses: the receptor points which are part of the full street canyon receptor points (see end of §4.3.5) which are not part of the limited street canyon receptor points, filled with the interpolated IFDM roof top concentrations (Part A); In grey: the buildings; In red line: the border of the street canyon polygon; Background colors: interpolated concentrations within the street canyon polygon. Part D: The final result. In grey: the buildings; In red line: the border of the street canyon polygon; Background colors: the final merged concentrations. The legend is equal for all the different parts and datasets. _____ 67
- Figure 31 : The validation plots (NO₂, in µg/m³). Left: for all measurements. Right: for the measurements in the two weeks with the most measurements. Every point represents the weekly averaged concentration (in µg/m³) measured (X-axis) and modelled (Y-axis). _____ 68
- Figure 32 : Validation plots for different steps in the methodology. Left: for RIO. Right: for the interpolated RIO. Every point represents the weekly averaged concentration (in µg/m³) measured (X-axis) and modelled (Y-axis). _____ 69
- Figure 33 : Validation plots for different steps in the methodology. Left: for RIO+IFDM. Right: the complete model chain. Every point represents the weekly averaged concentration (in µg/m³) measured (X-axis) and modelled (Y-axis). The black lines on the graph represent the street canyon contribution. _____ 70
- Figure 34 : The weekly averaged NO₂-concentration (in µg/m³) in the reference scenario (left), in the scenario with the homogenous NO₂/NO_x-fraction (middle) and the difference between both (right). _____ 74

- Figure 35 : The weekly averaged NO₂-concentration (in µg/m³) in the reference scenario (left), in the scenario with the homogenous low NO₂/NO_x-fraction (middle) and the difference between both (right). _____ 75
- Figure 36 : The weekly averaged NO₂-concentration (in µg/m³) in the reference scenario (left), in the scenario with the homogenous NO₂/NO_x-fraction in the addition phase (middle) and the difference between both (right). _____ 76
- Figure 37 : The weekly averaged NO₂-concentration (in µg/m³) in the reference scenario (left), in the scenario with the homogenous low NO₂/NO_x-fraction in the addition phase (middle) and the difference between both (right). _____ 77
- Figure 38 : The weekly averaged NO₂-concentration (in µg/m³) in the reference scenario (left), in the scenario without the correction for the double counting of the emissions in the IFDM-step (middle) and the difference between both (right). _____ 78
- Figure 39 : The weekly averaged NO₂-concentration (in µg/m³) in the reference scenario (left), in the scenario with a reduced road network (middle) and the difference between both (right). 79
- Figure 40 : The weekly averaged NO₂-concentration (in µg/m³) in the reference scenario (left), in the scenario with the reduced road network carrying the total traffic emissions for the region (middle) and the difference between both (right). _____ 80
- Figure 41 : The weekly averaged NO₂-concentration (in µg/m³) in the reference scenario (left), in the scenario with a reduced road network in the addition phase (middle) and the difference between both (right). _____ 81
- Figure 42 : The weekly averaged NO₂-concentration (in µg/m³) in the reference scenario (left), in the scenario with the reduced road network carrying the total traffic emissions for the region in the addition phase (middle) and the difference between both (right). _____ 82
- Figure 43 : The road type used in the simulations. In red: highways, in blue: major non-highways, in black: minor roads. Roads inside yunnels are not shown on this map. _____ 83
- Figure 44 : The weekly averaged NO₂-concentration (in µg/m³) in the reference scenario (left), in the scenario with emissions reduced by 20% in both the subtraction and the addition phase (middle) and the difference between both (right). _____ 84
- Figure 45 : The weekly averaged NO₂-concentration (in µg/m³) in the reference scenario (left), in the scenario with emissions increased by 20% in both the subtraction and the addition phase (middle) and the difference between both (right). _____ 85
- Figure 46 : The weekly averaged NO₂-concentration (in µg/m³) in the reference scenario (left), in the scenario with emissions reduced by 20% in the addition phase (middle) and the difference between both (right). _____ 86
- Figure 47 : The weekly averaged NO₂-concentration (in µg/m³) in the reference scenario (left), in the scenario with emissions reduced by 20% in both the addition phase (middle) and the difference between both (right). _____ 87
- Figure 48 : Locations of the measurements during the highway campaign. Figure is taken from Roet (2013). _____ 91
- Figure 49 : The location of Zwevegum (westernmost arrow), Idegem (central arrow) and Affligem (righternmost arrow). _____ 92
- Figure 50 : Model values (red), measurements (blue squares) and background concentrations (black line) (NO₂, all in µg/m³) plotted by their distance to the centre of the highway. Purple dots represent the location (and thus not the concentrations) of the different driving lanes. The red dashed lines shows the model values corrected for too high background concentrations, the new background is given in the dashed black line. _____ 93
- Figure 51 : Scatter plot of the modelled NO₂ concentration at AF07 on the measured concentration (both in µg/m³). Every symbol represents one week. The blue symbol represents the week ending on the 26th of October 2012. The red dots without a triangle represent the weeks at which the background concentrations from Idegem were unavailable. Three trendlines (1, 2, 3)

are plotted; one with all data (1); one without the week ending on the 26 th of October 2012 (2) and one without the week ending on the 26 th of October 2012 and the weeks lacking the Idegem background concentrations (3).	95
Figure 52 : Scatter plot of the weekly averaged BC concentrations (Y-axis, in $\mu\text{g}/\text{m}^3$) on the weekly averaged NO_2 concentrations (X-axis, in $\mu\text{g}/\text{m}^3$) for AF07. The week ending on the 26 th of October 2012 is the uppermost point of the graph (31.94; 6.73).	96
Figure 53 : Scatter plot of the modelled NO_2 concentration at AF02 on the measured concentration (both in $\mu\text{g}/\text{m}^3$). Every symbol represents one week. The blue diamonds represent the weeks with significant lack of Idegem background concentration data. Two trendlines (1,2) are presented: one of all the data (1), and one of only the red squares (2).	97
Figure 54 : Scatter plot of the modelled NO_2 concentration at AF03 on the measured concentration (both in $\mu\text{g}/\text{m}^3$). Every symbol represents one week. The blue diamonds represent the weeks with significant lack of Idegem background concentration data. Two trendlines (1,2) are presented: one of all the data (1), and one of only the red squares (2).	98
Figure 55 : Scatter plot of the modelled NO_2 concentration at AF04 on the measured concentration (both in $\mu\text{g}/\text{m}^3$). Every symbol represents one week. The blue diamonds represent the weeks with significant lack of Idegem background concentration data. Two trendlines (1,2) are presented: one of all the data (1), and one of only the red squares (2).	99
Figure 56 : Scatter plot of the modelled NO_2 concentration at AF05 on the measured concentration (both in $\mu\text{g}/\text{m}^3$). Every symbol represents one week. The blue diamonds represent the weeks with significant lack of Idegem background concentration data. Two trendlines (1,2) are presented: one of all the data (1), and one of only the red squares (2).	100
Figure 57 : Scatter plot of the modelled NO_2 concentration at AF06 on the measured concentration (both in $\mu\text{g}/\text{m}^3$). Every symbol represents one week. The blue diamonds represent the weeks with significant lack of Idegem background concentration data. Two trendlines (1,2) are presented: one of all the data (1), and one of only the red squares (2).	101
Figure 58 : Measured (blue) and modelled (red) concentrations (left scale, in $\mu\text{g}/\text{m}^3$) averaged over all measurement locations for NO_2 . The difference between these lines is given by the purple line (left scale, in $\mu\text{g}/\text{m}^3$). The green line represents the difference of the background concentration with the minimum of the six measurement locations for that week (left scale, in $\mu\text{g}/\text{m}^3$). The light blue line on the bottom of the graph represents the percentage of the time that Idegem was not available for the background concentrations (right scale, in %). The red dashed line is model value corrected for the background deviation (left scale, in %).	102
Figure 59 : Scatter plot comparing the difference of the background concentration and the minimum of the six measurement locations for that week (Y-axis, in $\mu\text{g}/\text{m}^3$) with the percentage of the time that Idegem was not available for the background concentrations (X-axis, in %).	103
Figure 60 : Model values (red), measurements (blue squares) and background concentrations (black line) (BC, all in $\mu\text{g}/\text{m}^3$) plotted by their distance to the centre of the highway. Purple dots represent the location (and thus not the concentrations) of the different driving lanes. A constant background concentration of $0.88 \mu\text{g}/\text{m}^3$ has been used.	104
Figure 61 : Scatter plot of the modelled BC concentration (without background) at AF07 on the measured concentration (both in $\mu\text{g}/\text{m}^3$). Every symbol represents 30 minutes.	106
Figure 62 : Scatter plot of the modelled BC concentration (without background) at AF02 on the measured concentration (both in $\mu\text{g}/\text{m}^3$). Every symbol represents 30 minutes.	107
Figure 63 : Scatter plot of the modelled BC concentration (without background) at AF04 on the measured concentration (both in $\mu\text{g}/\text{m}^3$). Every symbol represents 30 minutes.	108
Figure 64 : Scatter plot of the modelled BC concentration (without background) at AF05 on the measured concentration (both in $\mu\text{g}/\text{m}^3$). Every symbol represents 30 minutes.	109

Figure 65 : Scatter plot of the modelled BC concentration (without background) at AF07 on the measured concentration (both in $\mu\text{g}/\text{m}^3$). Every symbol represents one day. _____	110
Figure 66 : Scatter plot of the modelled BC concentration at AF02 on the measured concentration (both in $\mu\text{g}/\text{m}^3$). Every symbol represents one day. _____	111
Figure 67 : Scatter plot of the modelled BC concentration at AF04 on the measured concentration (both in $\mu\text{g}/\text{m}^3$). Every symbol represents one day. _____	112
Figure 68 : Scatter plot of the modelled BC concentration at AF05 on the measured concentration (both in $\mu\text{g}/\text{m}^3$). Every symbol represents one day. _____	113
Figure 69 : Scatter plot of the modelled BC concentration at AF07 on the measured concentration (both in $\mu\text{g}/\text{m}^3$). Every symbol represents one week. _____	114
Figure 70 : Scatter plot of the modelled BC concentration at AF02 on the measured concentration (both in $\mu\text{g}/\text{m}^3$). Every symbol represents one week. _____	115
Figure 71 : Scatter plot of the modelled BC concentration at AF04 on the measured concentration (both in $\mu\text{g}/\text{m}^3$). Every symbol represents one week. _____	116
Figure 72 : Scatter plot of the modelled BC concentration at AF05 on the measured concentration (both in $\mu\text{g}/\text{m}^3$). Every symbol represents one week. _____	117
Figure 73 : Scatter plot of the weekly averaged BC concentrations (Y-axis, in $\mu\text{g}/\text{m}^3$) on the weekly averaged NO_2 concentrations (X-axis, in $\mu\text{g}/\text{m}^3$) for AF04. _____	118
Figure 74 : Average BC concentration (Y-axis, in $\mu\text{g}/\text{m}^3$), per stability class (X-axis). Full lines: measurements. Dashed lines: Model values (without background). AF07 = blue; AF02 = red; AF04 = green; AF05 = purple. _____	120
Figure 75 : Average BC concentration (Y-axis, in $\mu\text{g}/\text{m}^3$), per wind speed (X-axis, in m/s, rounded to the nearest integer). Full lines: measurements. Dashed lines: Model values (without background). AF07 = blue; AF02 = red; AF04 = green; AF05 = purple. _____	121
Figure 76 : Average BC concentration (Y-axis, in $\mu\text{g}/\text{m}^3$), per wind direction (X-axis, in 36 classes, for which the centre is given on the X-axis, in $^\circ$). Full lines: measurements. Dashed lines: Model values (without background). AF07 = blue; AF02 = red; AF04 = green; AF05 = purple. _____	121
Figure 77 : Same as Figure 75, but only for wind directions quasi parallel ($\pm 20^\circ$) to the highway. _____	122
Figure 78 : Same as Figure 75, but only for wind directions quasi perpendicular ($\pm 20^\circ$) to the highway. _____	122
Figure 79 : Average BC concentration (Y-axis, in $\mu\text{g}/\text{m}^3$), per day of the week (X-axis). Full lines: measurements. Dashed lines: Model values (without background). AF07 = blue; AF02 = red; AF04 = green; AF05 = purple. _____	123
Figure 80 : Average BC concentration (Y-axis, in $\mu\text{g}/\text{m}^3$), per hour (X-axis, local time). Full lines: measurements. Dashed lines: Model values (without background). AF07 = blue; AF02 = red; AF04 = green; AF05 = purple. _____	123
Figure 81 : Average BC concentration (Y-axis, in $\mu\text{g}/\text{m}^3$), per month (X-axis, 1=January 2013; 2 = February 2013; 4 = April 2012; 5 = May 2012; ... ; 12 = December 2012). Full lines: measurements. Dashed lines: Model values (without background). AF07 = blue; AF02 = red; AF04 = green; AF05 = purple. _____	124
Figure 82 : $\text{PM}_{2.5}$ Model values (red), measurements (blue squares) and background concentrations (black line) ($\text{PM}_{2.5}$, all in $\mu\text{g}/\text{m}^3$) plotted by their distance to the centre of the highway. Purple dots represent the location (and thus not the concentrations) of the different driving lanes. A constant background concentration of $12 \mu\text{g}/\text{m}^3$ has been used to obtain best fit. _____	125
Figure 83 : PM_{10} Model values (red), measurements (blue squares) and background concentrations (black line) (PM_{10} , all in $\mu\text{g}/\text{m}^3$) plotted by their distance to the centre of the highway. Purple dots represent the location (and thus not the concentrations) of the different driving lanes. A constant background concentration of $19 \mu\text{g}/\text{m}^3$ has been used to obtain best fit. _____	125
Figure 84 : Scatter plot of the modelled NO_x -concentration at AF07 on the measured concentration (both in $\mu\text{g}/\text{m}^3$). Every symbol represents 30 minutes. _____	126

Figure 85 : Scatter plot of the modelled NO _x -concentration at AF07 on the measured concentration (both in µg/m ³). Every symbol represents one day. _____	127
Figure 86 : Scatter plot of the modelled NO _x -concentration at AF07 on the measured concentration (both in µg/m ³). Every symbol represents one week. _____	128
Figure 87 : Scatter plot of the modelled NO ₂ -concentration at AF07 on the measured concentration (both in µg/m ³). Every symbol represents 30 minutes. _____	129
Figure 88 : Scatter plot of the modelled NO ₂ -concentration at AF07 on the measured concentration (both in µg/m ³). Every symbol represents one day. _____	130
Figure 89 : Scatter plot of the modelled NO ₂ -concentration at AF07 on the measured concentration (both in µg/m ³). Every symbol represents one week. _____	131
Figure 90 : Same as Figure 50, but with the urban parameterization added in green lines. _____	132
Figure 91 : Same as Figure 90, but only for the correct model values. The added blue dashed line is the simulation as with the green line but with meteorology from Luchtbal. _____	133
Figure 92 : Normalized PM _{2.5} emission equivalents per hour of day (X-axis). In blue: the sum of the driving lanes towards Brussels; in red: the sum of the driving lanes towards Ghent. In green: the weighted average of the blue and red line. In black: the time factors used in the model. _____	134
Figure 93 : Normalized PM _{2.5} emission equivalents per hour of day (X-axis). In red: average for a weekday. In green: average for a weekend day. In purple: the weighted average of the green and red line. In black: the time factors used in the model. _____	135
Figure 94 : Normalized PM _{2.5} emission equivalents per day of the week (X-axis). In blue: the sum of the driving lanes towards Brussels; in red: the sum of the driving lanes towards Ghent. In green: the weighted average of the blue and red line. In black: the time factors used in the model. _____	135
Figure 95 : Normalized PM _{2.5} emission equivalents per month of the year (X-axis). In blue: the sum of the driving lanes towards Brussels; in red: the sum of the driving lanes towards Ghent. In green: the weighted average of the blue and red line. In black: the time factors used in the model. _____	136
Figure 96 : Average speed (in km/h) of passenger cars per hour of the day (X-axis). In blue: the average of the driving lanes towards Brussels; in red: the average of the driving lanes towards Ghent. In green: the weighted average of the blue and red line. _____	137
Figure 97 : Average speed (in km/h) of passenger cars per hour of the day (X-axis). In red: the average on weekdays.; in green: the average on weekend days. In blue: the weighted average of the green and red line. _____	137
Figure 98 : Time profiles for the different hours of the day (on the X-axis). In red: old time factors; in blue: new time factors; in green: new time factors without the speed component. _____	139
Figure 99 : Same as Figure 62, but after model adaptations. _____	140
Figure 100 : Same as Figure 80, but after model adaptations. _____	141
Figure 101 : Same as Figure 75, but after model adaptations. _____	141
Figure 102 : Same as Figure 75, but with only adaptations to the emissions, not to the model. _____	142
Figure 103 : Same as Figure 76, but with model adaptations. _____	142
Figure 104 : The RMSE (Y-axis, in µg/m ³) between measurements and model values at different locations (colors) for different aggregation times (X-axis, in periods of 30 minutes). _____	143
Figure 105 : The correlation (Y-axis) between measurements and model values at different locations (colors) for different aggregation times (X-axis, in periods of 30 minutes). _____	144
Figure 106 : The time-averaged NO ₂ (above) and O ₃ (below) concentration maps of Belgium for the year 2009 as simulated by RIO-IFDM. Units: µg/m ³ . _____	150
Figure 107 : Above: The time-averaged EC concentration map of Belgium for the year 2009 as simulated by AURORA-IFDM. Units: µg/m ³ . Below: the number of hours exceeding an NO ₂ concentration of 200 µg/m ³ for the year 2009 as simulated by RIO-IFDM. Units: hours. _____	151

Figure 108: Target plot for PM _{2.5} for the year 2009 comparing the model performance of IFDM (starting from RIO background concentrations), RIO and other available models. The figure on the left gives a separate value per measuring station; on the right the average over all measuring stations is depicted. The comparison is made applying the ‘leaving one out’ technique for all models except IFDM.	153
Figure 109: Target plots for NO ₂ , O ₃ , PM ₁₀ and PM _{2.5} . Values are averaged over all available measuring stations including the traffic stations. Comparison of validation for RIO and RIO-IFDM.	155
Figure 110: Target plots for PM ₁₀ split up per region in Belgium. Values are averaged over all available measuring stations. Validation is performed for RIO and RIO-IFDM.	156
Figure 111: Target plots spatial validation NO ₂ , O ₃ , PM ₁₀ and PM _{2.5} for RIO and RIO-IFDM	158
Figure 112: Scatter plots of the year average concentrations, simulations vs. measurements, for NO ₂ , O ₃ , PM ₁₀ and PM _{2.5} per measuring station. The linear regression line is plotted in red, the orange line represents ideal correlation.	159
Figure 113: NO ₂ scatter plots of year-average simulation vs. measurement concentrations split up per region in Belgium. Top plot: Flanders; middle plot: Wallonia; bottom plot: Brussels.	160
Figure 114: Daily average EC concentrations (µg/m ³) of the AURORA-IFDM simulations (dashed lines) vs. the experimental data (VMM) for the background stations Aarschot, Moerkerke and Retie.	161
Figure 115: Daily average EC concentrations (µg/m ³) of the AURORA-IFDM simulations (dashed lines) vs. the experimental data (VMM) for the hotspot stations Borgerhout, Evergem and Zwijndrecht.	161
Figure 116: Daily average EC concentrations (µg/m ³) of the AURORA-IFDM simulations (dashed lines) vs. the experimental data (VMM) for the hotspot stations Roeselare, Zwevegem and Oostrozebeke	162
Figure 117: Scatter plots of the EC simulated daily –average concentrations (Y-axis) vs. the measured concentrations (X-axis) per station. Units: µg/m ³	163
Figure 118: Correlation between EC and NO ₂ measurements (left) and simulations (right) for the station Oostrozebeke. Units: µg/m ³	164
Figure 119: Scatter plot annual average EC concentration AURORA-IFDM simulation vs. measured data (VMM) per station.	165

LIST OF TABLES

Table 1 : Summary table with the different studies used in this report. This table is a copy of Table 4.	III
Table 2 : Comparison of different simulations (Lefebvre et al., 2011b) with the measurements (Case 1). The measurement values are collected in column “Meas”. The AUR07 column describes the AURORA run for 2007, while the AUR10 column describes the AURORA run for 2010. The CK1_comp and CK2_comp column respectively denote the IFDM simulations for ChemKar 1 and ChemKar2. The “Combined” column combines the “CK1_comp” and the “CK2_comp” column by taking the value of the CK1_comp column if the measurement is performed during the Chemkar1 campaign and of the CK2_comp column otherwise. This table is part of Table 7.	IV
Table 3: Validation parameters of the comparison with the measurement for the SBO-case for different pollutants, for year-long RIO-IFDM simulations within the SBO-Mase project (Case 2). MAB = Mean Absolute Bias; RMSE = Root mean square error; BCRMSE = Bias corrected root mean square error ; Mean = Average of observations. This table is part of Table 8.	VIII
Table 4 : Summary table with the different studies used in this report.	2
Table 5 : The ratio EC/PM2.5 as used in this study for the different SNAP-sectors, based on Schaap et al. (2004) except for S7. The last column is the estimated Flemish emission of EC per snap-sector based on the latest estimations of the PM2.5-emissions from the Flemish Environment Agency (VMM) for 2007	17
Table 6 : Characteristics of the different simulations used in this study. The resolutions ‘IFDM regular’ and ‘IFDM road following’ are described in §3.4. The “mean conc” column denotes the modelled mean concentration (in $\mu\text{g}/\text{m}^3$) averaged over all monitoring sites available in at least one measurement campaign (and counting Aarschot and Borgerhout only once).	18
Table 7 : Comparison of the different simulations with the measurements. The measurement values are collected in column “Meas”. The “Combined” column combines the “CK1_comp” and the “CK2_comp” column by taking the value of the CK1_comp column if the measurement is performed during the Chemkar1 campaign and of the CK2_comp column otherwise. All model and measurement values are in $\mu\text{g}/\text{m}^3$. The mean value is based on the averaged value of all data, counting both the Aarschot and the Borgerhout data for both years (and thus double for the model simulations).	19
Table 8: Validation parameters of the comparison with the measurement. MAB = Mean Absolute Bias; RMSE = Root mean square error; BCRMSE = Bias corrected root mean square error ; Mean = Average of observations.	48
Table 9 : The number of measurements, and the number of measurements used in this validation for the different measurement weeks. The concentrations measured over different times are identified by season and week number. Measurements in late Spring or late Autumn are denoted by respectively S and A. The sample week is indicated by w1-w5 for week 1 up to week 5 respectively and by wAll for sampling performed over all locations simultaneously. Combining these time-related indicators, this results in e.g. S_w2 for the second week in the Spring campaign and A_wAll for the week in autumn in which all locations were measured simultaneously.	60
Table 10 : Validation parameters for the model, for the autumn week with most measurements, the spring week with most measurements and both weeks combined. Bias and RMSE are expressed in % of the average of the measurements. The slope represents the slope of the linear regression of the model values on the measurements. The rows ‘Ratio of stdev’ give the ratio of the standard deviation of the model values on the measurement values (in %). The	

rows '# locations > 40 $\mu\text{g}/\text{m}^3$ ' denote the number of locations at which concentrations larger than the annual limit of 40 $\mu\text{g}/\text{m}^3$ are modelled (left number) or measured (right number).	61
Table 11 : Same as First part of Table 10, but with validation parameters for only the street canyons.	61
Table 12 : Validation parameters for the reference and the sensitivity runs (for labels see Table 13) for both the combined spring and autumn week, the spring week and the autumn week alone. The bottom line is the average of the absolute value of the bias (in %), the RMSE (in %), one minus the R^2 and the absolute value of one minus the slope. A lower value is better.	88
Table 13 : The scenario numbers.	89
Table 14 : Correction factor to σ_y in case of neutral and stable conditions.	138

CHAPTER 1 INTRODUCTION

Atmospheric dispersion models are used world-wide, for instance to determine if air quality and odour norms are being met, to planify new plants in an intelligent way, to determine the most suitable stack height, to determine the contribution of sources to a certain air quality problem, to evaluate certain measures for mitigation of air pollution, to predict episodes of air pollution, to predict air pollution due to accidents, to determine the influence of objects on the atmospheric dispersion, ...

The Immission Frequency Distribution Model (IFDM) is developed as a Gaussian model for applications in the framework of Environmental Impact Assessments of point sources. Its basic equations are described in annex 4.4.1 of title II of Vlareem. The dispersion equations used in IFDM are those of Bultynck and Malet (1972). A commercial version of the IFDM software (IFDM-PC) has been developed in the nineties and is since the most used tool for Environmental Impact Assessments of point sources in Flanders.

During the development of IFDM, and in the years after this period, several validation studies for point sources have been performed (e.g. Kretzschmar et al., 1976; Cosemans et al., 1981; Kretzschmar et al., 1984; Olesen, 1995). It was shown in these studies that IFDM performs very well in the typical applications for point sources in Flanders.

Thereafter, IFDM has been further developed for point sources, including a building downwash module (Cosemans et al., 2012) for the description of the effect of buildings on the local dispersion of the plumes. Other extensions are the Emiad-tool for inverse modeling, the extension for modelling odour contours and recently the extension with a module for UFP (Ultra Fine Particles).

Next to these adaptations, a new field of applications has been introduced for the IFDM-model. The introduction of line sources into IFDM and an extension of possibilities of coupling the IFDM-model with other models enables the use of IFDM in regional/urban cases, mainly for road sources. Since then, this application has been used in several projects (e.g. Lefebvre, 2010b; 2011a; 2011c; 2011d; 2012). Furthermore, a web application, IFDM-traffic for use of IFDM in this context has been implemented for Environmental Impact Assessments (Lefebvre et al., 2010a; 2010b). The 'Richtlijnenboek Lucht, 2012' states that the IFDM-traffic is the appropriate tool for use in reporting of Environmental Impact Assessments in an open neighbourhood. Only in special cases and with thorough arguments, a different tool can be used.

This report aims in presenting the validation studies that have been made during the last years in this new application field, i.e. the use of IFDM in an regional/urban scale, mainly for line sources. In some of these validation studies, IFDM was coupled to a regional model (RIO/AURORA), in some cases IFDM was coupled to a street box model (OSPM). The following studies are presented:

- Case 1: Spatial validation of the EC-concentration in Flanders simulated by the AURORA-IFDM model and the measurements during the ChemKar-campaign (Lefebvre et al., 2011b).
- Case 2: Comparisons of the RIO-IFDM model chain over Flanders and Brussels with the measurements of the telemetric measurement network (Lefebvre et al., 2013a).
- Case 3: Spatial validation of the RIO-IFDM-OSPM model chain over Antwerp for NO₂ and measurements with passive samplers (Lefebvre et al., 2013b).
- Case 4: Sensitivity study of the RIO-IFDM-OSPM model chain over Antwerp for NO₂ (not previously published).
- Case 5: Spatial and temporal validation of the IFDM-model against measurements close to the E40 at Affligem (ATMOSYS highway campaign, not previously published).
- Case 6: Spatial and temporal validation of the RIO-IFDM model chain over Belgium with measurements of the telemetric measurement network (ATMOSYS action 9, not previously published).

A summary is given in Table 4.

Number	Regional Model	Street canyon model	Pollutants	Spatial (S), temporal (T) cyclical (C) validation	Measurement campaign (M) or Telemetric network (T)	Regional (R), Urban (U) or Local (L)
Case 1	AURORA	none	EC	S	M	R
Case 2	RIO	none	NO ₂ , O ₃ , PM ₁₀	S & C	T	R
Case 3	RIO	OSPM	NO ₂	S	M	U
Case 4	RIO	OSPM	NO ₂	Sensitivity study		U
Case 5	none	none	NO ₂ , BC, PM ₁₀ , PM _{2.5}	S, T & C	M	L
Case 6	RIO	none	NO ₂ , O ₃ , PM ₁₀ , PM _{2.5}	S, T	T	R
	AURORA		EC	S, T	M	

Table 4 : Summary table with the different studies used in this report.

CHAPTER 2 VALIDATION USING THE CHEMKAR-MEASUREMENTS, ON A FLEMISH SCALE

In this chapter the paper Lefebvre et al. (2011b) is reproduced, which describes this validation exercise.

Validation of the MIMOSA-AURORA-IFDM model chain for policy support: modelling concentrations of elemental carbon in Flanders

Wouter Lefebvre*, Jordy Vercauteren#, Liesbeth Schrooten*, Stijn Janssen*, Bart Degraeuwe*, Willy Maenhaut[§], Ina de Vlioger*, Jean Vankerkom*, Guido Cosemans*, Clemens Mensink*, Nele Veldeman*, Felix Deutsch*, Stijn Van Looy*, Wim Peelaerts*, Filip Lefebvre*

* Flemish Institute for Technological Research (VITO), Boeretang 200, 2400 Mol, Belgium

Flemish Environment Agency, Air Quality Networks, Kronenburgstraat 45, 2000 Antwerpen, Belgium

[§] Institute for Nuclear Sciences, Department of Analytical Chemistry, Ghent University, Proeftuinstraat 86, 9000 Gent, Belgium

Abstract

The ability of a complex model chain to simulate elemental carbon (EC) concentrations was examined. The results of the model chain were compared to EC concentration measurements made at several locations, every sixth day. Two measurement campaigns were taken into account, one in 2006-2007 and one in 2008-2009. The model results compare very well for both periods, with an R^2 of 0.74, a bias of $0.02 \mu\text{g}/\text{m}^3$ and a RMSE of $0.32 \mu\text{g}/\text{m}^3$. Sensitivity analyses to different meteorology inputs and changing emissions from year to year were performed. The differences between the two measurement periods were also investigated. It is shown that somewhat more than half of these differences is due to meteorology. However, emission changes also play an important role.

Keywords: Elemental carbon, validation, policy support, Flanders

2.1. INTRODUCTION

Elemental carbon (EC) is considered to have a significant effect on human health (Dijkema et al., 2008; Patel et al., 2009; Lefebvre et al., 2011a). It has also been found to be a suitable indicator of road traffic and it has been shown that exposure to abundant road traffic has significant impacts on several aspects of human health (Hoek et al., 2002; Gaudermann et al., 2007; Mills et al., 2007). Therefore, the measurement and modelling of this parameter is gaining increasing attention. The Flemish Environment Agency (VMM) has set up two measurement campaigns at different locations in Flanders, in order to assess the chemical composition of PM_{10} (PM = particulate matter smaller than $10 \mu\text{m}$), including EC and organic carbon (OC) concentrations. These campaigns were called Chemkar1 and Chemkar2. The first measurement campaign (Vercauteren et al., 2011), which was carried out at six different locations, was intended to assess the PM composition at various

representative locations in Flanders. The second one was used to examine a number of hotspot locations for PM₁₀ to obtain a better understanding of the reason for their hotspot-status.

The current European directive for air pollution (2008/50/EC) requires Member States to meet several air quality standards in every place within their territory. As it is impossible to measure at every location, it is strongly advised to combine air quality models with measurements at several well-chosen locations. This European guideline imposes limits on annual averaged concentration values or annual numbers of days/hours in exceedance of a threshold value. Therefore, it is necessary that a model is also validated on its capacity to simulate these annual statistics.

During the last decades, models have been developed and validated for several pollutants such as ozone or particulate matter. However, as science evolves, the focus changes and presently, it is aimed at more specific pollutants (e.g. PM₁, Ultrafine Particles (UFP) and EC). Therefore, as measurements are performed for these new pollutants, it is obvious that models should be tested and validated against these new datasets.

For the detailed simulation of air quality in larger domains, such as large urban areas or countries, a combination of several air quality models is required. The combination of models needs to be validated before it can be used in such an assessment. Since the seventies, validation and comparison studies have been performed on the models used in this study (e.g. Cosemans et al., 1981; Olesen, 1995; Thunis et al., 2009).

In this paper, the capability of the model chain, which consists of the traffic emission model MIMOSA, the Eulerian 3D grid dispersion model AURORA and the bi-Gaussian plume model IFDM, in simulating the EC concentrations is validated, not only at rural and urban background monitoring sites, but also at the more difficult hot-spot locations. Furthermore, we try to assess the effect of the meteorology on the yearly mean concentrations. The same MIMOSA-AURORA-IFDM model chain is used for policy support in the framework of the EU Air Quality Directive.

The models have been applied to Flanders, the northernmost part of Belgium. It is a flat and densely populated area, with more than 6 million people residing on a surface area of more than 13500 km², resulting in a population density of more than 450 persons/km². The area can be confined in a rectangle extending 238 km from west to east and 94 km from north to south.

2.2. MODEL DESCRIPTION

2.2.1. EMISSIONS

For the road traffic emissions, MIMOSA4 was used. MIMOSA4 is the most recent version of MIMOSA (Mensink et al., 2000; Vankerkom et al., 2009), which generates hourly output for different types of emissions, such as NO₂, PM₁₀ and PM_{2.5} for Flanders (see also Lefebvre et al., 2011a). The latest version of MIMOSA4 relies on the COPERT 4 methodology (COPERT 4, 2007) for the energy consumption and emission functions for the conventional fuels (diesel, petrol and LPG). Next to this data, it is necessary to distribute the road network over the selected domain, together with the

number and type of vehicles that use each road segment (De Vlieger et al., 2011). The model not only aims at calculating total emission evaluations, but also calculates geographically distributed emissions over time. Indeed, the goal is not only to obtain the total emission over Flanders over a complete year, but to obtain emission data for each particular road segment for every hour.

The MIMOSA4 model had not yet the possibility to directly derive EC emissions. Therefore the model was extended for this new pollutant. The assumption was made that EC traffic emissions account for 66.11% of the PM_{2.5} total traffic primary emissions. This fraction is based on the COPERT 4 emission factors for EC for the Flemish fleet composition. The high value can be explained by the large diesel fraction of the newly purchased vehicles over the last few years in Flanders (Lefebvre et al., 2011a).

Although traffic emissions play a major role in this study, a complete emission inventory over all sectors is required for the dispersion model evaluation. Therefore, the non-traffic emissions of the different pollutants such as NO_x, PM₁₀ and PM_{2.5} for Flanders are based on the emission inventory compiled by the Flemish Environment Agency. For the other regions, the EMAP-tool (Maes et al. 2009) is used which provides gridded emissions based on the EMEP data set. The EC emissions are calculated based upon the PM_{2.5} emissions per Selected Nomenclature for Air Pollution (SNAP) sector. The percentage of EC in PM_{2.5} was taken from Schaap et al. (2004), except for road transport where 66.11% was used (see Table 5). In fact, Schaap et al. (2004) discusses BC and not EC. We have assumed that the EC fraction is equal to the BC fraction. This corresponds to the literature on this subject (Venkatachari, 2006; Hitzenberger, 2006; Quincey et al., 2009), which estimates the BC/EC regression slope consistently in the immediate neighborhood of 1.

2.2.2. AURORA

The atmospheric dispersion model used for simulation of the regional air quality in this study is 'Air quality modelling in Urban Regions using an Optimal Resolution Approach' (AURORA, Mensink et al. 2001). The AURORA model uses the method of nested simulations. In this model, the vertical diffusion is calculated with the Crank-Nicholson method (De Ridder and Mensink, 2002), while the horizontal advection uses a Walcek (2000) scheme. The gas phase chemistry is treated by the Carbon-Bond IV scheme (Gery et al., 1989), which has been enhanced to take into account biogenic isoprene emissions. For particulate matter (PM₁₀ and PM_{2.5}), a distinction was made between primary and secondary particles. Both the amount and distribution of green vegetation cover are based on SPOT-VEGETATION satellite imagery. Terrain height is taken from the Global 30 Arc-second Elevation Data Set, distributed by the U.S. Geological Survey. Meteorological fields, required as input for AURORA, were simulated using the Advanced Regional Prediction System (ARPS) model, a non-hydrostatic mesoscale atmospheric model developed by the University of Oklahoma (Xue et al., 2000; 2001). More information on the AURORA model can be found in the European Model Database (<http://air-climate.eionet.europa.eu/databases/MDS/index.html>).

A validation of the combined ARPS-AURORA model setup can be found in De Ridder et al. (2008) and in Van de Vel et al. (2010) for the Ruhr area and the Lake Baikal region respectively. The model has also been validated for Flanders in several projects. The AURORA model has been used to simulate, with a high spatial resolution of 1x1km², air pollution over Belgium (including Flanders) and for several European cities such as Rotterdam and Prague as part of the GMES-PROMOTE project. In this

project, it has been demonstrated (PROMOTE, 2009a; 2009b) that the AURORA model is able to accurately simulate air quality in urban regions. Analyses of the air quality over the Po-Valley in Italy for the POMI project show that the AURORA model performance is in general in line with respect to other similar high resolution models (Thunis et al., 2009). This model is also validated for the city of Shenyang, China (Lefebvre et al., 2010). Finally, the coupling of AURORA with both the MIMOSA emission model and an activity-based traffic model is validated in Beckx et al. (2009).

2.2.3. IFDM

The Immission Frequency Distribution Model (IFDM) model is a bi-Gaussian plume model, designed to simulate non-reactive pollutant dispersion on a local scale. The Gaussian dispersion parameters are dependent on the stability of the atmosphere and the wind speed following the Bultynck and Malet formulation based on the Bulk Richardson number (Bultynck and Malet, 1972). Line sources are treated as in Venkatram and Horst (2006), except for the cases where the wind is parallel or almost parallel to the road. In the latter case, numerical integration of a series of point sources is applied. Area sources are treated as a set of equivalent parallel line sources perpendicular to the wind. Currently, the IFDM model only uses meteorology from one fixed point for the complete domain. The model will be adapted in the future, in order to use spatially differentiated meteorology measurement data. As IFDM is a receptor-model, it can be used for every grid setup, whether it is regular or not. More information on the IFDM model can be found in the European Model Database (<http://air-climate.eionet.europa.eu/databases/MDS/index.html>).

2.2.4. AURORA-IFDM COUPLING

As mentioned in the introduction, air quality models can be used as tools for policy support for the new EU Air Quality Directive. However, in such a framework air pollution has to be simulated over a large area such as the Flemish region (13522 km²) with sufficient detail to account for the large gradients along highways and major point sources. Therefore, it is insufficient to rely only on a 1-3km scale 3D grid model such as AURORA, as its results are not at a high enough resolution or a 25m-1km scale bi-Gaussian plume model such as IFDM. In order to combine the best of both worlds, the two models are coupled to cover both the regional aspects of the air pollution phenomenon and the large gradients along the major line and point sources.

One major problem that has to be accounted for in the coupling procedure is the double counting of emission sources. For example: when the result of the bi-Gaussian plume model is simply superimposed on top of the 3x3km² grid concentration of the regional air quality model, all emissions taken into account by the plume model are counted twice. In our approach, the AURORA and IFDM model are coupled by using a simple algorithm to avoid double counting of the sources:

1. First of all, AURORA simulates air pollution on a resolution of 3x3km², using all sources (case A in Figure 7).
2. Secondly, IFDM simulates on a regular grid (finer than AURORA, 488x194 points on a 0.48x0.48 km² resolution, 39 IFDM grid points per AURORA cell) the air pollution from (traffic) sources which are of interest (in this case, traffic emissions on the major roads) (case B in Figure 7).

3. Thirdly, the concentration in each AURORA-cell is adapted cell by cell, by subtracting from its hourly concentrations, the spatial mean of the hourly concentrations of all IFDM receptor points in this cell (case C in Figure 7). This results in AURORA-concentrations without the effect of the local traffic sources which are of interest (case D in Figure 7). These AURORA concentrations are interpolated on the IFDM-grid (see below), using a bi-linear interpolation technique (case E in Figure 7).
4. Finally, IFDM simulates the air pollution due to the traffic sources which are of interest (same sources as in the second point). In this step, the model uses a road following grid (ranging from 1000x1000m² away from the roads till 25x600m² close to the roads following a similar methodology as in Lefebvre et al. (2011a)), in order to have more receptor points available where the largest gradients are expected. These IFDM-results are added to the concentrations calculated in point 3. As a result, a detailed hourly concentration field is created with a regional pattern and steep gradients along the major line (and point, if applicable) sources (case F in Figure 7), without double counting.

The AURORA-IFDM coupling procedure is similar to the one used in Lefebvre et al. (2011a).

2.3. MEASUREMENT CAMPAIGN

2.3.1. SAMPLING SITES

For Chemkar1, sampling was done at six sites in Flanders, Belgium (Figure 8) from September 2006 to September 2007. The sites were chosen to obtain a reasonable spread in location and type of site. The six sites were located in Houtem (rural background), Zelzate (industrial), Mechelen (suburban), Borgerhout (urban), Aarschot (rural background) and Hasselt (suburban). For Chemkar2 sampling was done at nine sites in Flanders, Belgium, between October 2008 and November 2009. Six of the sites were considered PM₁₀ hot spots: Borgerhout (same site as in Chemkar1), Roeselare, Oostrozebeke, Zwevegem, Evergem and Zwijndrecht; three were considered rural background sites: Aarschot (same as in Chemkar1), Moerkerke and Retie.

2.3.2. SAMPLING AND EC/OC ANALYSIS

For a detailed description of the Chemkar approach we refer to Vercauteren et al. (2011). In short, 24-hour sampling was carried out simultaneously on all locations on every sixth day with a PM₁₀ low-volume sampler (Leckel SEQ 47/50). With this apparatus 55 m³ of air was sampled on a 47 mm diameter quartz fiber filter (pre-fired Whatman QM-A). After weighing, the filters were cut for different types of analysis. For EC/OC determination a 1 or 1.5 cm² punch was analyzed by means of a thermal-optical transmission (TOT) method with a Sunset Laboratory (Tigard, OR, USA) Lab OCEC analyzer using the NIOSH 5040 protocol (Birch, 2003). This method is known to give relatively low EC values compared to some other techniques and protocols, but at the same time the NIOSH-EC is probably the best indicator for traffic emissions.

2.3.3. METEOROLOGY MEASUREMENTS

Where measured meteorology has been used in this study, it is taken from the Luchtbal pylon in Antwerp. At this urban location, temperature, wind speed and direction are measured at a height of 30m.

2.4. MODEL SETUP AND SIMULATIONS

Up until now, a very detailed hourly by hourly simulation methodology has been described. However, as EC is a passive pollutant and as we estimate that the background emissions do not show much inter-annual variability, we can use the annual mean background calculations for the different years, all made with 2007 meteorology.

To validate the coupled model chain with the measurements collected during the two Chemkar campaigns, several simulations with the different models were made (Table 6):

- AURORA simulations, nested in 60x60 km² BelEUROS-output (Deutsch et al., 2008a; 2008b; 2009) at resolutions of respectively 25x25 km², 9x9 km² and 3x3km² for the years 2007 and 2010. As the simulations were made in 2010, i.e. before emission and meteorology data for 2010 were available, emission projections by the Flemish Environmental Agency in cooperation with VITO have been used. Furthermore, meteorology from 2007 was used for both simulations and is calculated by ARPS based on the ECMWF-reanalysis for the year 2007. Thus, differences between 2007 and 2010 are due to changes in emissions. The simulations at 3x3 km² are named *AUR07* and *AUR10*.
- IFDM traffic EC simulations for the years 2007 and 2010 using the ARPS-meteorology for 2007. Only Flemish traffic emissions derived by the MIMOSA4 model are taken into account. These simulations are named *I07_ARPS_r* and *I10_ARPS_r* on the regular IFDM-grid and *I07_ARPS* and *I10_ARPS* on the road-following grid.
- IFDM traffic EC simulations using measured meteorology data from the years 2006, 2007, 2008 and 2009, with EC emissions from the year 2007. Only Flemish traffic emissions are taken into account. These simulations are named *I_06_07*, *I_07_07*, *I_08_07*, *I_09_07* respectively.
- IFDM traffic EC simulations using measured meteorology data for the collection dates of the measurement campaigns with EC emissions both for the year 2007 and for the year 2010. These simulations are named *I_CK1_07*, *I_CK2_07*, *I_CK1_10* and *I_CK2_10* respectively. Only Flemish traffic emissions are taken into account.

Using the results from the first two bullet points, background concentrations without the roads for the year 2007 and 2010 can be calculated (steps A-C, Figure 7) in the AURORA-IFDM coupling. The results are called *BACK07* and *BACK10*. Thereafter, depending on the situation, one of the IFDM simulations can be used to create the final concentration set.

The Chemkar measurement campaigns, Chemkar1 and Chemkar2, were conducted mostly during the year 2007, and the year 2009 respectively. Therefore, in order to compare the simulated results with the results of the Chemkar1 campaign, only emission data for 2007 were used (*BACK07+I_CK1_07*,

we call this the *CK1_comp*). For the Chemkar2 campaign however, a blend of both 2007 and 2010 data were used ($\frac{1}{3}*(BACK07+I_CK2_07)+\frac{2}{3}*(BACK10+I_CK2_10)$), we call this the *CK2_comp*). These are the datasets that will be validated and discussed in this paper.

For the location of the cities mentioned in this chapter, we refer to Figure 8. The different contributions to the overall *CK1_comp* simulation are presented in Figure 9. In the top panel, the AURORA-results are shown. Increased concentrations are observed around the major highways and in the major cities (especially around Ghent, Antwerp and Brussels). However, another area with high EC concentration is apparent in the southwestern part of Flanders. On analyzing the AURORA results, it is shown to be related to a significant import of EC from the highly urbanized region around Lille in northern France.

In the middle panel of Figure 9, the effect of the Flemish road emissions, smoothed out over a 3x3 km² grid is shown. As can be observed, these emissions are mainly located around the urban city centers of Ghent, Brussels, Antwerp and Kortrijk and around some major highways (especially, the highways Kortrijk-Ghent-Antwerp, Ghent-Brussels and Brussels-Antwerp). As explained before, the simulation *BACK07* is created by subtracting these results from the *AUR07*-simulation. The high resolution impact of the roads can be examined in the bottom panel of Figure 9. In this figure all major roads are clearly visible. It is clear that large gradients exist in the immediate neighborhood of these traffic sources. At a certain distance away from these roads the EC concentrations are low. However, close to the important traffic emission sources, the EC concentrations are very high with a maximum of about 9 µg/m³ on the Ring of Antwerp. The resulting simulation, *CK1_comp* is shown in the top panel of Figure 10. As expected high concentrations are revealed around the major highways and in the city centers of Antwerp and Ghent. Furthermore, high concentrations can be found at the Flanders-France border south of Kortrijk.

2.5. RESULTS

2.5.1. COMPARISON TO MEASUREMENTS

In order to compare the results of the MIMOSA-AURORA-IFDM model chain to measurements, measurements of the Chemkar1-campaign are compared with the *CK1_comp*-dataset and the measurements of the Chemkar2-campaign with the *CK2_comp*-dataset, using the average over the complete time series per station.

As can be seen in Figure 11, the results of the comparison are very promising. The R² value is 0.739, while the bias (about 0.02 µg/m³) and the RMSE (about 0.32 µg/m³) are small. Furthermore, the regression line (model $\approx 1.2407*\text{measurement}-0.2414$) is not too far from the 1:1-line. Apart from this comparison, the different parts of the simulation chain can also be evaluated. This evaluation is summarized in Table 7. Herein the combined version performs best with a high R², a very small bias and a low RMSE. However, the different components do not perform too badly either. For instance, the AURORA simulations themselves (including traffic) show an even lower RMSE, although the R² is somewhat lower. The bias is also low in this case. The Flemish traffic simulations only resulted in an R² close to 0.7. However, the bias and as a result also the RMSE are much higher. This is logical, as only part of the existing emissions are used in these simulations. Finally, the simulations without the

Flemish traffic emissions also exhibit a larger bias and a larger RMSE combined with a lower R^2 . This again can be explained as part of the emissions is also missing.

2.5.2. ESTIMATION OF THE EC CARBON CONCENTRATIONS DUE TO FLEMISH ROAD EMISSIONS

Based on these analyses (§2.6 and 4.1), it can be concluded that, on average¹ about 25 to 31% of the EC concentrations can be attributed to Flemish traffic (Table 6, see also lower panel Figure 9, and upper panel Figure 10). This number can be calculated by, for instance for the year 2007, comparing the mean of the I_CK1_07 simulation to the mean of the CK1-comp simulation ($0.40/1.11 = 31\%$). The remaining part is due to Flemish non-traffic emissions or to non-Flemish (both traffic and non-traffic) emissions. The proportion due to Flemish traffic emissions varies from about 1% in Houtem to about 50% in Mechelen and Borgerhout (Table 7). The percentage due to Flemish traffic is slightly higher when the 2007 emissions are used instead of the 2010 emissions. This indicates that in this period EC traffic emissions are decreasing faster than other sector contributions, thanks to renewal of the car technology and despite the increasing use of diesel cars during this period.

2.5.3. FURTHER SENSITIVITY TESTS

The results of further sensitivity tests can be found in the supplementary material (§2.7).

2.6. DISCUSSION AND CONCLUSIONS

Based on the results of the comparison (with the measurements) presented in this paper, we can conclude that the MIMOSA-AURORA-IFDM model chain presented here is well capable of simulating the spatial variability of EC concentrations averaged over a longer period. Furthermore, it is shown that the meteorology can play an important role in the EC concentrations. However, when annual mean concentrations are considered, the meteorology effects are reduced. Further sensitivity tests have been made and were discussed in the supplementary material. Finally, it can be concluded that on the basis of these results, the currently used EC/PM_{2.5} ratio in the Flemish road emissions inventory yields good results.

The EC concentrations in Flanders are shown to be between 0.6 and 1 $\mu\text{g}/\text{m}^3$ in rural areas away from major roads (Figure 10) and between 1 and 3 $\mu\text{g}/\text{m}^3$ in urban areas, excluding street canyons. These figures are comparable to the ones found in the supplementary material of Putaud et al. (2010) for the rural case in Northwestern Europe and lower than the values in Central Europe. However, the methodology used to determine EC is different from study to study and the difference in the results can reach as high as 100% (Putaud et al., 2010). We know that the methodology used in our study results in low EC concentrations and therefore, it is not possible to claim a significant difference between our results and those in the rest of Europe. Furthermore, as we have shown, EC concentrations are decreasing in time, at least in Flanders. Therefore, it can be problematic to compare EC concentrations from studies ranging over two decades.

¹ averaged over all monitoring sites in the Chemkar dataset and depending on the simulation

The maps resulting from this effort can be used by the Flemish government and other interested parties in determining the possible risks of the population to the exposure to elemental carbon. Furthermore, this model chain can be used in order to assess elemental carbon concentrations at locations where no measurements are available. As measurements of elemental carbon are expensive, this model chain can provide a relative cheap way in determining which locations risk being exposed to high elemental carbon concentrations. Furthermore, it can assist the responsible agency to determine suitable measurement locations for elemental carbon.

Acknowledgements

This work was partially funded by the department 'Leefmilieu, natuur en energie' of the Flemish government and partially by the LIFE+ programme of the European Union. (LIFE+ 2009 project ENV/BE/000409, www.life-atmosys.be).

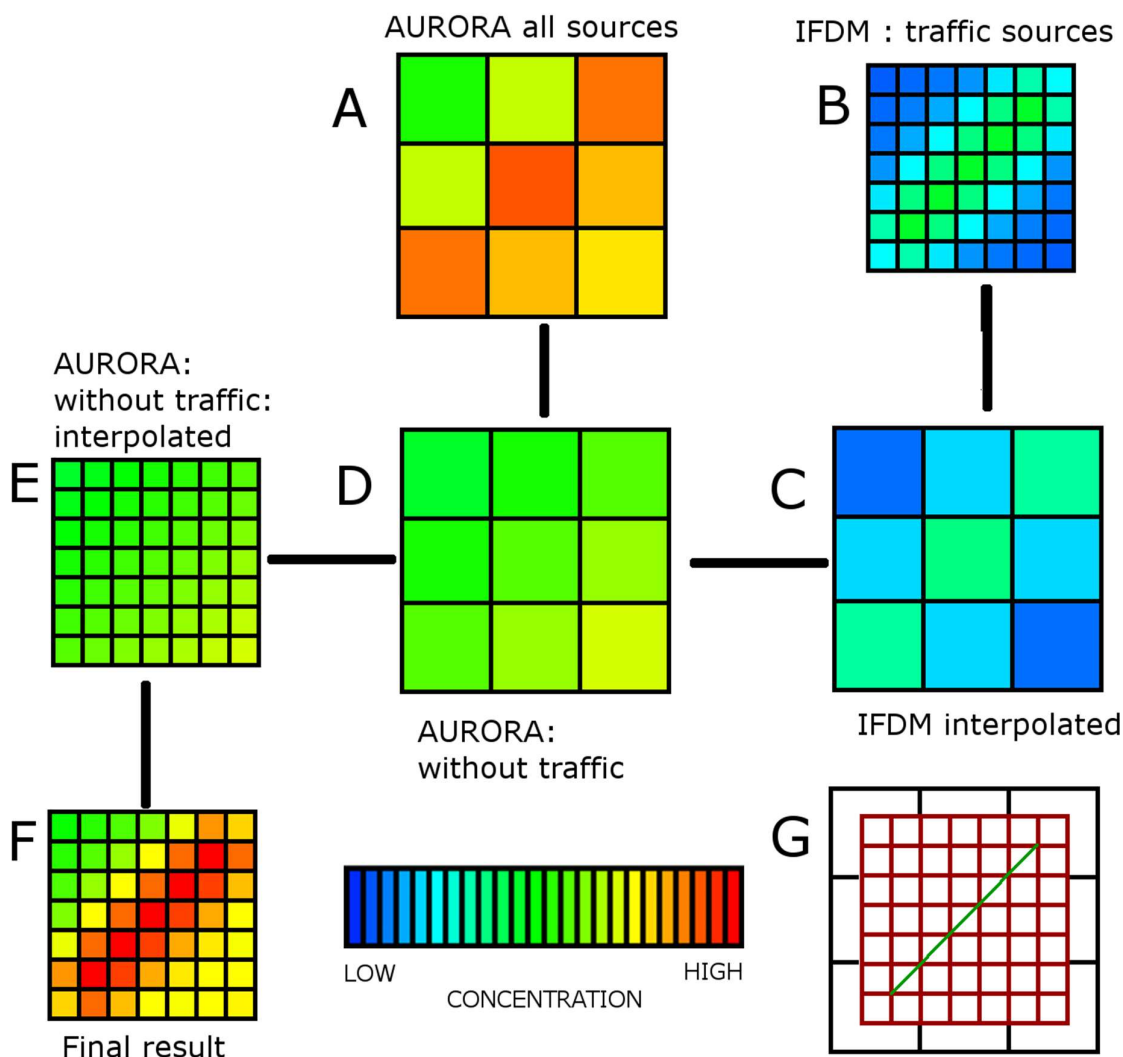


Figure 7 : The different steps in the coupling of AURORA and IFDM. Case G denotes the different grids: in black AURORA, in red IFDM. In this example, in order to keep the figure simple, only a regular IFDM grid has been shown. The green line is a road as the major emission source in this example.

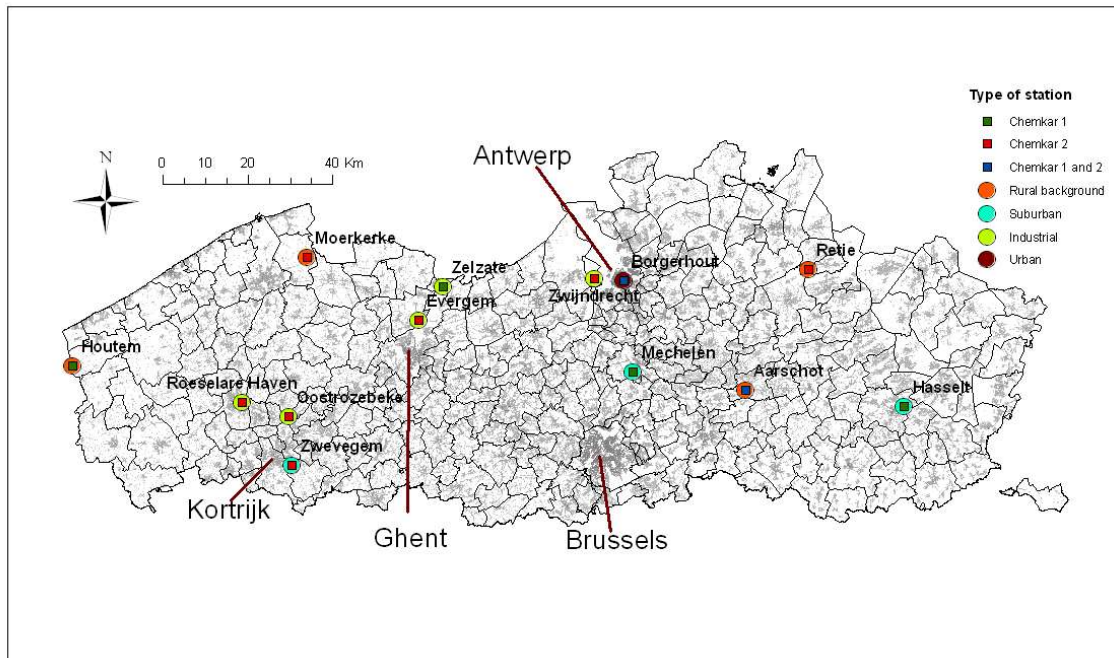


Figure 8 : The locations of the Chemkar monitoring sites, superimposed on a population map of Flanders and Brussels (gray = densely populated). In circles, the type of monitoring site is shown (e.g. rural background, suburban, ...). The squares within the circles show the Chemkar-campaign in which the monitoring site was included.

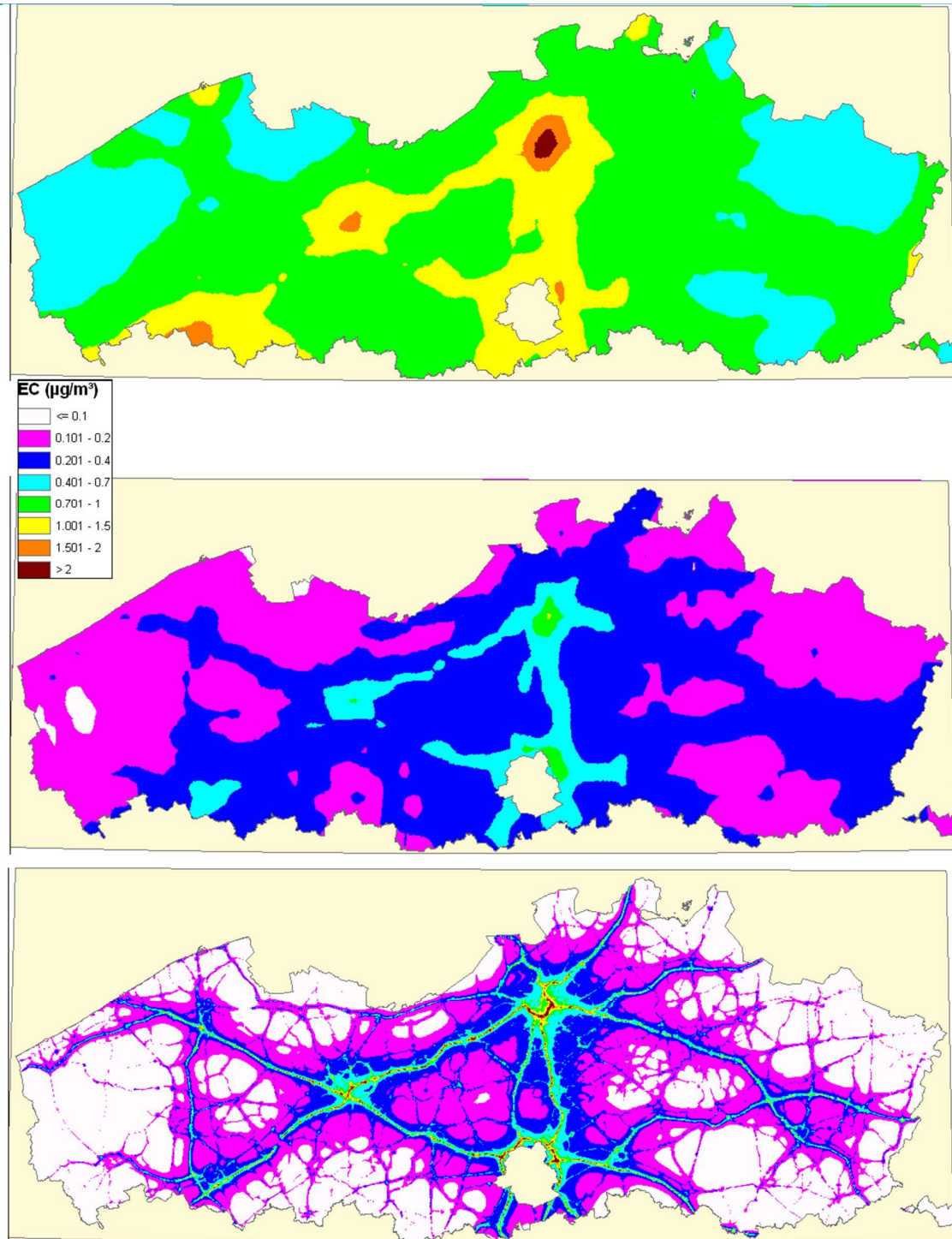


Figure 9 : The different components of the EC concentration (in $\mu\text{g}/\text{m}^3$). Top: the EC concentration as simulated in AUR07. Middle: the concentration as simulated in I07_ARPS_r averaged out over $3 \times 3 \text{ km}^2$. Bottom: the concentration as simulated in I_CK1_07, the road contribution. The final simulation CK1_comp is calculated as the upper panel minus the middle panel plus the lower panel and is shown in the top part of Figure 4.

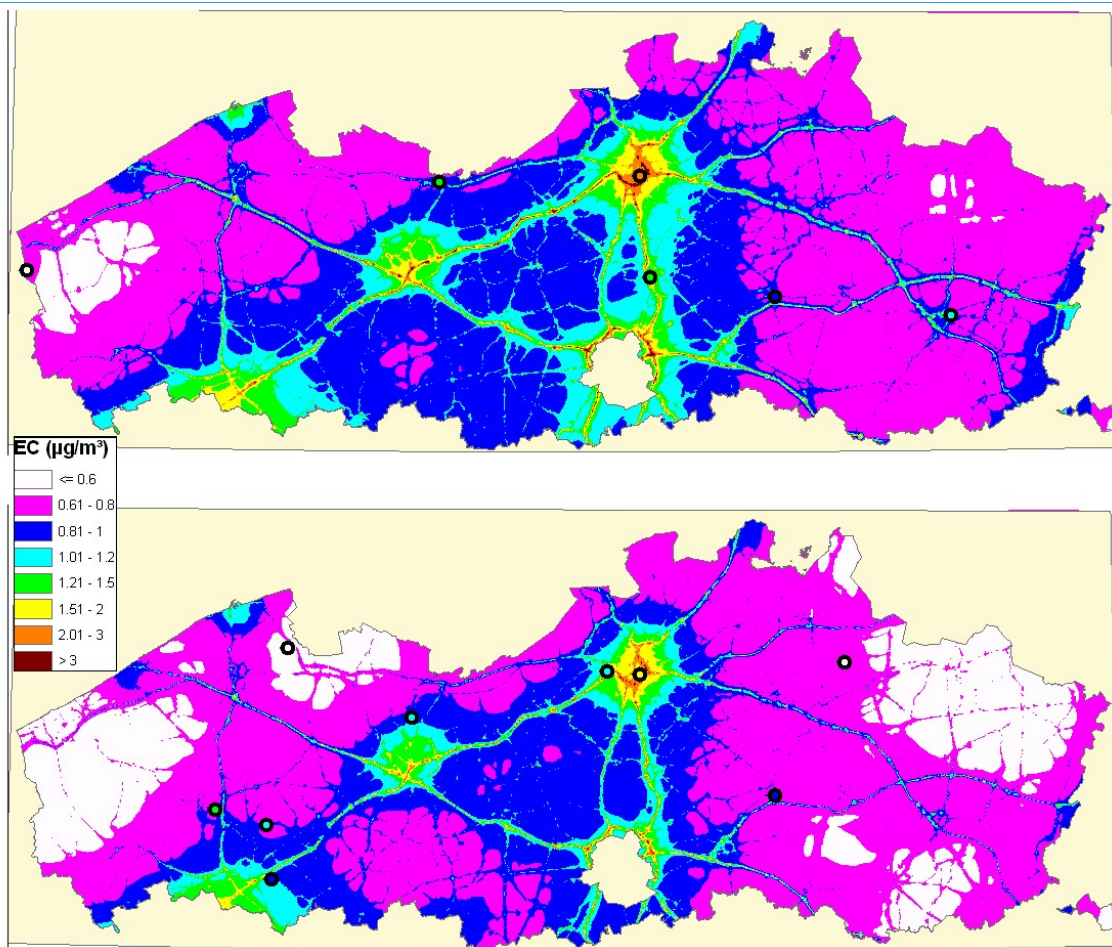


Figure 10 : The modelled EC concentration (in $\mu\text{g}/\text{m}^3$) in the CK1_comp simulation (top) and in the CK2_comp simulation (bottom). The circles are the monitoring sites and are filled corresponding to the measured concentrations.

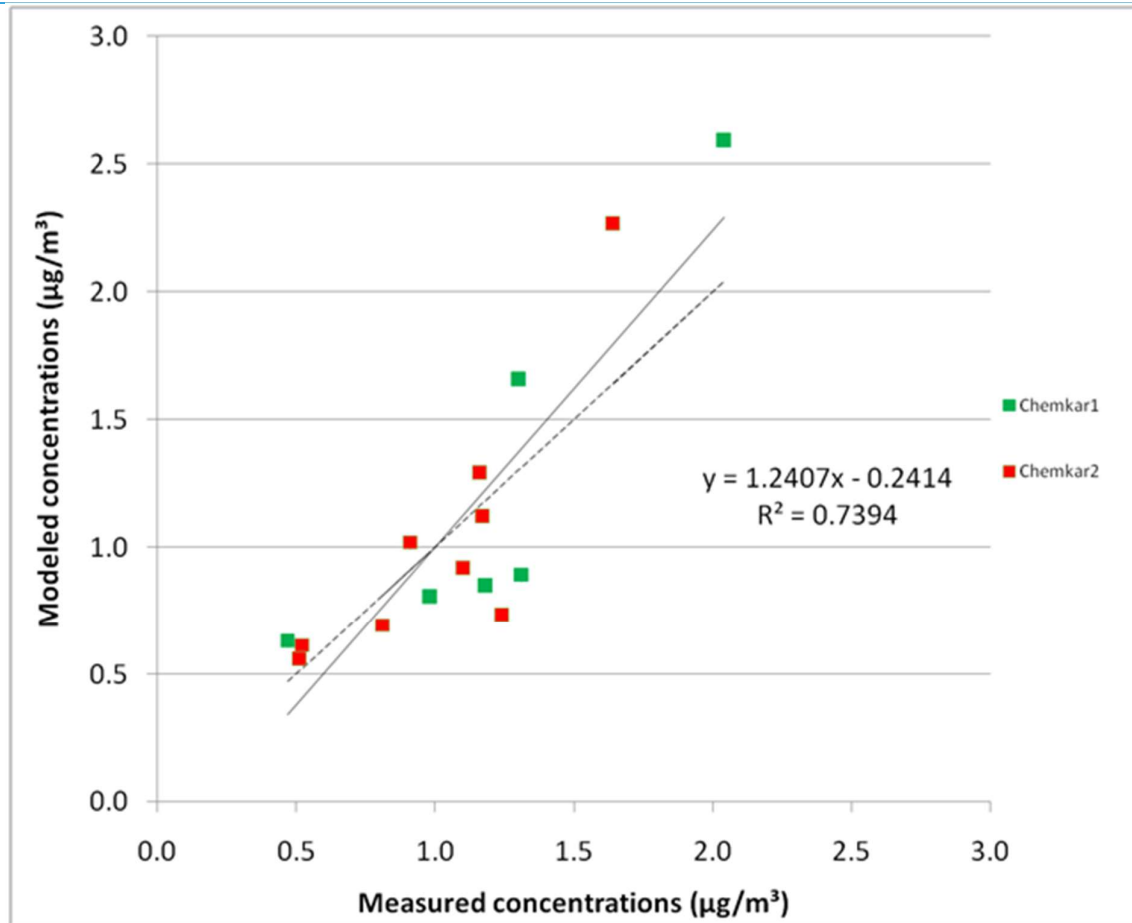


Figure 11 : The validation graph for the campaign-mean EC concentrations. On the X-axis: the measured EC concentrations in $\mu\text{g}/\text{m}^3$. On the Y-axis: the modelled EC concentrations in $\mu\text{g}/\text{m}^3$, using CK1_comp results for Chemkar1-monitoring sites and CK2_comp results for Chemkar2-monitoring sites. Every dot represents one monitoring site during one campaign: green for Chemkar1, red for Chemkar2. The dashed line is the 1-1 line. The black full line shows the regression between the measurements and the model, for which the equation and the R^2 are shown on the right side.

Number	Description	EC/PM _{2.5}	EC (ton/yr)
S1	Combustion in energy and transformation industries (stationary sources)	0.11	88
S2	Non-industrial combustion plants (stationary sources)	0.21	498
S3	Combustion in manufacturing industry (stationary sources)	0.25	404
S4	Production processes (stationary sources)	0	0
S5	Extraction and distribution of fossil fuels and geothermal energy	0.85	0
S6	Solvent use and other product use	0	0
S7	Road transport	0.6611	2213
S8	Other mobile sources and machinery	0.52	1634
S9	Waste treatment and disposal	0.004	1
S10	Agriculture	0.17	85
S11	Other sources and sinks	0	0

Table 5 : The ratio EC/PM_{2.5} as used in this study for the different SNAP-sectors, based on Schaap et al. (2004) except for S7. The last column is the estimated Flemish emission of EC per snap-sector based on the latest estimations of the PM_{2.5}-emissions from the Flemish Environment Agency (VMM) for 2007

Simulation	Resolution	Model	Emissions	Emission year	Meteorology	Mean conc ($\mu\text{g}/\text{m}^3$)
AUR07	3x3 km ²	AURORA	All	2007	Modelled 2007	1.03
AUR10	3x3 km ²	AURORA	All	2010	Modelled 2007	0.91
I07_ARPS_r	IFDM regular	IFDM	Flemish Roads	2007	Modelled 2007	0.26
I10_ARPS_r	IFDM regular	IFDM	Flemish Roads	2010	Modelled 2007	0.21
I07_ARPS	IFDM road following	IFDM	Flemish Roads	2007	Modelled 2007	0.34
I10_ARPS	IFDM road following	IFDM	Flemish Roads	2010	Modelled 2007	0.28
I_06_07	IFDM road following	IFDM	Flemish Roads	2007	Measured 2006	0.32
I_07_07	IFDM road following	IFDM	Flemish Roads	2007	Measured 2007	0.30
I_08_07	IFDM road following	IFDM	Flemish Roads	2007	Measured 2008	0.31
I_09_07	IFDM road following	IFDM	Flemish Roads	2007	Measured 2009	0.27
I_CK1_07	IFDM road following	IFDM	Flemish Roads	2007	Measured Chemkar1	0.34
I_CK1_10	IFDM road following	IFDM	Flemish Roads	2010	Measured Chemkar1	0.28
I_CK2_07	IFDM road following	IFDM	Flemish Roads	2007	Measured Chemkar2	0.29
I_CK2_10	IFDM road following	IFDM	Flemish Roads	2010	Measured Chemkar2	0.23
BACK07	3x3 km ²	AUR07-I07_ARPS_r				0.77
BACK10	3x3 km ²	AUR10-I10_ARPS_r				0.70
CK1_comp	IFDM road following	BACK07+CK1_07				1.11
CK2_comp	IFDM road following	$1/3*(\text{BACK07}+\text{CK2_07})+2/3*(\text{BACK10}+\text{CK2_10})$				0.97
CK2-CK1	IFDM road following	CK1_comp-CK2_comp				-0.14
ΔE_b	IFDM road following	$2/3*(\text{BACK10}-\text{BACK07})$				-0.05
ΔE_l	IFDM road following	$2/3*(\text{CK2_10}-\text{CK2_07})$				-0.03
ΔM_l	IFDM road following	CK2_07-CK1_07				-0.06

Table 6 : Characteristics of the different simulations used in this study. The resolutions 'IFDM regular' and 'IFDM road following' are described in §3.4. The "mean conc" column denotes the modelled mean concentration (in $\mu\text{g}/\text{m}^3$) averaged over all monitoring sites available in at least one measurement campaign (and counting Aarschot and Bergerhout only once).

Nr	Cp	Location	Meas	AUR07	AUR10	BACK07	BACK10	I_CK1_07	I_CK2_07	I_CK2_10	CK1_comp	CK2_comp	Combined
1	CK1	Houtem	0.47	0.6450	0.5430	0.6228	0.5325	0.0080	0.0120	0.0090	0.6308	0.5726	0.6308
2	CK2	Moerkerke	0.51	0.6270	0.5540	0.5605	0.5035	0.0520	0.0430	0.0350	0.6125	0.5602	0.5602
3	CK2	Retie	0.52	0.7050	0.5970	0.6216	0.5273	0.0690	0.0590	0.0510	0.6906	0.6124	0.6124
4	CK1	Aarschot	0.98	0.8420	0.7250	0.5999	0.5233	0.2070	0.1600	0.1360	0.8069	0.6928	0.8069
	CK2	Aarschot	0.81	0.8420	0.7250	0.5999	0.5233	0.2070	0.1600	0.1360	0.8069	0.6928	0.6928
5	CK2	Zwevegem	0.91	1.1580	0.9680	1.0739	0.9050	0.0740	0.0650	0.0530	1.1479	1.0183	1.0183
6	CK2	Evergem	1.10	0.9780	0.9010	0.8121	0.7607	0.2000	0.1530	0.1360	1.0121	0.9195	0.9195
7	CK2	Zwijndrecht	1.16	1.4290	1.3110	0.8599	0.8497	0.5270	0.5000	0.4090	1.3869	1.2924	1.2924
8	CK2	Oostrozebeke	1.17	0.8900	0.7760	0.7585	0.6695	0.6100	0.4600	0.4060	1.3685	1.1232	1.1232
9	CK1	Hasselt	1.18	0.8550	0.7390	0.6382	0.5543	0.2130	0.1590	0.1340	0.8512	0.7246	0.8512
10	CK2	Roeselare H	1.24	0.8690	0.7680	0.6774	0.6129	0.1270	0.1130	0.0930	0.8044	0.7341	0.7341
11	CK1	Mechelen	1.30	1.2020	1.0490	0.8354	0.7491	0.8240	0.6240	0.5290	1.6594	1.3385	1.6594
12	CK1	Zelzate	1.31	0.8530	0.7630	0.6735	0.6134	0.2180	0.1680	0.1470	0.8915	0.7874	0.8915
13	CK1	Borgerhout	2.04	2.3030	2.1560	1.2673	1.2988	1.3270	1.1100	0.9120	2.5943	2.2663	2.5943
	CK2	Borgerhout	1.64	2.3030	2.1560	1.2673	1.2988	1.3270	1.1100	0.9120	2.5943	2.2663	2.2663
		R²	<i>1.000</i>	0.675	0.680	0.543	0.611	0.696	0.692	0.694	0.703	0.698	0.739
		Mean ($\mu\text{g}/\text{m}^3$)	<i>1.09</i>	1.10	0.98	0.79	0.73	0.40	0.33	0.27	1.19	1.04	1.11
		Bias ($\mu\text{g}/\text{m}^3$)	<i>0.00</i>	0.01	-0.11	-0.30	-0.36	-0.69	-0.76	-0.82	0.10	-0.05	0.02
		RMSE ($\mu\text{g}/\text{m}^3$)	<i>0.00</i>	0.29	0.30	0.41	0.45	0.73	0.80	0.85	0.37	0.30	0.32

Table 7 : Comparison of the different simulations with the measurements. The measurement values are collected in column “Meas”. The “Combined” column combines the “CK1_comp” and the “CK2_comp” column by taking the value of the CK1_comp column if the measurement is performed during the Chemkar1 campaign and of the CK2_comp column otherwise. All model and measurement values are in $\mu\text{g}/\text{m}^3$. The mean value is based on the averaged value of all data, counting both the Aarschot and the Borgerhout data for both years (and thus double for the model simulations).

2.7. SUPPLEMENTARY MATERIAL

2.7.1. EFFECT OF METEOROLOGY

→ Effect of meteorology

In this section, the impact of the meteorology on the observed and simulated EC concentrations is examined.

Modelled versus measured meteorology

To assess the impact of meteorology on the model simulation, we compare the dispersion simulations using modelled ARPS meteorology (I07_ARPS) versus measured meteorology (I07_07). Only the Flemish traffic contribution is compared here. The simulated concentrations with the ARPS meteorology are always lower than the ones with the measured meteorology. The differences in Flemish traffic contributions range from 1% in Oostrozebeke to 18% in Houtem (although the absolute EC concentration due to Flemish traffic is very low here). The mean difference between both approaches is about 10%. The difference seems to be due to two reasons. On the one hand, the modelled wind speed, when reduced to the height of the measurements, is on average about 21% higher than the observed measurements. Overestimation of the modelled wind speed is pronounced at low wind speeds, while at high wind speeds, the model bias is small. On the other hand, the ARPS model displays a somewhat more stable atmosphere than what is observed in the measurements, which can be expected to result in higher concentrations. Clearly, the wind speed effect is larger than the stability effect, leading to slightly lower concentrations in the model runs using modelled wind speeds.

Year-to-year differences

As 4 years were simulated with the same Flemish traffic emissions (year 2007) and with only differences in the meteorology year (performing a simulation for every year using the meteorological parameters of that year) (2006-2009), the effect of meteorology on the concentration levels can be estimated. The standard deviation of the four annual mean concentrations, divided by the four-year-average concentration, leads to a deviation of 2% in Roeselare Haven to 12% in Zwevegem and Oostrozebeke. The average over all monitoring sites is 8%. The maximum difference between two years amounts to 18% averaged over all monitoring sites, ranging from 3% in Roeselare Haven to 27% in Oostrozebeke. This large difference can be explained by the specific road configuration in the neighborhood of the latter monitoring site. There is only one major road in the vicinity of the Oostrozebeke monitoring site and year to year differences in the prevailing winds result in a large difference in traffic-induced EC concentrations. As a comparison, equally important roads surround the measurement location in Roeselare Haven. However, changes in prevailing winds do not lead to large differences between the years which explains the 3% effect at this location.

→ Differences between the two measurement periods

At two monitoring locations meteorological data were collected during both Chemkar campaigns. Both monitoring sites exhibit a significantly lower concentration during the second campaign compared to the first one. In this paragraph it will be investigated whether or not the model is able to reproduce this behavior, and if so, what is the origin of the differences. On the assumption of a marginal linear contributions we can assume that the difference in concentration (ΔC) can find its origin in four different components:

$$\Delta C = \Delta El + \Delta Eb + \Delta Ml + \Delta Mb \quad (1)$$

where ΔEl is the concentration change by changing Flemish traffic emissions, ΔEb by other emission changes, ΔMl because of the effect of the different meteorology on the concentrations originating from the Flemish traffic emissions and ΔMb because of the effect of the different meteorology on the concentrations originating from the other emissions. The ΔMb term cannot be assessed with the model runs performed here. However, for the other terms an evaluation can be made. Their method of calculation is given in Table 3. The results are shown in Figure 12 and Figure 13. The changes because of background emissions (ΔEb , Figure 12, bottom) are small in the northern part of Flanders and slightly increase (up to about $0.1 \mu\text{g}/\text{m}^3$) in the southern part. This term, averaged over the monitoring sites, accounts for about 33% of the difference between the *CK2_comp* and the *CK1_comp* simulations. The change in Flemish road emissions (ΔEl , Figure 13, top) is only important very close to the major roads. This term, averaged over the monitoring sites accounts for about 21% of the difference between the *CK2_comp* and the *CK1_comp* simulations. The change because of the impact of changing meteorology on the Flemish road emissions (ΔMl , Figure 13, bottom) is only important close to the major roads. However, at these locations, this term is quite important, with changes over $0.2 \mu\text{g}/\text{m}^3$ at several places. This term, averaged over the monitoring sites, accounts for about 46% of the difference between the *CK2_comp* and the *CK1_comp* simulations. Finally, the size of the ΔMb term can be estimated, based on the model results and data collected at the two measurement locations (Aarschot and Borgerhout) which participated in both Chemkar-campaigns. The difference between both campaigns is up to $0.17 \mu\text{g}/\text{m}^3$ in Aarschot and up to $0.4 \mu\text{g}/\text{m}^3$ in Borgerhout. The sum of the three first terms at the right hand side of Eq.(1) at these locations shows a difference of respectively 0.11 and $0.33 \mu\text{g}/\text{m}^3$ in Aarschot and Borgerhout. Therefore we can assume that the ΔMb term accounts for about $0.06 \mu\text{g}/\text{m}^3$ in Aarschot and for about $0.07 \mu\text{g}/\text{m}^3$ in Borgerhout. This would be respectively 33% and 18% of the total measured difference. As a result, we can assume that this term is important and of the same order as the other three terms.

If we estimate this ΔMb term as about 25% of the total concentration change, this would lead to contributions of the other terms (by multiplying the remaining 75% with respectively the 33%, 21% and 46% contributions derived above) of respectively 25%, 16% and 34% for ΔEb , ΔEl and ΔMl . In conclusion, the differences in concentrations between both Chemkar campaigns (i.e. the distinct higher concentrations of EC in the first Chemkar campaign compared to the second one) could be explained for about 60% by changed meteorology and 40% by changed emissions.

→ Measuring one out of every six days as a proxy for an entire year

In the Chemkar measurement campaigns, measurements were taken once every six days during an entire year allowing a fair representation of samples over working days, weekends and holidays.

However, it is questionable whether the weather conditions of the measurement days were representative for the full period. Therefore, we compare the I_CK1_07 simulation with the I_07_07 simulation. Both simulations are based on the Flemish traffic emission only. In I_CK1_07 only the measurement days are taken into account, while for I_07_07 the entire year 2007 is included. If the meteorology of the Chemkar1-campaign days were representative for the entire year 2007, one would expect the same average concentrations in both simulations. The average over all monitoring sites (counting Aarschot and Borgerhout only once) in the I_CK1_07 simulation is $0.34 \mu\text{g}/\text{m}^3$, while in the I_07_07 simulation, the average amounts to only $0.30 \mu\text{g}/\text{m}^3$ (see Table 2).

An analogous comparison can be made for the Chemkar2-campaign, by comparing the I_CK2_07 simulation with the I_09_07 simulation. Here, the simulation using only the Chemkar2-campaign days amounts to $0.28 \mu\text{g}/\text{m}^3$, while the average in the I_09_07 simulation amounts to $0.27 \mu\text{g}/\text{m}^3$ (Table 2). Based on those model results, it can be stated that the “one out of six” strategy led, in this case, to a small overestimation of the effective annual averaged EC concentrations. Moreover continuous measurements over the entire years 2007 and 2009 would have led to smaller differences between both campaigns than the current methodology. However, these conclusions are based on model results and preferably should be confirmed by measurements. However, one location (Retie) was included in Chemkar2 for which samples were taken each day of the campaign. The data of this full 365 days series showed that for the 6 possible ‘one out of six’ datasets, the average absolute difference was 7% and the maximum absolute difference was 10%. This is comparable to the modelled differences obtained above.

2.7.2. EXTRA INFORMATION ON THE METEOROLOGY DURING THE MEASUREMENT CAMPAIGNS

In Figure 14, the wind roses for both Chemkar campaigns and the total period 2006-2009 can be found. It can be seen that while the roses resemble each other, the differences remain large. However, thanks to the methodology procedure of modelling each period with the exact meteorology measured during this period, this poses no problem for the comparison with the model values. Furthermore, in Figure 15 and Figure 16, a complete overview of the meteorology during these campaigns is given.

For the reader which is interested in more detail in the meteorological conditions during the Chemkar-campaigns, the backward trajectories for every measured day are available in ‘Bijlage A’ from VMM (2009) and VMM (2010).

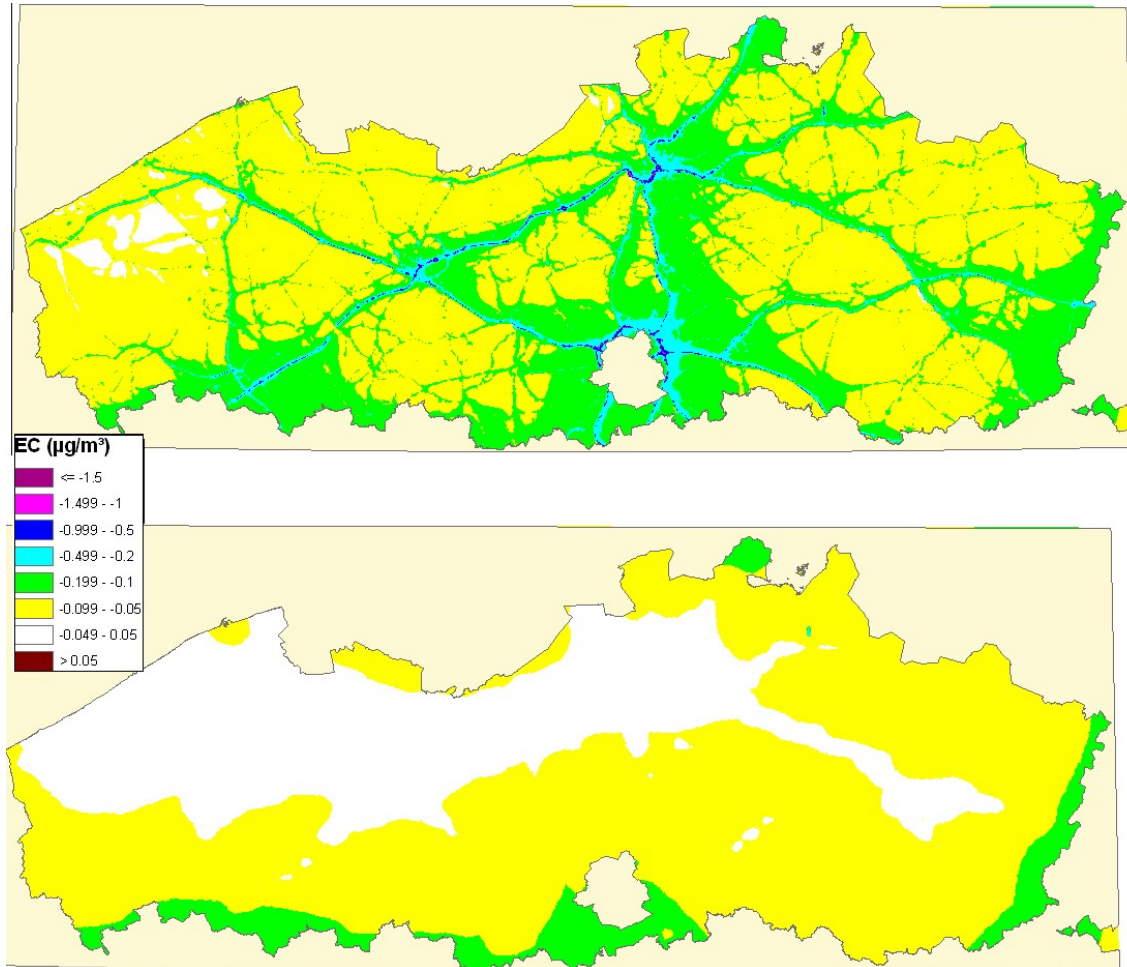


Figure 12 : The difference in the modelled EC concentration (in $\mu\text{g}/\text{m}^3$) between the CK2_comp and the CK1_comp simulation (top) and the ΔEb term (bottom).

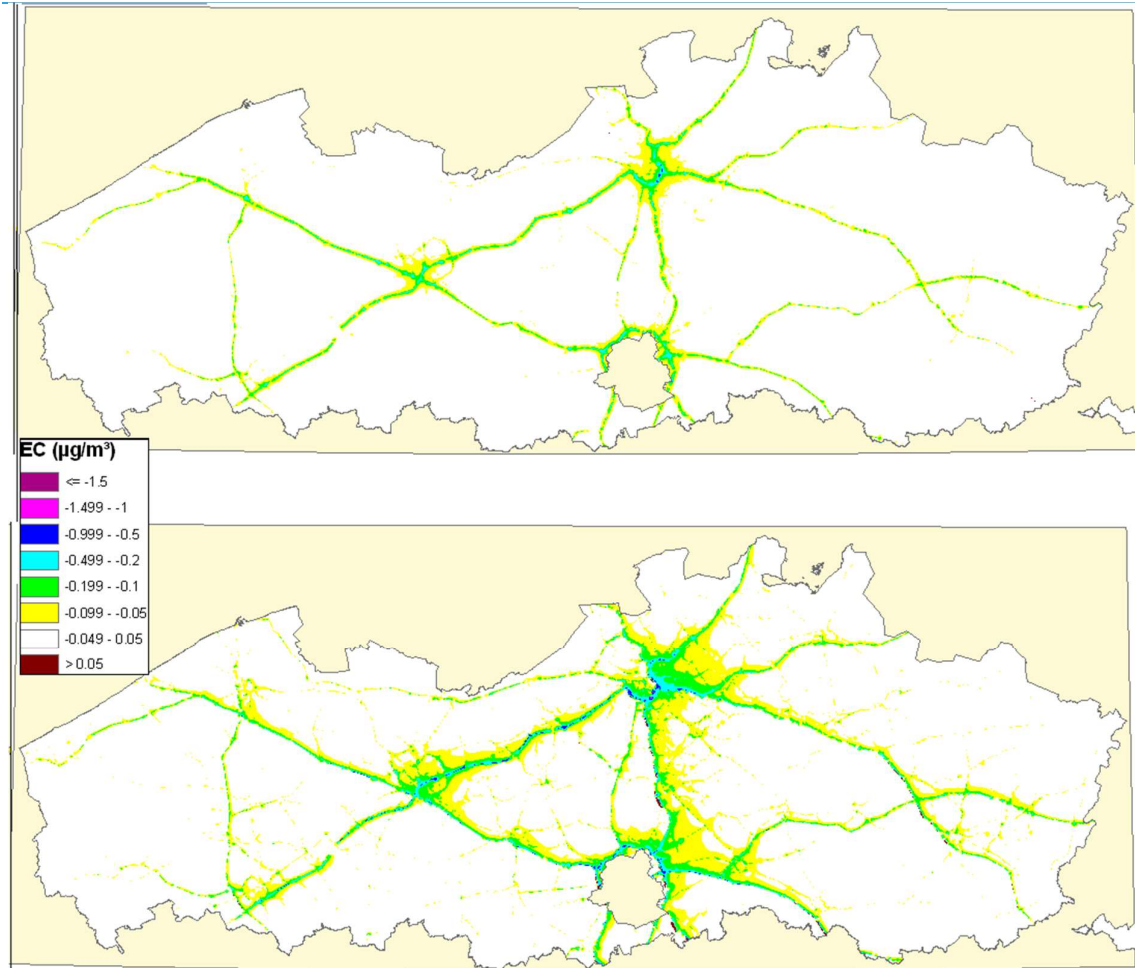


Figure 13 : The ΔEI (top) and the ΔMI term (bottom) (in $\mu\text{g}/\text{m}^3$).

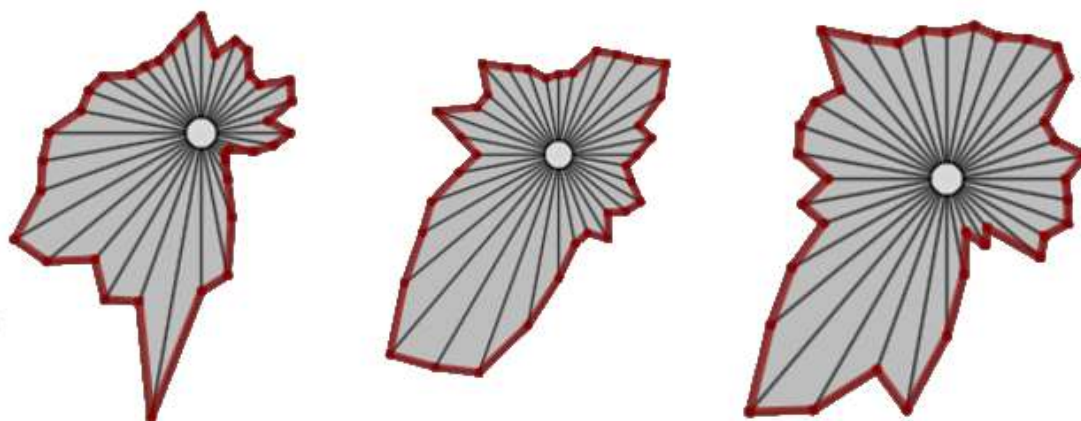


Figure 14 : The wind roses for the first Chemkar-campaign (left), the second Chemkar-campaign (right) and the mean over the period 2006-2009 (middle).

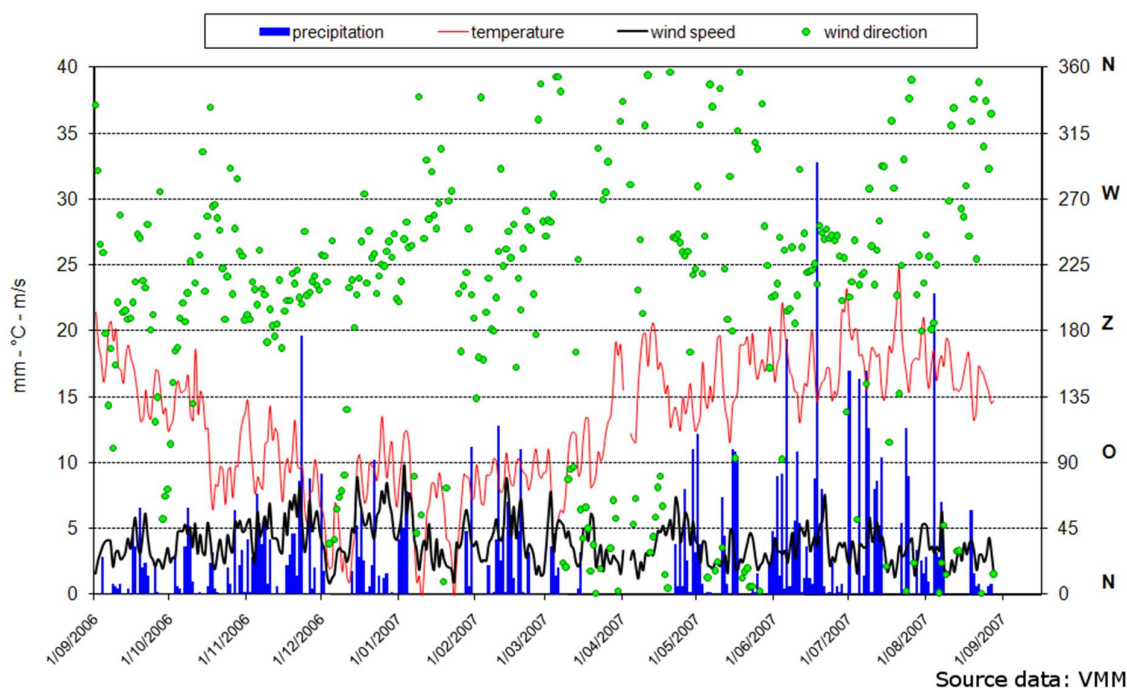


Figure 15 : Meteorological conditions during the first Chemkar-campaign.

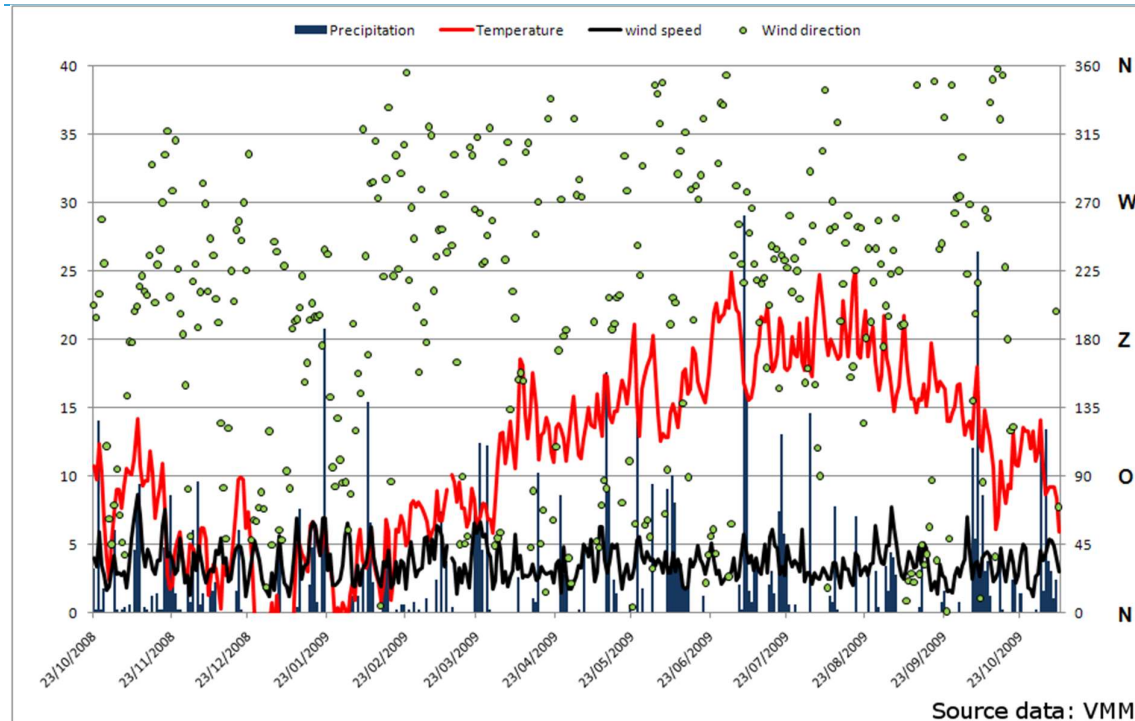


Figure 16 : Meteorological conditions during the second Chemkar-campaign.

2.8. FURTHER WORK ON THIS SUBJECT SINCE THE PUBLICATION OF THE PAPER

Since the publication of the paper, the results for the third ChemKar-campaign have become available. The validation Figure of the paper has thus since been extended to include the results from this campaign.

As no street canyon model was available in this model chain, and as the station R802 is found in a street canyon, this point was added in a different way. In the study made for the city of Antwerp we found a EC concentration (annual mean) for 2015 of $1.9 \mu\text{g}/\text{m}^3$ at R801 and $2.7 \mu\text{g}/\text{m}^3$ at R802. This difference ($0.8 \mu\text{g}/\text{m}^3$), I added to the modelled value at R801 in order to obtain the modelled results for R802. This results in Figure 17.

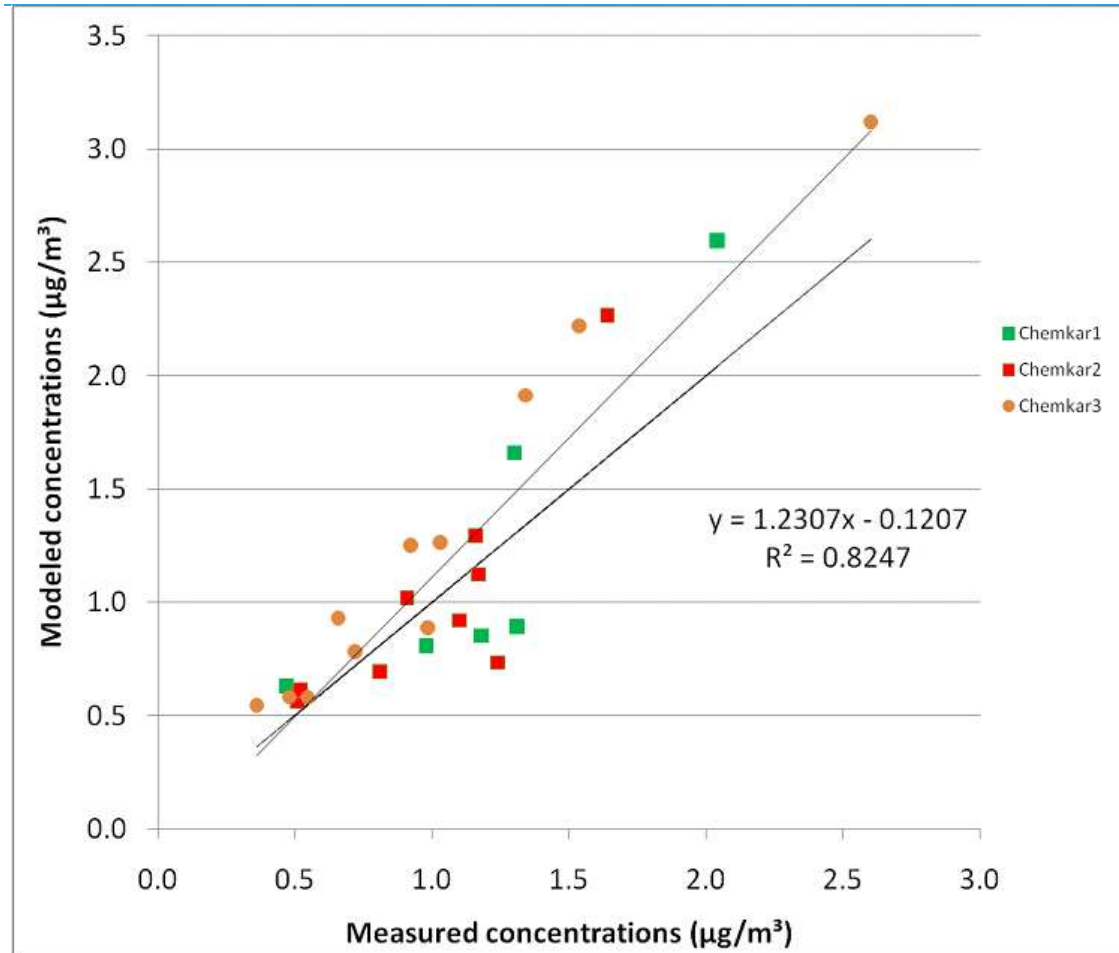


Figure 17 : Update of Figure 5 of Lefebvre et al. (2011b) (Figure 11) to include the Chemkar 3 campaign.

As can be seen, the addition of the Chemkar3-campaign improves the results even more, with a better slope and a better R^2 when taking into account these data.

CHAPTER 3 CONCLUSIONS FROM THE SBO-MASE PROJECT, RELEVANT TO THIS VALIDATION EXERCISE

In this chapter the paper Lefebvre et al. (2013a) is reproduced, which describes a validation exercise done within the SBO-Mase project.

Presentation and evaluation of an integrated model chain to respond to traffic- and health-related policy questions

Lefebvre W.*, Degraeuwe B.*, Beckx C.*, Vanhulsel M.*, Kochan B.#, Bellemans T.#, Janssens D.#, Wets G.#, Janssen S.*, de Vlieger I.*, Int Panis, L.*#, Dhondt S.‡

* Vlaams Instituut voor Technologisch Onderzoek (VITO), Boeretang 200, 2400 Mol

Transportation Research Institute (IMOB), Faculty of Applied Economics, Hasselt University, Wetenschapspark 5 Box 6, B-3590 Diepenbeek, Belgium

‡ Department of Medical Sociology and Health Sciences, Vrije Universiteit Brussel, Laarbeeklaan 103, 1090 Brussel

Abstract

There is often a large discrepancy between the questions raised by policy makers and the responses offered by scientists. Current modelling approaches do not answer some of the typical questions that decision-makers face, as they do not provide solutions to policy-makers dealing with concrete political negotiation and decisions. In this paper, we try to bridge the gap by creating an integrated model chain that can respond to such concrete policy questions. The paper describes a model chain consisting of an activity-based transport model, a road traffic emission model, a bi-gaussian atmospheric dispersion model and a concentration measurement interpolation model. Subsequently results are compared to observations, in order to test its usability for simulating air quality and assessing dynamic exposure. The model is shown to represent the main cycles governing air quality, such as the intra-daily, the intra-weekly and the intra-annual cycle. Finally, this paper provides an example of the use of such a model chain by assessing the impact of different trip motives on the intra-daily NO₂ cycle.

Highlights

- An integrated model chain designed to respond to specific policy questions is presented.
- The chain is evaluated with air quality measurements, showing a very good agreement.
- The intra-daily, intra-weekly and intra-annual cycles are presented in the model results.
- An example of the use of the model chain is provided.

Keywords

Air quality, integrated model chain, evaluation, policy questions

3.1. INTRODUCTION

There is often a large discrepancy between the questions raised by policy makers and the responses offered by scientists. Scientists in the domain of air pollution modelling are well able to respond to questions such as: 'If a new road with an annual emission of 10 tonnes of NO_x is built, how will this affect the air pollution at certain measurement stations nearby?' However, policy makers are more interested in questions such as: 'If the new road network proposed by the public transport authority is implemented, what will be the impact in the region in terms of traffic loads, pollution concentration levels and resulting health risks for the population?'

Previous efforts have been made to estimate concentrations of air pollutants as an aid for policy in reducing exposure and thereby improving health (e.g. Borrego et al., 2006; Marshall et al., 2006; Hatzopoulou and Miller, 2010; Hatzopoulou et al., 2011). However, human travel behaviour can not only be used to assess exposure, i.e. by including time-activity patterns, but it can also be seen as a driving force for emissions (Beckx et al., 2009a; Hatzopoulou and Miller, 2010). To account for this latter, an activity-based transport demand model was integrated in an environmental modelling framework. The advantages of using such an activity-based model for air quality purposes are described in numerous other publications and are presented briefly in the next section (section 2). A more accurate assessment of vehicle emissions and population exposure of the 'reference situation' are often mentioned as the key advantages. Additionally, activity based models can cover a nationwide region, while still providing sufficient detail to assess effects on a local scale and for different population subgroups (Dhondt et al., 2012a). The benefits of estimating the impact of specific policy measures are not yet fully explored. Furthermore, improvements in the spatial resolution can be made in order to better capture the steep concentration gradients caused by local vehicle emissions. Hereby, it is important to take into account both these large concentration gradients along the major line and point sources as well as the regional aspects of the air pollution.

This paper presents a model chain which enables us to answer these type of questions at a sufficiently high spatial resolution and thus provides a tool to bridge the gap between policy makers and scientists. In this chain, it is necessary to combine models describing human behavior as well as traffic emission and atmospheric dispersion.

Thus, this paper has three distinct goals:

- 1) Explain and discuss the model setup;
- 2) Show that the model chain reproduces the measurements;
- 3) Give an example of the use of the model chain.

3.2. AN ACTIVITY-BASED MODELLING APPROACH FOR AIR QUALITY PURPOSES

By simulating activity-travel patterns for individuals in a population, activity-based transport models provide information on why, when and where people travel (Arentze and Timmermans, 2004).

Although the activity-based model was originally developed to gain more insight into travel behavior, the activity-based approach for transport modelling also offers other advantages. Integrating an activity-based transport model in an air quality modelling framework has numerous advantages for modelling traffic demand, emissions, dispersion and exposure. We briefly discuss some of the main benefits of using an activity-based approach for air quality purposes and refer to Beckx et al. (2008, 2009a) for a more detailed overview of all advantages.

Due to the richer set of concepts which are involved in activity-based transportation models the estimation of some important transportation variables can be improved by using an activity-based approach (Shiftan, 2000; Shiftan and Suhrbier, 2002). Vehicle emissions depend not only on distance and the driving speed, but also on the number of trips, the time between them, and whether the engine was hot or cold when started (Recker and Parimi, 1999). The activity-based prediction of trips as parts of a tour can identify whether a trip is a cold or a hot start. Furthermore, an activity-based model, by predicting which activities are conducted, where, when, for how long, with whom and the transport mode involved, gives additional information about other important transportation variables such as, travel by time of day and time/location of starts. These variables all are relevant and important for both vehicle emission analysis and atmospheric modelling but are not generally available from classical traffic models. In most traffic air pollution studies aiming at a temporal differentiation of traffic emissions, either hourly traffic counts are used or the emission model applies normalized distribution factors expressing the time dependency of traffic with respect to peak values (e.g. Schrooten et al., 2006). An activity-based approach however does not work with traffic counts nor peak hour predictions, but simulates entire activity-travel schedules covering a complete day and takes into account local and temporal variations in travel behavior. Extraction of the simulated travel information can therefore provide temporal travel and emission values more accurately (Beckx et al., 2009a). And, finally, since an activity-based model provides information on people's location during the day, this approach can be used to assess the exposure to pollutants at different locations and different moments.

Epidemiological studies typically use concentrations from fixed site monitoring stations (Pope et al., 2009) or concentrations modelled at the home location (Brunekreef et al., 2009). It has however been argued that both approaches may contribute to bias in the health effect estimates (Setton et al., 2011). Attempts to assess dynamic exposure are very rare and often focus on long time scales (e.g. De Ridder et al., 2008a; 2008b). However, when temporal information is available on both the sources (i.e. the emissions) and the receptors of the air pollution (i.e. the population), a dynamic exposure procedure can be established as for example demonstrated by Beckx et al. (2008) who used the Dutch ALBATROSS model (Arentze et al., 2003; Arentze and Timmermans, 2004) and by Hao et al. (2010) including the activity-based travel demand model TASHA for the Toronto area. Moreover, by taking advantage of information on 'which activity is performed' or 'who is performing the activity', the activity-based procedure allows for a disaggregated exposure analysis according to different subgroups. This information can for example give more insights into the subgroups most at risk and identify the activities contributing disproportionately to the exposure (Marshall, 2006; Beckx et al., 2009b; Dons et al., 2011a).

3.3. THE TEN STEPS ON DEVELOPMENT AND EVALUATION OF ENVIRONMENTAL MODELS

In 2006, Jakeman et al. published a paper outlining ten steps which a development and evaluation cycle for environmental models ideally should contain. Applications of these ten steps on very diverse models can be found in Welsh (2008) for water modelling, Robson et al. (2008) for a biogeochemical model of aquatic systems, Piuleac et al. (2010) for modelling of electrolysis processes by using neural networks and Blocken et al. (2012) for a Computational Fluid Dynamics model. It has also been applied for modelling of air quality (e.g. Mensink and Cosemans, 2008). Following their example, we briefly address each of the ten model building steps given in the Jakeman et al. (2006) paper.

The purpose (1) of the model combination presented in this paper is defined in the introduction: an integrated model chain that helps policy makers answer questions related to air quality and traffic. Automatically, this sets the modelling context and scope (2): how to model concentrations (and in a next step the exposure) in a region and how it is affected by changes in behavior due to measures taken by the policy makers. The model concept (3) is defined in Figure 18. Input data include, but are not limited to, hourly activity diary data, road networks, hourly freight traffic, hourly meteorology data, hourly air quality measurements and land use (yellow parallelograms on Figure 18). Prior (empirical and theoretical) knowledge and assumption on behavior and dispersion processes are included in the different models within the chain. The selection of these models (4) is based on long-term satisfying experience in application and testing of these models or their precursors. For instance, more than 30 years of experience for the IFDM model is present. The choice of using a land use regression model instead of a chemical transport model is explained in §4.3. The model structure and parameter values (5, 7) are defined for each model building block and based on specific expertise in the relevant domain (for instance, the bi-gaussian dispersion modelling concept in IFDM). Concerning performance criteria and techniques to evaluate these criteria (6), it is worthwhile to mention the large effort which was undertaken in Europe to obtain a common reference frame for testing Gaussian models (Olesen, 1995). For instance, the IFDM model has been tested against several experimental datasets that are presented in the Model Validation Kit. The other models are also tested against comprehensive datasets and are found to be adequate for the underlying exercise (see next sections and supplementary material). Whereas the individual model components have been tested extensively (8), the combination of all these models is new and thus validation of the model chain is needed, the strategy of which can be found in §5.2. This validation will be presented in section 5. Model uncertainty (9) is difficult to quantify, since it depends strongly on the simulated pollutants as well as on the quality of the input data. However, the model evaluation (section 5), gives rise to some insight in the uncertainty in the model chain by comparing the model results to the observations (10).

3.4. MODEL SETUP

An integrated model chain has been setup to assess air quality, including both regional changes as well as local variation of air pollution. Figure 18 presents an overview of this modelling framework. The first model in the chain, the FEATHERS model (§3.4.1), simulates origin destination matrices and spatially and temporally distributed person-hours, based on activity diary data and demographic and socio-economic data. The resulting origin-destination matrices are then attributed to the road

network by the Transcad model (§3.4.1). This yields road traffic loads which are the input for the MIMOSA4 emission model (§3.4.2). The resulting spatially and temporally distributed emissions are used in the bi-gaussian model IFDM (§3.4.4) in which they are coupled (§3.4.5) to regional concentration levels from the land-use regression model RIO (§3.4.3). The individual models, their setup and interconnections are briefly discussed in the following paragraphs. More detailed descriptions of the different models can be found in supplementary files.

3.4.1. FEATHERS AND TRANSCAD

The activity-based model FEATHERS (Forecasting Evolutionary Activity-Travel of Households and their Environmental RepercussionS) is an agent-based simulation framework to model travel behavior in the regions of Flanders and Brussels (Belgium) (Bellemans et al., 2010). It is an adaptation of the Dutch ALBATROSS model developed by Arentze and Timmermans (Arentze and Timmermans, 2004). FEATHERS simulates how individuals build up their activity-travel schedules during the day and, as a result, predicts for all individuals within a synthetic population which activities are conducted, when, where, for how long and the transport mode involved. The activity-based model treats travel as being derived from the demand for activity participation distributed in space and time. Trip information for the individual agents in the population is then presented as origin-destination matrices, for every hour of an average week. Similar to the approach of Beckx et al. (2009a) these origin-destination matrices were in a next step assigned to a road network by applying the traffic assignment functionalities of the Transcad model (Caliper). As a result, the number of vehicles and the average speed per road segment and per time of day were provided, which are needed for the emission modelling.

For this study the zone-level was chosen as the spatial unit for the location assignment procedure. The 1145 zones match with the former independent municipalities and have an average surface of 12 km². More information about these models can be found in the supplementary material (SM1).

3.4.2. MIMOSA

MIMOSA4 was used to estimate road traffic emissions based on the hourly information on traffic intensities and vehicle speed that resulted from the activity-based travel modelling step. MIMOSA4 is the most recent version of the traffic emission model MIMOSA (Mensink et al., 2000; Vankerkom et al., 2009), and relies on the COPERT4 methodology (Gkatzoflias et al. 2012) to generate hourly output for different types of emissions, such as NO₂, NO_x, PM₁₀ and PM_{2.5} (see also Lefebvre et al., 2011a). To deal with the ozone chemistry, MIMOSA generates both total NO_x and NO₂ emissions. More information about this model can be found in the supplementary material (SM2) and in Beckx et al. (2009a) where its application to activity-based models is also fully described.

3.4.3. RIO

The RIO model is a validated land use regression model for Flanders and the Netherlands (Hooyberghs et al., 2006; Janssen et al., 2008). RIO estimates hourly pollutant concentrations in a 3x3

km² square, based on the pollution data collected in the official fixed site monitoring network and a land use (CORINE) derived covariate. Therefore, statistical relationships between land use and long term average hourly concentrations are determined (trend functions). I.e., for each hour of the day, the hourly-trend function gives the relationship (regression line) between the long term average at that particular hour and the same underlying land use. In that respect, the RIO model is able to estimate hourly pollutant concentrations by taking into account the trends with respect to land use valid for that particular hour of the day. Note that also a distinction between week & weekend is made (so separate sets of parameterisations for the relationship between land use and the long term average concentrations). As an output RIO produces hourly concentration maps for the pollutants PM₁₀, PM_{2.5}, NO₂, O₃ and SO₂. Based on those results, annual statistics (annual mean, number of exceedances) can be derived. Recently, the model was extended to estimate uncertainties associated with the interpolated air quality maps. RIO has been shown to be very accurate in estimating the pollution over Belgium (Janssen et al., 2008). It is clear that the method of interpolating measurements in an intelligent way will yield better results than using an Eulerian dispersion model (as in e.g. Beckx et al., 2009b), because limitations due to incomplete emission inventories and uncertainties in dispersion modelling are avoided. The RIO model currently is the most accurate means of mapping air pollutant concentrations for Belgium (e.g. Janssen et al., 2008), the methodology has been extensively validated both via cross-validation (leaving one out) and independent measurement campaigns. Furthermore, it is known that many dispersion models still lack accuracy when simulating PM₁₀ (e.g. Mues et al., 2012). Furthermore, chemical transport models (CTMs) are used instead of a Gaussian model. However, using a CTM up to the resolution which is applied here for IFDM (up to 25m close to the major roads), would result in a very long simulation time and the use of enormous amounts of computer calculation time, which is not infinitely available to the model community. Doubling the horizontal resolution of a CTM multiplies the calculation time of the model with at least a factor 4. As a result, using a CTM would lead to a maximum time upon which the model could be applied (e.g. one day instead of one year) which diminishes both the accuracy of the model (as the advection from the previous day is not well represented) and the robustness of the conclusions (as specific meteorological conditions during the simulated day could make generalization of the model results very difficult). As norms on air quality are often described upon the period of a year, being able to simulate a complete year is very important and using the RIO-IFDM coupling enables this, although a validation using temporal data up to one hour resolution is undertaken (Section 5).

3.4.4. IFDM

The IFDM (Immission Frequency Distribution Model) model is a bi-Gaussian plume model, designed to simulate non-reactive pollutant dispersion at a local scale. An additional chemistry module describes the chemical equilibrium of nitrogen oxides and ozone (similar to the one used in Berkowicz et al. (1997)). As IFDM is a receptor model, it can be used for both regular and irregular grids. On top of a regular 1 by 1 km² grid, an irregular line source following grid was defined in order to account for the steep concentration gradients along the roads. This approach is similar to the methodology used by Lefebvre et al. (2011a; 2011b) and ensures that more receptor points are available where the largest concentration gradients are expected. More information on the IFDM

model can be found in the supplementary material (SM3) and in the European Model Database (<http://air-climate.eionet.europa.eu/databases/MDS/index.html>).

3.4.5. COUPLING OF RIO AND IFDM

It is encouraged to use air quality models as tools for policy support by the EU Air Quality Directive (2008/50/EC). However, for a hotspot as Flanders (13522 km²), in which exceedances are widespread, it is recommended to simulate the air pollution over a large area but with sufficient detail to account for the large gradients along highways and major point sources. Therefore, it is insufficient to rely only on a 3x3 km² scale interpolation model such as RIO, as its results are not as detailed enough. On the other hand, a bi-Gaussian plume model such as IFDM is not capable to account for the regional air pollution patterns. In order to combine the best of both worlds, the two models are coupled to cover both the regional aspects of the air pollution phenomenon and the large gradients along the major line and point sources. A coupling procedure, eliminating the double counting of emission sources, is used. This is done by eliminating the marginal concentration increase resulting from traffic emissions from the RIO low resolution background scale (elimination step), before adding the concentrations generated by IFDM due to these emissions (addition step) on a higher resolution. The complete description of the coupling and the double counting correction for passive species can be found in detail in Lefebvre et al. (2011b).

However, this scheme is slightly adapted for chemically reactive pollutants such as NO₂ and O₃. First of all, RIO simulates the background concentrations for both NO₂ and O₃. For every time step (1 hour) and every RIO grid cell, background NO concentrations in equilibrium with the NO₂ and O₃ background levels. The coupling procedure is then applied for the NO_x, the NO₂ and the NO concentrations separately, using the total NO_x, the NO₂ and the NO emissions respectively, which are all provided by the MIMOSA model. The ozone concentrations are not adapted, as no primary ozone emissions exist. After the coupling procedure and correction for double counting of emissions, the IFDM chemistry module is applied, in order to arrive at the final concentrations. Herein solar height and temperature are used as input parameters for the reaction rates and the conservation of total NO_x and O_x is used as additional constraints.

3.4.6. MODEL SETUP AND SIMULATIONS

The model chain described above has been applied for the year 2007 to the Flanders and Brussels region, the two northern regions of Belgium. It is a rather flat and densely populated area (13522 km²) with approximately 7.4 million inhabitants, resulting in an average population density of almost 550 persons/km². The area can be confined in a rectangle extending 238 km from west to east and 94 km from north to south.

3.5. RESULTS OF THE MODEL CHAIN

3.5.1. CONCENTRATION MAPS

The resulting annual mean concentration maps of PM₁₀, NO₂ and O₃ are shown respectively in Figure 19, Figure 20 and Figure 21. In each map, the corresponding measurement values are depicted. The model chain results in high resolution maps, especially for NO₂ and O₃, which are heavily influenced by local traffic at the highways and in the urban areas such as Brussels and Antwerp. Furthermore, it is seen that the effect of primary traffic emissions on the PM₁₀ concentrations is small, leading to much lower gradients close to the roads, compared to the other pollutants. Due to the small local contributions, the PM₁₀ concentration maps are close to the RIO-concentration maps, with a large regional west-east gradient. Finally, there is a strong inverse relation between the NO₂ and the O₃ concentrations, with higher NO₂ levels in regions with lower O₃ values and vice versa. This is due to the prevalence of high NO₂ concentrations in regions with a lot of traffic emissions, leading locally to high NO and lower ozone concentrations. This effect can also be seen in the intra-weekly cycle (Figure 22), with respectively lower and higher concentrations in the weekend for NO₂ and ozone.

3.5.2. EVALUATION METHODOLOGY

In this section, we compare the modelled pollutant concentrations with measurements. We want to test if the different cycles are well represented in the model and if the model setup will lead to a correct representation of real world conditions. Before discussing this, it is important to stress at all component of the model chain have been evaluated and validated in the recent past:

- The FEATHERS model has been validated recently (Kochan et al., 2012). Furthermore, FEATHERS is based on the ALBATROSS model, which has been compared to measurements in Beckx et al. (2009a).
- RIO has already been validated using the “leaving one out” methodology (Janssen et al., 2008), where it was demonstrated that the RIO approach outperforms inverse distance weighted or Ordinary Kriging interpolation techniques.
- IFDM has been validated at several occasions (Cosemans et al., 1981; Olesen, 1995; Lefebvre et al., 2011a; 2011b).
- The coupling as described above (between the low resolution RIO and the high resolution IFDM model) has been validated already for passive pollutants (Lefebvre et al., 2011a; 2011b). Furthermore, in these papers, the combination of MIMOSA, RIO and IFDM has been validated.
- Barely any traffic stations were available during the year 2007 in the Flanders-Brussels region. A validation using the “leaving one out” methodology would thus lead to a repetition of the validation of the RIO model.

Nevertheless, in the publications mentioned above, several points have not yet been assessed:

- Is there an important loss in accuracy related to the interpolation step which preprocesses the RIO regional scale output as input for IFDM?

- Is the coupling procedure also valid for the NO₂-O₃-NO-equilibrium. Lefebvre et al. (2011a; 2011b) have only shown that this methodology is valid for passive pollutants.
- Are the different cycles, such as the intra-daily (hourly variation of concentrations during the day), the intra-weekly (daily variation of concentrations during the week) and the intra-annual (monthly variation of concentrations during the year) well represented by the model chain? If so, it is possible to perform a dynamic exposure assessment where information on the temporal and spatial distribution of the population during the day is combined with spatio-temporal information on the pollutant concentrations? This is important as traffic is at the origin of a major cycle observed in the concentration patterns (see also later). Furthermore, the location of the people also reveals a daily cycle, as people travel daily from their place of living to their workplaces (see, for instance, Beckx et al., 2008; Dhondt et al., 2012a).
- In summary, can this data be used to assess the effect of human travel behavior on human exposure, taking into account complex effect such as differences in the chemical equilibrium during the day and during the year?

In order to assess the latter points which are specifically related to the capabilities of the model chain, the validation analysis in this paper includes the following parameters:

- For PM₁₀, NO₂ and O₃ we make a comparison of the:
 - Temporal variability: mean absolute bias, RMSE, R², bias corrected RMSE on an hourly averaged time series over all stations.
 - Spatial variability: bias, RMSE, R² and bias corrected RMSE of the annual mean concentrations of all stations.
 - Intra-daily cycle: for all stations the mean intra-daily cycle is determined. The average over all stations is then compared (by a RMSE, R² and bias corrected RMSE) to the averaged measured intra-daily cycle.
 - Intra-weekly cycle: the same as for the intra-daily cycle is done for the different days of the week.
 - Intra-annual cycle: the same as for the intra-daily cycle is done for the different months of the year.

3.5.3. EVALUATION

A comparison of the model results for the year 2007 with associated measurements is given in Table 8. In this table, it can be observed that the bias is small for all pollutants. The absolute mean bias ranges from 1.51 µg/m³ for O₃ to -3.08 µg/m³ for NO₂, while the relative mean bias is always lower than 10%. Furthermore, the mean over all stations of the absolute value of the bias maximally amounts up to maximum 15%. Also, the root mean square error is small, ranging from less than 10% to somewhat more than 30%. The R² is large and higher than 0.7 except for the spatial validation, where the R² ranges from 0.45 to 0.68.

The different cycles are well preserved throughout the model procedure with R² larger than 0.8 and relative root mean square errors lower than 10%. When correcting the root mean square error for

the biases, it becomes smaller than 3% for all discussed cycles and for all pollutants. The cycles are also shown in Figure 22.

As a result, we can conclude that the loss of accuracy due to the RIO interpolation is small, that the coupling procedure also works well for the chemically reactive pollutants and that the different cycles are well preserved throughout the model chain. Therefore it can be stated that these results are applicable to assess the effect of human travel behavior on human exposure, taking into account the high resolution gradients along the line sources.

3.5.4. COMPARISON OF THE DAILY CYCLE

Having the model chain described, we give a small example of the strengths of this type of application by looking at the intra-daily NO₂-cycle. This cycle (Figure 22, upper left) exhibits two well expressed peaks during the day: one in the morning and one in the evening. The concentrations during midday and during the night are significantly lower compared to the two peaks. Both the measurements and the modelled data are an average over all monitoring stations in Flanders and Brussels. To analyze this pattern, we split up the data set in three groups of eight hours: the peak concentrations (5-9 UTC and 17-21 UTC), the lowest concentrations (11-14 UTC and 23-04 UTC) and the remaining hours. Based on the measured values, the first group has a mean NO₂-concentration of 39.25 µg/m³, while the second group has a concentration of 29.70 µg/m³ and the third group has a concentration of 34.13 µg/m³. This represents a (measured) concentration gap of 9.55 µg/m³ between the peak and the lowest group and 5.12 µg/m³ between the peak and the middle group. This daily cycle is well represented in the model with respectively concentrations of 35.93, 26.98 and 31.19 µg/m³ amounting to gaps of 8.94 µg/m³ and 4.73 µg/m³. These characteristics of the daily cycle are close to the observed values (see also Figure 22, upper left). We will come back to the intra-daily NO₂-cycle later and try to find out what causes this cycle.

3.6. LIMITATIONS OF THE INTEGRATED MODEL CHAIN AND IMPLICATIONS FOR EXPOSURE ASSESSMENT

The processing of intra-zonal traffic in this model chain is a first point of attention. The concept of zones (1145 in total) used within the FEATHERS model eliminates the rerouted intrazonal traffic in the subsequent TransCAD, i.e. the traffic departing and arriving in the same zone. As a result, only the passenger car trips between two different zones are taken directly into account. As such, short, intra-zonal trips travelled by car are ignored when looking at the traffic data of the modelling framework. However, the environmental impact of these trips are taken into account by the use of the RIO interpolation model. Since RIO uses measurements in which all emissions are implicitly taken into account, these trips are present in the background concentration data. As these trips are not taken into account during the traffic assignment modelling, and thus also not in emissions coming from MIMOSA, they are neither eliminated from the background data (elimination step in coupling procedure), nor added up to the background data (addition step in coupling procedure), but they remain present in the low resolution background data. As such, they are taken into account, but only implicitly and at a low resolution. As a consequence, the model chain is not capable to assess any impact of planning scenario's dealing with this intra-zonal traffic.

A second issue, also partly related to the issue of intra-zonal traffic, concerns the calculation of cold start emissions. It is impossible for this model chain to include cold start emissions in a coherent way, as no intra-zonal traffic is explicitly taken into account. This intra-zonal traffic, usually at the beginning or at the end of a trip chain will account for a large part of the cold start emissions. In our model chain, cold start emissions are calculated for the inter-zonal trips and spread evenly over all model segments with road traffic. This is not ideal, but at least the total amount of cold start emissions for these trips is present in the model, albeit not necessarily on the correct road segments.

Thirdly, TransCAD is a static traffic assignment model and our approach of a link-by-link emission calculation has therefore relied on average speed emission functions. This is a limitation that may have resulted in an underestimation of emissions especially because idling and start-stop emissions are not fully accounted for in congested urban driving. Hao et al. (2010) have overcome this limitation through the use of TASHA, a dynamic agent-based traffic assignment model linked with speed dependent emission factor look-up tables. While this approach resulted in 7% higher fuel consumption and up to 19% higher pollutant emission estimates in Toronto Canada (mainly because it makes TASHA more sensitive to effects of congestion), the main benefit of their fully agent-based approach is probably that the link between individuals, trips and emissions is preserved throughout their modelling chain. In addition their look-up table approach may be more accurate and require less computer time than the evaluation of speed and acceleration based emission functions such as those presented in Int Panis et al. (2006). On the other hand the Flanders modelling area presented here is evaluated over an entire meteorological year and is much larger than the greater Toronto area, including many rural areas. In this case the underestimation resulting from using a static traffic assignment and average speed emission functions is probably smaller. Following the work of Hao et al. (2010), it would be interesting to use fully dynamic model chains for future work focusing on urban areas.

Finally, the choice of the spatial resolution of the activity based model influences the accuracy of the exposure results. As in this case a zone-based model is used, only variability (of population movement) between zones can be taken into account when determining exposure. As a result, variability within zones nor individual exposure can be determined by this model chain. A thorough discussion of the limitations of this model chain for exposure assessment has been given in Dhondt et al. (2012a).

3.7. EXAMPLE OF USE OF THE MODEL CHAIN: THE ORIGIN OF THE DAILY NO₂-CYCLE.

We will now further investigate the origin of the NO₂ intra-daily cycle. Therefore, we will evaluate if traffic emissions can explain the majority of this cycle. In order to discern the effect of traffic, the coupling procedure as explained above (§4.5) is slightly adapted. The subtraction step is kept (with all traffic emissions), but instead of adding the effect of all traffic emissions back again to the concentrations, none of the emissions are added again. As a consequence, the effect of traffic can be attributed as the difference between the run with all the emissions, minus the run with the traffic eliminated. If we eliminate the traffic emissions, a much smaller daily cycle is observed. The modelled concentration averages for the three groups as described in section 5 are equal to 24.57

$\mu\text{g}/\text{m}^3$, $22.54 \mu\text{g}/\text{m}^3$ and $23.97 \mu\text{g}/\text{m}^3$, resulting in gaps of $2.03 \mu\text{g}/\text{m}^3$ and $0.59 \mu\text{g}/\text{m}^3$. These gaps are only one fifth of the original concentration gaps, showing that much of the daily NO_2 cycle originates from the local traffic emissions (Figure 23, above). Furthermore, we can see that the intra-weekly NO_2 cycle (Figure 23, middle) is also diminished in strength, however, not as much as the daily cycle. The intra-annual cycle (Figure 23, below) is not affected in a significant way.

The added value of using the FEATHERS-activity model in the presented model chain is that FEATHERS does not only predict where and when people are travelling, but also for which purpose. As a consequence, we are able to analyze the contribution of each trip type to the daily NO_2 cycle (Figure 24). We can see that the morning peak is primarily created by people going to work and transit traffic (mostly people from the region going to work outside or vice versa). The evening peak is primarily created by people going home and again transit traffic. Heavy duty vehicles contribute to increasing NO_2 concentrations almost equally throughout the day. The increased concentration levels due to heavy duty vehicles during the night and the morning are linked to the worse dispersion at these times. Finally, it can be seen that despite the ozone chemistry, the NO_2 -concentrations behave rather linearly, as the sum of all concentrations due to the different traffic components is close to the total traffic contribution (compare complete bars with black squares in Figure 24). The deviation can be attributed as the ozone chemistry effect.

3.8. CONCLUSIONS AND APPLICATIONS OF THE MODEL CHAIN

In this paper, we have presented an integrated model chain destined to answer specific policy questions. The model chain consists of an activity-based transport model, a vehicle emission model, a land use regression model and a dispersion model. Results demonstrate that the concentrations resulting from this model chain correspond to measured concentration levels and represent well the different cycles present in air pollution.

This approach takes into account the different underlying links between activities, trips, emissions and concentrations. An important added value of this approach is therefore that the specific contribution of each vehicle trip on the pollutant concentration levels can be distinguished. To illustrate this, the impact of different trip motives on the intra-daily NO_2 -cycle was presented.

The presented modelling framework also allows to perform a more detailed population exposure assessment since the activity-based transport model predicts where people spend their time (and are exposed). It was shown in Dhondt et al. (2012a) that when combining the daily cycle of NO_2 and O_3 concentrations with the daily cycle of population movements, the exposure to NO_2 was slightly underestimated (about 1.2% on average) if passive exposure was used instead of dynamic exposure, while O_3 exposure was slightly overestimated (Dhondt et al., 2012a). These results were due to the fact that people travel during the day to urban centers with high NO_2 concentrations. As a result, the estimated population exposure was higher than assuming that people are always at home. Due to the inverse NO_2 - O_3 relationship, exposure to O_3 was for the same reasons slightly overestimated compared to concentrations.

Applications of this model chain can thus focus on its advantages for exposure assessment, as shown above (Dhondt et al., 2012a), and on health impact assessment, answering questions such as ‘What is the effect of increased fuel prices (Dhondt et al., 2012b) or changing shop-opening hours (Dons et al., 2011b) on human exposure to air pollution?’ or ‘What is the impact of teleworking on population health?’. Also, by disaggregating the exposure by population subgroup, socio-demographic differences in exposure and health effects can be examined. Because of its ability to evaluate the impact of concrete policy measure, the modelling chain can aid in developing protective policies.

Acknowledgments

This research has been supported by the Institute for the Promotion of Innovation by Science and Technology in Flanders.

3.9. SUPPLEMENTARY MATERIAL

The supplementary material of this paper was deemed to be not relevant for validation enough in order to add it to this report.

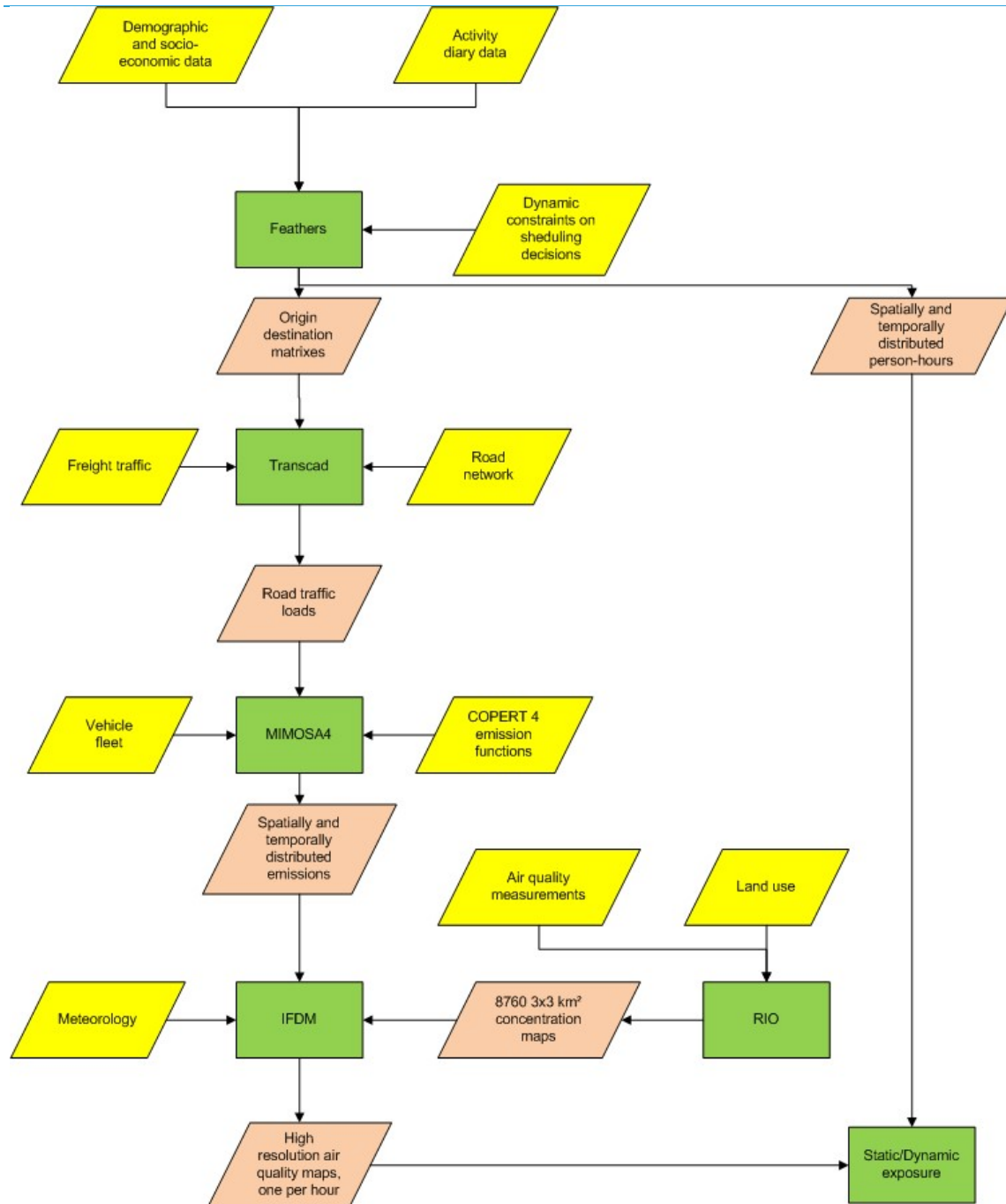


Figure 18: The model chain. In yellow parallelograms: the input data. In green squares: the model chain components. In orange parallelograms: the output of the models, used as input for the next model in the chain.

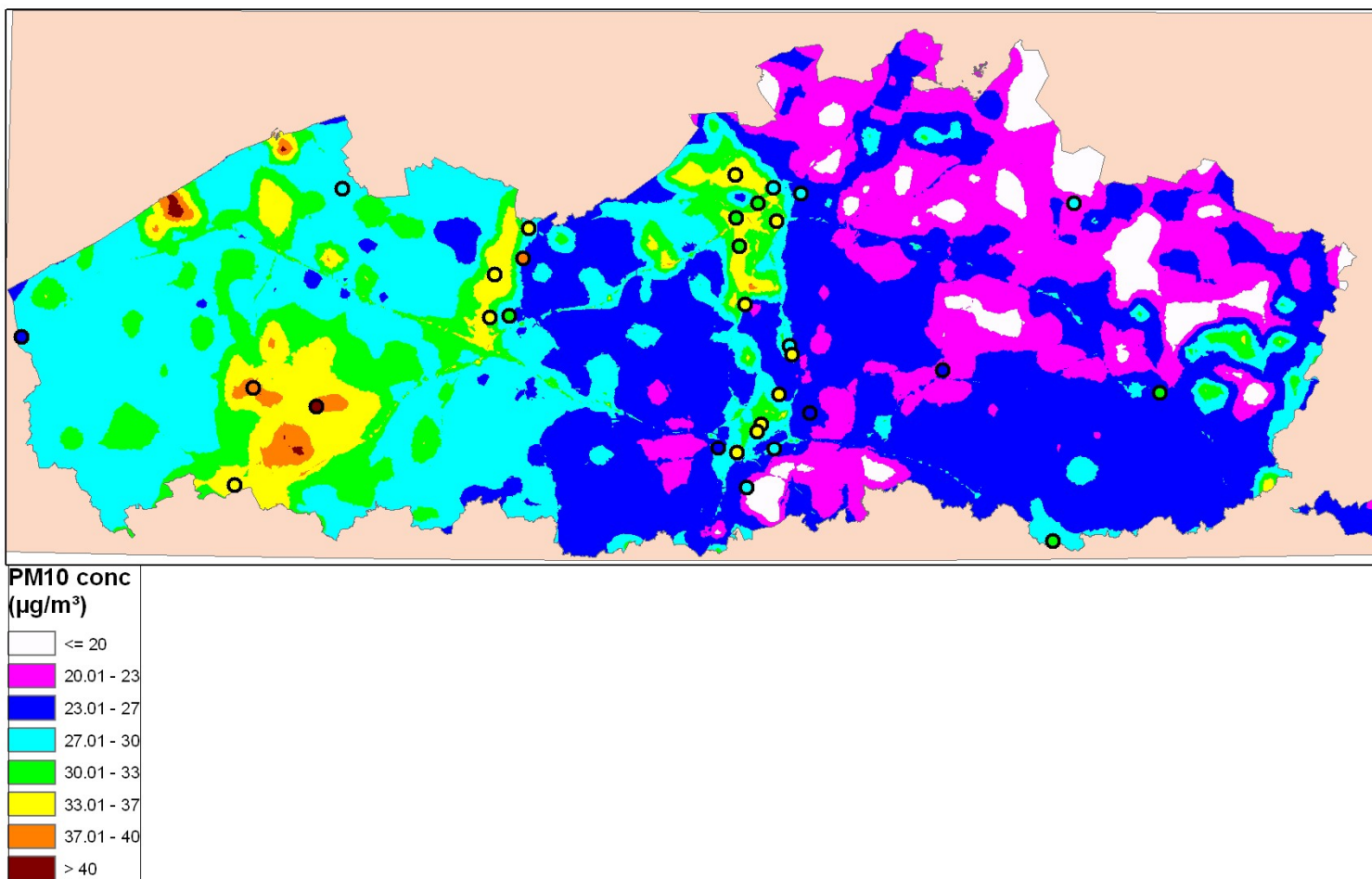


Figure 19: Annual mean PM₁₀ concentration (2007). The background map shows the modelled concentrations. In the circles, the annual mean concentrations of the measurements are shown.

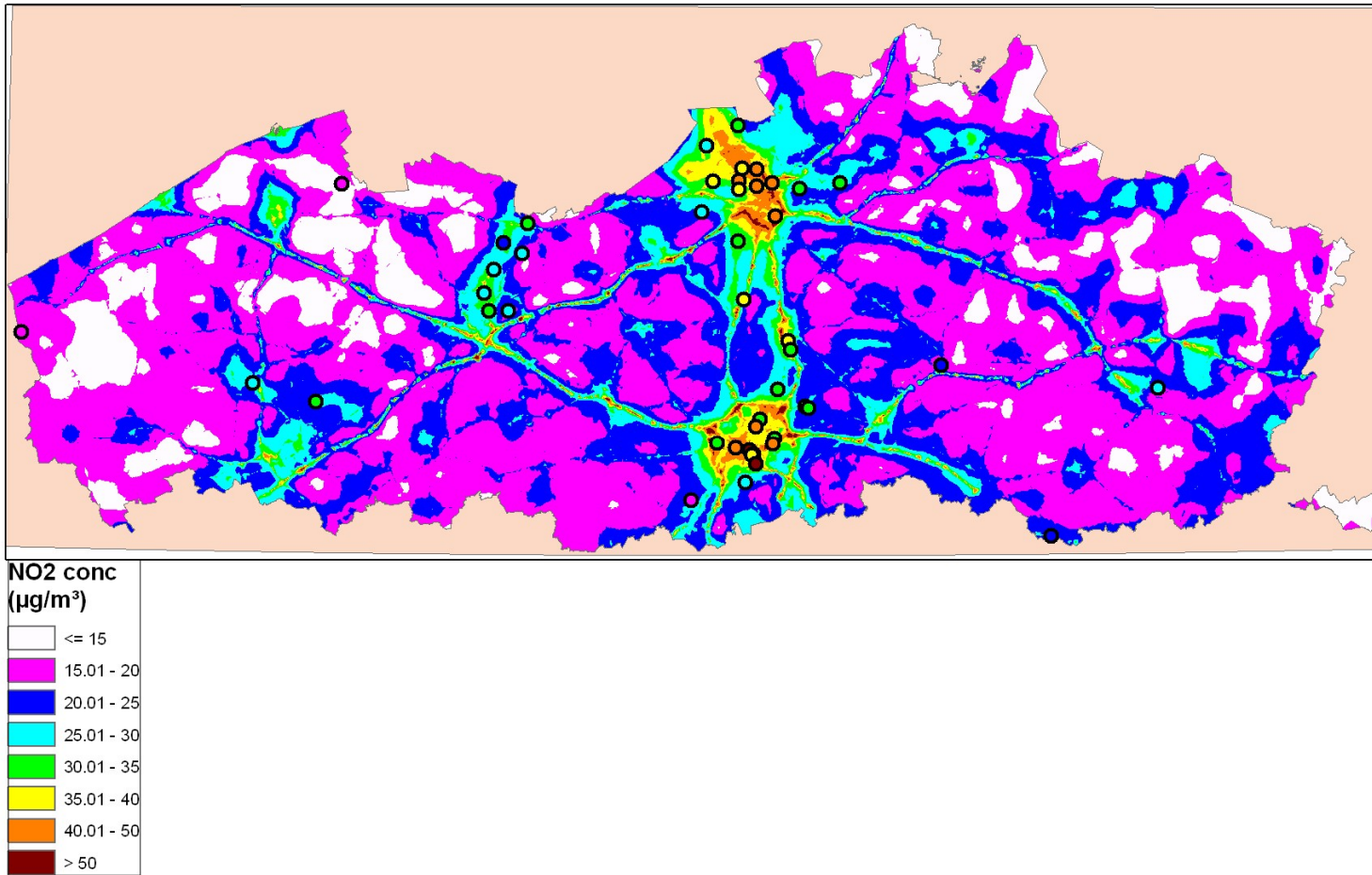


Figure 20 : Annual mean NO₂ concentration (2007). The background map shows the modelled concentrations. In the circles, the annual mean concentrations of the measurements are shown.

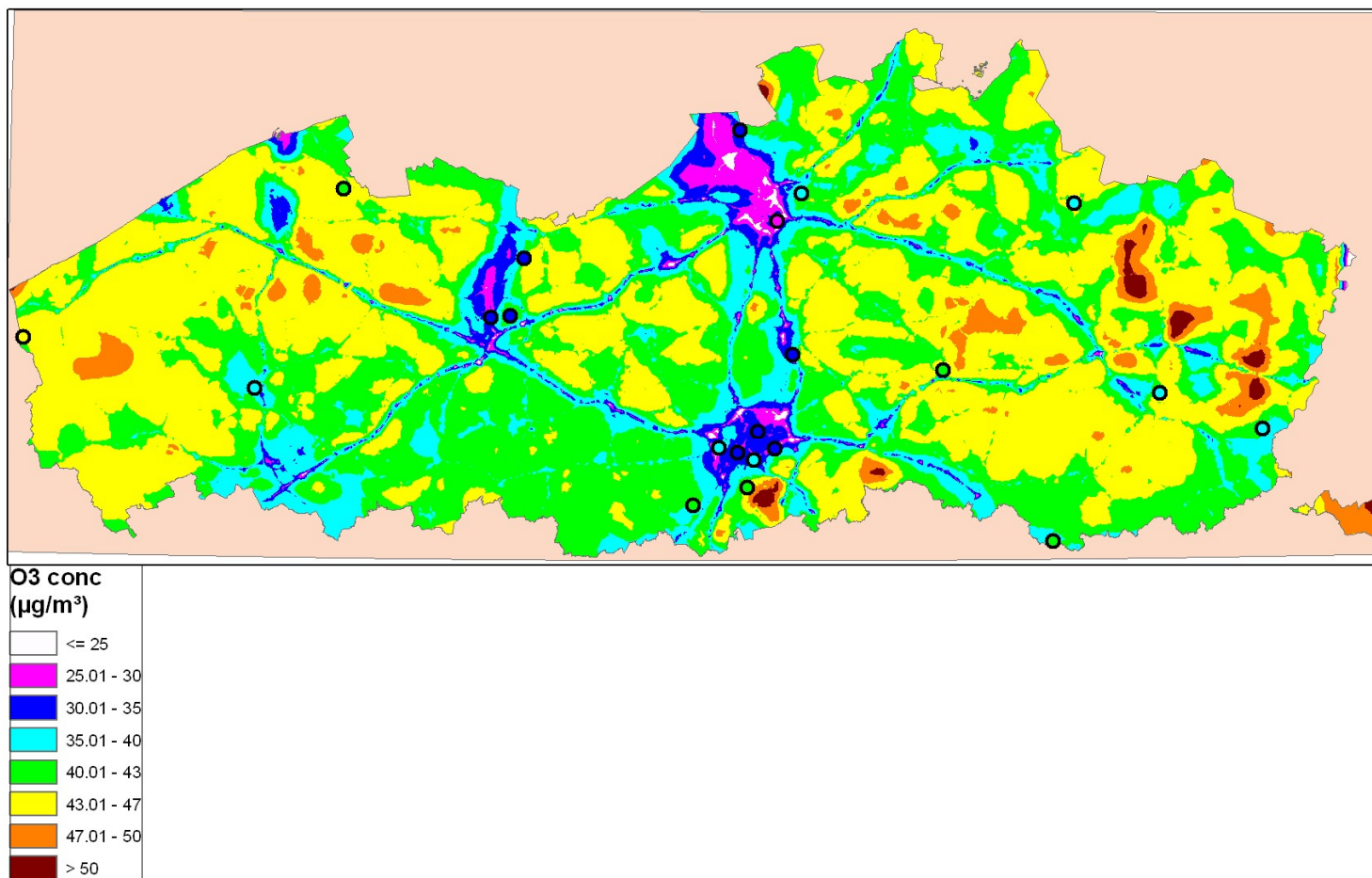


Figure 21 : Annual mean O₃ concentration (2007). The background map shows the modelled concentrations. In the circles, the annual mean concentrations of the measurements are shown.

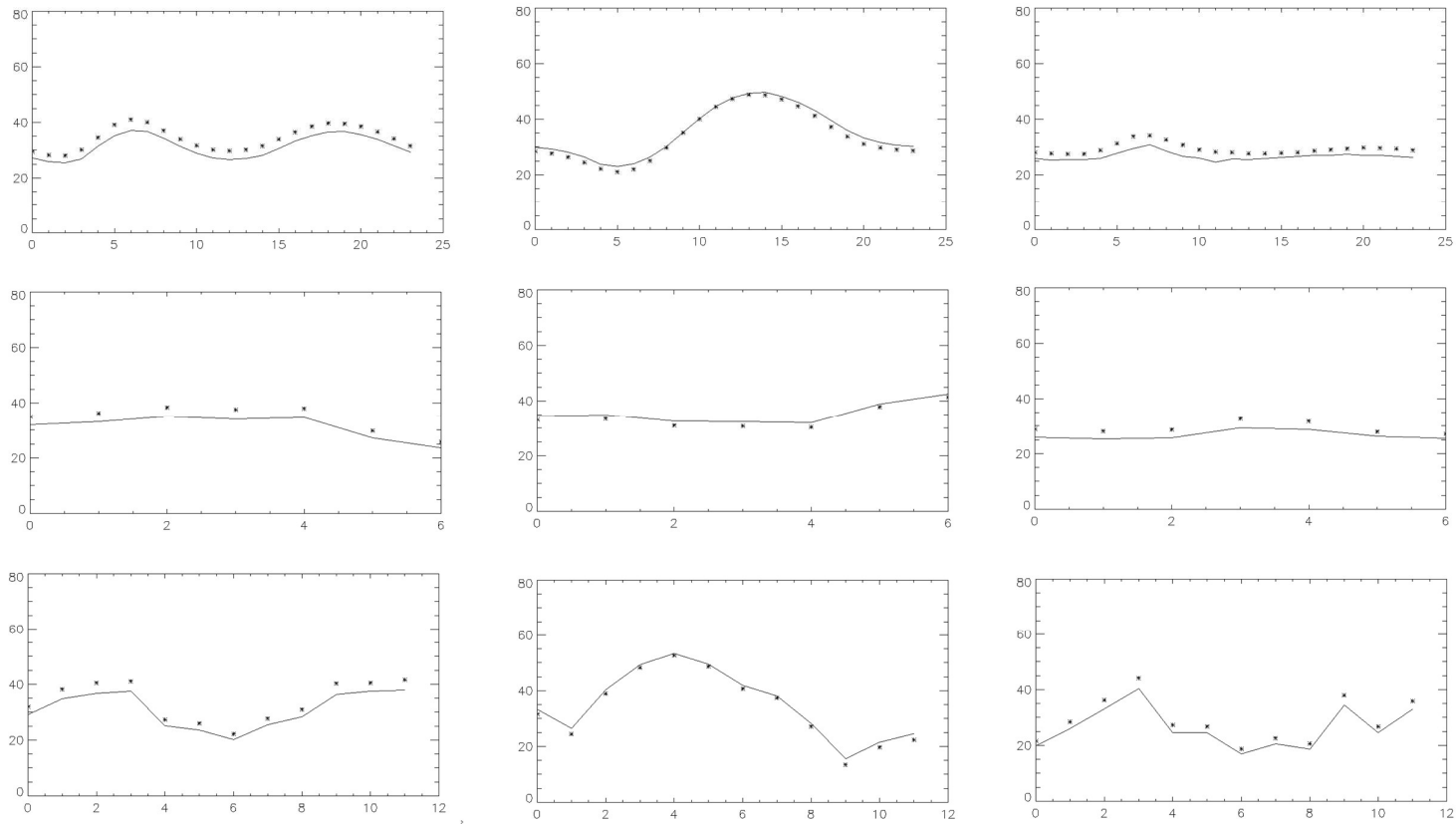


Figure 22: Validation results for NO₂ (left), O₃ (middle) and PM₁₀ (right). Shown are the intra-daily cycle (top figures, x-axis: 0 = first hour of the day, 23 = last hour of the day; GMT), the intra-weekly cycle (middle, x-axis: 0 = Monday, 6 = Sunday) and the intra-annual cycle (bottom, x-axis: 0 = January, 11 = December). Asterisks: measurements, line: model. Shown is the mean over all measurement stations. Y-axis: mean concentration (in µg/m³, ranging from 0 to 80).

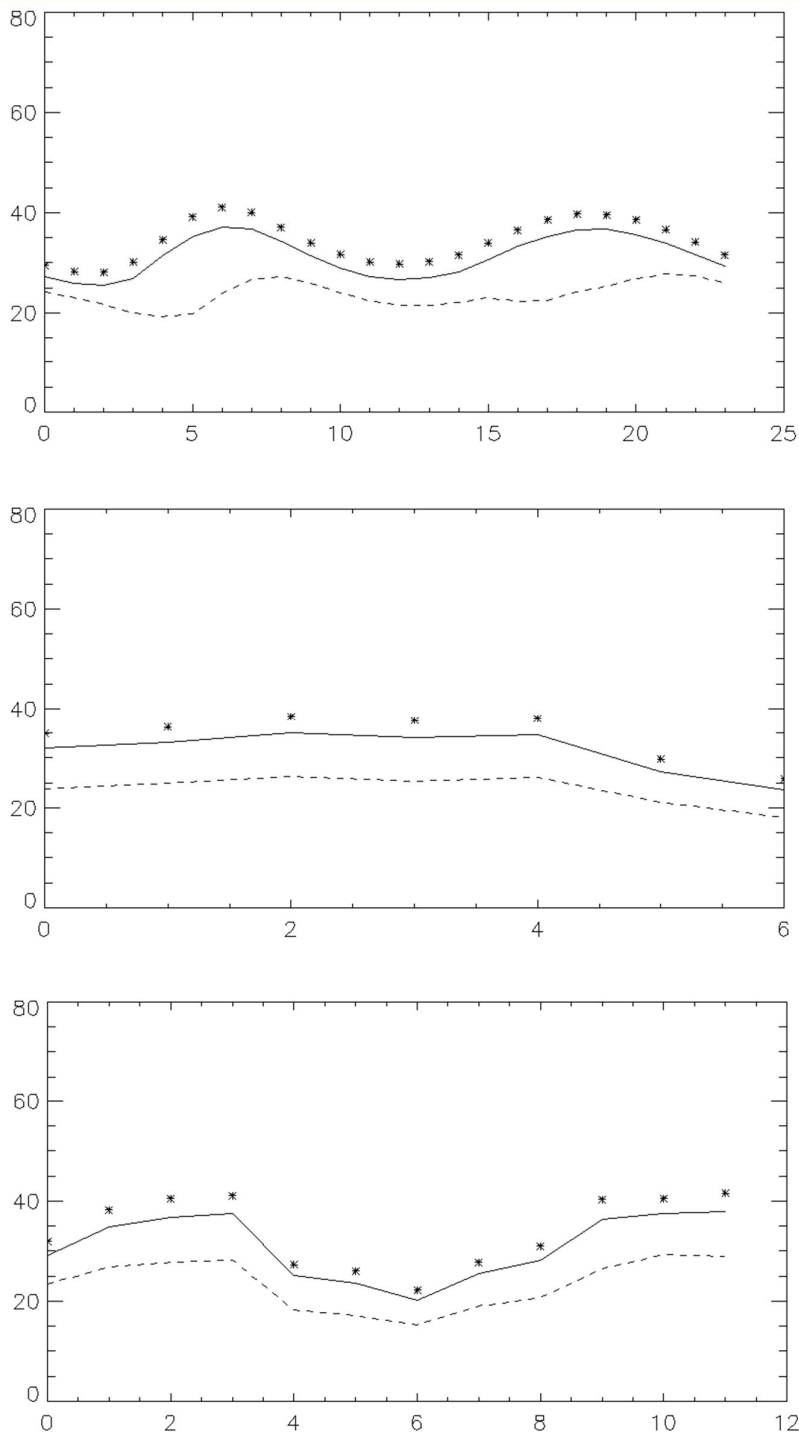


Figure 23: The intra-daily cycle (above, x-axis: 0 = first hour of the day, 23 = last hour of the day; GMT), the intra-weekly cycle (middle, x-axis: 0 = Monday, 6 = Sunday) and the intra-annual cycle (below, x-axis: 0 = January, 11 = December) for NO_2 . Asterisks: measurements, line: model with traffic emissions included. Dashed line: model with traffic emissions excluded. Shown is the mean over all measurement stations. Y-axis: mean concentration (in $\mu\text{g}/\text{m}^3$, ranging from 0 to 80).

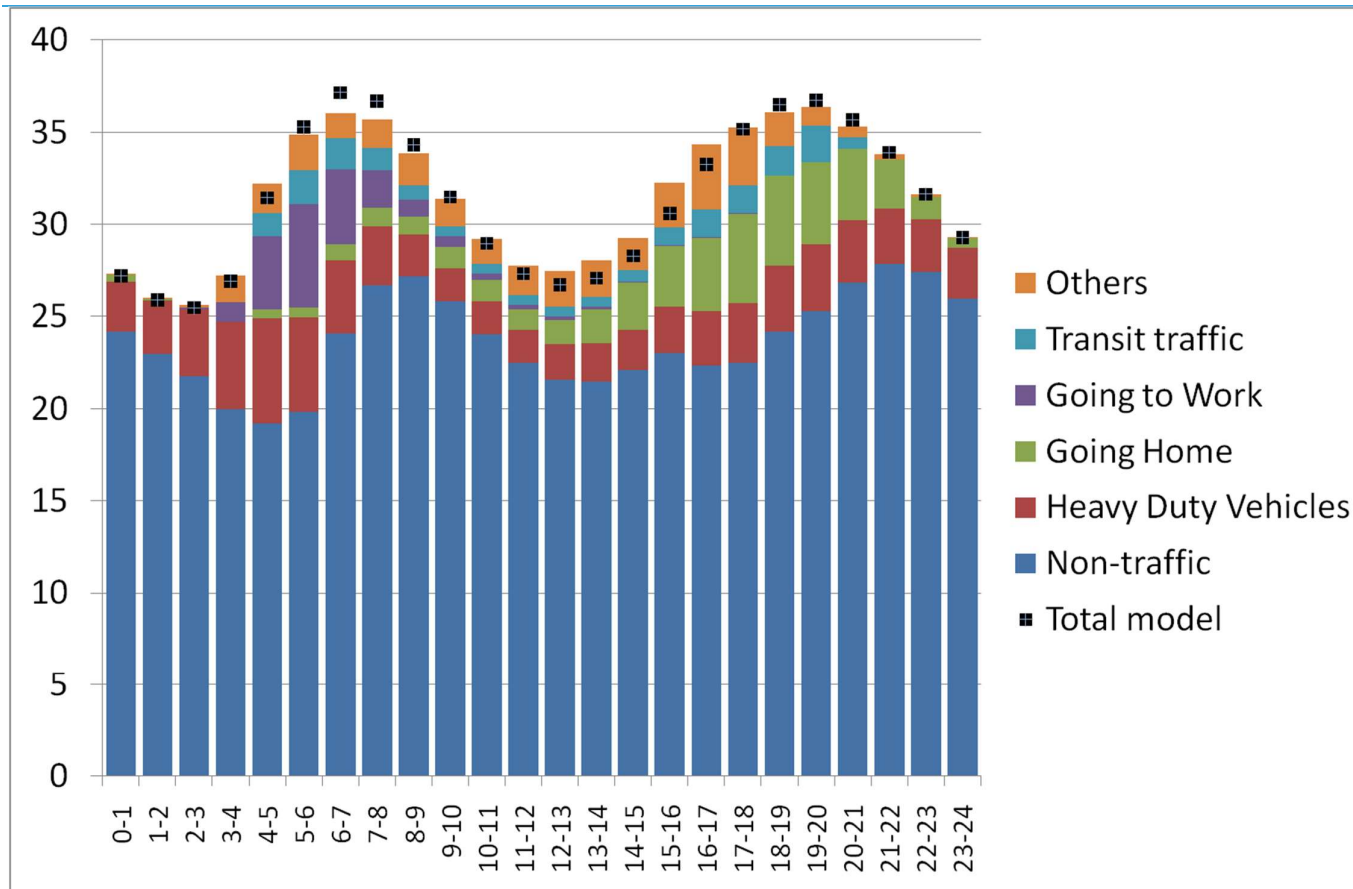


Figure 24: Bar-chart of the intra-daily cycle (x-axis: hours in GMT, y-axis: NO₂-concentration averaged over all days and all measurement locations). In black squares: model results with all traffic emissions included. Blue bars: model results with traffic emissions excluded. Other bars: model results for heavy duty vehicles (red), for person cars going home (green bars), for person cars going to work (purple bars), for person cars in transit through the region (light blue bars) and for person cars with other motives (orange bars).

		Bias	MAB	RMSE	BCRMSE	R ²	Bias or MAB /Mean	RMSE /Mean	BCRMSE /Mean
		µg/m ³	µg/m ³	µg/m ³	µg/m ³		%	%	%
NO ₂	Spatial comparison	-3.08		7.56	6.91	0.68	-8.8%	21.7%	19.8%
	Temporal comparison, averaged over all stations		5.08	11.58	9.44	0.76	14.6%	33.2%	27.1%
	Intradaily cycle			3.03	0.47	0.99		8.7%	1.4%
	Intraweekly cycle			3.03	0.46	1.00		8.7%	1.3%
	Intra-annual cycle			3.03	0.66	1.00		8.7%	1.9%
PM ₁₀	Spatial comparison	-2.84		4.39	3.35	0.45	-8.9%	13.7%	10.5%
	Temporal comparison, averaged over all stations		3.59	10.67	9.31	0.84	11.2%	33.3%	29.0%
	Intradaily cycle			2.73	0.84	0.84		8.5%	2.6%
	Intraweekly cycle			2.67	0.64	0.92		8.3%	2.0%
	Intra-annual cycle			2.64	0.66	1.00		8.2%	2.1%
O ₃	Spatial comparison	1.51		3.25	2.87	0.65	4.1%	8.8%	7.8%
	Temporal comparison, averaged over all stations		2.60	8.03	6.98	0.92	7.0%	21.7%	18.8%
	Intradaily cycle			1.55	0.69	1.00		4.2%	1.9%
	Intraweekly cycle			1.42	0.28	1.00		3.8%	0.8%
	Intra-annual cycle			1.52	0.55	1.00		4.1%	1.5%

Table 8: Validation parameters of the comparison with the measurement. MAB = Mean Absolute Bias; RMSE = Root mean square error; BCRMSE = Bias corrected root mean square error ; Mean = Average of observations.

CHAPTER 4 EVALUATION OF THE RIO-IFDM-STREET CANYON MODEL CHAIN

In this chapter the paper Lefebvre et al. (2013b) is reproduced, which describes this validation exercise.

Evaluation of the RIO-IFDM-street canyon model chain

W. Lefebvre*, M. Van Poppel*, B. Maiheu*, S. Janssen*, E. Dons*[#]

* VITO, Boeretang 200, 2400 Mol, Belgium

[#] Transportation Research Institute, Hasselt University, Wetenschapspark 5 bus 6, 3590 Diepenbeek, Belgium

Abstract

Integration of all relevant spatial scales in concentration modelling is important for assessing the European limit values for NO₂. The local NO₂-concentrations are influenced by the regional background, the local emissions and the street canyon effects. Therefore, it is important to consistently combine all these contributions in the model setup which is used for such an assessment. In this paper, we present the results of a integrated model chain, consisting of an advanced measurement interpolation model, a bi-Gaussian plume model and a canyon model to simulate the street-level concentrations over the city of Antwerp, Belgium. The results of this model chain are evaluated against independent weekly averaged NO₂ measurements at 49 locations in the city of Antwerp, during both a late autumn and a late spring week. It is shown that the model performed well, explaining between 62% and 87% of the spatial variance, with a RMSE between 5 and 6 µg/m³ and small biases. In addition to this overall validation, the performance of different components in the model chain is shown, in order to provide information on the importance of the different constituents.

Graphical abstract

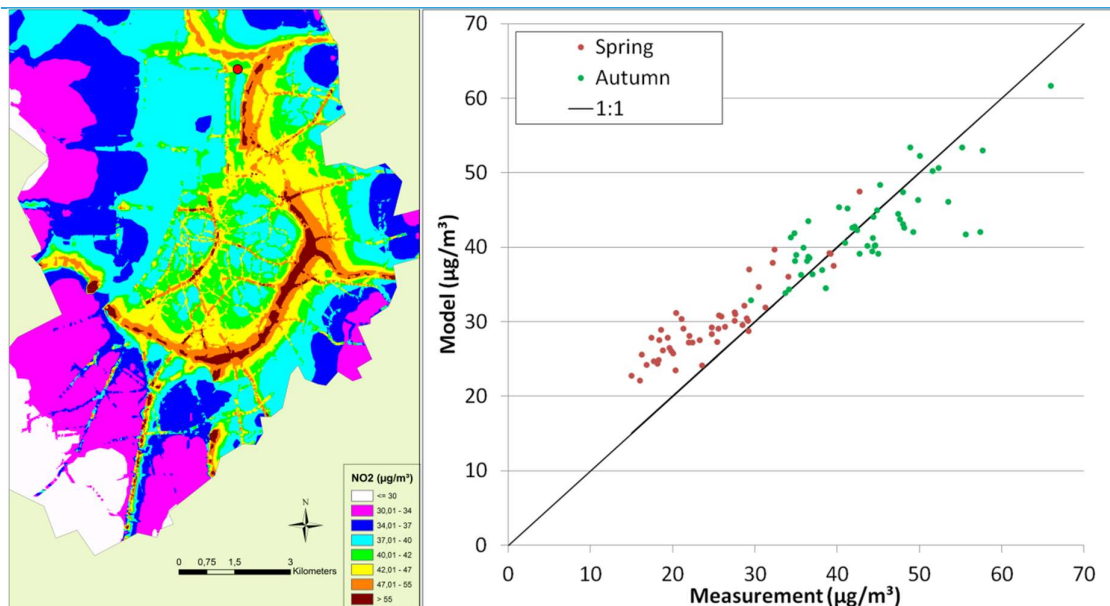


Figure 25 : The graphical abstract

Highlights:

- Setup of model chain ranging from regional to local scale
- High resolution air quality maps for urban environments
- Comparison to independent measurement data leads to very good validation results
- Step-by-step analysis on the importance of the different model components

Keywords: validation, street canyons, NO₂ concentrations, passive samplers, Antwerp (Belgium)

4.1. INTRODUCTION

There is an old joke about a statistician who drowns in a river of on average half a meter deep. The same joke could apply to someone who wants to test the European NO₂ limits and uses a spatial average over a complete region, although it is questionable whether much laughter would be drawn from the public.

The European annual NO₂ limit of 40 $\mu\text{g}/\text{m}^3$ has to be reached at every location. However, Eulerian models have limited spatial resolution and will provide an average concentration over a larger zone, typically about 1 km². A concentration in this zone which is lower than the limit is not instructive in assessing whether the limit is reached at every location within this zone (Thompson and Selin, 2012).

Measurements can solve this problem partially as they can measure at specific hotspots, although they are typically limited in space or time. As such, measurements do not provide concentrations averaged over a certain zone but result in point concentrations. While a well-distributed measurement network can thus give reliable information about exceedances of the European

limits, it is in fact a series of point measurements. As a result, compliance to European Union limit values at all air quality monitoring stations does not necessarily imply a compliance at every location in the area.

A number of experimental campaigns have quantified the spatial variability of urban pollutant concentration levels (Da Silva et al., 2006; Thornburg et al., 2009; Vardoulakis et al., 2011). These papers have shown that for an assessment of the exposure of the population to air pollution, it is important to take into account both the heterogeneous spatial and temporal concentration distribution and the changing locations of the exposed population (e.g. Wilson et al., 2005; Beckx et al., 2009a; Setton et al., 2011; Dons et al., 2012; Dhondt et al. 2012). Furthermore, many questions can be raised about the representativeness of existing in-situ measurement sites (Buekers et al., 2011). There were recent attempts to characterize the spatial representativeness of air quality monitoring stations based on different approaches (Spangl et al., 2007; Joly and Peuch, 2011; Janssen et al., 2012). However, to our best knowledge, a unique robust methodology to assess the representativeness of in-situ measurements has not yet been achieved, especially on a street-level scale. It is therefore essential to create a reliable modelling framework which is able to capture both the spatial diverseness of the concentrations on a street-level scale, while still providing complete coverage over the studied region.

Several types of models have been applied in recent years to tackle this problem (e.g. Vardoulakis et al., 2003; Holmes and Morawska, 2006). The first group of models are the box models, such as OSPM (Berkowicz, 1997), which parameterize the effect of street canyons at the local scale. However, these models are unable to take into account the effect on the concentration by neighboring roads in a systematic way. Furthermore, these models need detailed inputs on the street-building configuration. As a result, these models are often applied only at one or some streets or at one or some locations (e.g. Hirtl and Baumann-Stanzer, 2007; Wang and Xie, 2008) or with reduced accuracy on the street-building configuration (e.g. Assael et al., 2008). Gaussian plume models, such as AERMOD, can easily take into account a complete city area. However, they lack the street canyon effect in their simulations, which can be significant for busy roads confined by continuous building-walls. An alternate approach is to apply CFD (Computational Fluid Dynamics) –based dispersion models, such as MISCAM. These models explicitly resolve the 3D geometry of the city and enable one to directly compute the dispersion in the street-canyon flow. However, due to computational restrictions typical for CFD models, it is currently practically unfeasible to apply them for a whole city and to simulate a complete year (Schatzmann and Leitl, 2011). For this reason there are only a very limited number of CFD applications used for operational policy support, although recent studies have been successful in demonstrating the potential of combining CFD calculations with a meteorostatistics approach (Parra et al, 2010; Solazzo et al, 2011), albeit for a limited spatial domain.

Combinations between Gaussian models and box models, such as UBM-OSPM and ADMS-urban, have already been applied to some cities (Hirtl and Baumann-Stanzer, 2007; Berkowicz et al., 2008; Righi et al., 2009). When combined, these models can both perform yearlong simulations for a complete city and do this in a reasonable computing time, while taking into account both the street canyon effect and the effect of the neighboring roads. These model combinations have challenges

in being consistent (e.g. eliminating double counting of emissions which are present both in the Gaussian model and in the box model, both in dispersion and in the chemistry, Lefebvre et al., 2011b), in devising a system in which detailed and accurate street-building geometry information is present for all street canyons (Jensen et al., 2001; Righi et al., 2009), in assimilating the known measurements in the city and thus correcting for eventual model biases or wrong estimations in the emissions, ...

This paper evaluates such a consistent integrated modelling framework against independent measurements in the city of Antwerp. A comparison with measured concentration over two seasons is presented and the performance of different model components is discussed. This paper focuses on spatial validation. As such, we can be assured that major characteristics of the spatial concentration distribution are captured by the model. Nevertheless, this paper does not have the aim of validating the model framework in a complete fashion such as proposed in Jakeman et al. (2006) and Dennis et al. (2010). It will merely demonstrate its use for policy makers and thus will provide only part of what is needed to validate a model thoroughly in the framework of Jakeman et al. (2006) and Dennis et al. (2010).

4.2. MEASUREMENT CAMPAIGN

Measurements reported in this paper are part of a larger multidisciplinary study (HAEPS; Health Effects of Air Pollution in Antwerp Schools; Van Poppel et al., 2012) dealing with health impact of traffic related air pollution on school children. To assess the exposure of the children at home, air quality measurements were performed at selected home locations.

NO₂ was measured over 7 days at selected locations in an urban area using diffusive sampling tubes (IVL, Sweden; Ferm and Svanberg (1997)) resulting in weekly average concentrations. The locations are characterised by differences in traffic exposure and street characteristics (e.g. street canyon locations, urban traffic locations and urban background locations), chosen to represent different ranges in concentration fields in an urban area. Diffusive samplers are placed in a dedicated rain shield attached to a rainwater pipe, a balcony or a streetlamp, near the front door, at a height of 2-3m.

At each location, NO₂ was monitored during late spring (May – June 2011) and late autumn (November – December 2011). In both seasons, measurements were performed at 8 locations simultaneously during 5 consecutive weeks resulting in 40 locations sampled. In addition, all 40 locations were sampled simultaneously for one week in each season, including also 12 extra locations, resulting in 52 locations. During the entire sampling campaign, NO₂ was measured at an urban location of the AQ monitoring network.

To test reproducibility of the sampler a triple measurement was performed in spring at one location resulting in an average concentration of 25.9 ± 0.39 (SD) $\mu\text{g}/\text{m}^3$. Passive samplers were compared to reference monitors (Chemiluminescence) during the monitoring campaign at the urban location of the AQ monitoring station (5 weeks each season) and at a street location (1 week each season) resulting in 12 co-located measurements. Monitor data were averaged over the

sampling period and plotted against the diffusive sampler values resulting in a regression line with intercept 2.95 (95% CI: -2.15 – 8.04) and slope 0.95 (95% CI: 0.84 – 1.06). The concentrations measured over different times are identified by season and week number. Measurements in late Spring or late Autumn are denoted by respectively S and A. The sample week is indicated by w1-w5 for week 1 up to week 5 respectively and by wAll for the week that sampling was performed over all locations simultaneously. Combining these time-related indicators, this results in e.g. S_w2 for the second week in the Spring campaign and A_wAll for the week in autumn in which all locations were measured simultaneously (Table 9).

Measurements for which the location was separated from the adjacent road by buildings (2 measurement locations), or the location was situated outside of the city of Antwerp (4 measurement locations) were not taken into account in this validation (Table 9). The omission of the stations outside the street canyon is done because the locations available were denoted by the addresses and for these stations, their exact location was not clear. As a result, we end up with 185 weekly average NO₂ concentrations. From these 185 measurements, 52 were taken in street canyons (15 in week S_wAll, 15 in week A_wAll and 22 otherwise). The resulting monitoring locations are presented in Figure 26.

The advantage of relative inexpensive passive samplers, providing possibilities for good spatial city coverage, is countered by the absence of a good time resolution in the measurements. Only weekly averages of NO₂ concentrations are available and it is thus impossible to evaluate the model capacity of reproducing short-term episodes. However, this is not a large constraint for the application of the model for regulatory purposes in Europe, as the most stringent NO₂ limit value is defined on annual averages. Indeed, an exceedance value based on the hourly concentrations of NO₂ exists in Europe, but it has been found (e.g. Lefebvre et al., 2011c) that when this limit is exceeded, the annual limit is also (strongly) violated. It is expected that annual limit values are exceeded at several locations within the urban area; therefore, model validation in this paper focusses on spatial variability.

4.3. MODEL DESCRIPTION AND SETUP

4.3.1. OVERVIEW AND SETUP

An integrated model chain has been set up to assess the air quality at the local (street level) scale, including both regional variability as well as local variation in sources of air pollution. The model chain is shown in Figure 27 and the different components are discussed in the next paragraphs. The MIMOSA4 emission model (Mensink et al., 2000; Vankerkom et al., 2009) is used to calculate local traffic emissions. The resulting spatially and temporally distributed emissions are used in the bi-Gaussian model IFDM (Lefebvre et al., 2011a; 2011b). These results are coupled to output of the land-use regression model RIO (Hooybergs et al., 2006; Janssen et al., 2008). A method to avoid double counting of the (local) emissions by the different models is applied (Lefebvre et al., 2011b). Finally the output of the IFDM model is coupled as boundary conditions to the IFDM street canyon module. In all these coupling steps, care is taken to consistently take into account the fast NO_x-O₃-

chemistry. Finally, the results of the IFDM model and the IFDM street canyon module are combined using a post processing tool, so that the street canyon concentrations are confined to the street canyons, and the IFDM roof top concentrations are used outside of the canyons.

The integrated model chain has been used to perform simulations for the city of Antwerp, using meteorological data of a local meteo station, situated in the northern part of the city (see Figure 26). This meteorology source has been used in several other projects and has been found to be reliable and representative for the greater area of Antwerp.

4.3.2. RIO

RIO (Hooyberghs et al., 2006; Janssen et al., 2008) is a land use regression model for the interpolation of hourly pollutant concentrations as measured by the official monitoring network in Belgium (Figure 28). The model is based on a residual kriging interpolation scheme using a land use (CORINE) derived covariate. A polynomial regression determines the statistical relationship (trend functions) between the long term averaged concentrations at each hour of the day and the underlying land use parameter. In addition, a distinction is made between week and weekend days to account for the obvious difference in traffic/industry related emissions. As a result, RIO produces hourly concentration maps for the pollutants PM₁₀, PM_{2.5}, NO₂ and O₃ on a 4x4 km² grid. Based on those results, annual statistics (annual mean, number of exceedances) can be derived. RIO has been shown to be very accurate in estimating the pollutant concentrations over Belgium (Janssen et al., 2008). The RIO-output for the A_wAll-week can be found in the upper left panel of Figure 29.

4.3.3. LOCAL EMISSIONS

MIMOSA4 was used to estimate road traffic emissions based on traffic intensities and vehicle speed from the city of Antwerp (SGS et al., 2010). MIMOSA4 is the most recent version of the traffic emission model MIMOSA (Mensink et al., 2000; Vanerkom et al., 2009), and relies on the COPERT4 methodology for the emission factors (Gkatzoflias et al., 2012) to generate hourly output for different types of emissions, such as NO₂, NO_x, PM₁₀ and PM_{2.5} (see also Lefebvre et al., 2011a). To deal with the ozone chemistry, MIMOSA generates both total NO_x and NO₂ emissions. More information about this model can also be found in Beckx et al. (2009b).

Industrial emissions were taken from estimations from the MilieuKostenModel (Lodewijks and Meynaerts, 2007), as described in Lefebvre et al., (2011c). Household and other emissions (non-traffic, non-industrial), accounting for about 37% of the local NO_x-emissions (estimations for the wider city region of Antwerp), were supposed to be spatially homogeneous on a city scale. Therefore the impact of these emission sources on the resulting concentrations is taken into account by RIO via the measurement network.

4.3.4. IFDM

The IFDM (Immission Frequency Distribution Model) model is a bi-Gaussian plume model, designed to simulate non-reactive pollutant dispersion at a local scale. As IFDM is a receptor model, it can be used for both regular and irregular grids. On top of a regular 200 by 200 m² grid, an irregular line source following grid was defined in order to account for the steep concentration gradients along the roads. This approach is similar to the methodology used by Lefebvre et al. (2011a; 2011b) and ensures that more receptor points are available where the largest concentration gradients are expected. More information on the IFDM model can be found in the European Model Database (<http://air-climate.eionet.europa.eu/databases/MDS/index.html>). IFDM takes into account the differences in NO_x-split per street, resulting from differences in the traffic segmentation in passenger cars and heavy duty vehicles. The chemical equilibrium in the NO_x-O₃ reaction is determined on the basis of temperature and the solar height and is based on the scheme proposed by Berkowicz (1997).

4.3.5. IFDM STREET CANYON

The IFDM street canyon module is a simplification of the OSPM-module (Berkowicz, 1997). The OSPM-module is simplified by assuming :

- The height of the buildings in the street is chosen to be equal to the average of the left side and the right side of the street.
- If buildings are only present at one side of the street, the street canyon effect is supposed to be equal to 0.
- The concentration in the street canyon is the average of the concentration at both sides of the street canyon. Thus, we neglect the leeward versus windward asymmetry inside the street canyon.

In addition, the chemistry is made consistent with the chemistry module of the IFDM model (see §3.4, thus eliminating the need for UV-radiation data.

The street canyon model is run on a grid with a receptor point every 10m on each line segment (the full street canyon receptor points, see also Figure 30). From these points, only points in the street canyon are used for the simulation (these points will be called the limited street canyon receptor points, see also Figure 30).

The model is applied as such that every receptor point has its set of characteristics (such as height of the street canyon, width of the street canyon and distance to the next crossing). As a result, the receptor point is supposed to be representative for its location and its location only. However, as analyzing air quality in this way is impossible, it is needed to assume that these receptor points are representative for their immediate neighborhood (up to the next receptor point, 10m further down the road). Several obstacles such as trees, road signals, ... can have an influence on the measurements (e.g. Solazzo et al., 2011; Vos et al., 2013). In this simulation, however, such

microscale effects are not taken into account. We therefore assume that due to the amount of sampling locations and the time-integrated measurements, the overall validation for the entire city should not be affected too much. In a way, this evaluation is therefore also an evaluation of the importance of common obstacles in streets for the assessment of the larger scale air quality in a city.

4.3.6. COUPLING OF DIFFERENT MODELS INTO ONE INTEGRATED MODEL CHAIN

The different models have to be coupled to each other, using a method to prevent double counting of emissions at the various model levels and taking into account the NO_x-O₃-chemistry at all scales. The coupling procedure is setup in several steps which are also presented in Figure 29:

- The RIO results are available for NO₂ and O₃ on an hourly basis. Chemical equilibrium, as a function of temperature and the solar angle, is imposed in order to calculate NO-concentrations on an hourly basis and at a 4x4km² grid.
- The RIO results are coupled to the IFDM results, using the procedure presented in Lefebvre et al. (2011a; 2011b; 2013a). This procedure starts by a bilinear interpolation of the RIO-concentrations to a continuous concentration field on the IFDM grid (Figure 29, upper right panel). Subsequently, the aggregated concentrations from local contributions (calculated by IFDM) are subtracted from the RIO maps, followed by a superposition of the spatially explicit local source contributions (calculated by IFDM). Finally, chemical equilibrium is imposed. This leads to the lower left panel of Figure 29.
- Coupling of IFDM to the IFDM street canyon module is done in a similar way. First, the local street contribution (calculated by IFDM) is removed from the IFDM result in the street canyon. Next the street canyon contribution is added back again for this receptor point taking into account the specific dispersion characteristics in the street canyon. Finally, chemical equilibrium is imposed.

4.3.7. POST PROCESSING

At this stage in the model chain, two sets of results are now available. First of all, we have the roof-top concentrations simulated by the IFDM model. Secondly, in the street canyons, we have receptor points with the street canyon concentrations coming from the IFDM street canyon model. Since both IFDM and IFDM street canyon are receptor models, the concentrations are available at point locations only. In order to arrive at one overall gridded air quality map, the results of the IFDM model and the IFDM street canyon model need to be merged in a consistent way (so that for instance roof-top concentrations are not used in the street canyons and vice versa). Therefore a polygon is created. This polygon encompasses every receptor point which is closer than 30m to a line segment, which is not part of a building and not separated from a road by a building (see red lines on Figure 30). We call this polygon the street canyon polygon, as only points within this polygon are candidates for points being in a street canyon. Thereafter, a series of GIS operations are being performed using SAGA-GIS, www.saga-gis.org (Böhner et al., 2006), giving rise to a gridded air quality map:

1. The IFDM-results (without street canyons) are being interpolated to a raster with a resolution of $5 \times 5 \text{m}^2$ (panel A of Figure 30).
2. The results on the full street canyon receptor points are composed of the street canyon concentrations for the points part of the limited street canyon receptor points and for the IFDM roof-top concentrations for the points not part of the limited street canyon receptor points (panels B and C of Figure 30).
3. The results from the previous step are being interpolated to a raster with a resolution of $5 \times 5 \text{m}^2$ (panel C of Figure 30).
4. The rasters from point 1 and point 3 are being combined, using the concentrations resulting from point 1 outside of the street canyon polygon and from point 3 inside the street canyon polygon (panel D of Figure 30).

An example of the results of this chain can be found in the lower right panel of Figure 29.

4.4. RESULTS

4.4.1. CORRELATION, RMSE AND BIAS OF THE INTEGRATED MODEL CHAIN

First of all, we compare all weekly model values to all weekly measurement values (Figure 31, left). This yields a very good correlation ($R^2=0.86$), combined with a small RMSE ($5.28 \mu\text{g}/\text{m}^3$) and a low bias ($1.5 \mu\text{g}/\text{m}^3$). However, as we have combined measurements at different locations in both seasons for several separate weeks the resulting correlation might be artificially increased. This is due to the fact that the late autumn concentrations are systematically higher than the late spring concentrations. As this seasonal effect is covered by RIO (which takes into account the concentrations measured in the stations of the telemetric network around Antwerp, Figure 28), we automatically get a large R^2 by using all the measurement values together. Therefore, we will focus our analysis on the two weeks with the majority of the data, one in autumn, and one in spring (Figure 31, right). This leads to a similar R^2 (0.87), RMSE ($5.31 \mu\text{g}/\text{m}^3$) and a somewhat higher bias ($1.91 \mu\text{g}/\text{m}^3$) (see also Table 10). However, if we only look at concurrent measurements, i.e., measurements that have been made during the same week, we get an R^2 of respectively 0.80 and 0.62 in spring and autumn, an RMSE between 5 and $6 \mu\text{g}/\text{m}^3$ for both weeks and a bias ranging from almost $5 \mu\text{g}/\text{m}^3$ in spring to about $-1 \mu\text{g}/\text{m}^3$ in autumn. The latter values do not mix spatial and temporal correlation and are thus a good indication of the spatial predictive power of the model. As can be seen in Figure 31, the model underestimates the higher concentrations and overestimates the lower concentrations. The spatial and temporal variability of the model is thus slightly too small (see also ratio of standard deviation in Table 10). The underestimation of the spatial variability is also represented by the slope of the linear regression of the modelled values on the measurements. This could be linked to the absence of microscale effects (such as trees, traffic signs, ...) in our model. This slope is found to be 0.67, well under the ideal case of slope 1.

4.4.2. IMPACT OF DIFFERENT MODEL STEPS ON IMPROVEMENT OF MODELLING RESULTS

In the previous section, the overall model performance was evaluated. In this section we want to investigate to what extent each of the different model steps improves the modelled

concentrations. This is done by comparing the slopes of the regression curve, correlation coefficients, RMSEs and biases for the different model steps. Improvements will result in respectively increasing the correlation coefficients and decreasing both the bias and the RMSE. Finally, improvements will also result in the approach of the slope of the regression towards 1.

For this analysis, we have repeated the validation exercise for the different steps in the model chain setup:

1. The RIO model (Figure 29, upper left panel; Figure 32, left panel; Table 10);
2. The interpolated RIO model (Figure 29, upper right panel; Figure 32, right panel; Table 10);
3. The interpolated RIO combined with IFDM (Figure 29, lower left panel; Figure 33, left panel; Table 10);
4. The full integrated model chain, taking into account street canyon effects (Figure 29, lower right panel; Figure 33, right panel; Table 10).

Figure 32, left panel and Table 10, show that the RIO model cannot account for the spatial variability of the measurements within an urban scale. This is as expected, as the RIO model has a resolution of only $4 \times 4 \text{ km}^2$. Indeed, all the measurement locations can be found in 4 RIO cells. However, the bias in the RIO model is already relatively small, as is the RMSE. Nevertheless, the R^2 is small when evaluating the autumn and the spring week separately, although it is quite high (0.65) for the combination of both seasons. This shows that RIO is representing correctly the difference between the autumn and the spring week. The difference in bias between the autumn and the spring week is about 16%, with underestimation of the concentrations in the autumn season and overestimation in the spring season. This shows that the RIO model is responsible for a large part of the (small) bias in the final results, although the bias in both RIO and the integrated model chain is quite limited (Table 10). Finally, within both the spring and the autumn week, the standard deviation in the model results is an underestimation of the measured standard deviation.

The interpolation of the RIO results ($4 \times 4 \text{ km}^2$) to the IFDM grid (Figure 32, right panel) does not lead to significant changes in the average modelled concentrations. However, the discrepancy between the seasonal biases increases, with a stronger negative bias in autumn and a stronger positive bias in spring. Indeed, the interpolation step increases concentrations in cells surrounded by cells with higher concentrations, while decreasing concentrations in cells surrounded by cells with lower concentrations. In spring, the RIO cells north of the study domain have higher concentrations. In autumn, the cells with the highest concentrations in the whole region are found inside the study domain. This difference can probably be attributed to the heating emissions inside the city centre which are much more important in late autumn than in late spring. As a result the city centre displays higher concentrations than its harbor in the North during autumn but not during spring. Next to the change in bias, there is an increase of correlation due to the interpolation and a decrease in the RMSE, although the skill still remains low at this local scale.

The addition of IFDM, taking into account local emissions and their characteristics, (Figure 33, left panel; Table 10) leads to an important change in the validation parameters. First of all, the R^2 values rise from 0.75 to 0.86. However, for the separate seasons, the rise is even more pronounced with values increasing from 0.46 to 0.53 in autumn and soaring from 0.34 to 0.74 in spring. The average modelled concentration is higher when IFDM is included, leading to an elimination of the

bias averaged over both seasons. However, the spread between the two seasons remains approximately at the same level as for the interpolated RIO results alone. Furthermore, the slope of the regression also increases strongly and the standard deviation of the model values increases strongly. Finally, the RMSE values decrease, confirming the increased skill of the model once IFDM is included.

The increase of the model skill with and without the street canyon model seems rather small (Figure 33, right panel; Table 10). However, this is due to the fact that many of the locations on which measurements were performed are not found in a street canyon and are thus not affected by the inclusion the street canyon model (Figure 33, right panel). Overall, the inclusion of the street canyon model increases slightly the R^2 , the bias and the RMSE. However, for individual locations, it increases the skill of the model and the standard deviation of the model values increases toward the standard deviation in the measurements (Table 10, Table 11). This can be seen in Figure 33 (right panel), where the black lines represent the street canyon contribution in order to show the effect of adding the street canyon model to the model chain. The resulting effect is also seen in the improvement of the slope of the regression curve (Table 10). The increases in skill are somewhat more clear when we only validate for street canyons (Table 11).

4.5. CONCLUSIONS

This paper presents an integrated model framework for calculating concentrations at the urban to street level scale. The method is validated by an NO_2 monitoring campaign, using passive samplers in a late spring and late autumn period. As a result, only an evaluation on the spatial correctness of the model was performed, not on the ability of reproducing the temporal variability of the concentration fields. The validation analysis show that the model is able to represent the spatial variability within an urban environment. As a result, the model can be used to improve the static exposure assessment of people living in the urban area and to complement fixed monitoring stations that are often only limited in number in a city.

The validation analysis was performed for the different steps in the model chain revealing the strengths of the different components in creating these concentration maps. First of all, it was shown that RIO is well able to represent the differences between the seasons. However, due to the relatively low resolution, it is not capable of representing the spatial variability between the different locations. Interpolating these RIO-results to the measured locations does not add much skill to the model. The use of the plume model improves strongly the accuracy of the results. In particular, the RMSE decreases and the R^2 soars. This last parameter improves even more when taking into account street canyons.

Acknowledgments

This work was partially funded by the Flemish Environment Agency (VMM, measurements) and partially by the LIFE+ programme of the European Union. (LIFE+ 2009 project ENV/BE/000409, www.life-atmosys.be). The authors want to thank the anonymous reviewers and participants of the measurement campaign.

Period name	Number of measurements	Number of measurements used in this validation
S_w1	10	7
S_w2	11	9
S_w3	11	8
S_w4	11	10
S_w5	11	9
S_wAll	55	49
A_w1	12	8
A_w2	11	9
A_w3	11	8
A_w4	12	10
A_w5	11	9
A_wAll	54	49
Total	220	185

Table 9 : The number of measurements, and the number of measurements used in this validation for the different measurement weeks. The concentrations measured over different times are identified by season and week number. Measurements in late Spring or late Autumn are denoted by respectively S and A. The sample week is indicated by w1-w5 for week 1 up to week 5 respectively and by wAll for sampling performed over all locations simultaneously. Combining these time-related indicators, this results in e.g. S_w2 for the second week in the Spring campaign and A_wAll for the week in autumn in which all locations were measured simultaneously.

		RIO	RIO interpolated	RIO+IFDM	RIO+IFDM + street canyon
Autumn + spring	Mean BIAS (%)	-1	-1	2	6
	RMSE (%)	22	21	16	15
	R ²	0.65	0.75	0.86	0.87
	Slope	0.48	0.46	0.61	0.67
Autumn	Mean BIAS (%)	-7	-9	-5	-2
	RMSE (%)	16	15	12	13
	R ²	0.09	0.46	0.53	0.62
	Slope	0.03	0.11	0.52	0.68
Spring	Mean BIAS (%)	9	12	14	20
	RMSE (%)	28	27	21	23
	R ²	0.02	0.34	0.74	0.80
	Slope	0.10	0.15	0.45	0.60

Table 10 : Validation parameters for the model, for the autumn week with most measurements, the spring week with most measurements and both weeks combined. Bias and RMSE are expressed in % of the average of the measurements. The slope represents the slope of the linear regression of the model values on the measurements. The rows 'Ratio of stdev' give the ratio of the standard deviation of the model values on the measurement values (in %). The rows '# locations > 40 µg/m³' denote the number of locations at which concentrations larger than the annual limit of 40 µg/m³ are modelled (left number) or measured (right number).

		RIO	RIO interpolated	RIO+IFDM	RIO+IFDM + street canyon
Autumn + spring	Mean BIAS (%)	-11	-13	-7	4
	RMSE (%)	25	24	18	16
	R ²	0.60	0.76	0.86	0.82
	Slope	0.43	0.42	0.58	0.64
	Ratio of stdev (%)	55	48	63	71
	# locations > 40 µg/m ³	14/15	9/15	8/15	15/15

Table 11 : Same as First part of Table 10, but with validation parameters for only the street canyons.

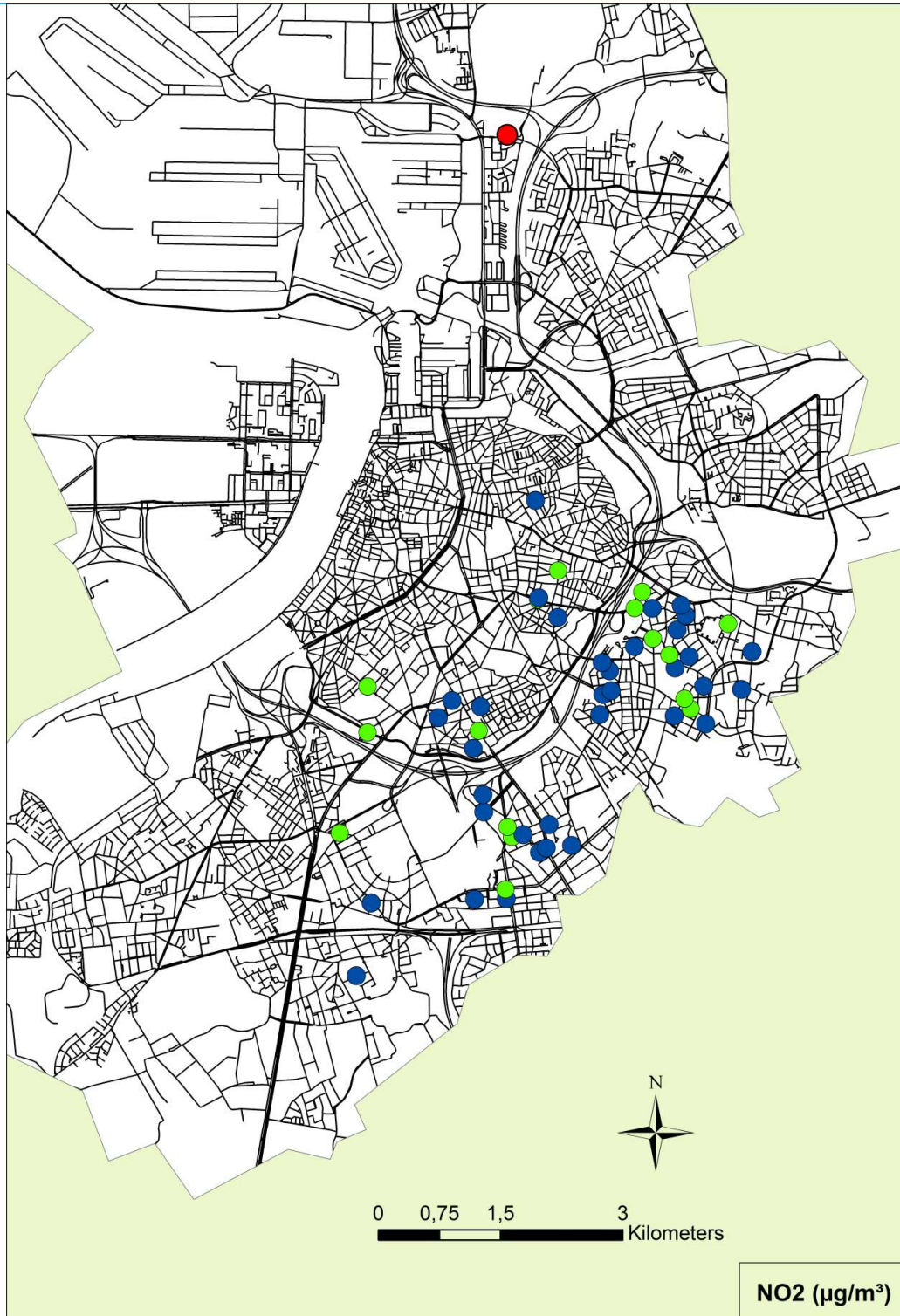


Figure 26 : The location of the NO₂-measurements. Green dots are measurement locations within street canyons; blue dots are found outside street canyons. In black: roads. The red dot represents the location where the meteorological measurements have been made. Only the area within the city limits of Antwerp is shown.

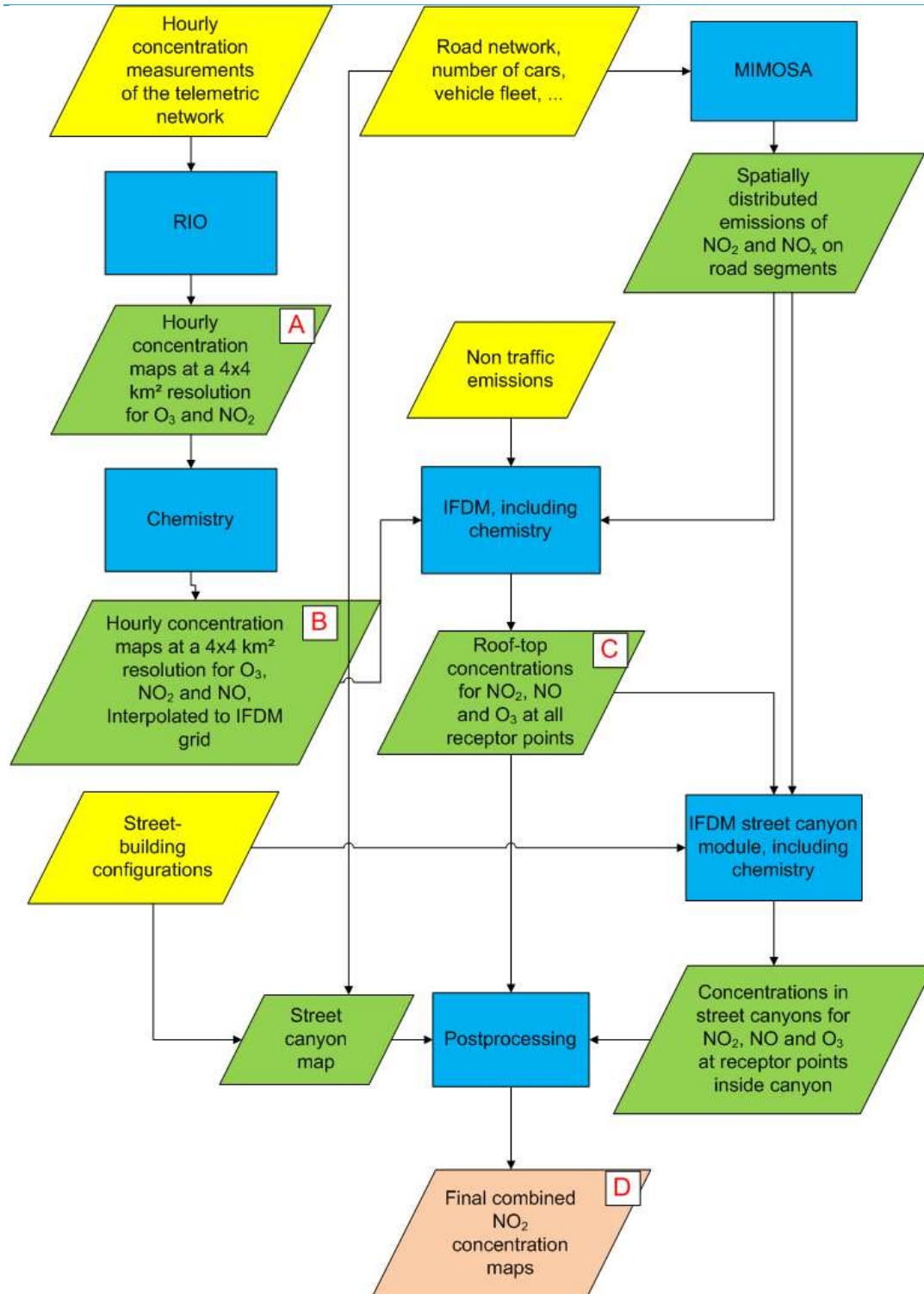


Figure 27 : The modelling chain. In yellow parallelograms: input data sets. In blue rectangles: the different processes. In green parallelograms: intermediate results. In the salmon-coloured parallelogram: the final result. The red letters A-D denote the model steps shown in Figure 29, Figure 32 and Figure 33.

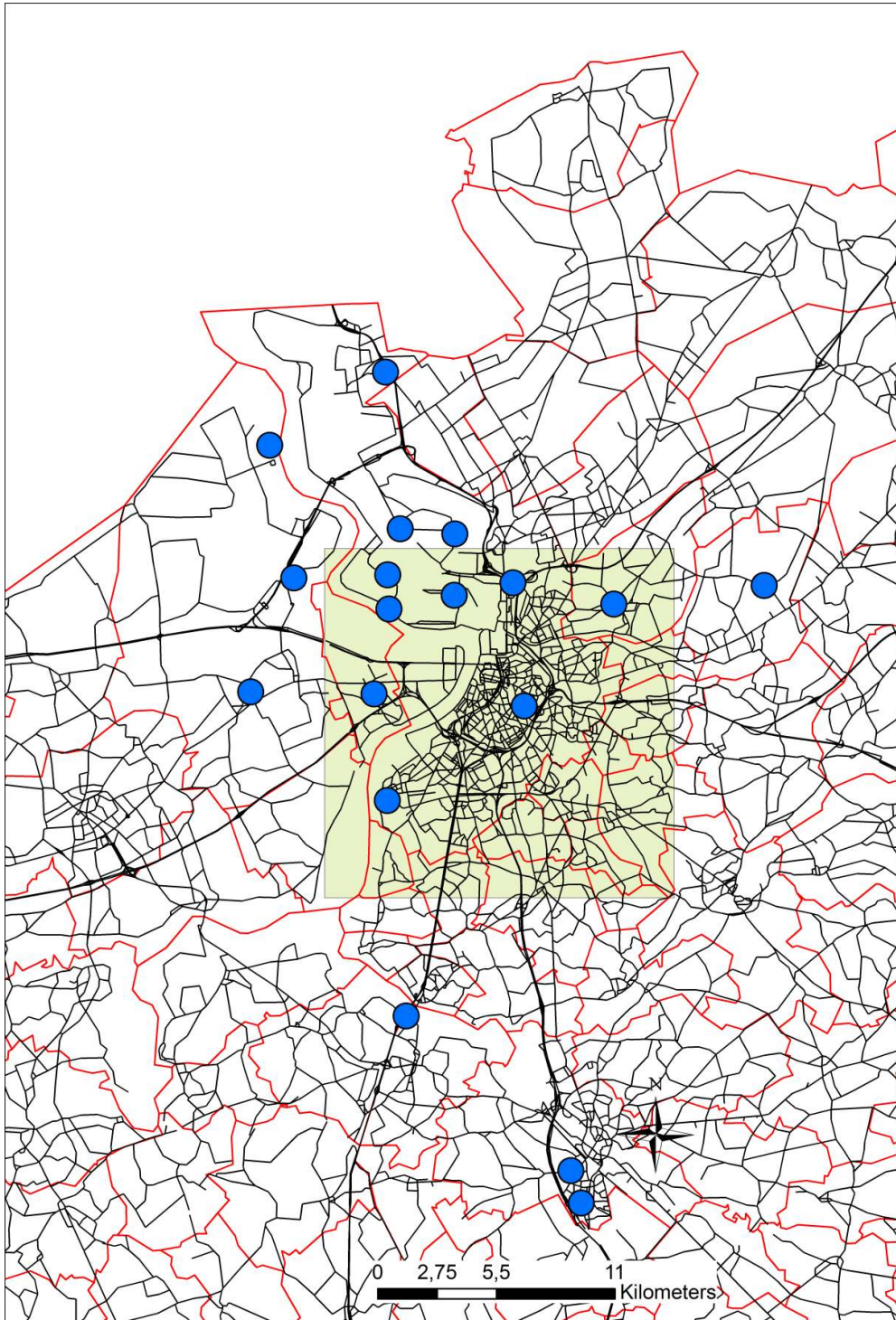


Figure 28: In red lines: the administrative boundaries of the communities in the region around Antwerp. In black lines: major roads. In blue dots: the measurement stations used by RIO. In the green cadre: the approximate region shown in Figure 29.

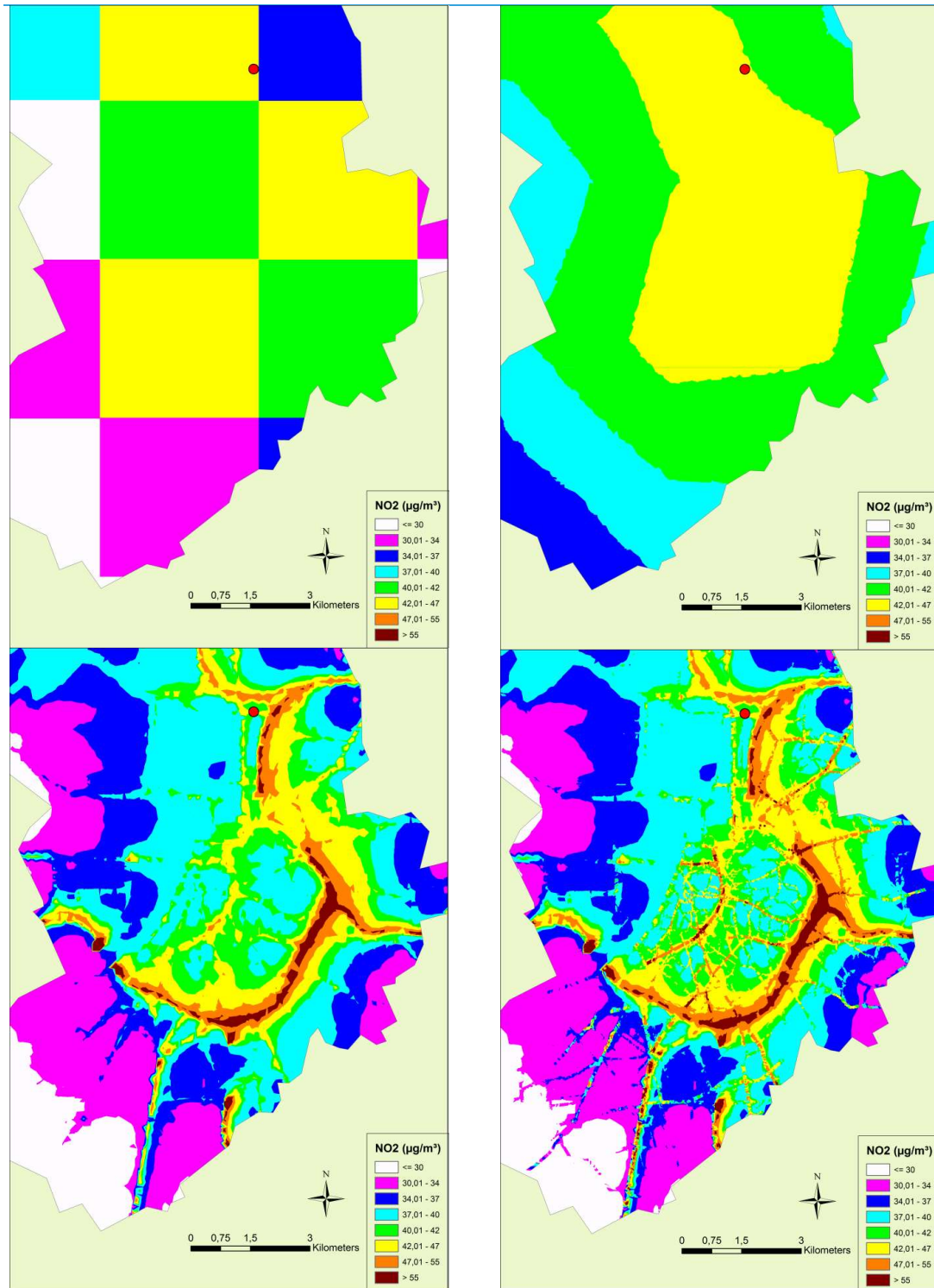


Figure 29 : Concentration maps (NO₂, in $\mu\text{g}/\text{m}^3$) in different steps of the methodology for the AwAll-week. Upper left: the RIO-map. Upper right: the interpolated RIO-map. Lower left: the concentration map including IFDM. Lower right: the complete map. The red dot is the location of the meteorology measurement. Only concentrations within the city of Antwerp are shown.

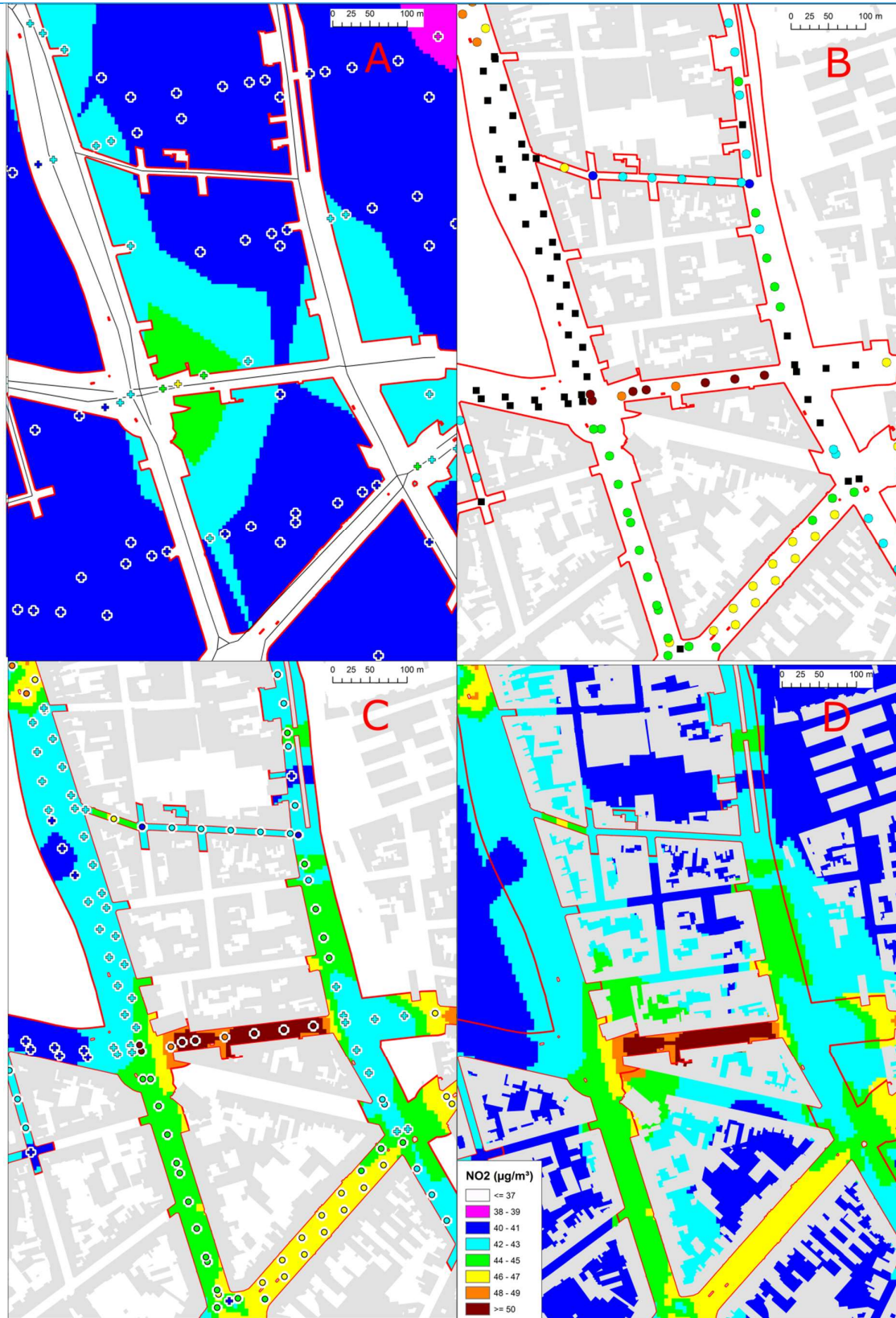


Figure 30 : Different steps in the postprocessing of the results, shown for a small region of the city of Antwerp. Part A: postprocessing of the IFDM roof-top results. In crosses: the concentrations at the receptor locations of the IFDM-grid; In black: road segments; Background colors: interpolated concentration results. In white with red border: the street canyon polygon (see §4.3.7). Part B: the initial situation before postprocessing the IFDM street canyon results. In circles: the concentrations given by the IFDM street canyon module at the locations of the street canyons for the limited street canyon receptor points (see end of §4.3.5); In black squares: the receptor points which are part of the full street canyon receptor points (see end of §4.3.5) which are not part of the limited street canyon receptor points; In grey: the buildings; In red line: the border of the street canyon polygon. Part C: the postprocessing of the IFDM street canyon results. In circles: the concentrations given by the IFDM street canyon module at the locations of the street canyons for the limited street canyon receptor points (see end of §4.3.5); In crosses: the receptor points which are part of the full street canyon receptor points (see end of §4.3.5) which are not part of the limited street canyon receptor points, filled with the interpolated IFDM roof top concentrations (Part A); In grey: the buildings; In red line: the border of the street canyon polygon; Background colors: interpolated concentrations within the street canyon polygon. Part D: The final result. In grey: the buildings; In red line: the border of the street canyon polygon; Background colors: the final merged concentrations. The legend is equal for all the different parts and datasets.

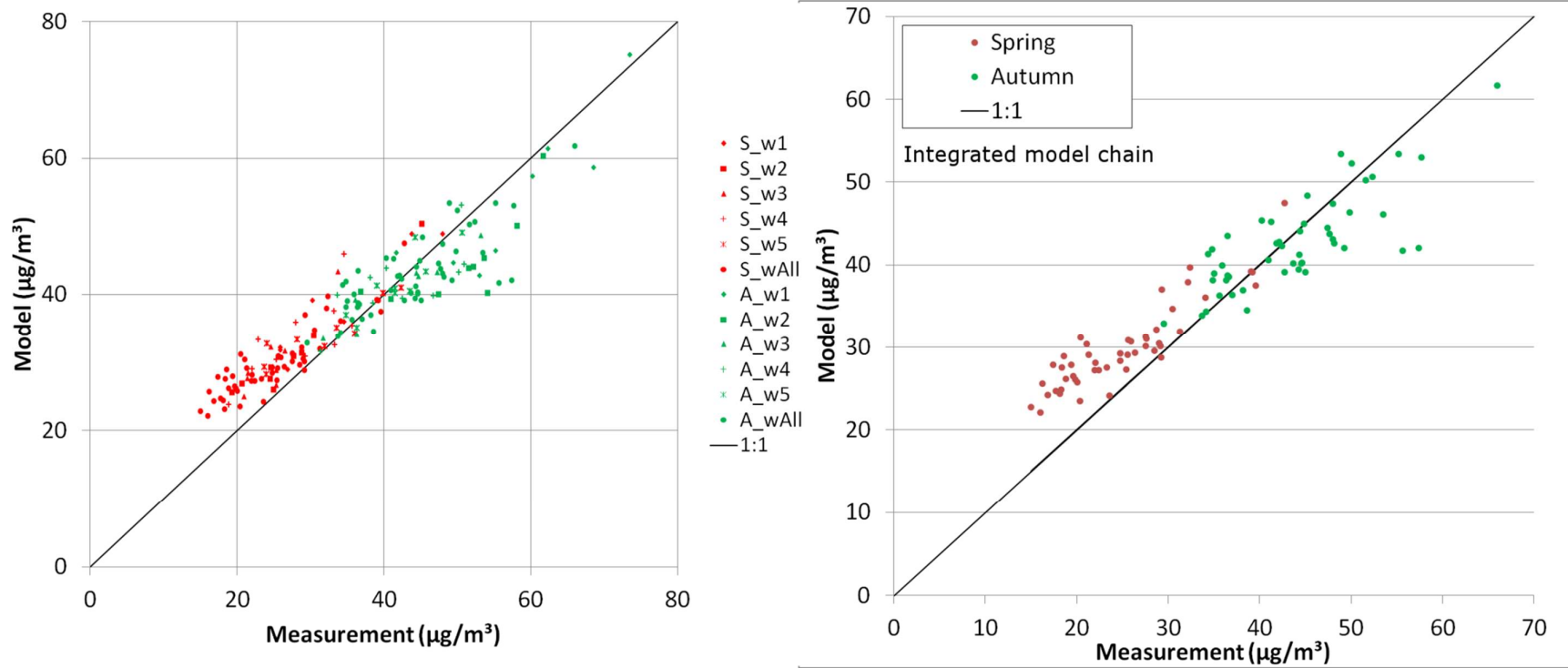


Figure 31 : The validation plots (NO₂, in µg/m³). Left: for all measurements. Right: for the measurements in the two weeks with the most measurements. Every point represents the weekly averaged concentration (in µg/m³) measured (X-axis) and modelled (Y-axis).

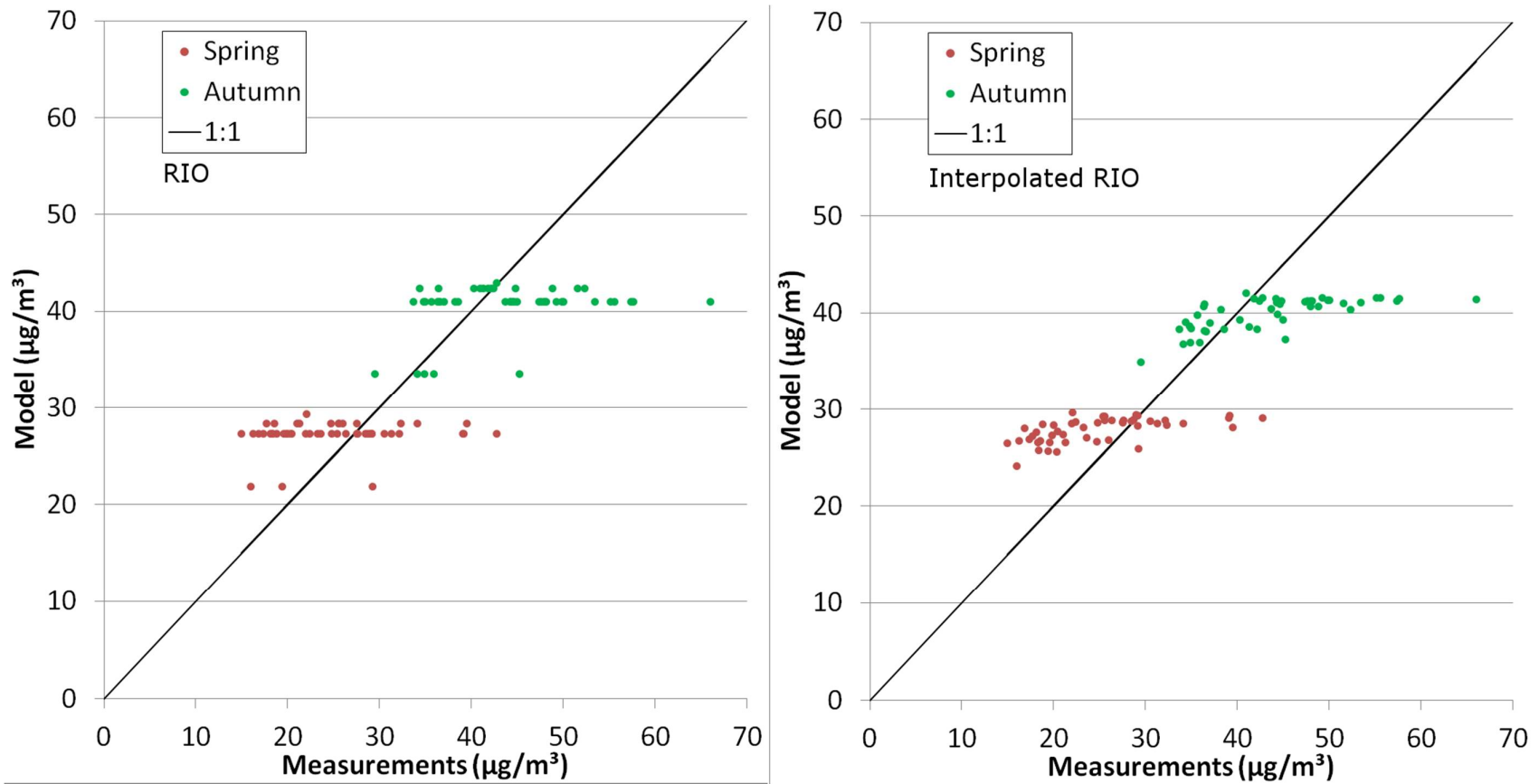


Figure 32 : Validation plots for different steps in the methodology. Left: for RIO. Right: for the interpolated RIO. Every point represents the weekly averaged concentration (in $\mu\text{g}/\text{m}^3$) measured (X-axis) and modelled (Y-axis).

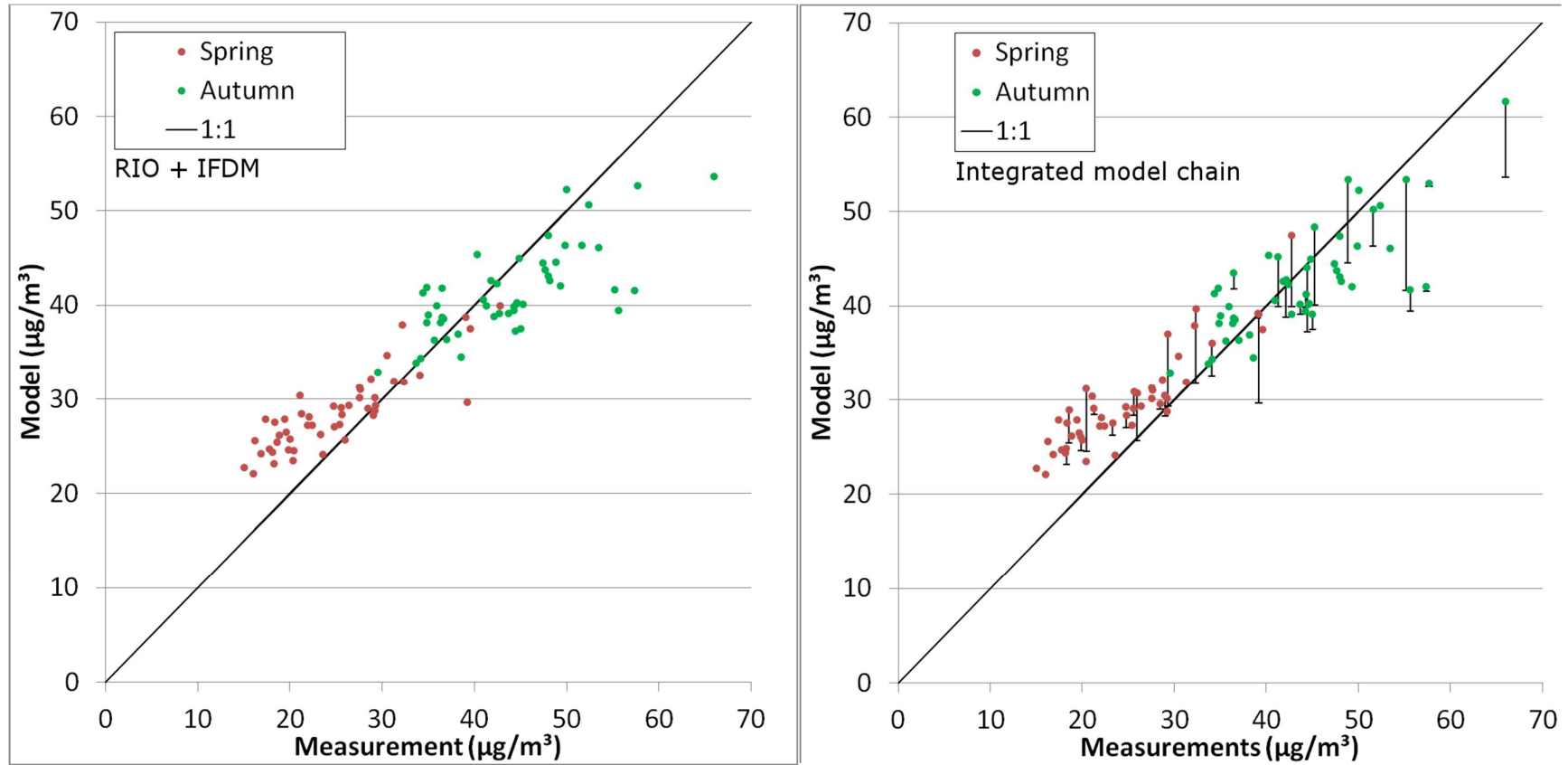


Figure 33 : Validation plots for different steps in the methodology. Left: for RIO+IFDM. Right: the complete model chain. Every point represents the weekly averaged concentration (in $\mu\text{g}/\text{m}^3$) measured (X-axis) and modelled (Y-axis). The black lines on the graph represent the street canyon contribution.

CHAPTER 5 SENSITIVITY TESTS

Some sensitivity tests have been performed on the Antwerpen-case (CHAPTER 4). The model runs have been performed for the late autumn week for which also measurements were available. This allows us to perform a validation of the different sensitivity runs and assess whether they could be considered as an improvement for the model setup.

5.1. SENSITIVITY TO THE NO₂/NO_x-RATIO

In order to assess the impact of the NO₂/NO_x-ratio, two scenarios are studied:

- All roads have the same NO₂/NO_x-ratio, i.e. the weighted average NO₂/NO_x-ratio of the roads in the study area (ratio of 0.315, as emissions are for the year 2015).
- All roads have an NO₂/NO_x-ratio of 0.05 (representative ratio for the early nineties).

In the reference run, the NO₂/NO_x-ratio is street specific and depends on the fleet composition and the road type. One of the major determining factors is the ratio of heavy duty vehicles on passenger cars.

The difference between the first scenario and the reference scenario is very small (Figure 34). Small increases are found on the highways (as on these locations the decrease in the NO₂/NO_x-ratio due to the large amount of heavy duty vehicles is not taken into account in the scenario run), whereas small decreases are found on the roads where the amount of heavy duty vehicles is relatively small.

The difference between the second scenario and the reference scenario is more important (Figure 35). Decreases in the concentration are found on all roads with a lot of traffic and are most easily seen in major street canyons and along the highways. It is clear that the model is sensitive to this action and thus that it is important to take into account the change of the average NO₂/NO_x-ratio throughout the years.

The validation results of the first scenario are similar to those of the reference scenario (Table 12). The second scenario exhibits a slightly higher R² but this is compensated by a lower slope of the regression line.

However, the effect of this ratio is larger than is shown here in the validation results, as, both in the subtraction step and the addition step, these changes are taken into account and cancel each other partly out. Therefore, we have made additional sensitivity simulations in which the changes to the NO₂/NO_x-ratio are only used in the addition step. Using the subtraction step from the reference scenario will lead to the same basic concentration maps on which the addition step of the ratio-scenarios will add the local concentrations. The maps can then be interpreted in two ways:

- What would happen if suddenly the changes we have added in the model are reality?
- What would be the difference if the changes were not made on the RIO-background but added to the concentrations of a background station?

For the scenario with the homogenous ratio, the differences with the reference remain small (Figure 36) and similar to the ones in Figure 34. However, the impact of a NO_2/NO_x -ratio of 0.05 becomes quite large, without the double counting cancellation effect (Figure 37). This confirms that it is important to take into account the changing NO_2/NO_x -ratio throughout the years.

5.2. SENSITIVITY TO THE DOUBLE COUNTING PROCEDURE

We study the effect of eliminating the double counting procedure for the IFDM roof-top concentrations. In this analysis IFDM concentrations are simply added on top of the (interpolated) RIO concentration fields. The double counting elimination for the street canyon procedures is kept in place in this analysis.

The effect of the double counting procedure is enormous (Figure 38). Eliminating this procedure leads to increases in NO_2 -concentrations up to more than $9 \mu\text{g}/\text{m}^3$. As a result, we can conclude that taking into account the possibility of double counting in the simulations is very important.

The validation results of this scenario are worse than the validation of the reference scenario (Table 12). Especially the increase in the biases and the RMSE is large. The R^2 and the slope of the regression line are slightly better than in the reference scenario, as locations in grid cells with higher local concentration components will be mostly impacted by the double counting procedure. As there is a slight underestimation of the highest concentrations by the model, eliminating the double counting procedure will lead to an increased slope of the regression line.

5.3. SENSITIVITY TO THE ROAD NETWORK

To assess the impact of the type of roads, two scenarios are studied:

- All roads of road type 3 (urban, black roads on Figure 43, about 64% of the road segments and 20% of the emissions) are eliminated (their emission is set to 0). The other roads are not affected.
- All roads of road type 3 (urban, black roads on Figure 43, about 64% of the road segments and 20% of the emissions) are eliminated (their emission is set to 0). The other roads are scaled up as to preserve the total traffic emissions within the area.

These scenarios create major changes in the concentration fields, especially in the city centre (Figure 39). The second scenario also increases the concentrations close to the major highways (Figure 40). Especially for calculating exposure of the population, the differences will be large as decreases are the highest in the densely populated areas. Furthermore, for assessment of limit values, eliminating part of the road network (although it accounts for only 20% of the emissions) is problematic.

The validation results of those sensitivity runs is also less good than in the reference scenario (Table 12). Although the bias is smaller and the RMSE is similar, the R^2 and the slope of the regression line are lower.

However, the effect of the omission of the local roads is larger than is shown here, as again, both in the subtraction step and the addition step, these changes are taken into account and cancel each other partly

out. Therefore, we have made additional sensitivity simulations in which the changes to the road network are only used in the addition step.

The differences in this setup (Figure 41, Figure 42) are even larger than in cases discussed above (Figure 39, Figure 40). This confirms that it is important to take into account the urban roads, especially for assessment of exposure and limit values.

5.4. SENSITIVITY TO THE EMISSIONS

In order to assess the impact of the emissions, two scenarios are studied:

- All emissions are reduced by 20%.
- All emissions are increased by 20%.

As can be expected, these scenarios create changes in the concentration fields, although the changes are at most locations smaller than in the previous case (§5.3). This is despite of the fact that emissions within the domain are reduced by about the same fraction (20%) in both scenarios. However, the reduction in the previous scenario is more concentrated in the city centre while the decrease in this scenario is more spread out (Figure 44). The second scenario shows the reverse effect (Figure 45).

The validation results are less good than in the reference case (Table 12) for the decreased emission scenario but are slightly better for the increased emission scenario, due to an increase in the slope of the regression line. This could lead to postulation of underestimation of the traffic emissions in the base case scenario.

As well as in the previous subsections, the effects studied here are partially canceled out in the subtraction and addition step. Therefore, the analysis is also performed with the sensitivity runs only included in the addition step.

The differences in these cases (Figure 46, Figure 47) are larger than in cases discussed above (Figure 44, Figure 45). Those results confirm that a change of 20% in urban traffic emissions would yield large effects on the NO₂-concentrations.

The analysis here and in the two previous sections demonstrates that the use of subtraction/addition steps strongly increases the robustness of the results, by tying the concentrations close to the background concentrations.

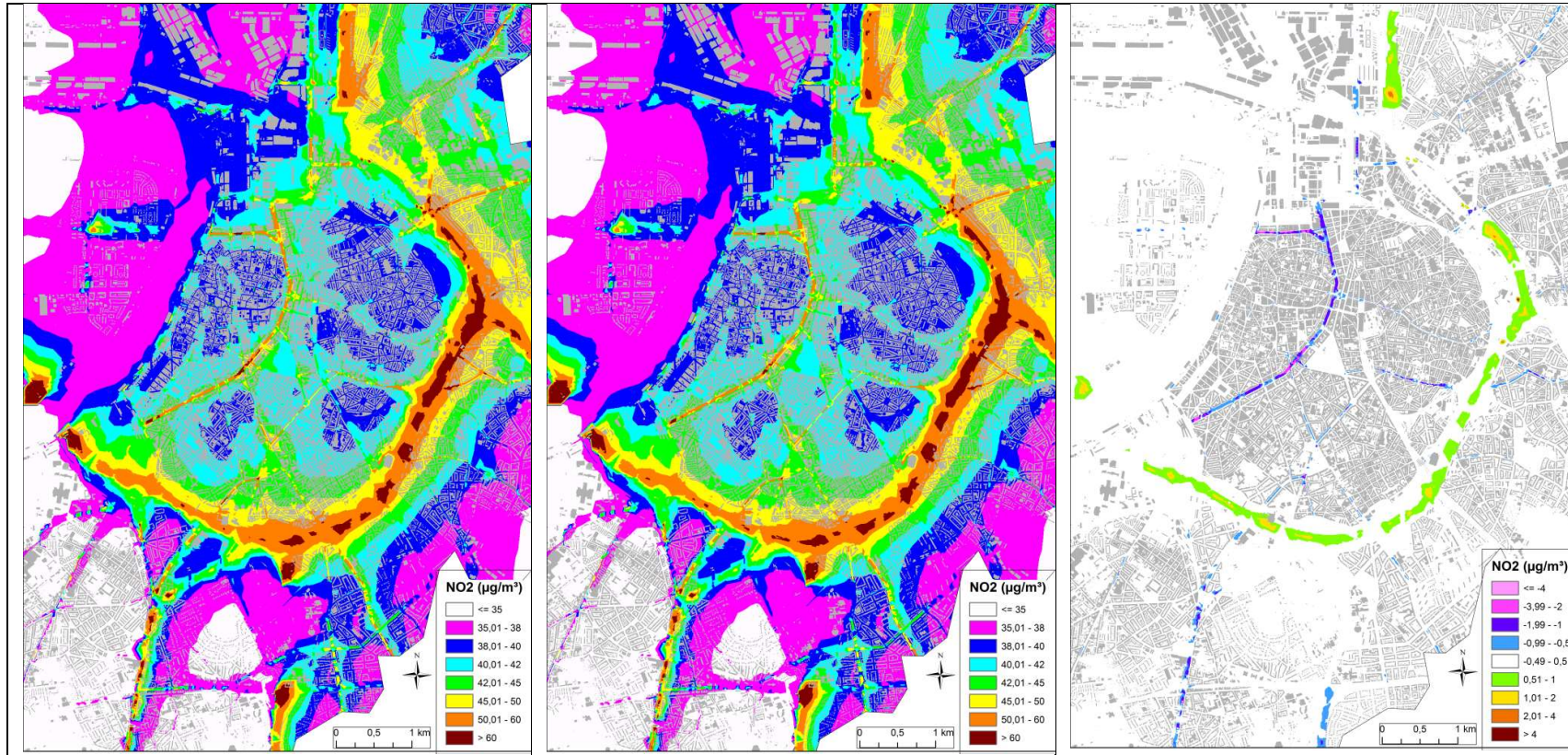


Figure 34 : The weekly averaged NO₂-concentration (in µg/m³) in the reference scenario (left), in the scenario with the homogenous NO₂/NO_x-fraction (middle) and the difference between both (right).

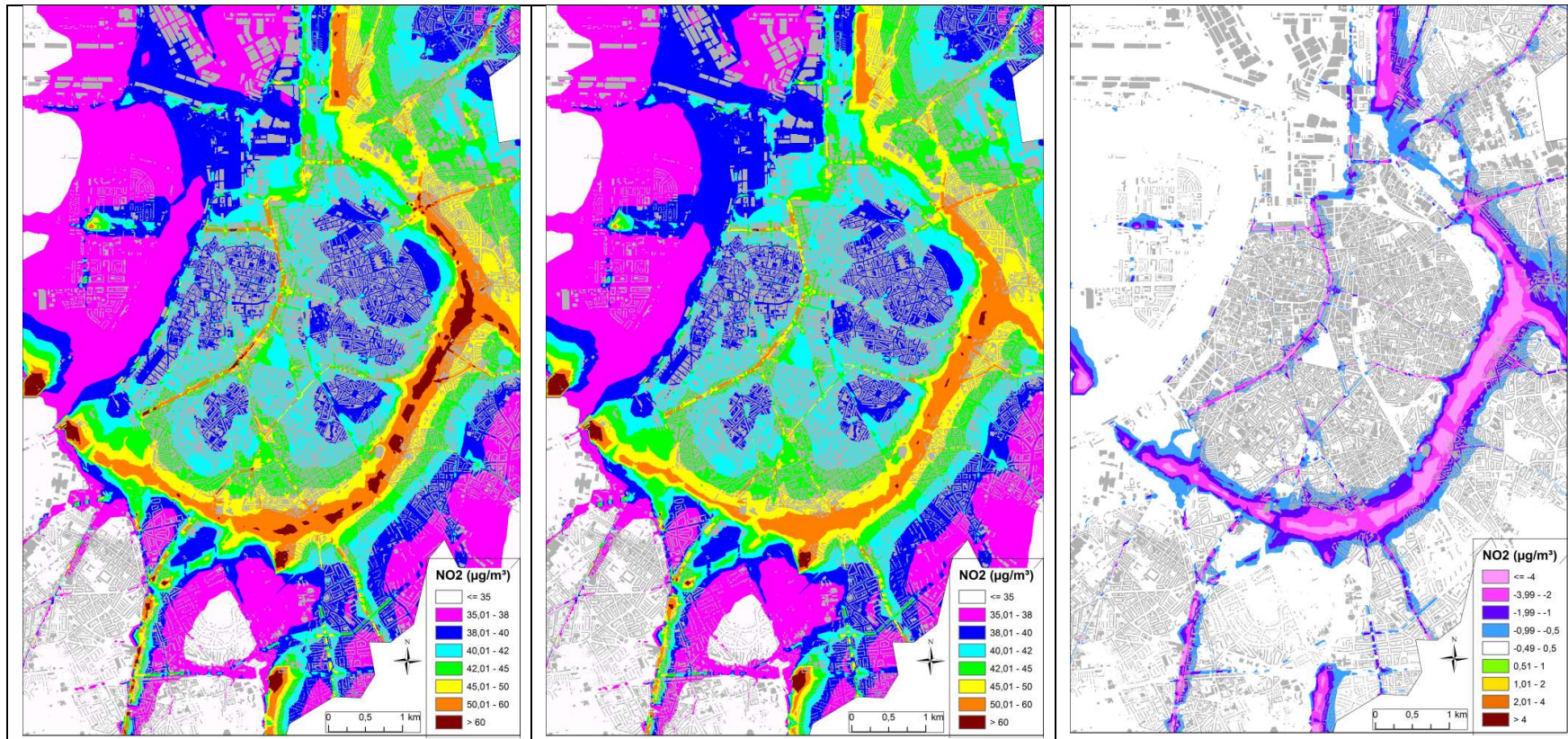


Figure 35 : The weekly averaged NO₂-concentration (in µg/m³) in the reference scenario (left), in the scenario with the homogenous low NO₂/NO_x-fraction (middle) and the difference between both (right).

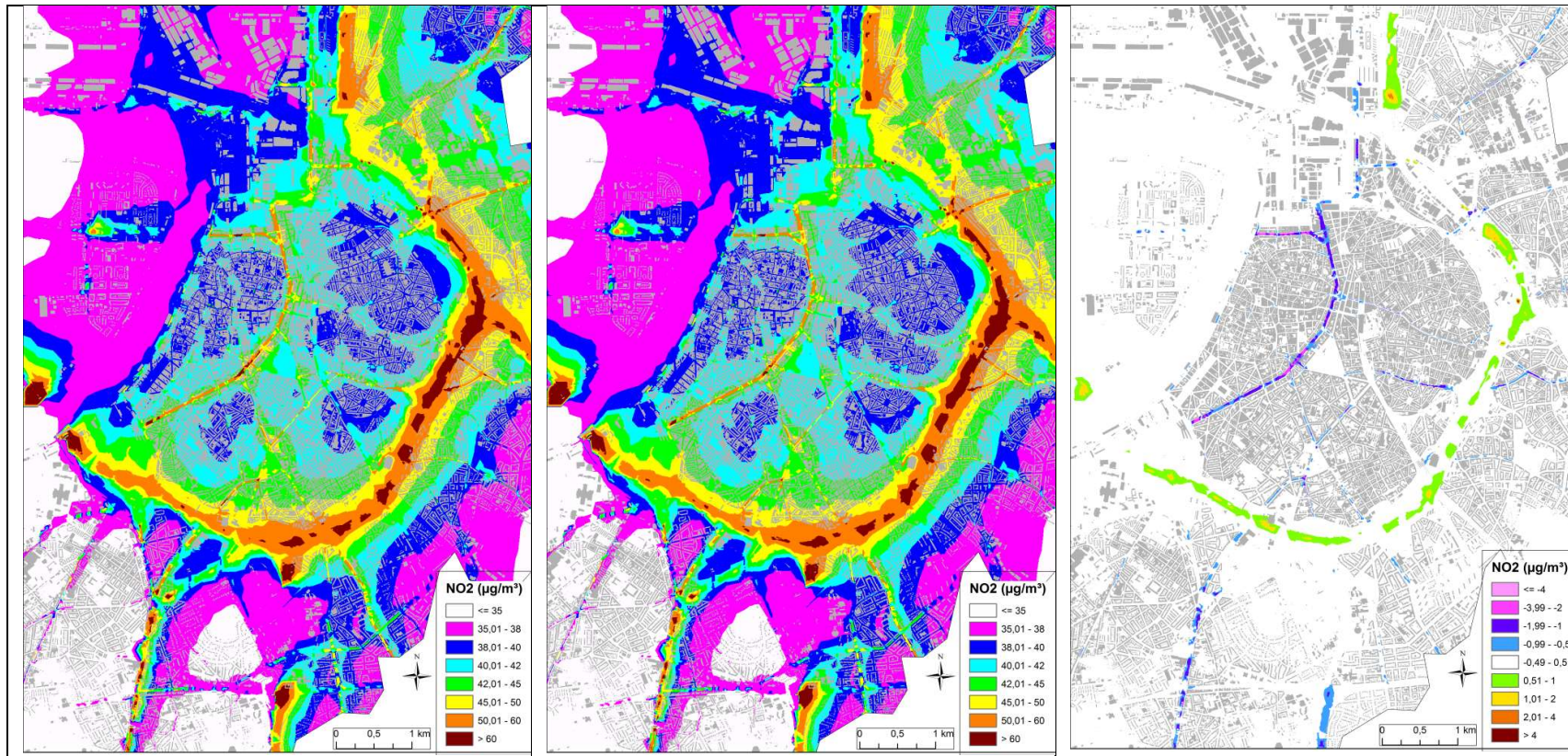


Figure 36 : The weekly averaged NO₂-concentration (in µg/m³) in the reference scenario (left), in the scenario with the homogenous NO₂/NO_x-fraction in the addition phase (middle) and the difference between both (right).

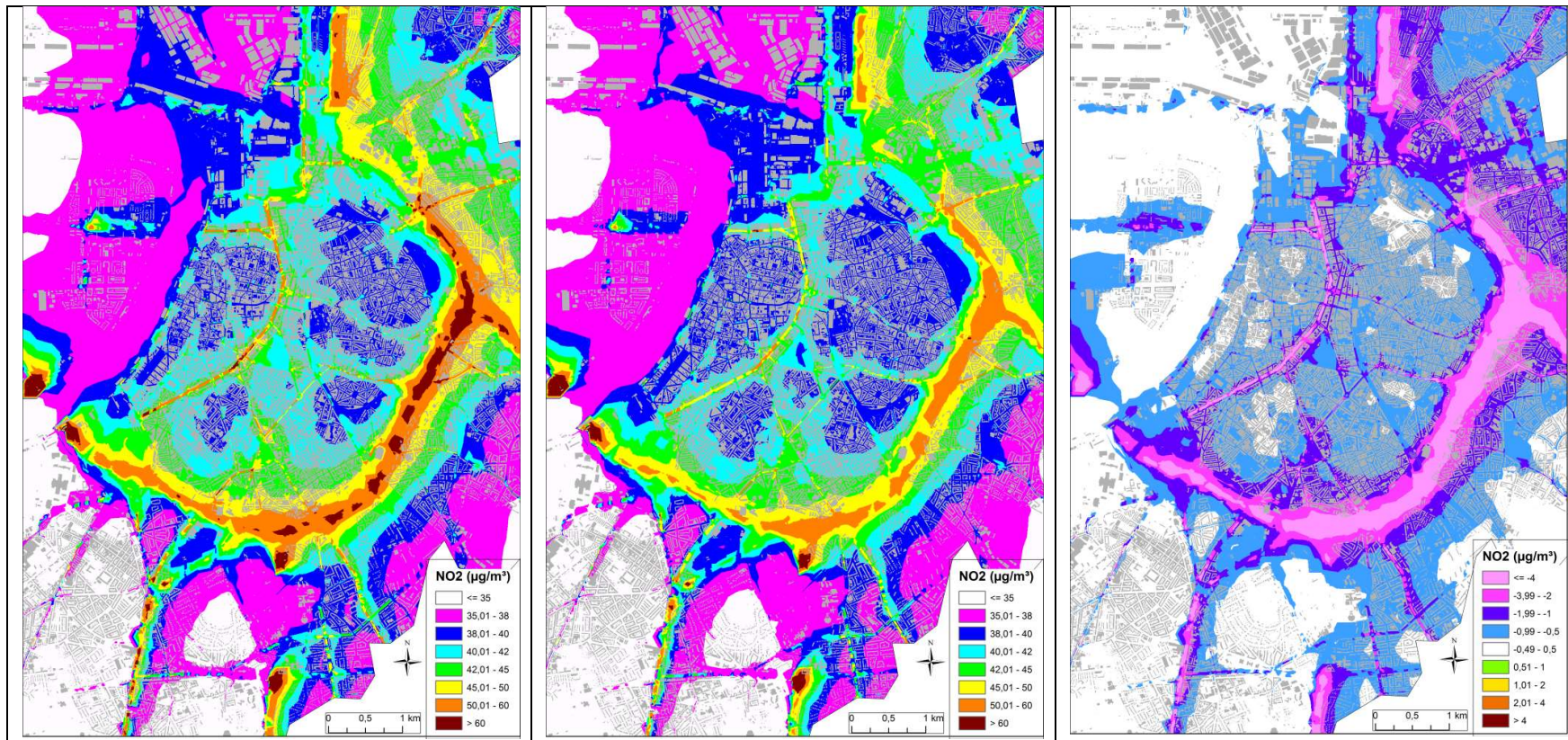


Figure 37 : The weekly averaged NO₂-concentration (in $\mu\text{g}/\text{m}^3$) in the reference scenario (left), in the scenario with the homogenous low NO₂/NO_x-fraction in the addition phase (middle) and the difference between both (right).

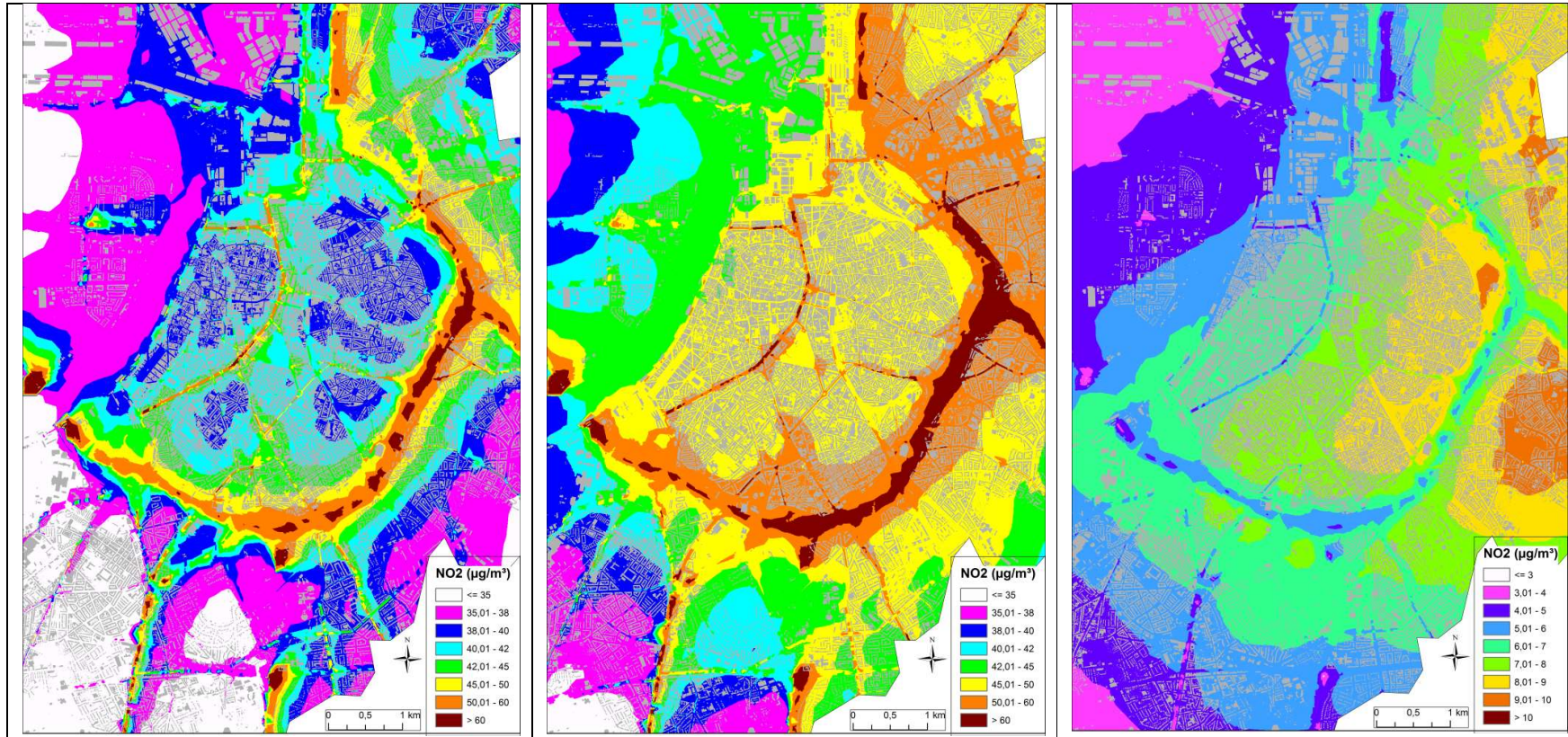


Figure 38 : The weekly averaged NO₂-concentration (in µg/m³) in the reference scenario (left), in the scenario without the correction for the double counting of the emissions in the IFDM-step (middle) and the difference between both (right).

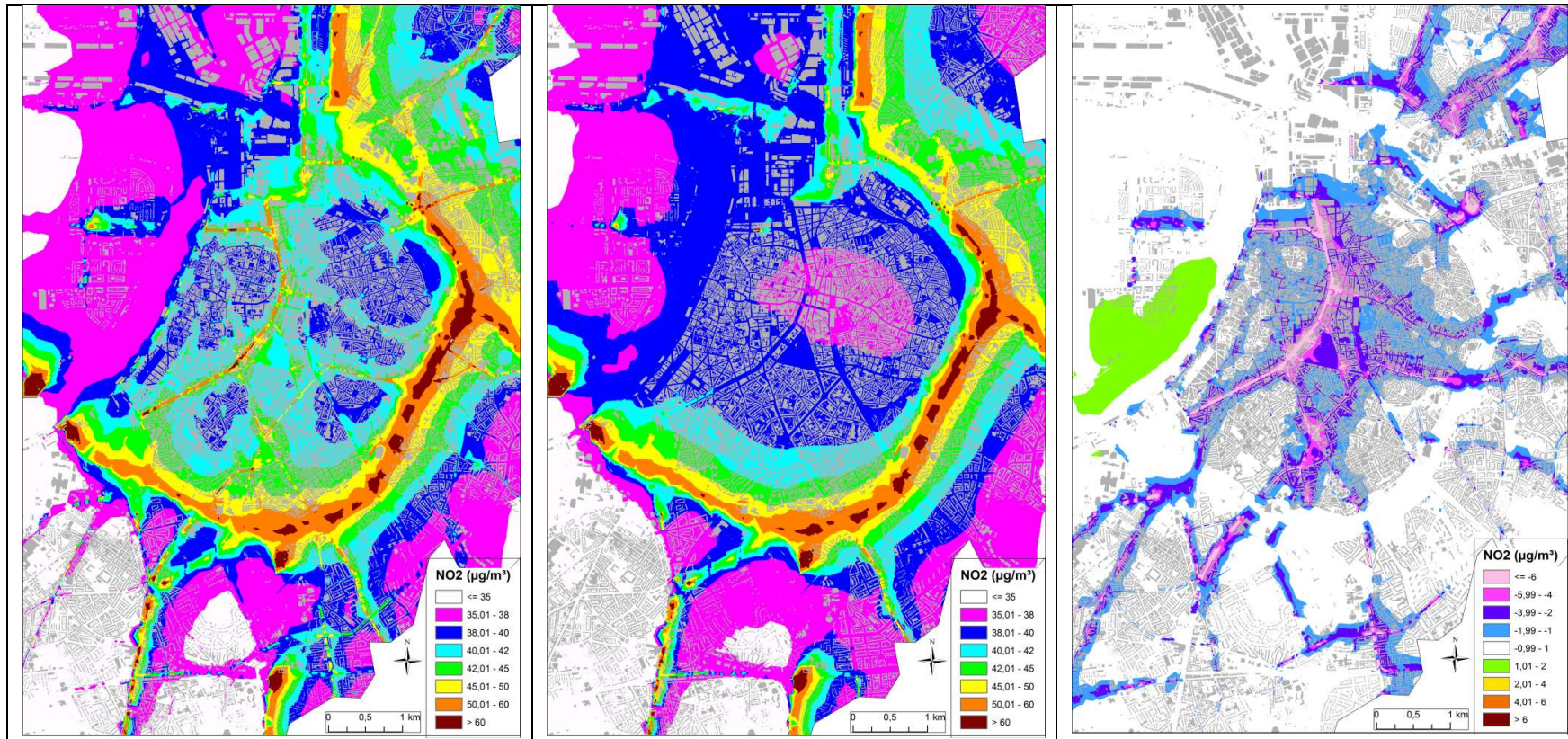


Figure 39 : The weekly averaged NO₂-concentration (in µg/m³) in the reference scenario (left), in the scenario with a reduced road network (middle) and the difference between both (right).

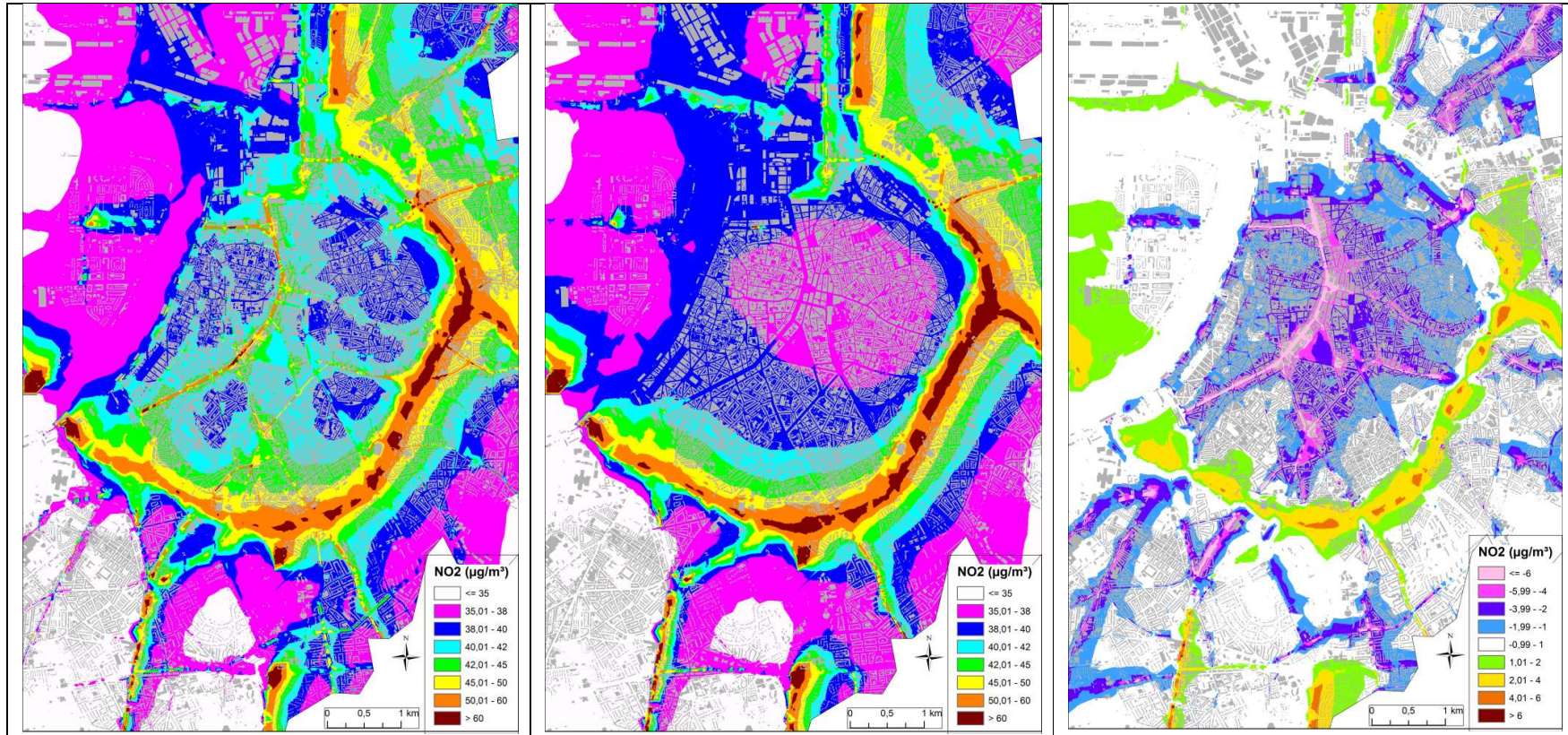


Figure 40 : The weekly averaged NO₂-concentration (in µg/m³) in the reference scenario (left), in the scenario with the reduced road network carrying the total traffic emissions for the region (middle) and the difference between both (right).

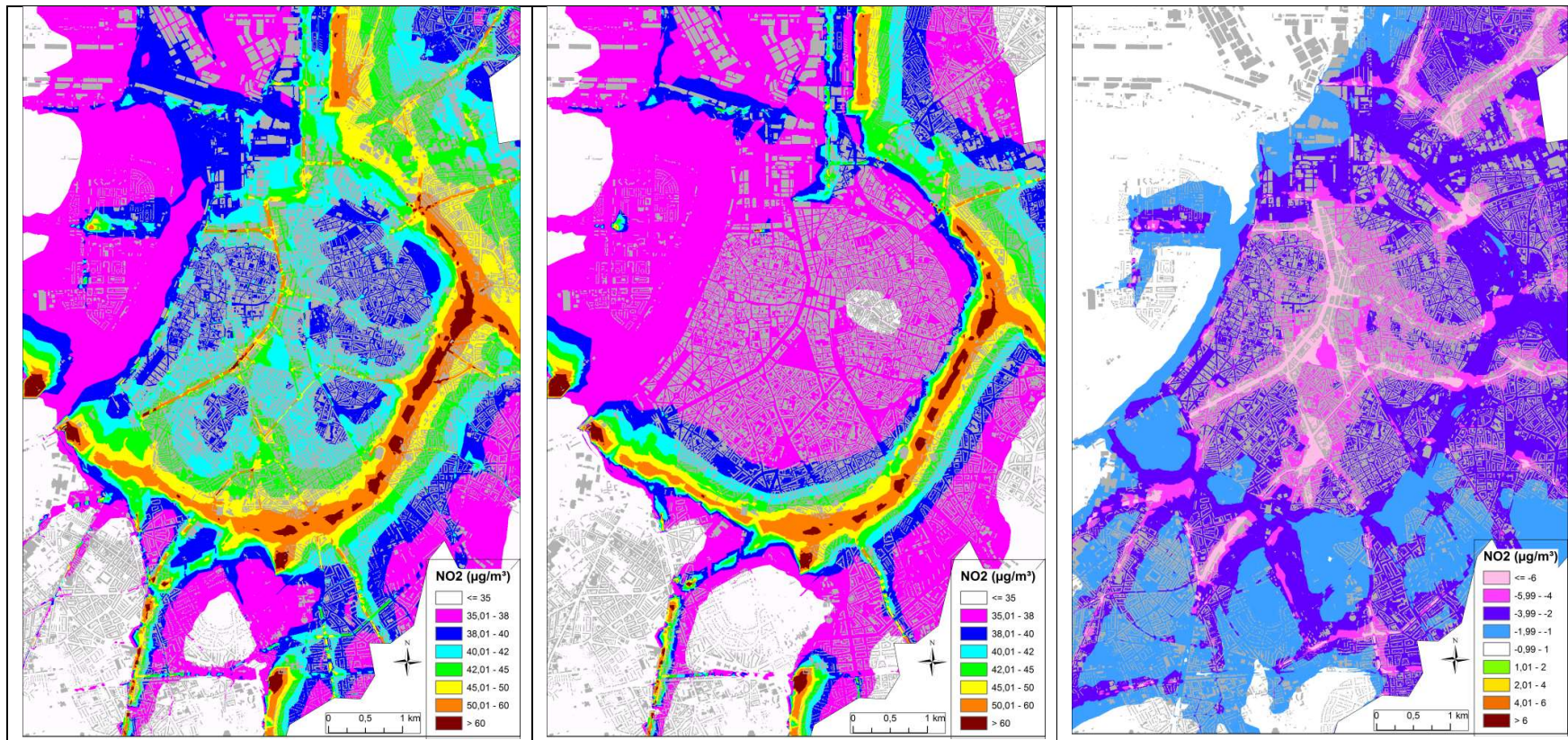


Figure 41 : The weekly averaged NO₂-concentration (in µg/m³) in the reference scenario (left), in the scenario with a reduced road network in the addition phase (middle) and the difference between both (right).

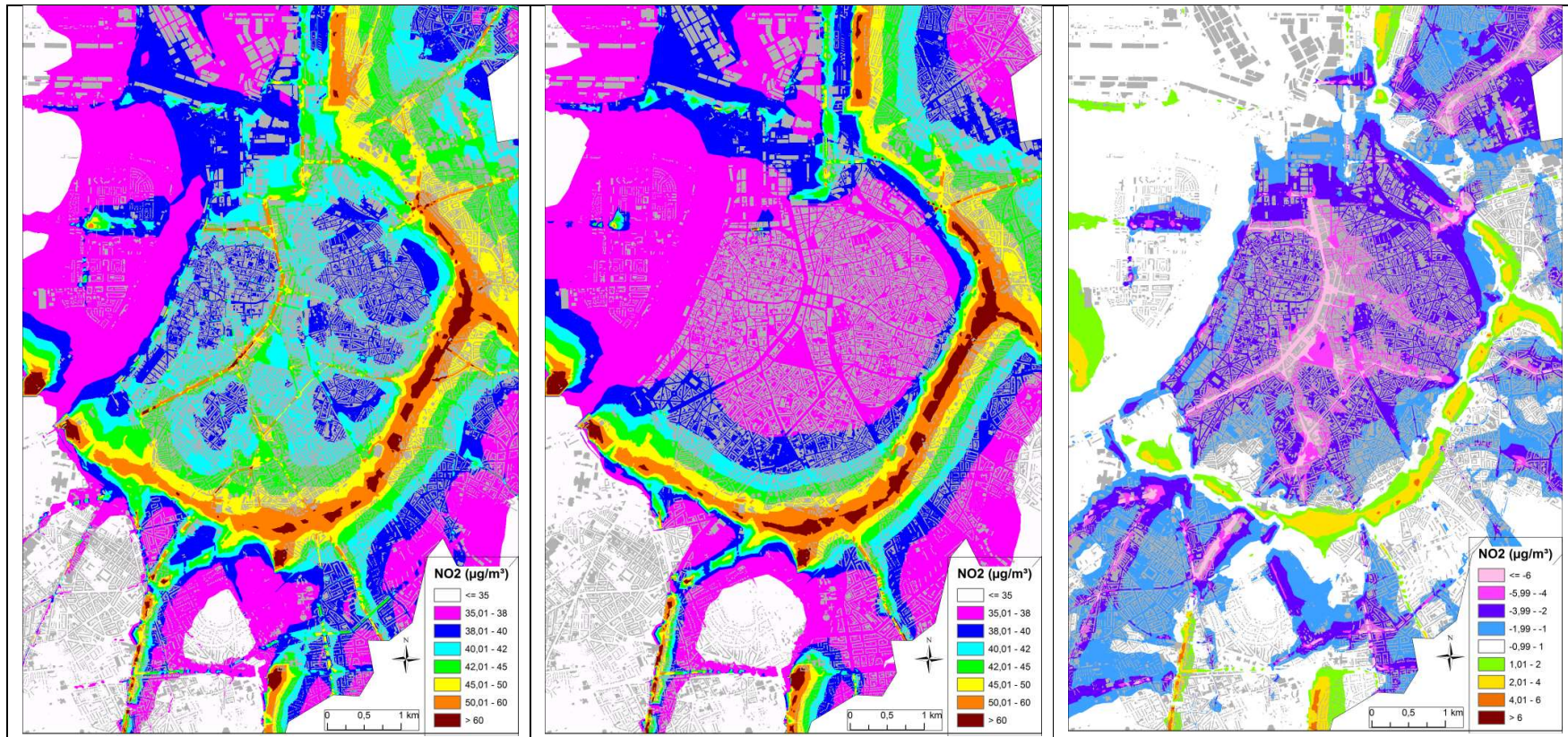


Figure 42 : The weekly averaged NO₂-concentration (in µg/m³) in the reference scenario (left), in the scenario with the reduced road network carrying the total traffic emissions for the region in the addition phase (middle) and the difference between both (right).

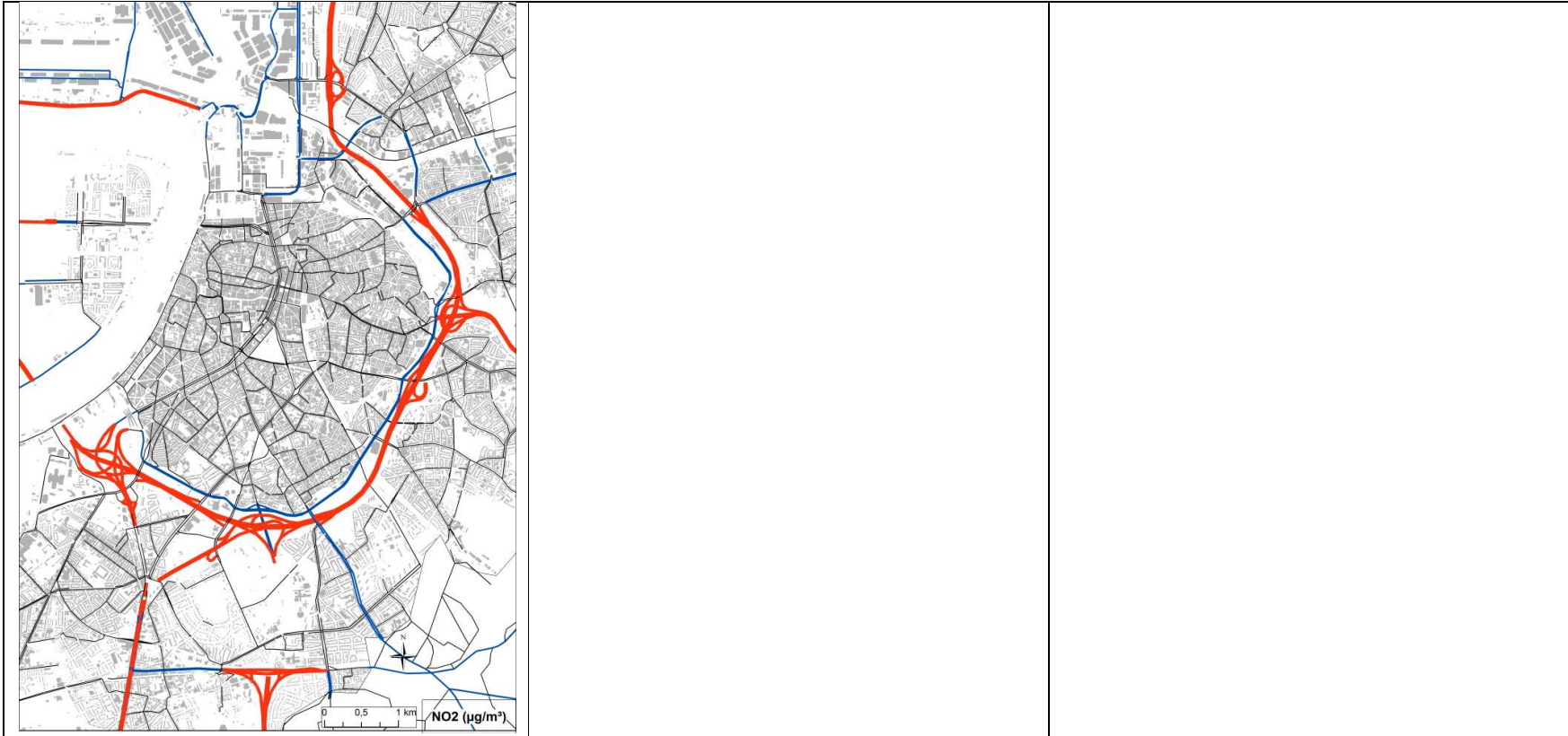


Figure 43 : The road type used in the simulations. In red: highways, in blue: major non-highways, in black: minor roads. Roads inside yunnels are not shown on this map.

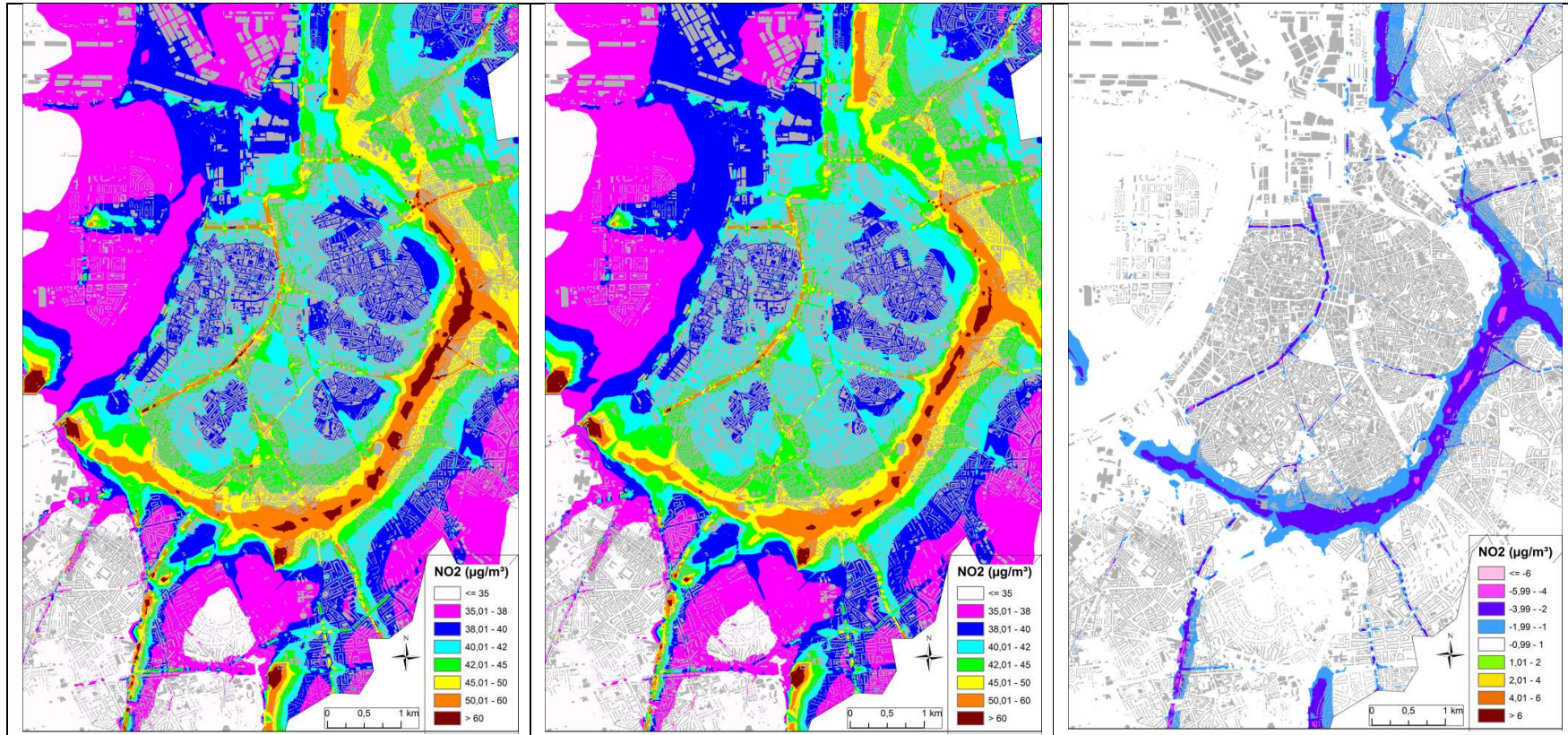


Figure 44 : The weekly averaged NO₂-concentration (in µg/m³) in the reference scenario (left), in the scenario with emissions reduced by 20% in both the subtraction and the addition phase (middle) and the difference between both (right).

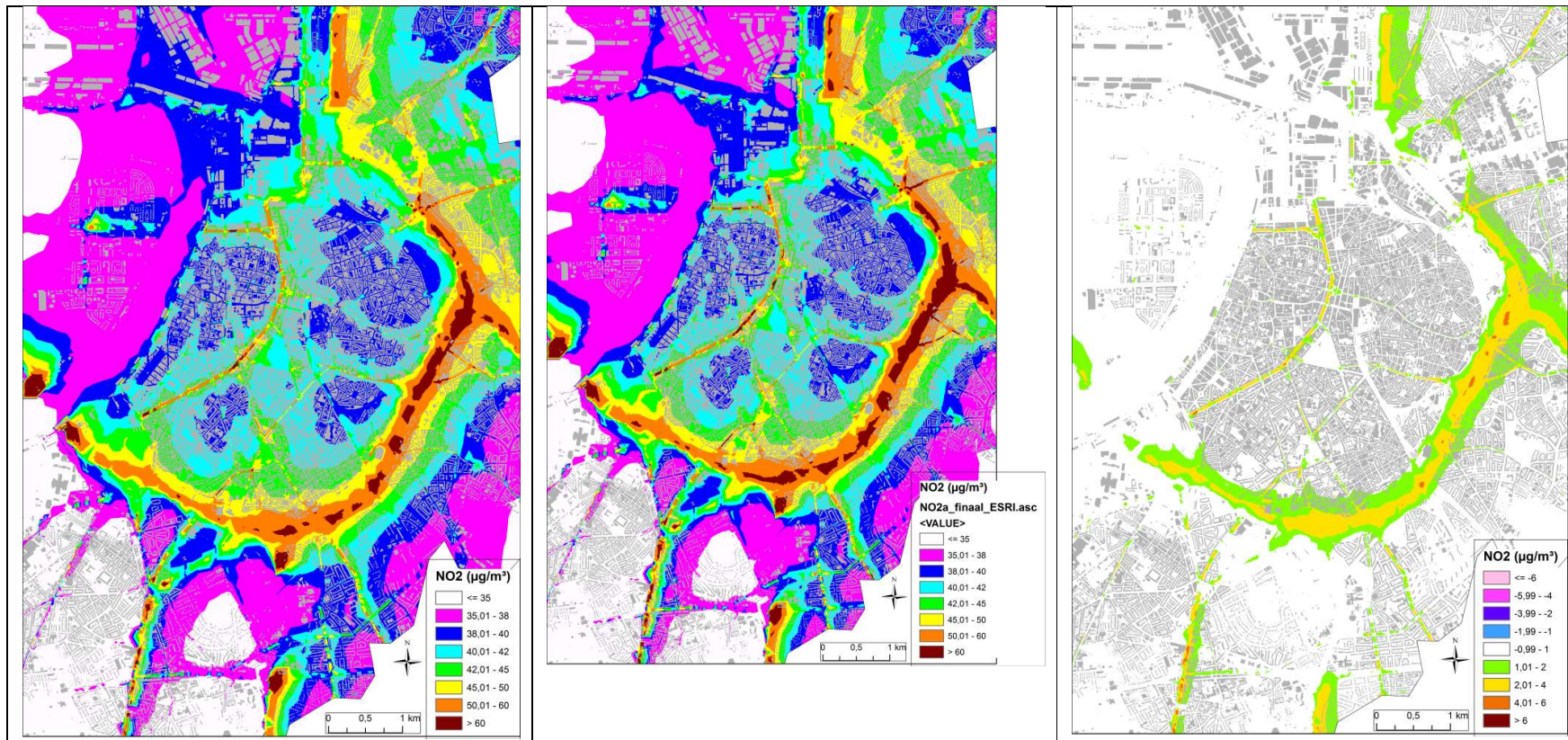


Figure 45 : The weekly averaged NO₂-concentration (in µg/m³) in the reference scenario (left), in the scenario with emissions increased by 20% in both the subtraction and the addition phase (middle) and the difference between both (right).

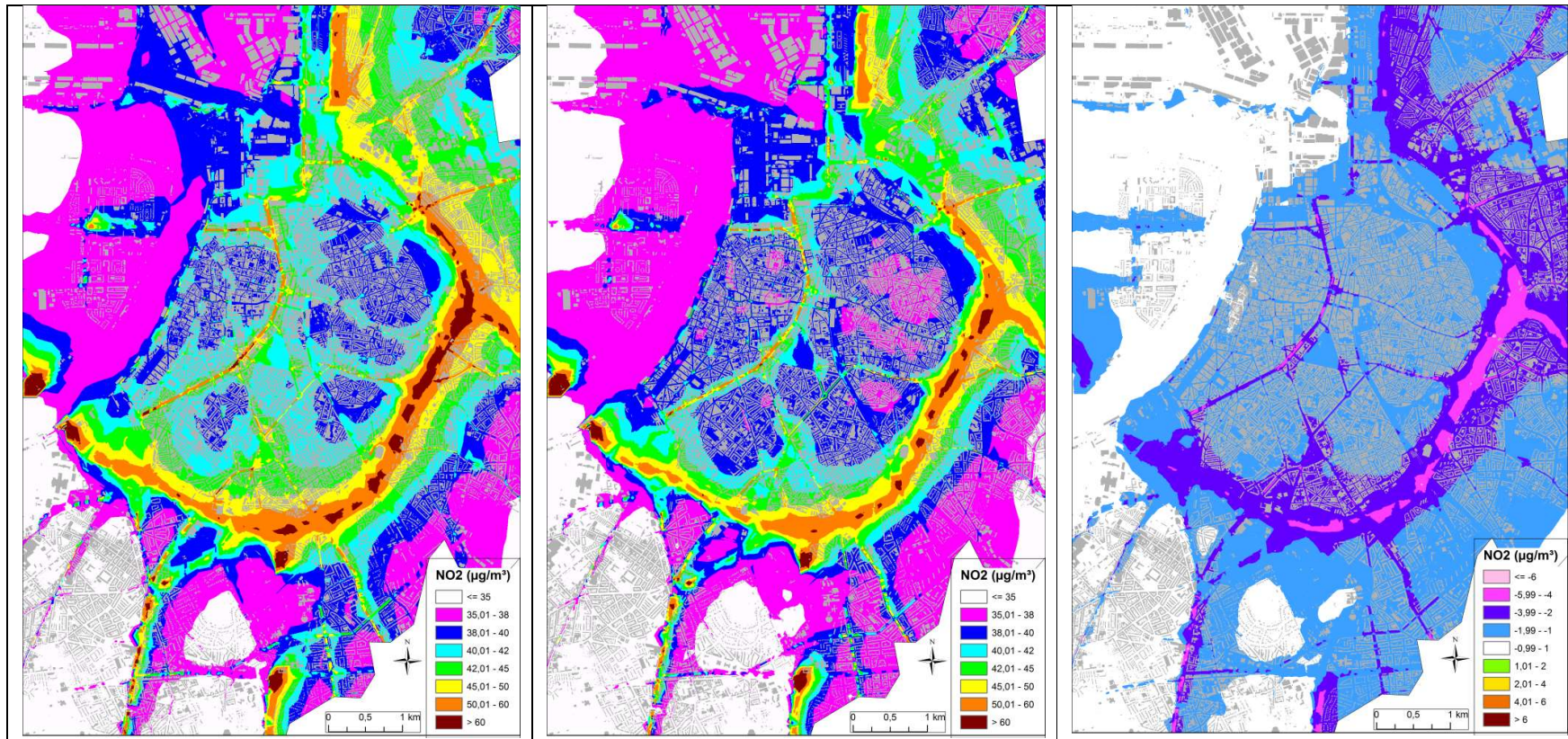


Figure 46 : The weekly averaged NO₂-concentration (in µg/m³) in the reference scenario (left), in the scenario with emissions reduced by 20% in the addition phase (middle) and the difference between both (right).

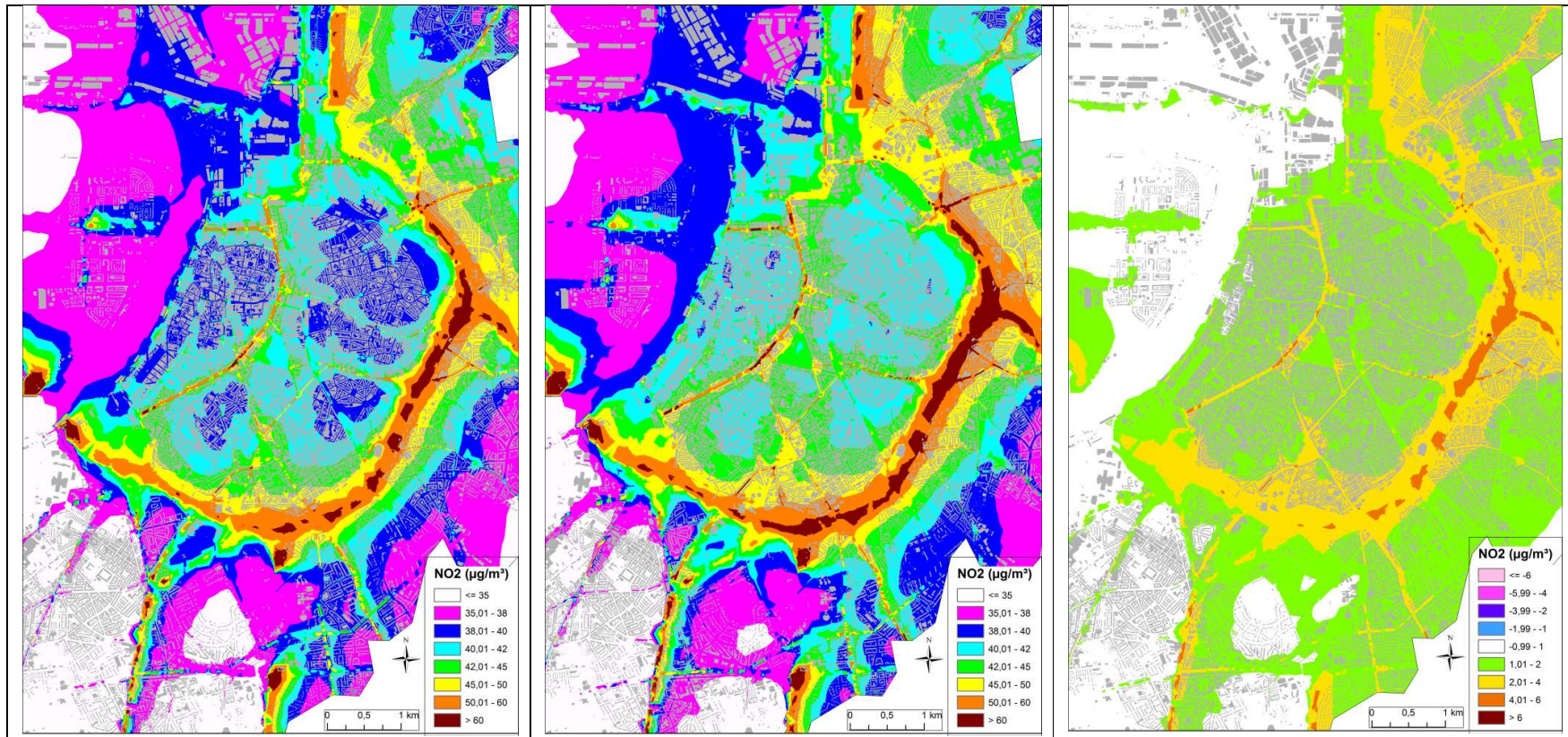


Figure 47 : The weekly averaged NO₂-concentration (in µg/m³) in the reference scenario (left), in the scenario with emissions reduced by 20% in both the addition phase (middle) and the difference between both (right).

		Ref	S1	S2	S6	S7	S3	S4	S5	S8	S9	S10	S11	S12	S13
BIAS	All	6%	5%	4%	5%	1%	25%	1%	1%	-5%	-1%	4%	7%	0%	10%
	Spring	20%	19%	17%	19%	14%	42%	14%	14%	7%	11%	18%	20%	13%	25%
	Autumn	-2%	-3%	-4%	-3%	-6%	15%	-7%	-7%	-12%	-9%	-4%	-1%	-7%	2%
RMSE	All	15%	15%	15%	15%	16%	28%	18%	17%	19%	18%	16%	16%	15%	17%
	Spring	23%	23%	22%	22%	20%	44%	22%	21%	19%	20%	23%	24%	19%	28%
	Autumn	11%	11%	12%	11%	13%	18%	15%	15%	18%	16%	11%	11%	13%	11%
R²	All	0.87	0.88	0.89	0.88	0.88	0.91	0.81	0.79	0.80	0.79	0.89	0.85	0.88	0.87
	Spring	0.80	0.80	0.80	0.80	0.79	0.82	0.65	0.64	0.62	0.63	0.80	0.79	0.78	0.80
	Autumn	0.62	0.62	0.63	0.62	0.60	0.71	0.42	0.40	0.38	0.39	0.63	0.61	0.60	0.63
Slope	All	0.67	0.66	0.62	0.66	0.61	0.74	0.57	0.60	0.54	0.58	0.63	0.71	0.61	0.72
	Spring	0.68	0.67	0.56	0.66	0.52	0.69	0.46	0.55	0.44	0.53	0.57	0.80	0.56	0.80
	Autumn	0.60	0.58	0.49	0.58	0.44	0.60	0.38	0.43	0.36	0.42	0.51	0.67	0.50	0.68
Weighted		21%	21%	23%	21%	24%	27%	29%	28%	30%	28%	23%	20%	23%	20%

Table 12 : Validation parameters for the reference and the sensitivity runs (for labels see Table 13) for both the combined spring and autumn week, the spring week and the autumn week alone. The bottom line is the average of the absolute value of the bias (in %), the RMSE (in %), one minus the R² and the absolute value of one minus the slope. A lower value is better.

Scenario number	Scenario name
S1	Homogeneous NO ₂ /NO _x -ratio of 0.315 in both the subtraction and addition step
S2	Homogeneous NO ₂ /NO _x -ratio of 0.050 in both the subtraction and addition step
S6	Homogeneous NO ₂ /NO _x -ratio of 0.315 in the addition step
S7	Homogeneous NO ₂ /NO _x -ratio of 0.050 in the addition step
S3	Without double counting correction
S4	All urban roads are eliminated (their emission is set to 0) in both the subtraction and addition step. The other roads are not affected.
S5	All urban roads are eliminated (their emission is set to 0) in both the subtraction and addition step. The other roads are scaled up as to preserve total traffic emissions.
S8	All urban roads are eliminated (their emission is set to 0) in the addition step. The other roads are not affected.
S9	All urban roads are eliminated (their emission is set to 0) in the addition step. The other roads are scaled up as to preserve total traffic emissions.
S10	Reduced emission with 20% in both the subtraction and the addition step.
S11	Increased emission with 20% in both the subtraction and the addition step.
S12	Reduced emission with 20% in the addition step.
S13	Increased emission with 20% in the addition step.

Table 13 : The scenario numbers.

CHAPTER 6 HIGHWAY-CAMPAIGN

6.1. INTRODUCTION

This chapter discusses the validation of the IFDM-model with the highway-campaign in Affligem. In §6.2 a short description of the measurement campaign is given, whereas the model setup is discussed in §6.3. The validation results for NO_2 for the daily samplers are studied in §6.4. The validation study for BC is given in §6.5. As the traffic contribution to BC is large and as the time resolution of the BC measurements is high, a sensitivity study is also performed in this section (§6.5.3). Validation results for PM_{10} and $\text{PM}_{2.5}$ are touched in §6.6. At one location, high resolution measurements for NO_x and NO_2 were made. The validation with these data can be found in §6.7. The sensitivity to another set of input parameters is discussed in §6.8, whereas in §6.9 is discussed what we can learn from the traffic data in this campaign. §6.10 proposes some model adaptations, whereas §6.11 discusses the effect of these adaptations on the validation. Thereafter (§6.12), we take a look at the influence of the aggregation time on the validation statistics. Finally, some conclusions (§6.13) are presented.

6.2. MEASUREMENT CAMPAIGN

In the framework of the ATMOSYS project, measurements have been made close to the E40-highway in Affligem. More information about the measurements itself can be found in Roet (2013). The measurement locations can be found in Figure 48. Measurements for BC, PM_{10} and $\text{PM}_{2.5}$ have been made at locations AF07, AF02, AF04 and AF05, high resolution measurements for NO_x and NO_2 only at AF07, while low resolution measurements for NO_2 have been done at all locations. Measurements were made from the 20th of April 2012 until the 28th of December 2012 for NO_2 (low resolution), until the 7th of January for PM_{10} and $\text{PM}_{2.5}$ and until the 7th of February 2013 for BC, NO_2 (high resolution) and NO_x .

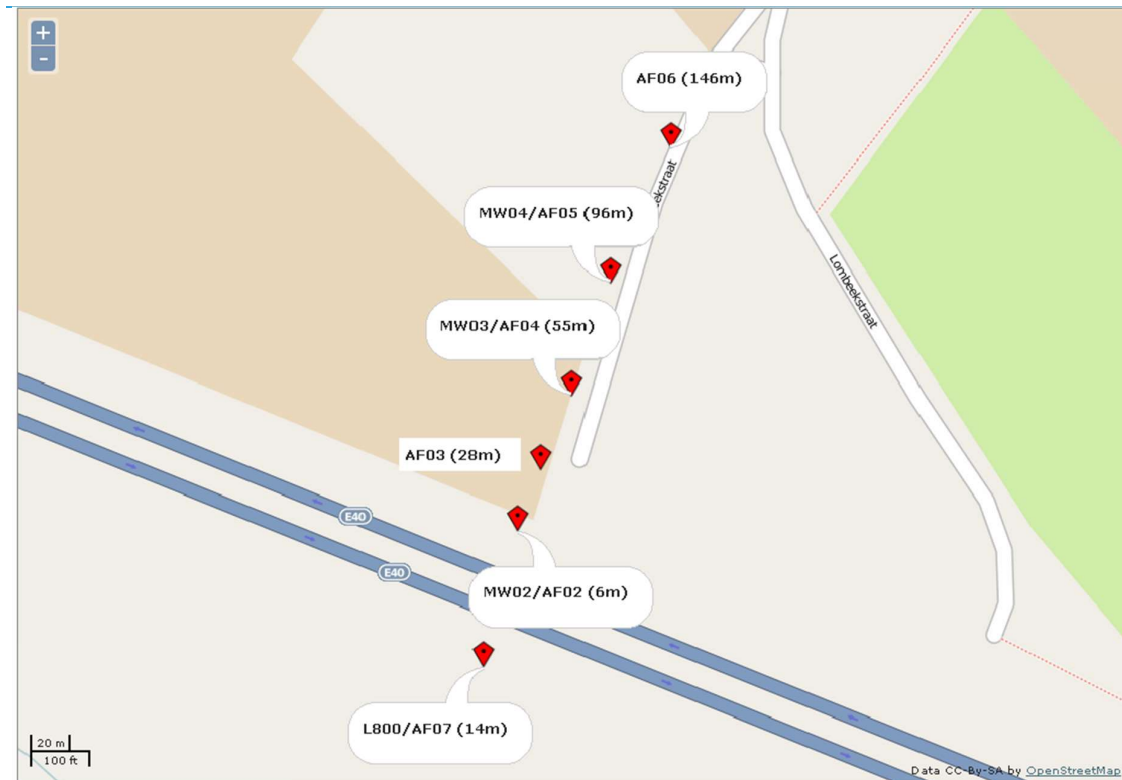


Figure 48 : Locations of the measurements during the highway campaign. Figure is taken from Roet (2013).

6.3. MODEL PARAMETRIZATION CHOICES AND INPUT DATA

- The parameterization that was used is the same as the parameterization used in the normal urban case (e.g. the web application IFDM-traffic; Lefebvre et al., 2010b; Lefebvre et al., 2013a) except for the parameters linked to the roughness length. Indeed, as the location in Affligem is rather open (low surface roughness), using an urban parameterization would lead to deviations from the reality (Op 't Eyndt et al., 2012) (see also §6.8).
- Background concentrations for NO₂, NO_x and O₃ are taken from Idegem, if available. Otherwise they are taken from Zwevegem (Figure 49).
- Meteorology is measured locally at AF07. If this data was missing, data from Ghent has been taken (8.8% of all cases).
- Emissions were based on the IMMI-2 2010BAU emissions and then, based on the estimates of this report (Lefebvre et al., 2010b) decreased with about 11% in order to obtain emissions for 2012. Also the NO₂/NO_x-ratio has been adapted for 2012 (to about 0.3). An emission spread over three traffic lanes 50, 30 and 20% has been estimated, for every direction, to take into account the extra heavy duty vehicle occupation on the righthernmost lanes.

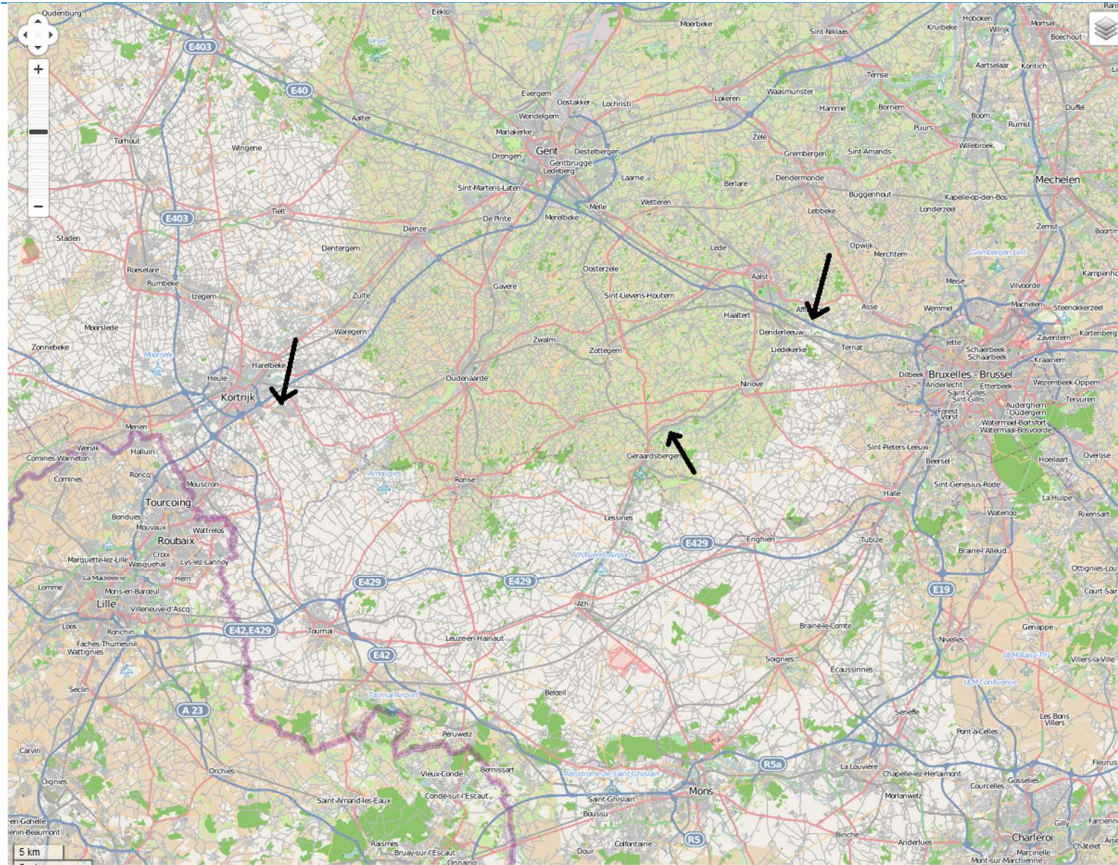


Figure 49 : The location of Zwevegem (westernmost arrow), Idegem (central arrow) and Affligem (righternmost arrow).

6.4. NO₂

6.4.1. SPATIAL VALIDATION

On Figure 50, the spatial validation for NO₂ is shown. The model slightly underestimates the concentrations at location AF02 and overestimates at all other locations. These overestimations are due to too high background concentrations (see later). When we correct for this (dashed lines), only the underestimation at AF02 remains. Furthermore, we see that the background concentrations are much lower than the measured/modelled concentrations and thus that the increase in concentrations due to the highway extends much further from the highway than the distance modelled/measured here.

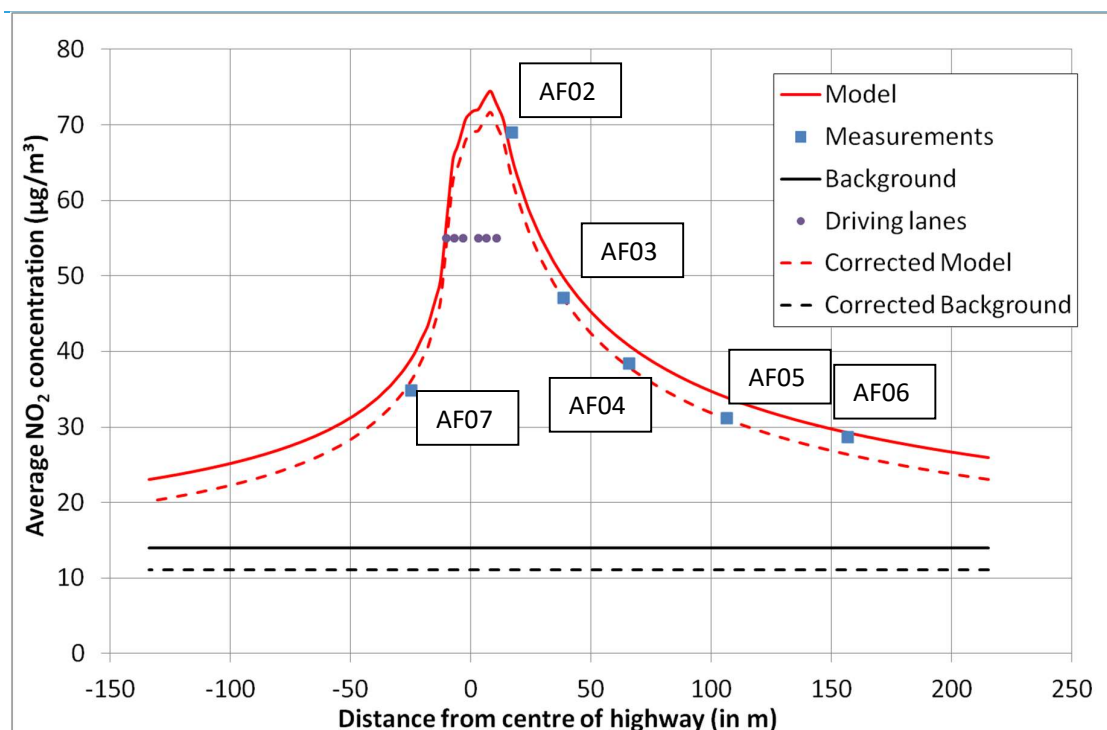


Figure 50 : Model values (red), measurements (blue squares) and background concentrations (black line) (NO_2 , all in $\mu\text{g}/\text{m}^3$) plotted by their distance to the centre of the highway. Purple dots represent the location (and thus not the concentrations) of the different driving lanes. The red dashed lines shows the model values corrected for too high background concentrations, the new background is given in the dashed black line.

6.4.2. TEMPORAL VALIDATION

Figure 51 shows the temporal validation plot for the location southwest of the highway. In general, the correlation between model results and measurements is good, with a relatively high R^2 , a slope of the regression line close to 1 and a small intercept of the regression line. However, there is one point (blue diamond on Figure 51) which cannot be explained by our model. The model estimates very high concentrations during this week at this location, while the measurements are relatively low. In order to find out if this is due to an anomaly in the model or to an anomaly in the measurements, we compare the weekly averaged BC measurements at AF07 with the NO_2 measurements at the same location (Figure 52). The week representing the blue diamond in Figure 51 is also an outlier in Figure 52. As a result, there can be doubts about the NO_2 measurement for this week at this location. Eliminating this outlier in Figure 51 increases the R^2 from 0.60 to 0.75.

For the other locations, the correlation between model and measurements is quite well, although slightly less good than for AF07 (Figure 53-Figure 56). Furthermore, the slopes of the regression lines remain close to 1, while the intercepts do not deviate too much from 0. The exception is the location which is the furthest from the highway (Figure 57, AF06). The source of this discrepancy is unknown for the moment.

Figure 58 shows the temporal evolution of the average of all the measurement locations both in model (red) and in the measurements (blue). The one striking feature in this graph is the large deviation of the model during some weeks at the end of the period. This can also easily be seen in the model bias (purple line). How can this be explained? A clue is given by the green line, which is constructed by subtracting from the background concentrations used in the model the minimum of the six measurements made in Affligem during the same week. This value is most of the time negative, which was to be expected, as during a week the highway will have had an influence on all of the measurement locations close to it (as winds will have blown from multiple directions during this week) and none of the measurements close to the highway will be a background value. However, during some weeks at the end of November and in December this value is positive, showing that we provided the model with background concentrations which are already higher (and in some cases more than $20 \mu\text{g}/\text{m}^3$) than the minimum of the 6 measurement locations close to the highway. This will automatically result in a model bias, as the highway will only be adding to this background concentration. The explanation can be found in the light blue line of Figure 58, which shows the percentage of the time that no data from Idegem was available. During this period, data from Zwevegem has been used. However, this location is further away from Affligem and is not a real background station. As a result, background concentrations are estimated too high and the model exhibits a bias. Can we correct for this bias? In Figure 59, a scatter plot shows the correlation between the percentage data lacking in Idegem and the difference between the background concentration and the minimum of the measurement locations. The slope of the regression line can tell us something about the overestimation of the background concentrations. This overestimation amounts to a whopping $19 \mu\text{g}/\text{m}^3$ when only data from Zwevegem is available. As 15% of the time (on average), the data from Idegem is missing, we can correct our temporal averages with $2.85 \mu\text{g}/\text{m}^3$, giving the dashed lines on Figure 50. In Figure 51 and Figure 53-Figure 57, the weeks with a data lack of at least 70% (no weeks have a data lack between 20% and 70%) have been given another symbol, as to distinguish them from the other data points. Eliminating these points from the trendlines leads in general to a higher R^2 and a lower slope of the regression line. This lower slope points to an overestimation of the low concentrations and an underestimation of the high concentrations, which has also been seen in other studies. However, the error made by the model close to the critical value of $40 \mu\text{g}/\text{m}^3$ is small, making the model sufficient performant for regulatory purposes, which are most important for NO_2 to be found in the annual limit value. This can also be concluded from the spatial validation, as there is only a small deviation from the measurements when averaged over a longer period, with the exception of AF06 (Figure 57).

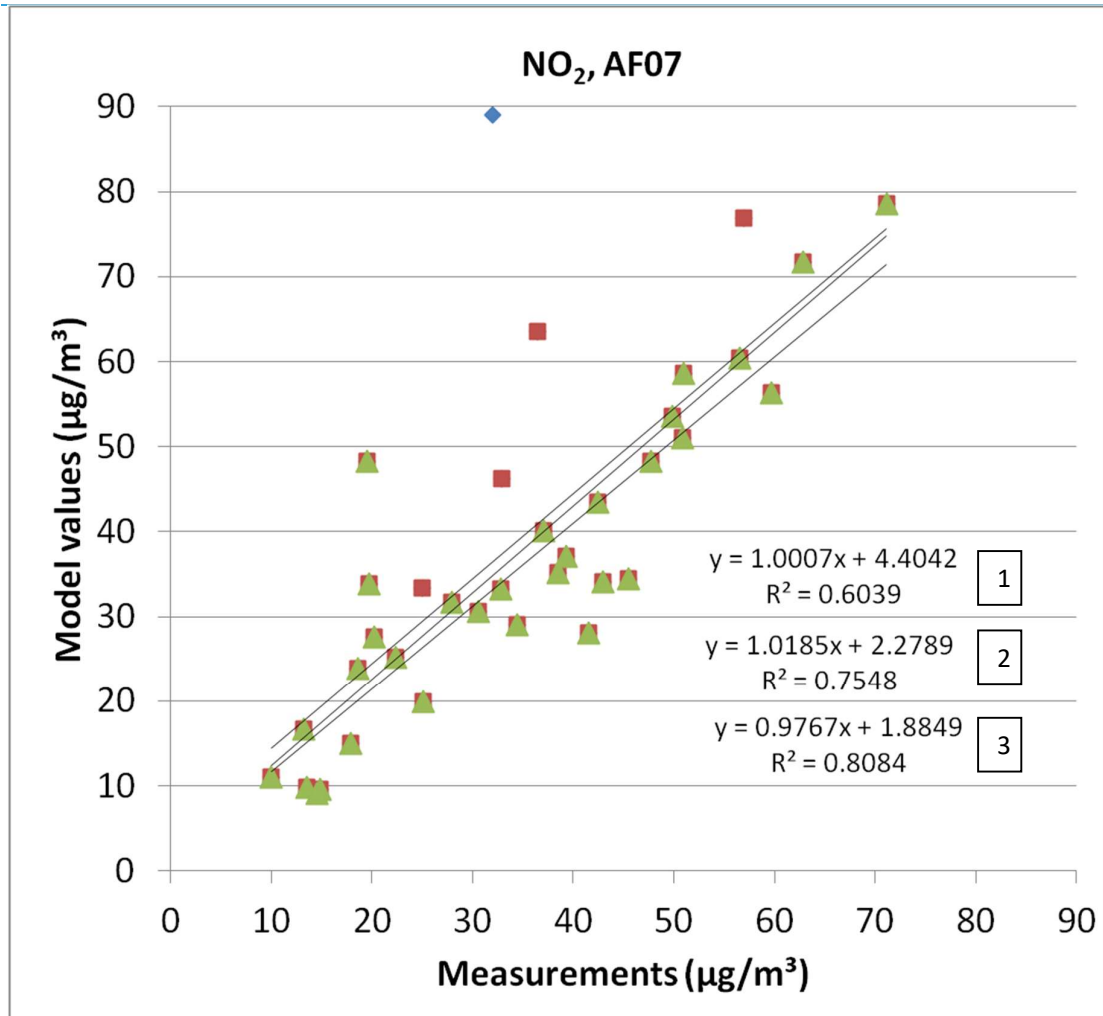


Figure 51 : Scatter plot of the modelled NO₂ concentration at AF07 on the measured concentration (both in µg/m³). Every symbol represents one week. The blue symbol represents the week ending on the 26th of October 2012. The red dots without a triangle represent the weeks at which the background concentrations from Idegem were unavailable. Three trendlines (1, 2, 3) are plotted; one with all data (1); one without the week ending on the 26th of October 2012 (2) and one without the week ending on the 26th of October 2012 and the weeks lacking the Idegem background concentrations (3).

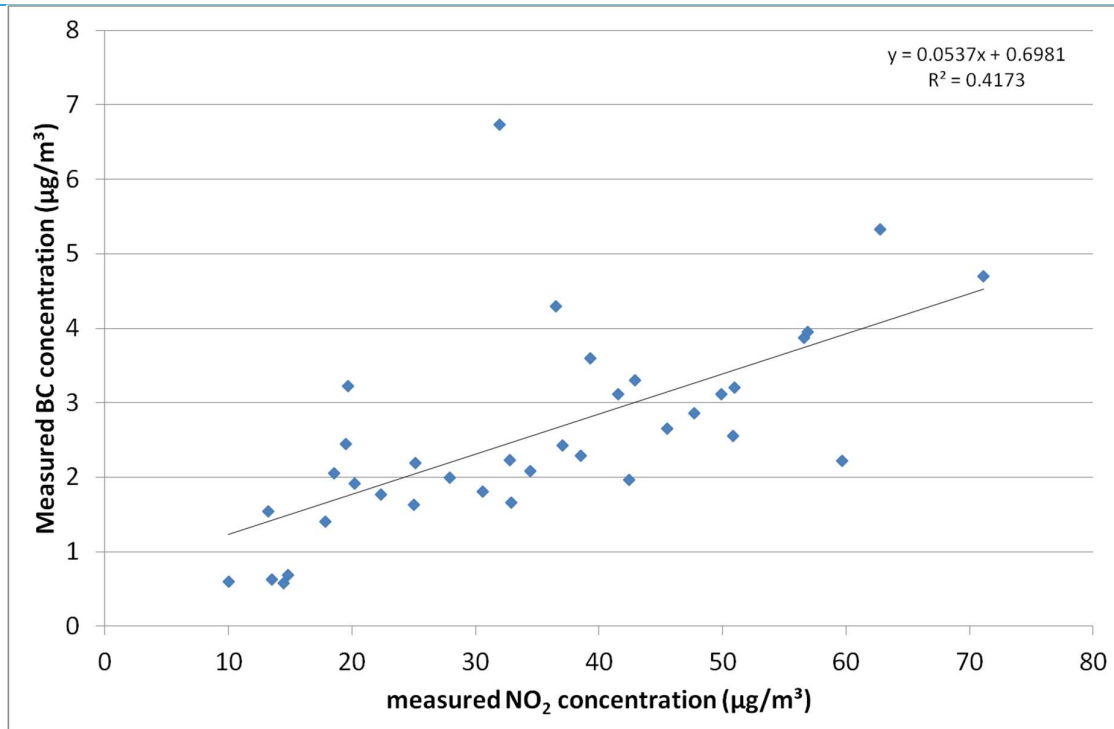


Figure 52 : Scatter plot of the weekly averaged BC concentrations (Y-axis, in $\mu\text{g}/\text{m}^3$) on the weekly averaged NO_2 concentrations (X-axis, in $\mu\text{g}/\text{m}^3$) for AF07. The week ending on the 26th of October 2012 is the uppermost point of the graph (31.94; 6.73).

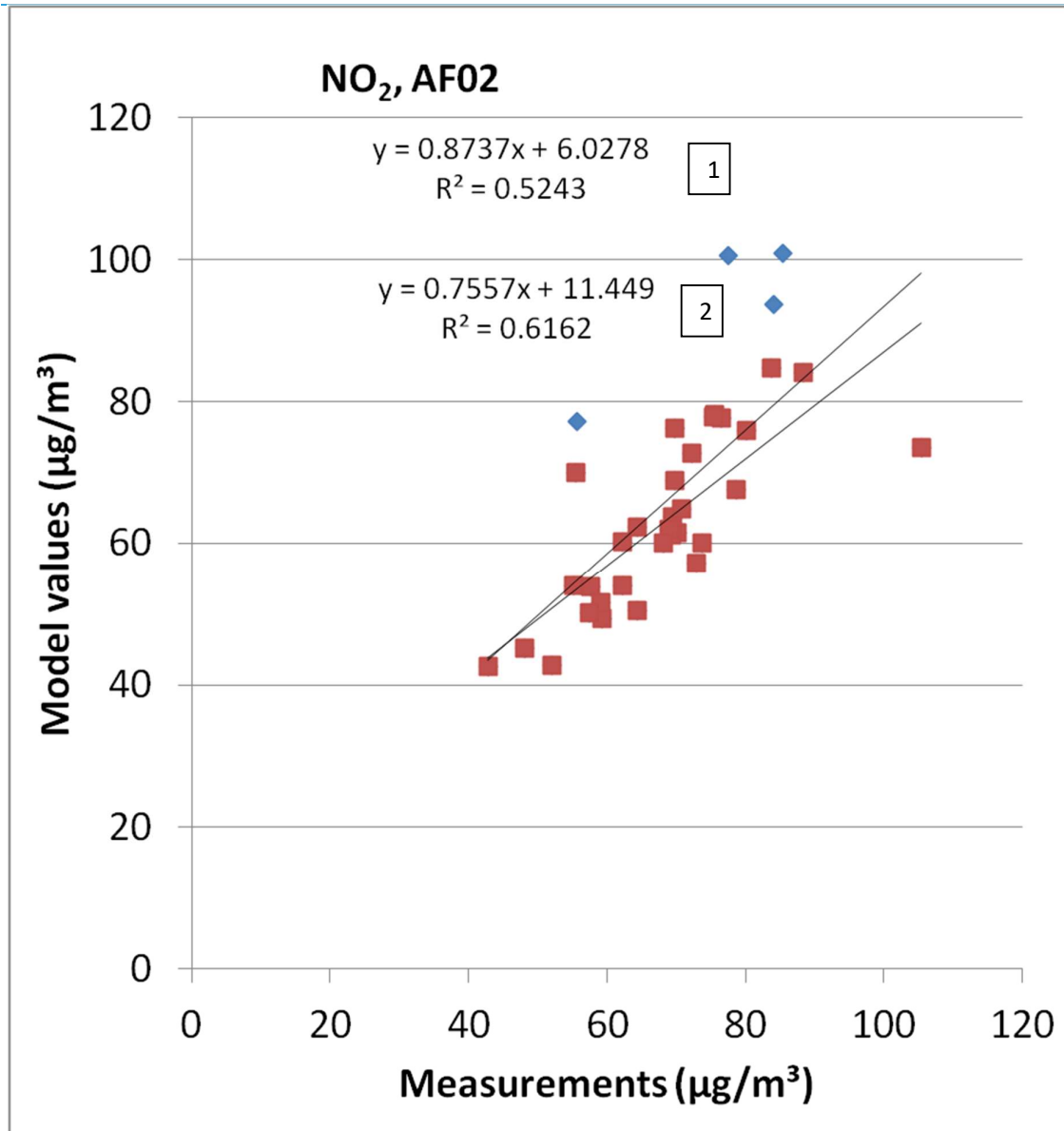


Figure 53 : Scatter plot of the modelled NO₂ concentration at AF02 on the measured concentration (both in $\mu\text{g}/\text{m}^3$). Every symbol represents one week. The blue diamonds represent the weeks with significant lack of Idegem background concentration data. Two trendlines (1,2) are presented: one of all the data (1), and one of only the red squares (2).

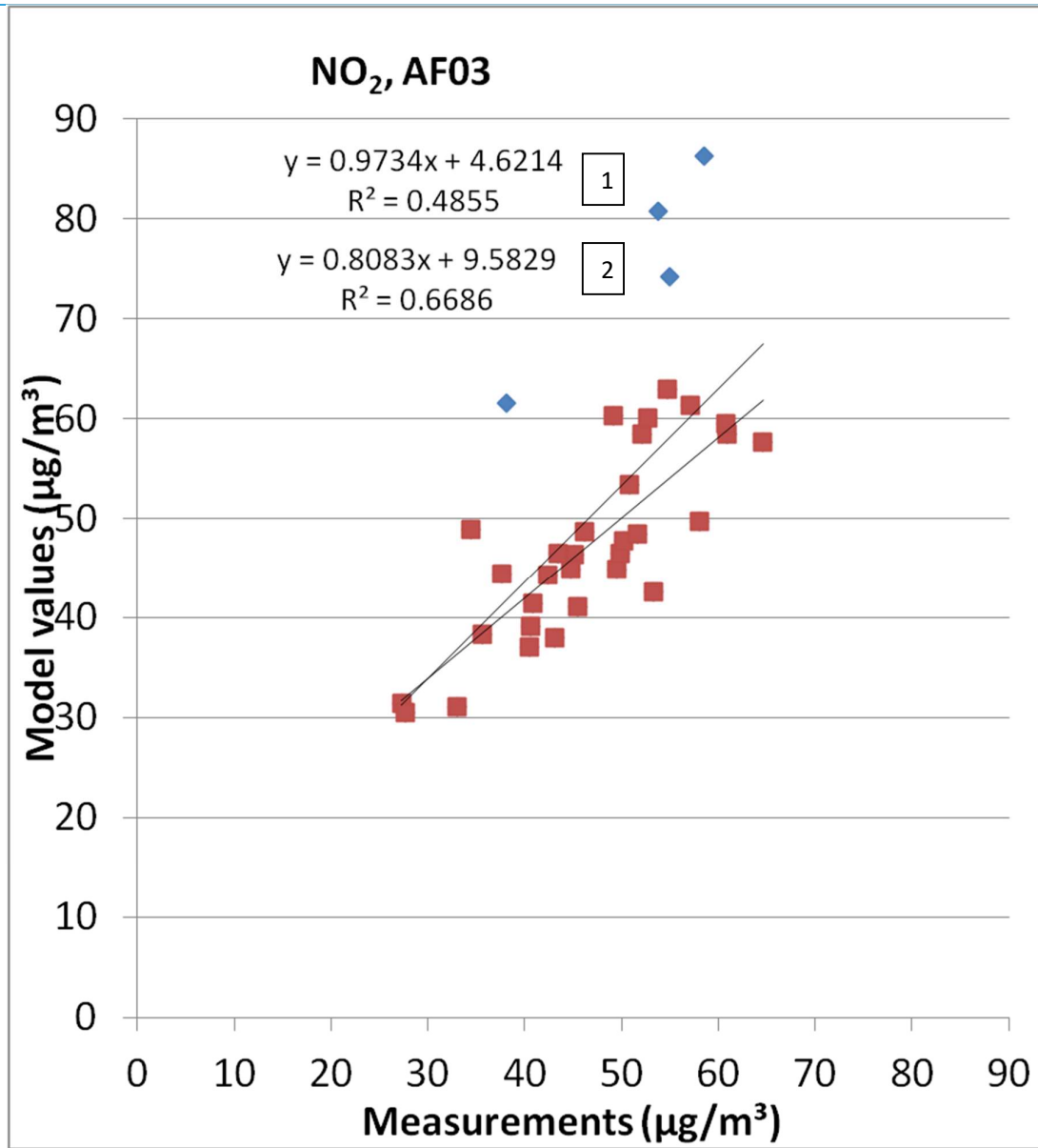


Figure 54 : Scatter plot of the modelled NO₂ concentration at AF03 on the measured concentration (both in µg/m³). Every symbol represents one week. The blue diamonds represent the weeks with significant lack of Idegem background concentration data. Two trendlines (1,2) are presented: one of all the data (1), and one of only the red squares (2).

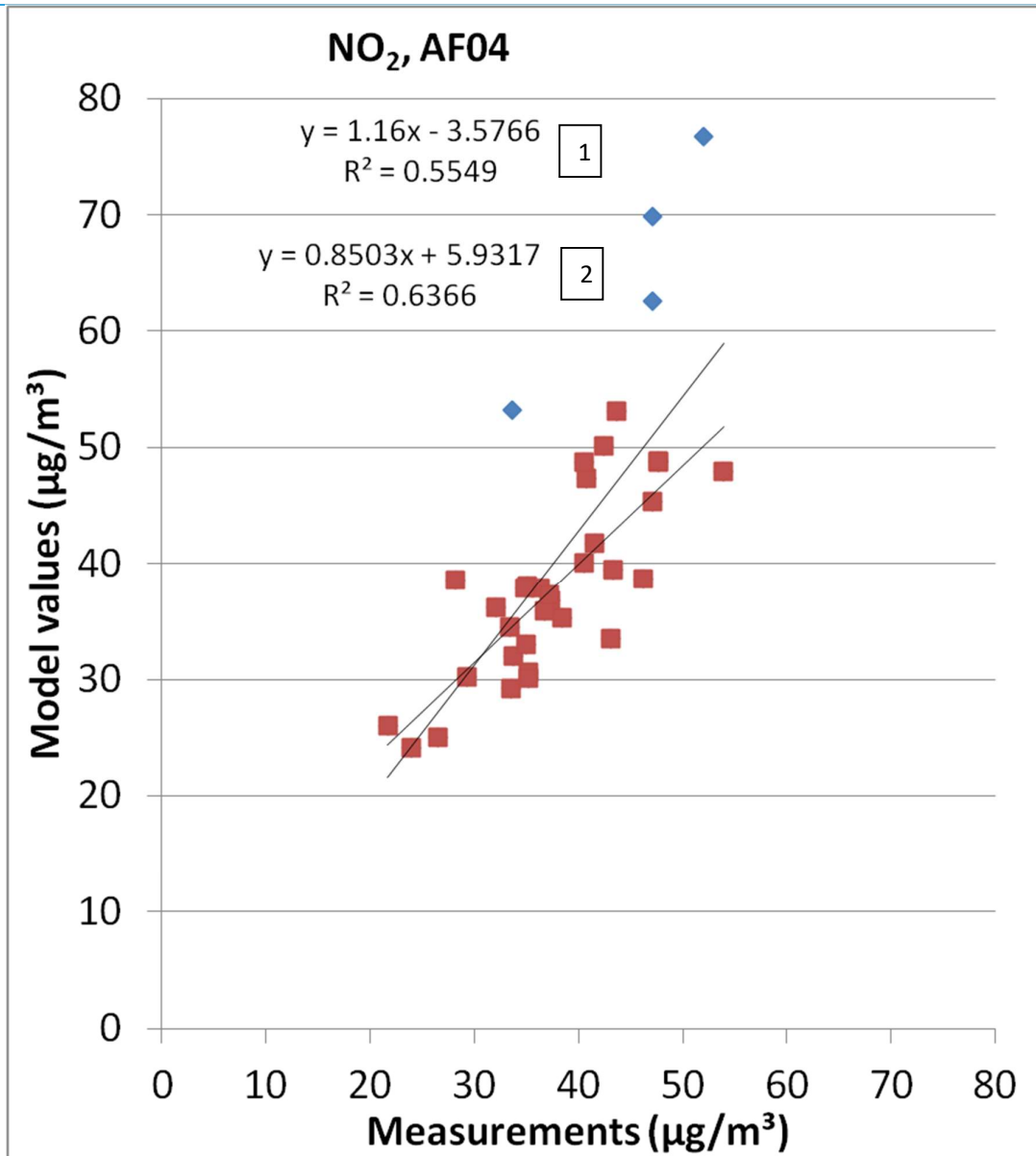


Figure 55 : Scatter plot of the modelled NO₂ concentration at AF04 on the measured concentration (both in $\mu\text{g}/\text{m}^3$). Every symbol represents one week. The blue diamonds represent the weeks with significant lack of Idegem background concentration data. Two trendlines (1,2) are presented: one of all the data (1), and one of only the red squares (2).

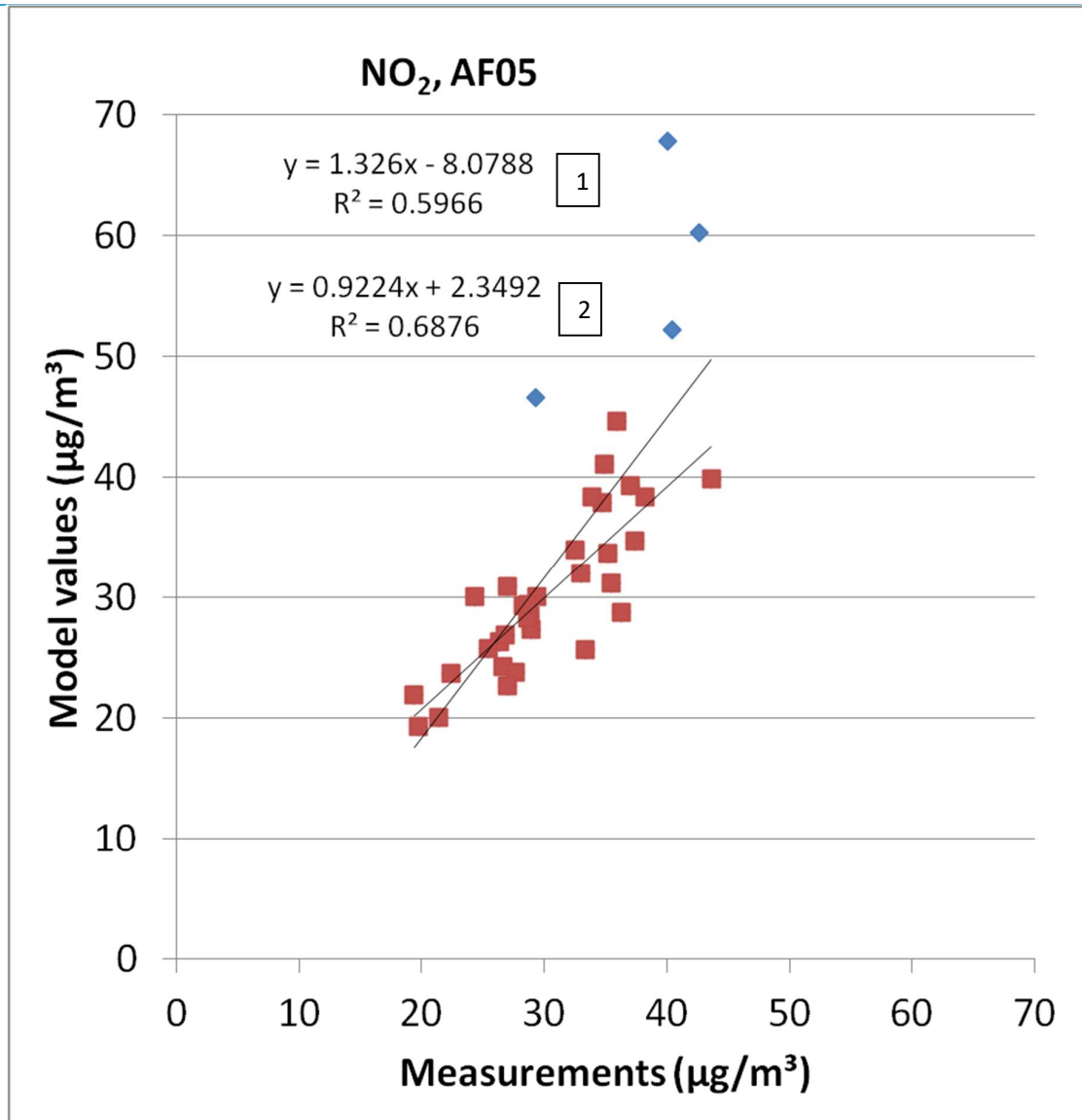


Figure 56 : Scatter plot of the modelled NO₂ concentration at AF05 on the measured concentration (both in $\mu\text{g}/\text{m}^3$). Every symbol represents one week. The blue diamonds represent the weeks with significant lack of Idegem background concentration data. Two trendlines (1,2) are presented: one of all the data (1), and one of only the red squares (2).

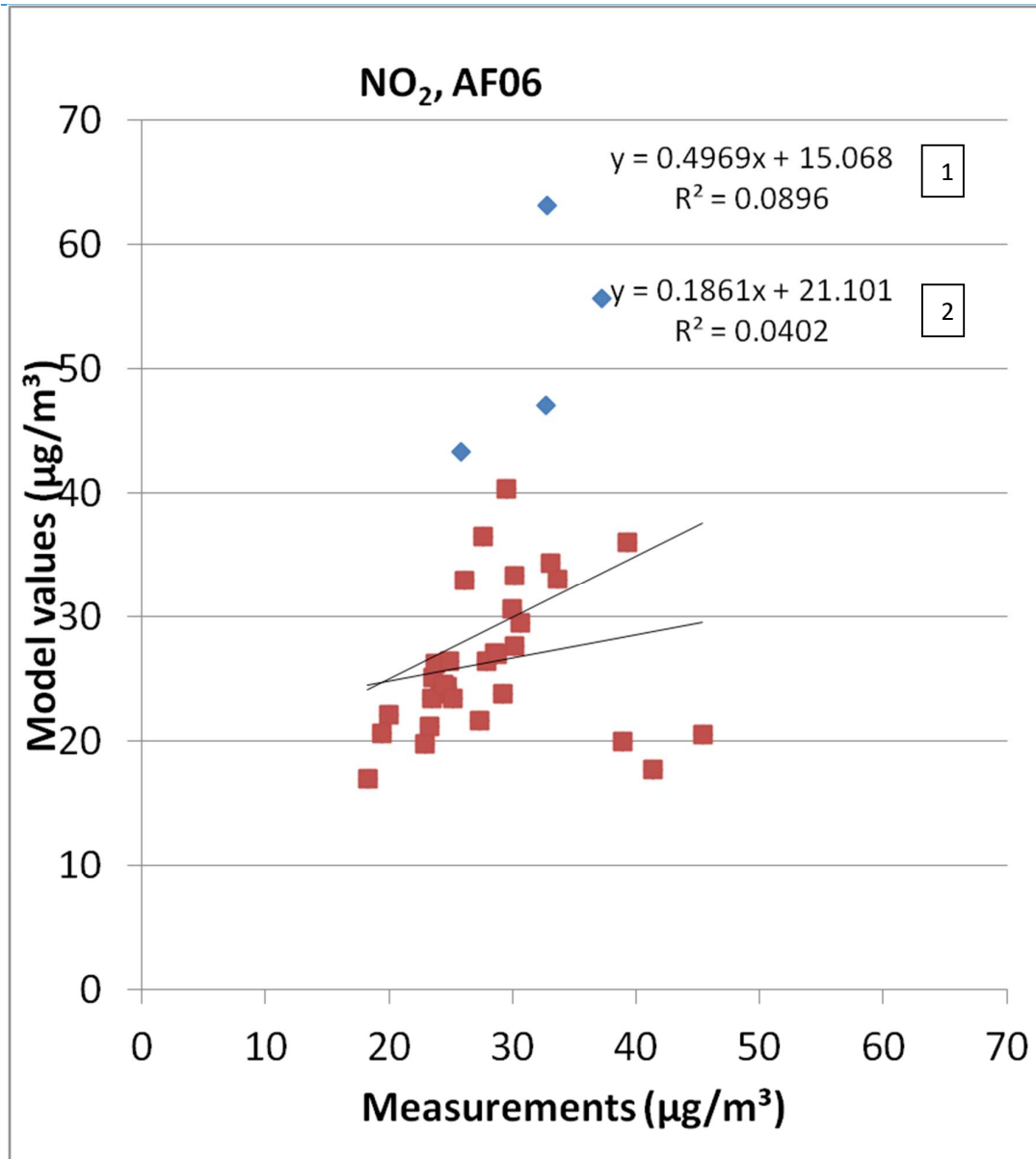


Figure 57 : Scatter plot of the modelled NO₂ concentration at AF06 on the measured concentration (both in $\mu\text{g}/\text{m}^3$). Every symbol represents one week. The blue diamonds represent the weeks with significant lack of Idegem background concentration data. Two trendlines (1,2) are presented: one of all the data (1), and one of only the red squares (2).

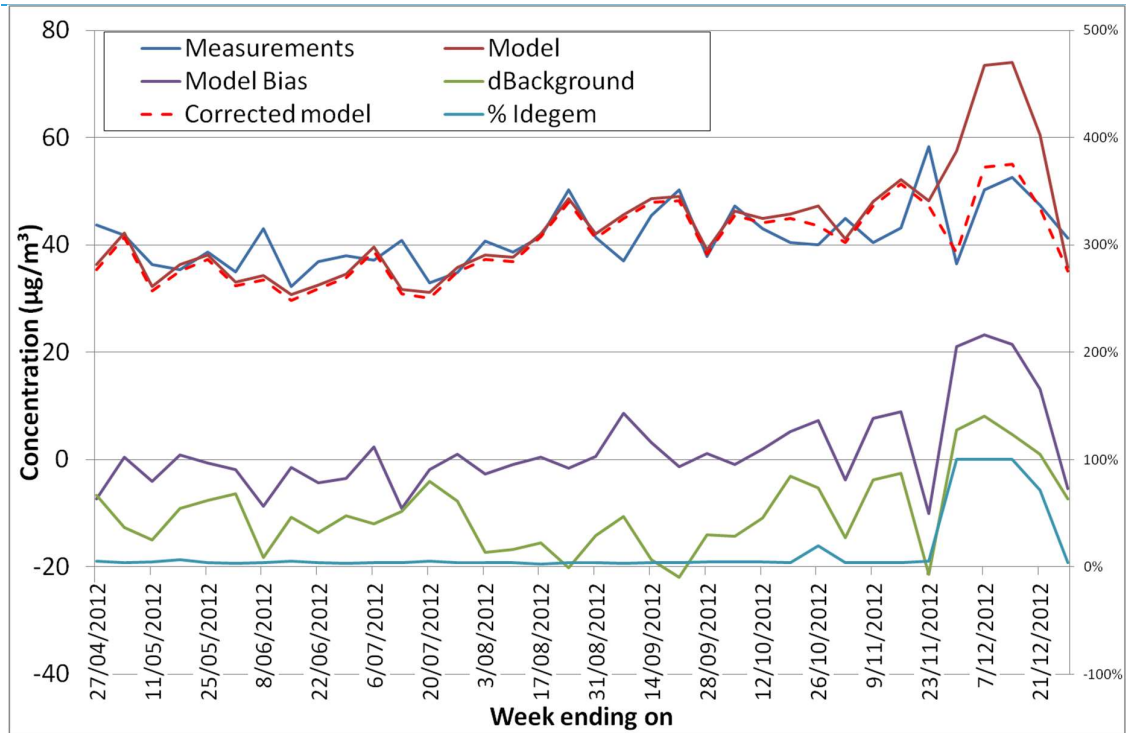


Figure 58 : Measured (blue) and modelled (red) concentrations (left scale, in $\mu\text{g}/\text{m}^3$) averaged over all measurement locations for NO_2 . The difference between these lines is given by the purple line (left scale, in $\mu\text{g}/\text{m}^3$). The green line represents the difference of the background concentration with the minimum of the six measurement locations for that week (left scale, in $\mu\text{g}/\text{m}^3$). The light blue line on the bottom of the graph represents the percentage of the time that Idegem was not available for the background concentrations (right scale, in %). The red dashed line is model value corrected for the background deviation (left scale, in %).

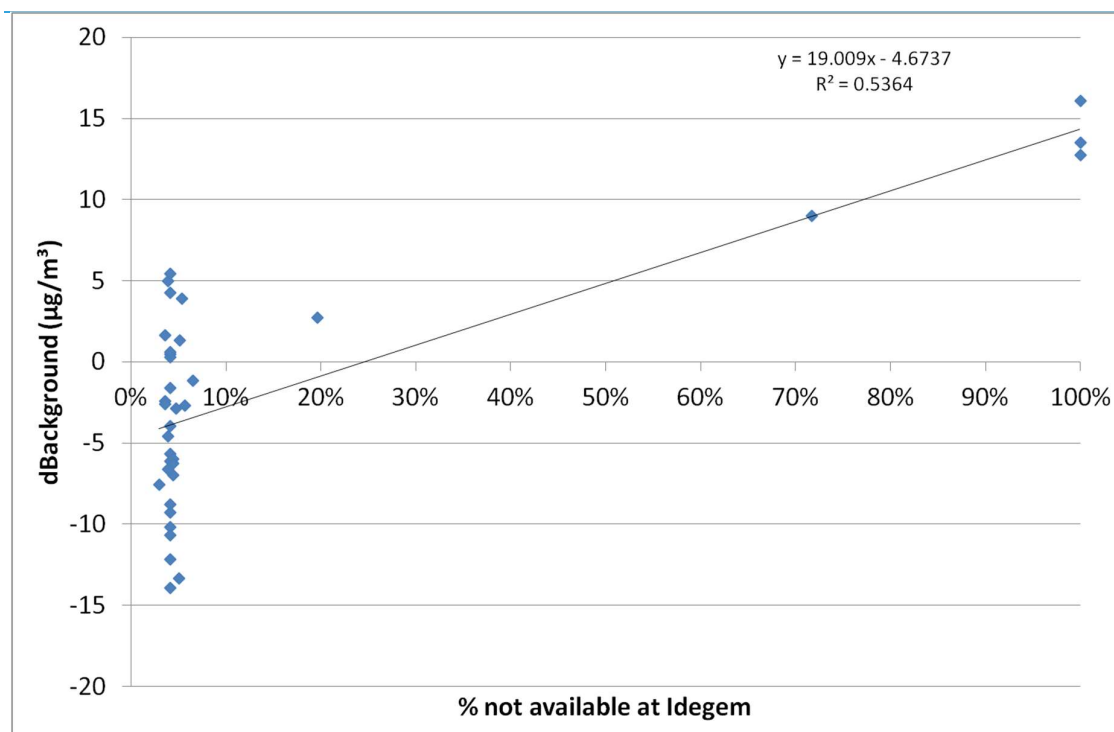


Figure 59 : Scatter plot comparing the difference of the background concentration and the minimum of the six measurement locations for that week (Y-axis, in $\mu\text{g}/\text{m}^3$) with the percentage of the time that Idegem was not available for the background concentrations (X-axis, in %).

6.5. BC

6.5.1. SPATIAL VALIDATION

First of all, no emissions were available for BC. However, emissions were available for the closely linked pollutant EC (Decoene, 2013). Therefore, we have done the simulations for EC, and we have used a transformation factor of 1.5 ($\text{BC}=1.5 \cdot \text{EC}$) (Van Poppel et al., 2012; Dons, personal communication) in order to obtain BC results. However it should be mentioned that this factor can be time and location dependant, which has not been taken into account in this study.

For BC, unfortunately no background concentrations are available. However, BC is supposed to be a passive pollutant and thus we can, at least for the spatial validation, estimate the background concentration ourselves and add it to the model values. This has been done in Figure 60. A background concentration of $0.88 \mu\text{g}/\text{m}^3$ has been estimated on the basis of these results (best fit between model and measurements, based on visual inspection of the graph).

A background concentration could also be estimated by taking, every half hour the minimum of the four measurements, supposing that at least one of the measurements is outside the influence of the highway. However, this gives a higher value which could be due to half hours with light but variable winds, on which none of the four measurement locations is a background location.

The spatial validation (of the gradients close to the highway, as the absolute values are used for the best fit of the background) of the BC-results is good, with only a slight overestimation at AF07 and good estimations at the other locations. As with NO₂, it is shown that the effect of the highway extends further down the road than the 200m distance which was modelled here.

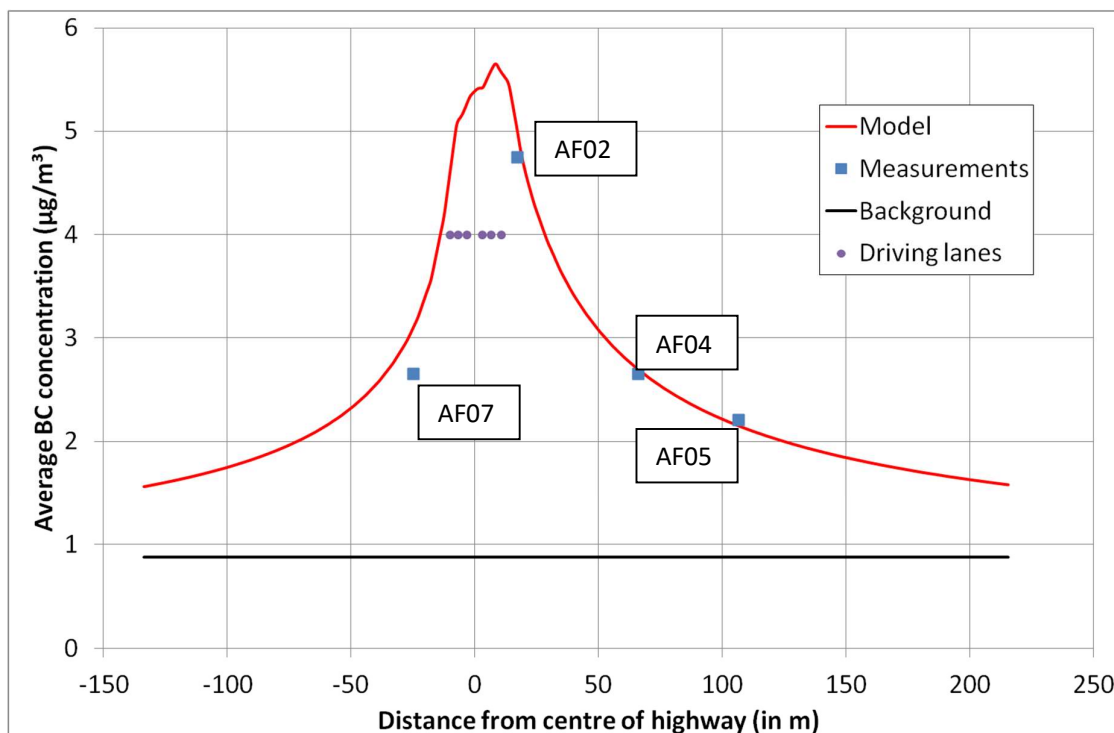


Figure 60 : Model values (red), measurements (blue squares) and background concentrations (black line) (BC, all in $\mu\text{g}/\text{m}^3$) plotted by their distance to the centre of the highway. Purple dots represent the location (and thus not the concentrations) of the different driving lanes. A constant background concentration of $0.88 \mu\text{g}/\text{m}^3$ has been used.

6.5.2. TEMPORAL VALIDATION

In this section, the half-hourly measurements and the half-hourly modelling values are compared for the different stations. For the measurements, the minimum value of the four measurements has been subtracted, while for the modelling, no background concentration has been taken into account.

For all stations (Figure 61-Figure 64), a large cloud of points can be found around the regression line. However, several points show very high model values compared to relatively low measurement values. The origin of these points will be discussed later. The regression line shows a slope reasonably close to 1 (albeit too high especially for AF07), a small intercept and a decrease of the R² from southwest (location AF07) to northeast.

Points on the X-axis (model values = 0) are in general measurements for which the wind does not blow from highway to the measurement location, so the concentrations modelled in these locations are zero. Nevertheless, the measurement is not the lowest of the four measurement locations during this half hour. Points on the Y-axis (measurement = 0) are for points where the measurement is the lowest of the four measurement locations during the corresponding half hour. However, the wind is directed from the highway to the measurement location, so there is a modelled concentrations different from zero.

It is thus clear that the model is not very good in estimating the halfhourly concentrations. However, is this still true for the daily averaged concentrations?

When taking the daily averages the situation improves strongly for the points closest to the highway (Figure 65-Figure 66). The correlation coefficients soar, while the slope and intercept remain close to respectively 1 and 0. For the points further away (Figure 67-Figure 68), this is not (or less) the case, with middling correlation coefficients, low slopes and high intercept values. The same can be said when averaging over one week (Figure 69-Figure 72).

The lack in model performance for the last points is strange, as for NO₂, the model performs well for these points (compare Figure 71 with Figure 55 and Figure 72 with Figure 56). The correlation between the model values for NO₂ and BC at these locations is high; however, this is not true for the measured concentrations (Figure 73). However, for the points closer to the highway, a high correlation is present (Figure 52). As a result, it is impossible for IFDM to simulate both NO₂ and BC well at the points further away from the highway. The source of the lack of correlation between NO₂ and BC in the points further way from the highway is still unknown.

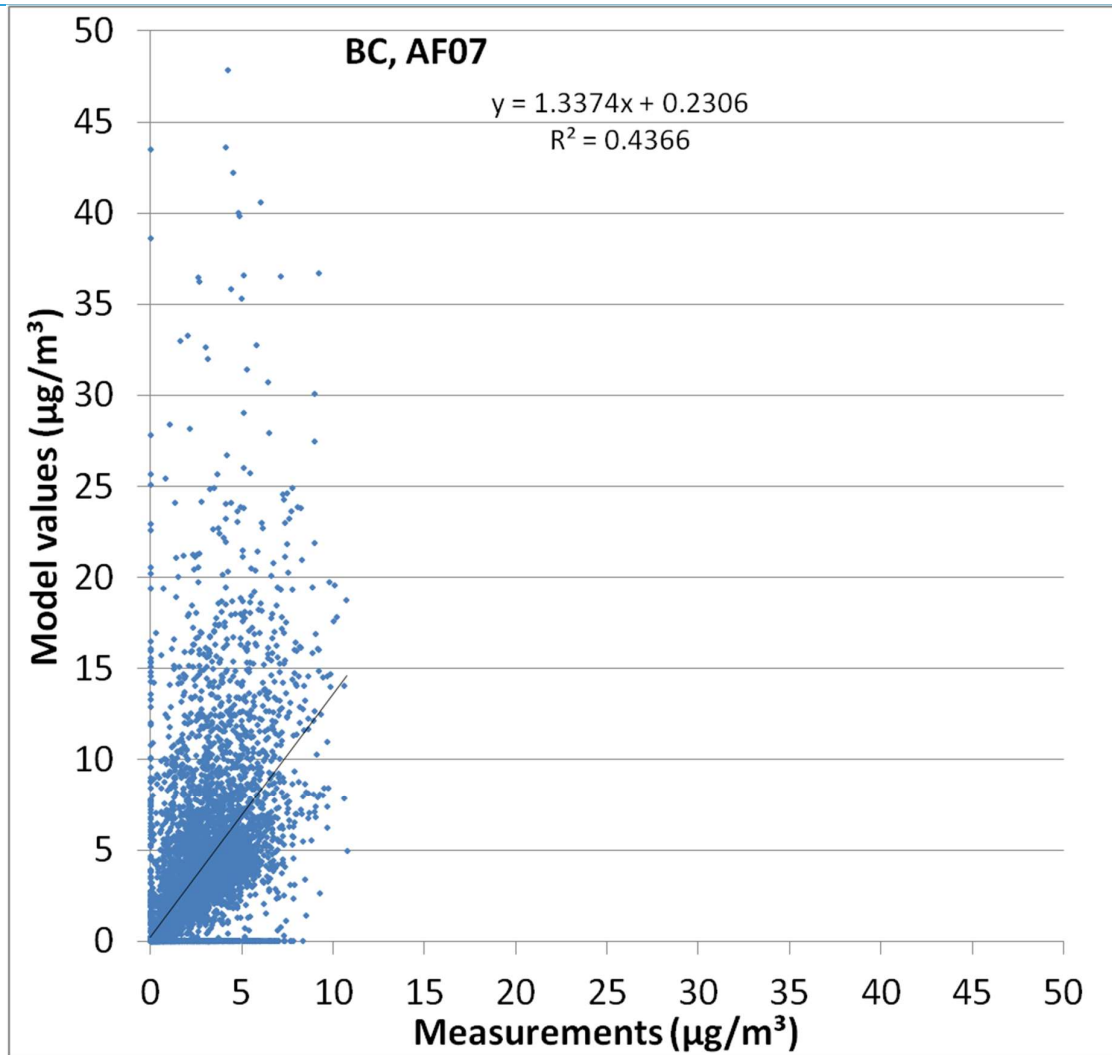


Figure 61 : Scatter plot of the modelled BC concentration (without background) at AF07 on the measured concentration (both in $\mu\text{g}/\text{m}^3$). Every symbol represents 30 minutes.

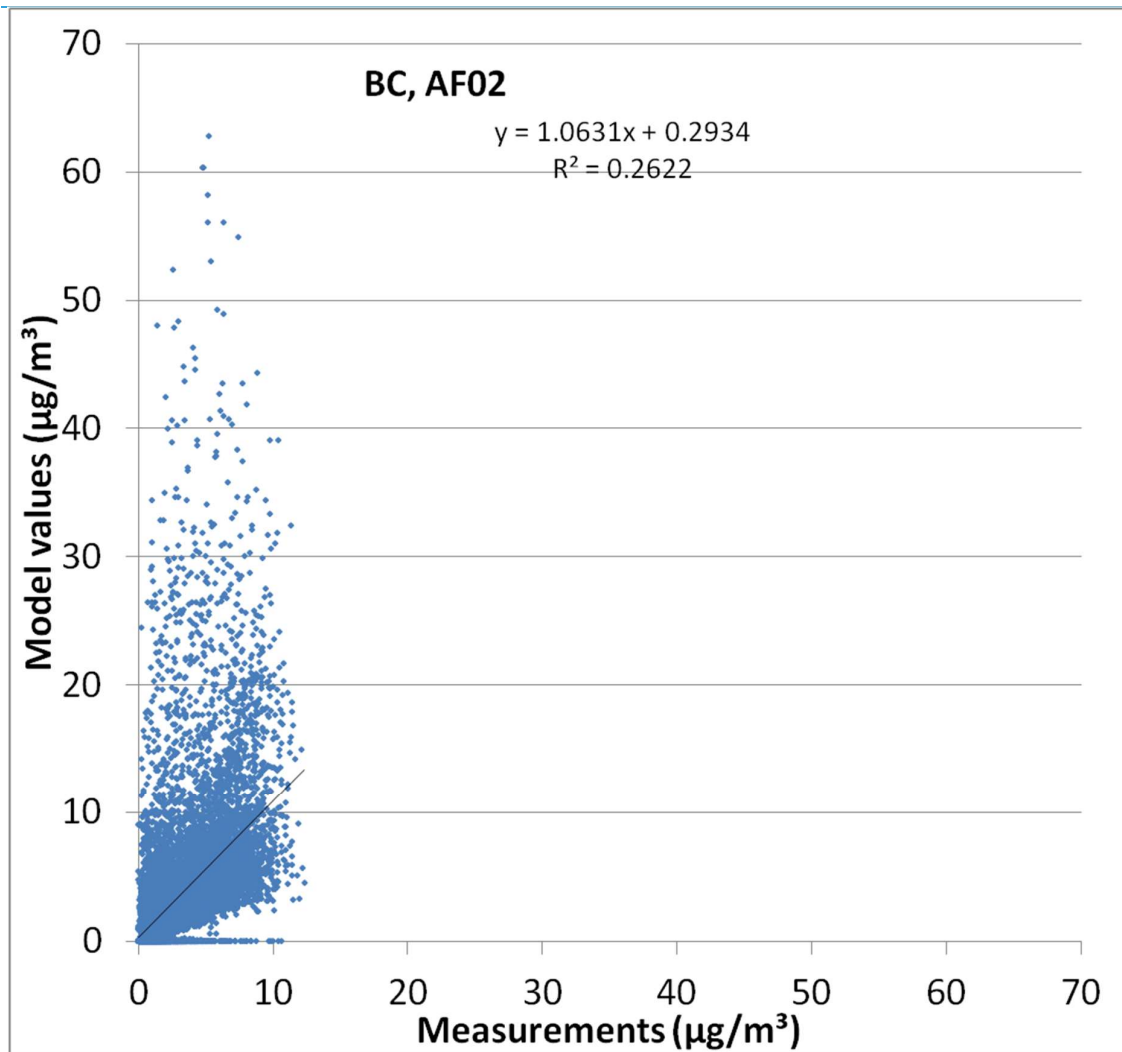


Figure 62 : Scatter plot of the modelled BC concentration (without background) at AF02 on the measured concentration (both in $\mu\text{g}/\text{m}^3$). Every symbol represents 30 minutes.

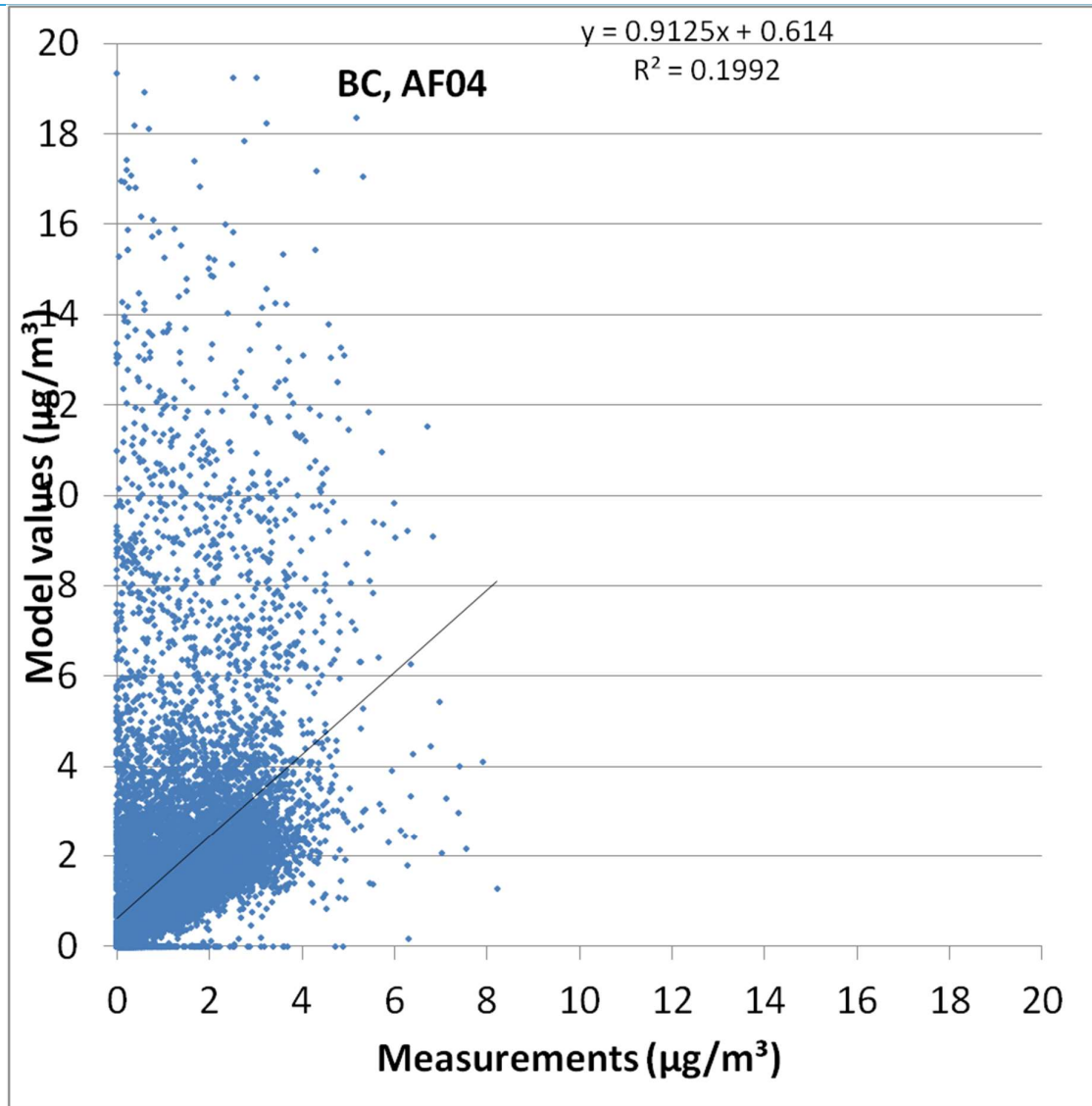


Figure 63 : Scatter plot of the modelled BC concentration (without background) at AF04 on the measured concentration (both in $\mu\text{g}/\text{m}^3$). Every symbol represents 30 minutes.

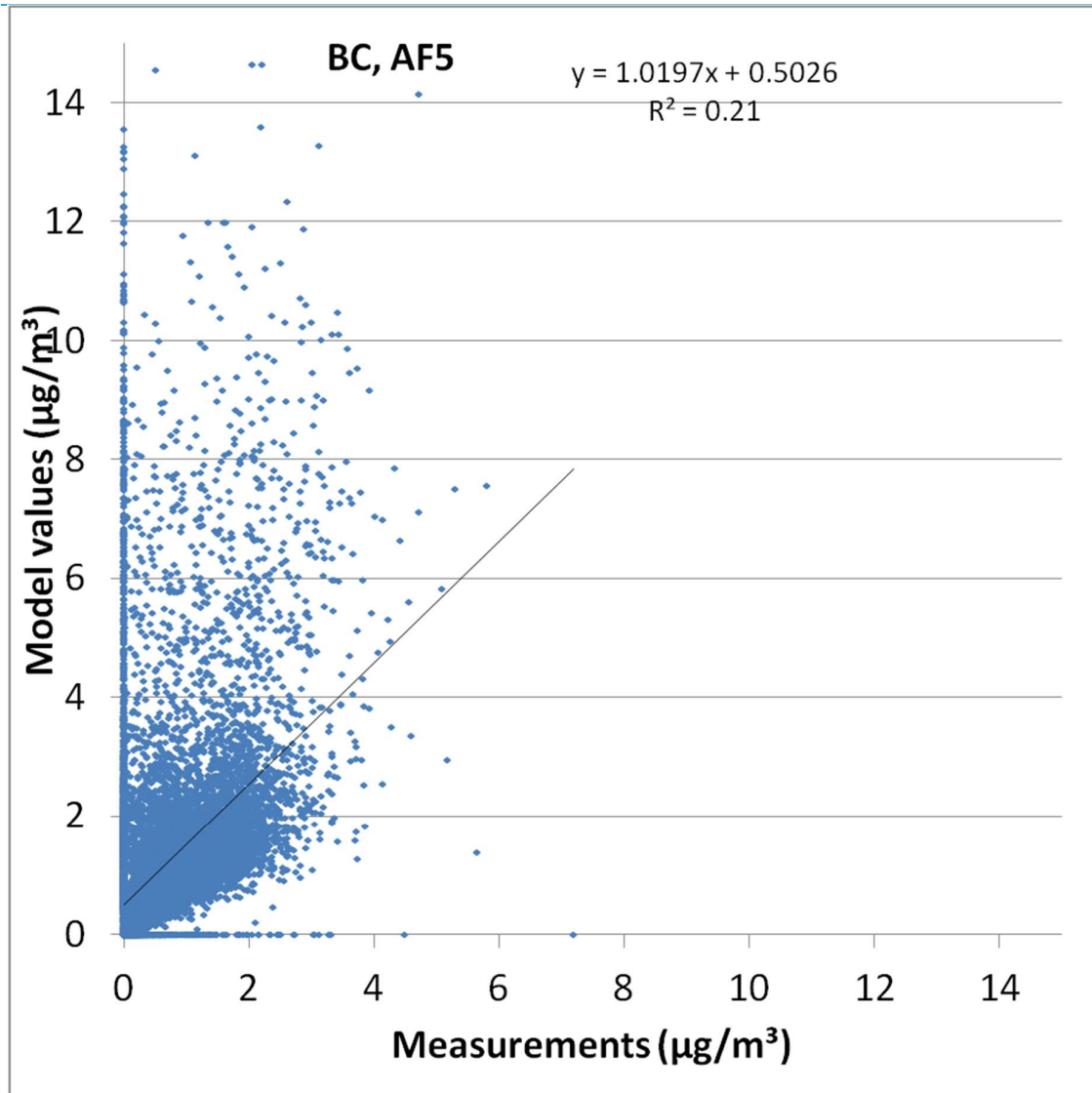


Figure 64 : Scatter plot of the modelled BC concentration (without background) at AF05 on the measured concentration (both in $\mu\text{g}/\text{m}^3$). Every symbol represents 30 minutes.

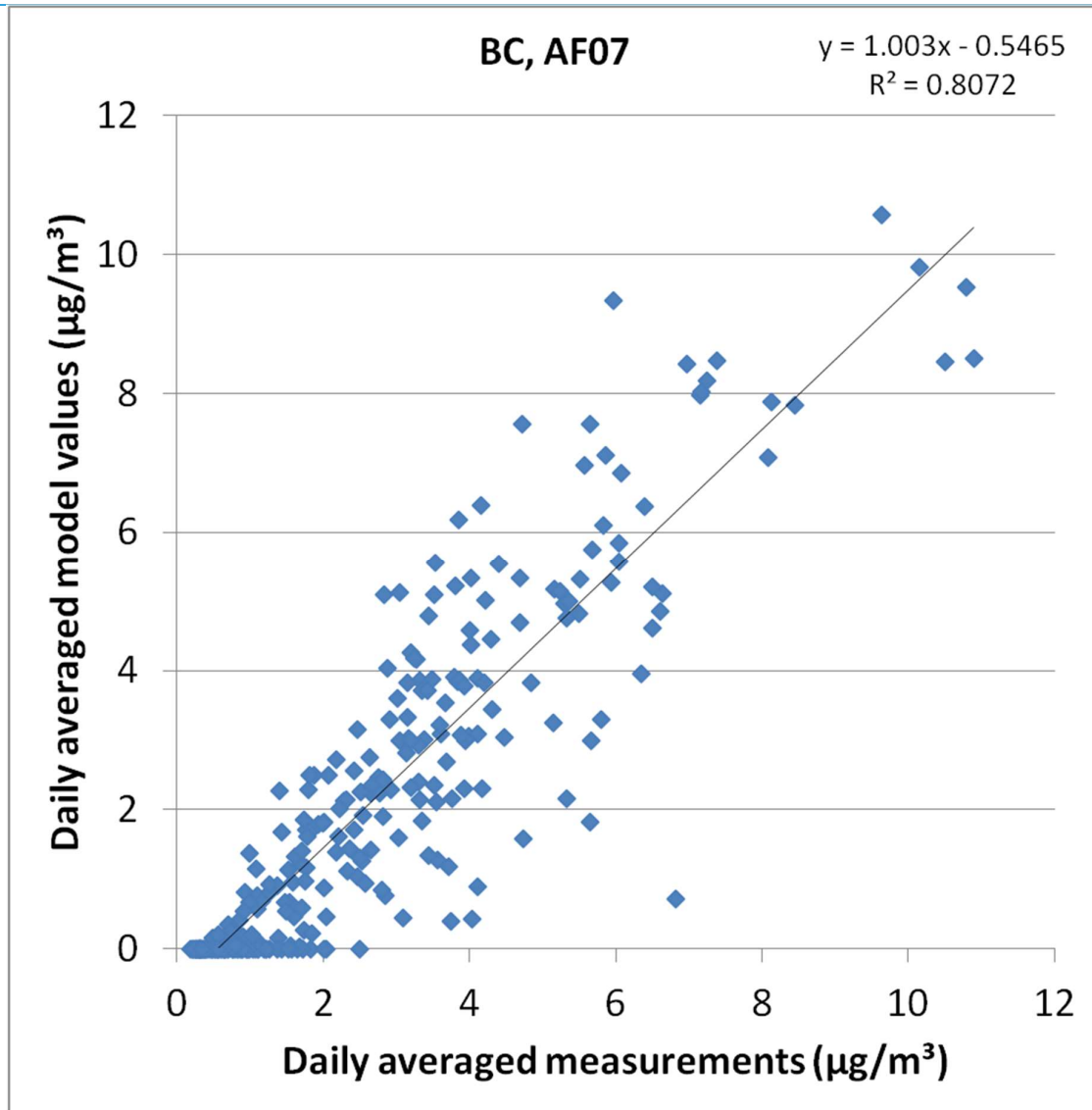


Figure 65 : Scatter plot of the modelled BC concentration (without background) at AF07 on the measured concentration (both in $\mu\text{g}/\text{m}^3$). Every symbol represents one day.

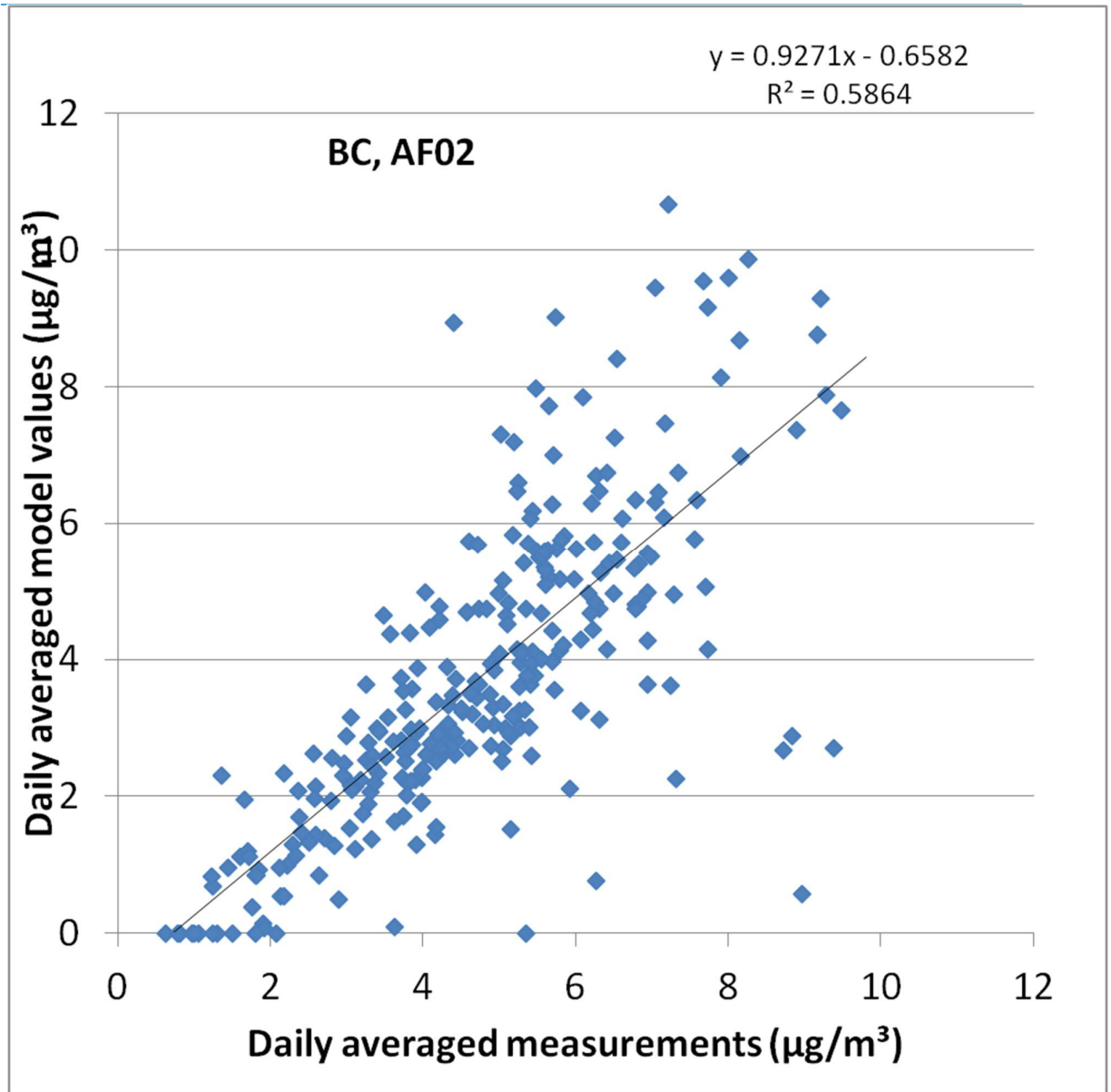


Figure 66 : Scatter plot of the modelled BC concentration at AF02 on the measured concentration (both in $\mu\text{g}/\text{m}^3$). Every symbol represents one day.

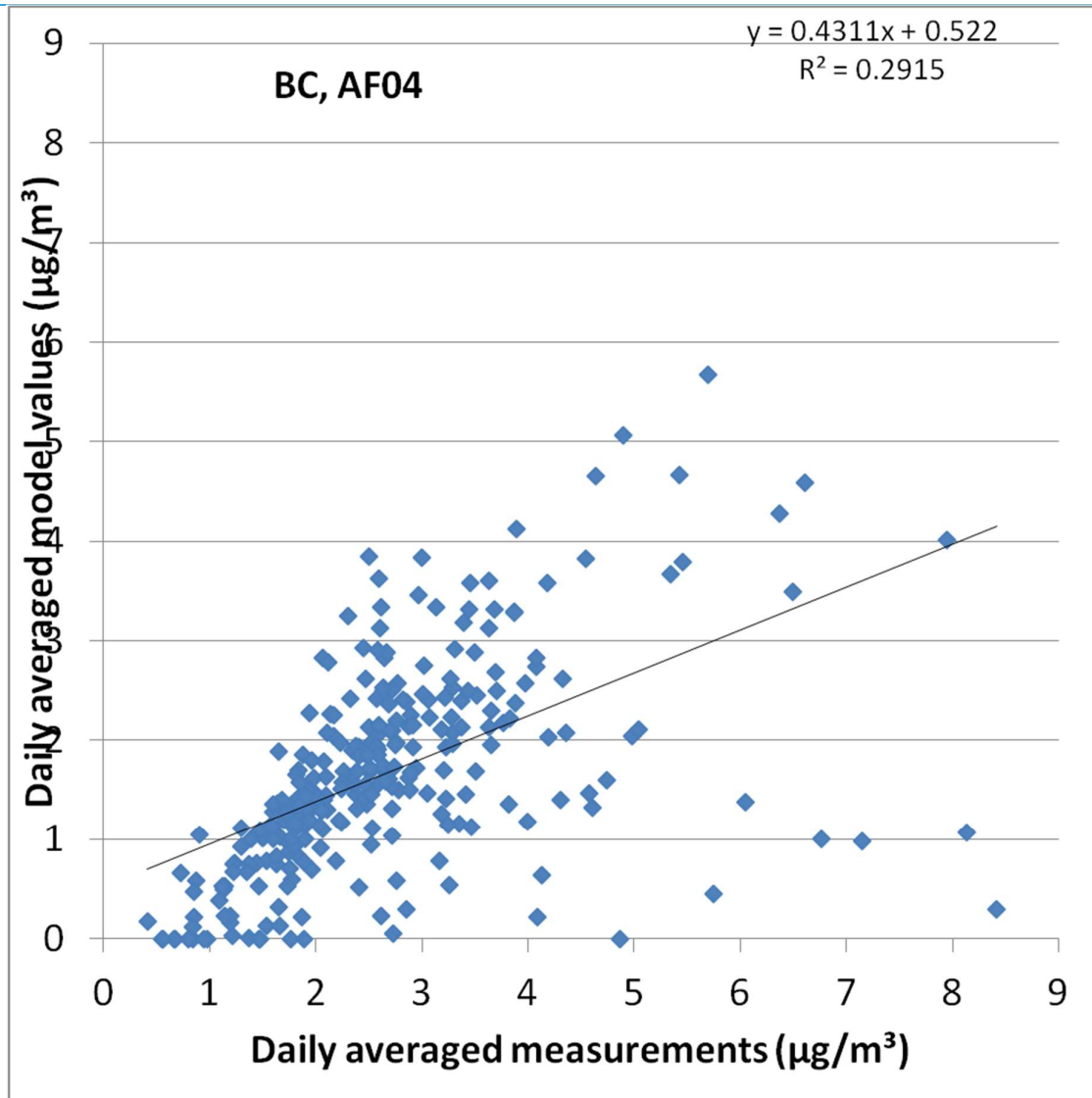


Figure 67 : Scatter plot of the modelled BC concentration at AF04 on the measured concentration (both in $\mu\text{g}/\text{m}^3$). Every symbol represents one day.

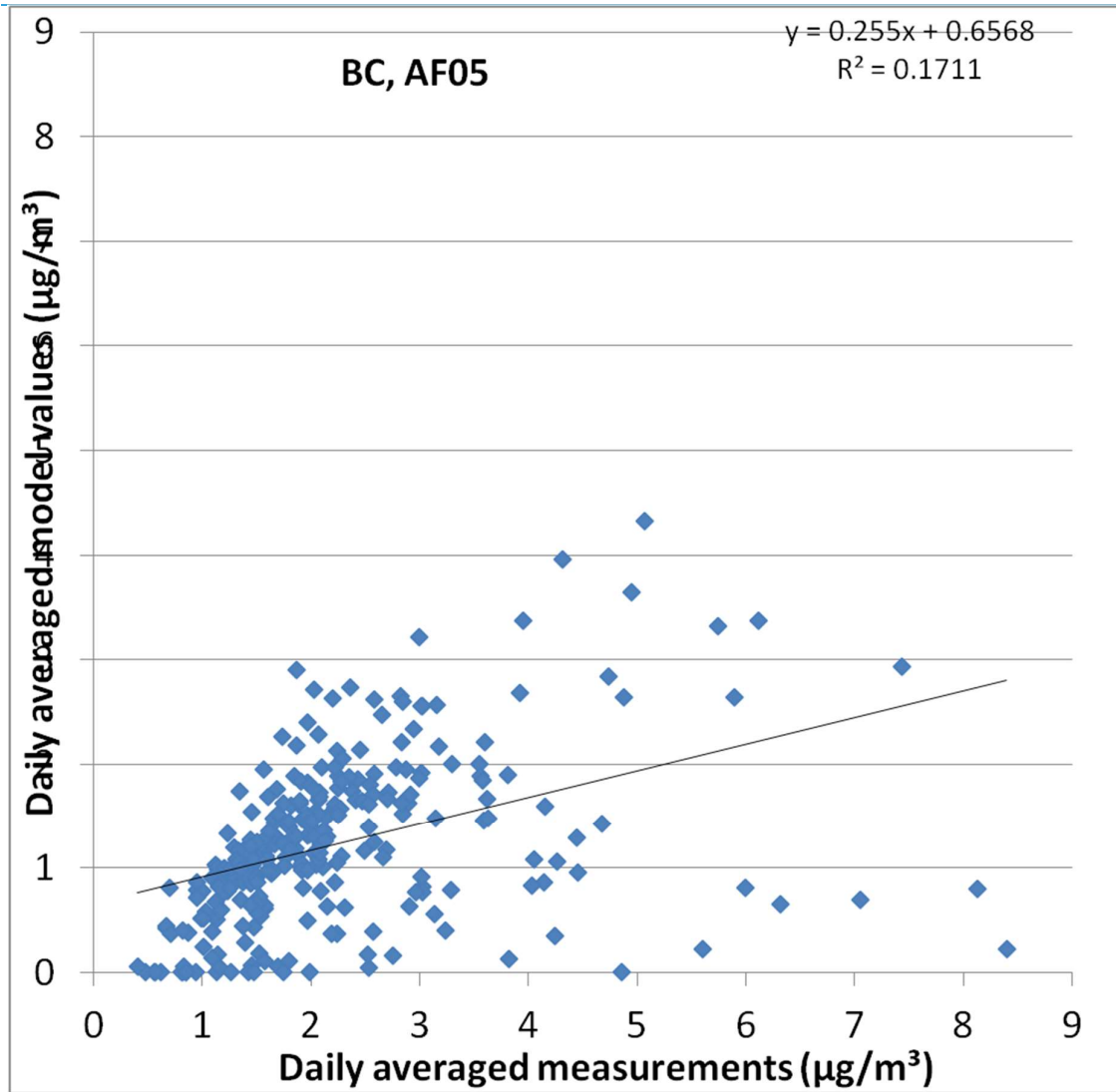


Figure 68 : Scatter plot of the modelled BC concentration at AF05 on the measured concentration (both in $\mu\text{g}/\text{m}^3$). Every symbol represents one day.

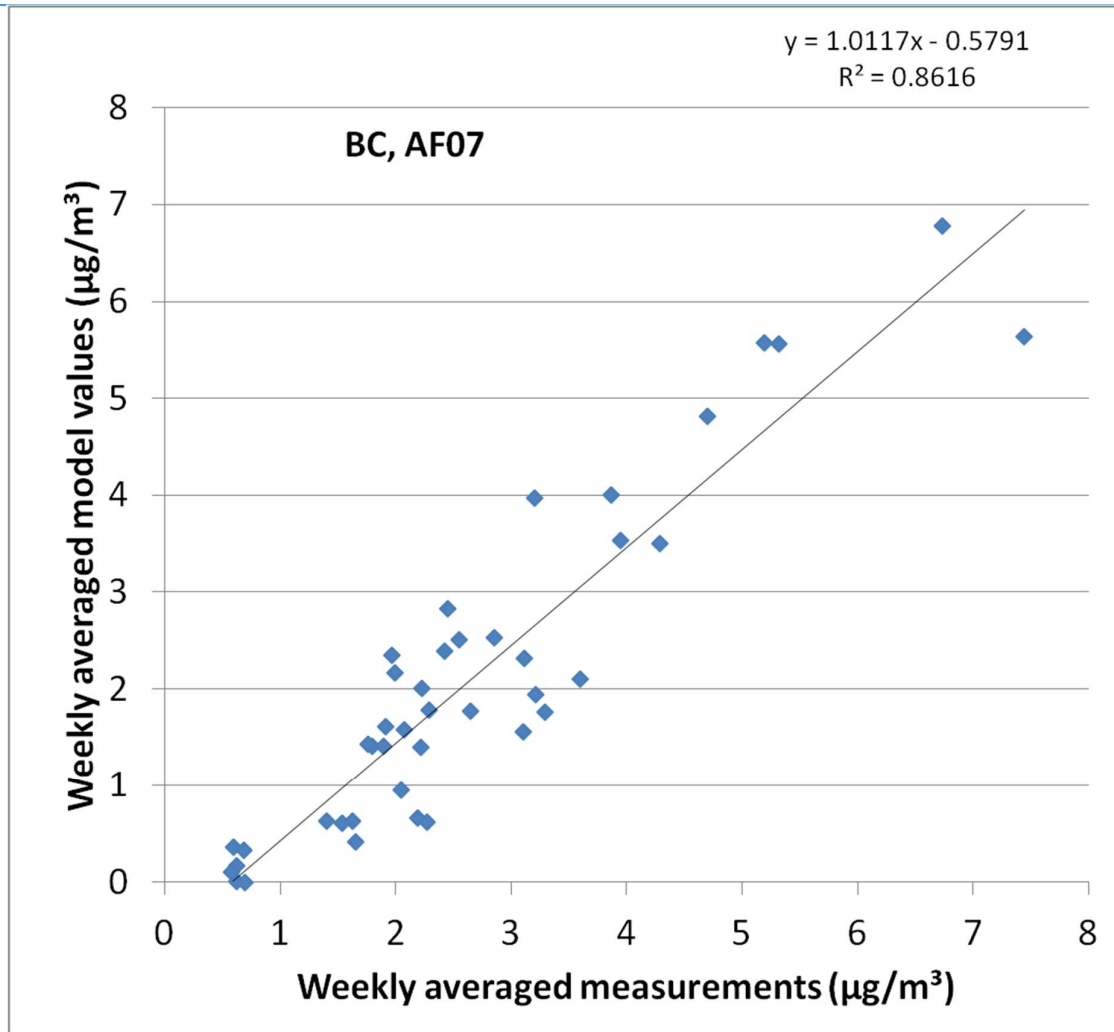


Figure 69 : Scatter plot of the modelled BC concentration at AF07 on the measured concentration (both in $\mu\text{g}/\text{m}^3$). Every symbol represents one week.

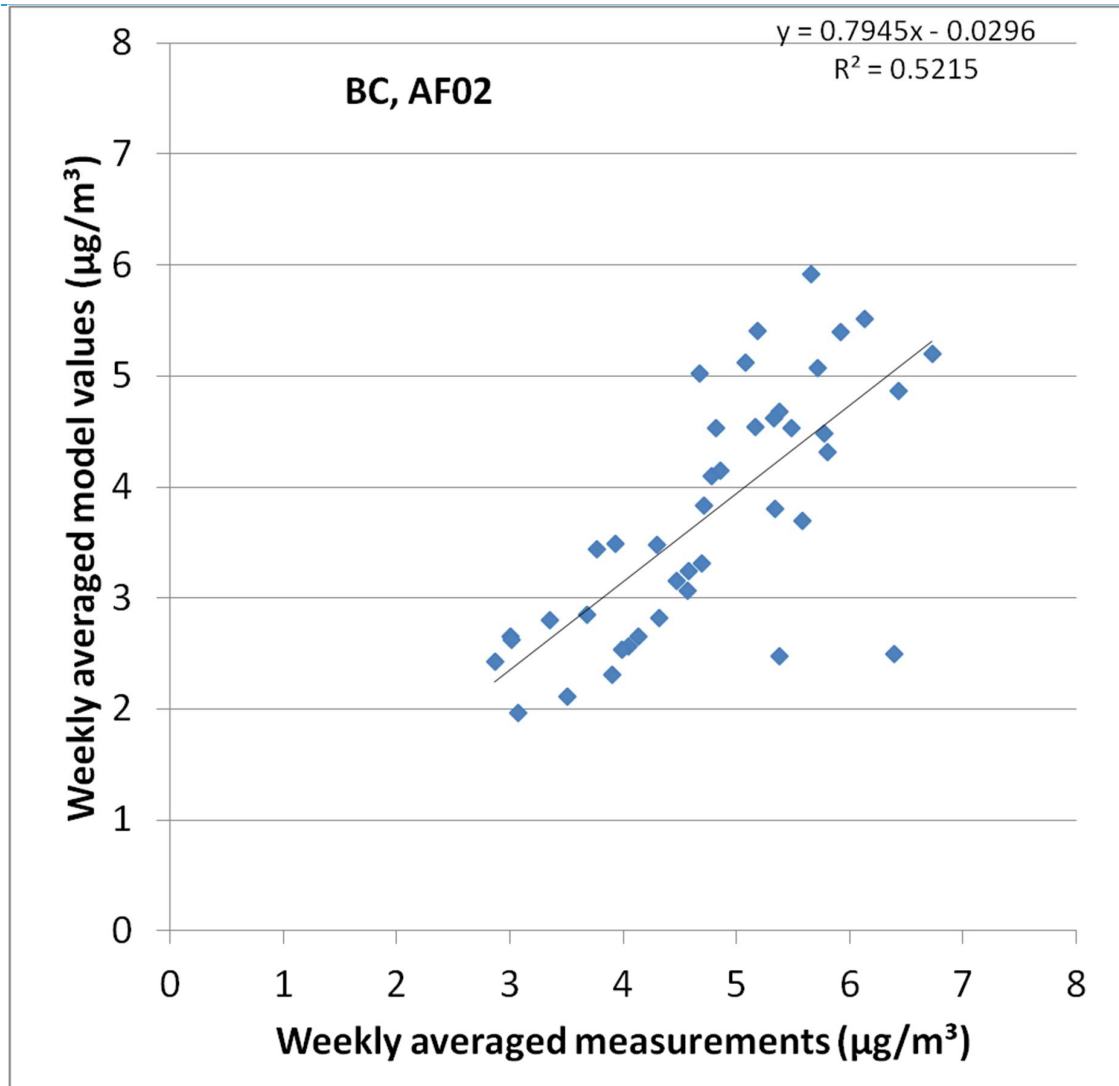


Figure 70 : Scatter plot of the modelled BC concentration at AF02 on the measured concentration (both in $\mu\text{g}/\text{m}^3$). Every symbol represents one week.

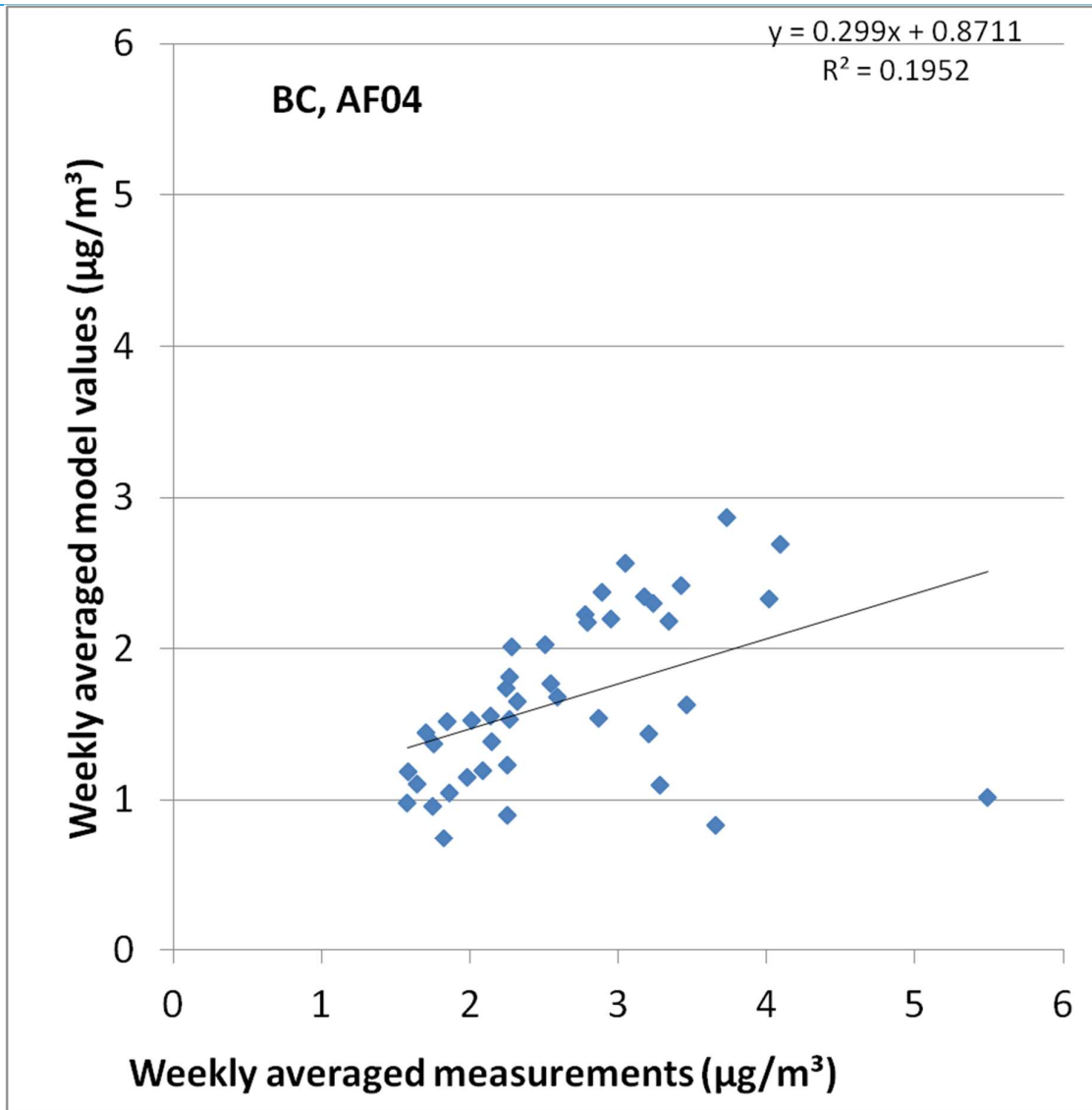


Figure 71 : Scatter plot of the modelled BC concentration at AF04 on the measured concentration (both in $\mu\text{g}/\text{m}^3$). Every symbol represents one week.

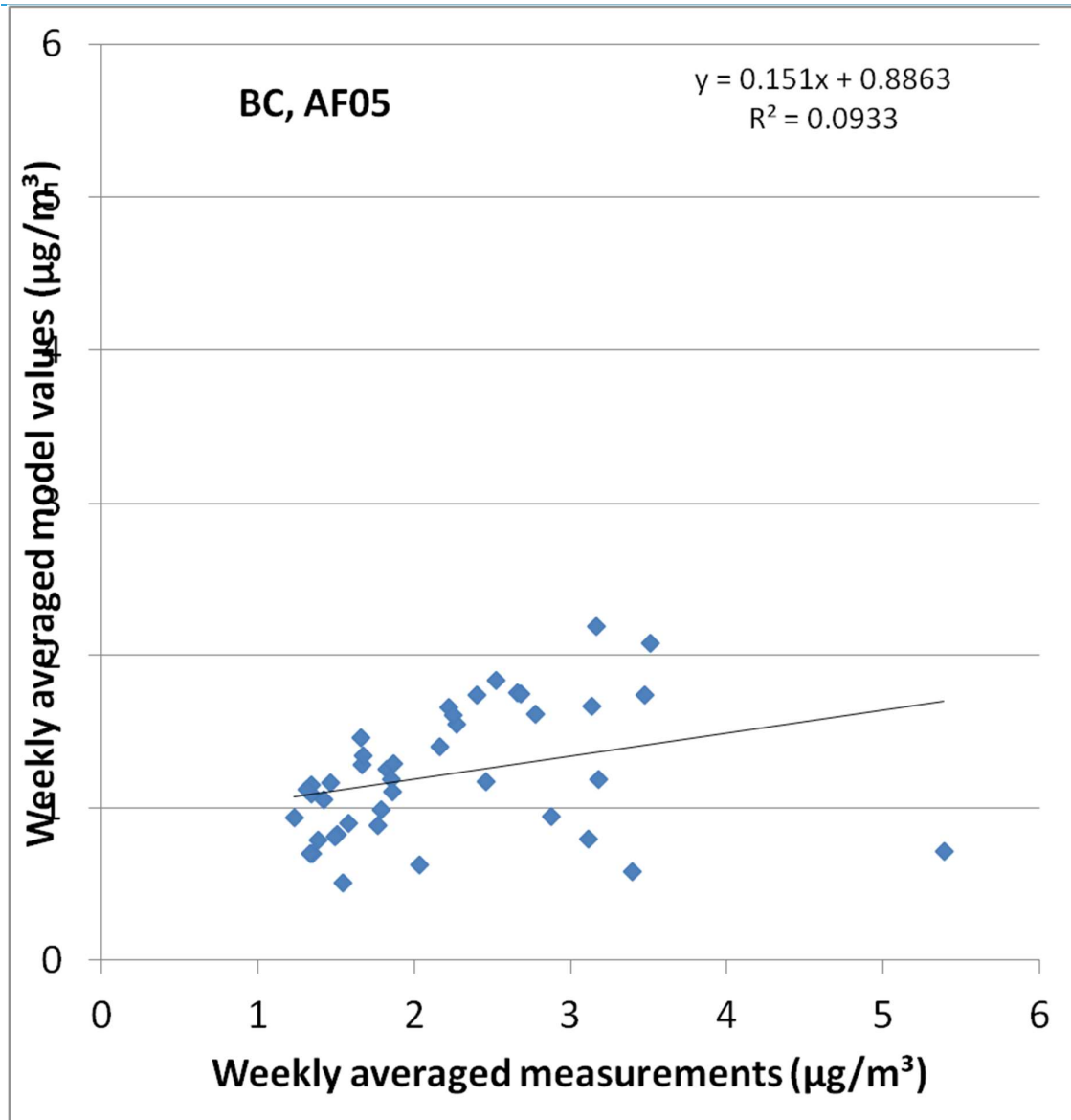


Figure 72 : Scatter plot of the modelled BC concentration at AF05 on the measured concentration (both in $\mu\text{g}/\text{m}^3$). Every symbol represents one week.

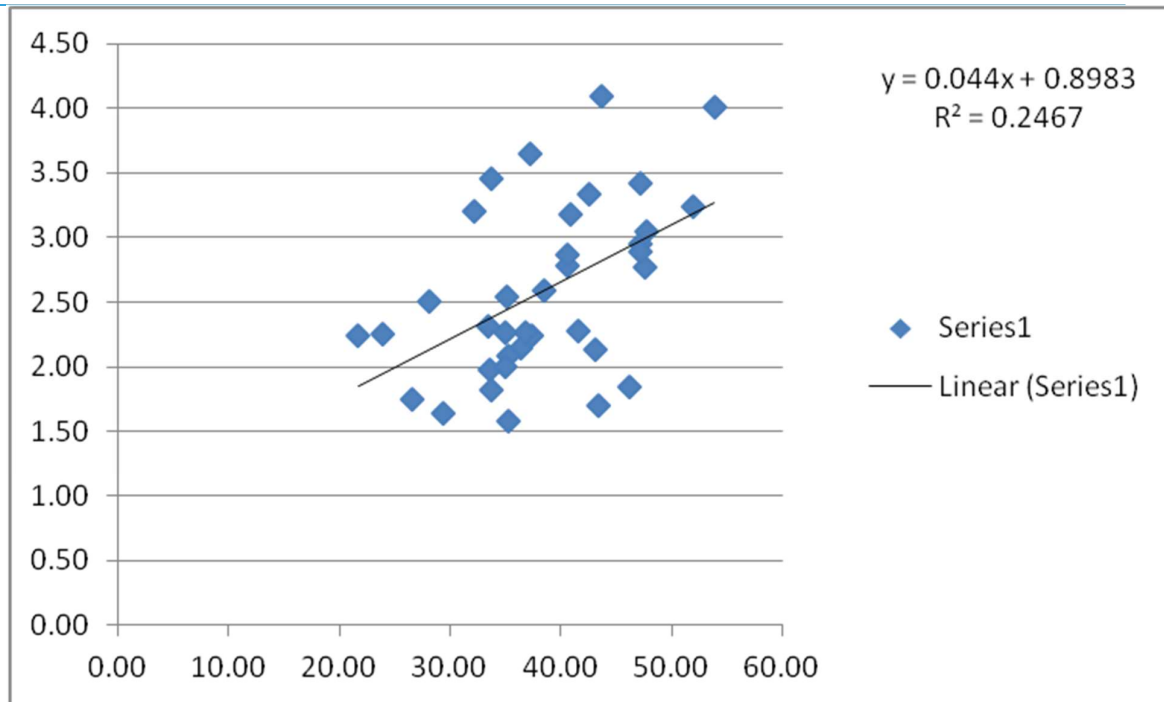


Figure 73 : Scatter plot of the weekly averaged BC concentrations (Y-axis, in µg/m³) on the weekly averaged NO₂ concentrations (X-axis, in µg/m³) for AF04.

6.5.3. SENSITIVITY ANALYSIS

In this section, we compare the average measurements (inclusive background) and the average modelling values (without background) for different stability classes, hours of the day, days of the week, wind speeds and wind directions.

There seems to be no direct influence of the stability class on the performance of the model (Figure 74). Indeed, the pattern of model and measurements is similar for all 4 locations. The measurements are higher than the model values, but this is logical as the first one includes the background while the second one does not.

For wind speed (Figure 75), there is a similar reasoning that can be made as for the stability class. However, for low wind speeds, the model seems to overestimate slightly the concentrations at the two stations close to the highway (AF07, AF02). This could be due to the treatment of the traffic-induced dispersion in the model (see text box). For the moment, the traffic-induced dispersion is treated by putting the initial vertical spread of the Gaussian distribution to a certain

Traffic-induced dispersion

The IFDM-model takes into account the traffic-induced dispersion. This is treated in the basic model as independent of the wind speed. This traffic-induced dispersion can be seen as the vertical distance over which the plume is spread when it leaves the highway.

The dispersion due to the meteorology is not included in the traffic-induced dispersion, as it is described by the Bultynck-Malet dispersion equations.

value. This value is not dependent on the wind speed. However, one can easily see that with very low wind speeds, the traffic-induced dispersion will not only be caused by the car that emits, but also by the following cars, as the pollution will not have been evacuated yet before the approach of the next car. The following cars spread out the pollution, inducing a larger dispersion. As a result, it could be possible that the traffic-induced dispersion is underestimated by the model at low wind speeds. An underestimated traffic-induced dispersion will lead to overestimated concentrations in the traffic plume, as not enough fresh (clean) air will be modelled to mix into the plume.

Furthermore, for higher wind speeds there seems to be an underestimation of concentrations at AF02. This could be explained by the same reasoning: a higher wind speed would lead to a quicker evacuation of pollution and thus a smaller number of cars will be on time to influence the traffic-induced dispersion and thus this traffic-induced dispersion will be lower. However, this quicker evacuation, and thus lower traffic-induced dispersion is not taken into account by the model. An overestimated traffic-induced dispersion will lead to underestimated concentrations in the plume, as too much fresh (clean) air will be modelled to mix into the plume.

The effect of the wind direction shows important deficiencies of the model (Figure 76). The model overestimates strongly at wind directions parallel to the highway, less strong (as model values and measurements are almost equal and no background concentrations are taken into account for the model) if the wind is directed from the highway to the measurement location and underestimates when the wind blows from the measurement location to the highway. All these could be explained by the variability of the wind speed during one half hour. Indeed, in reality, the wind direction is not constant, especially at low wind speeds, but is taken constant in the model. A wind blowing parallel to the highway will lead to very high concentrations close by. However, a slight deviation from this parallel would be enough to strongly decrease the measured concentrations. In the model however, the wind is kept constant. This effect is indeed the strongest (or even only existing) with low winds, both for the parallel and the perpendicular case (Figure 77 and Figure 78).

This wind direction variability explains also the remarkable model skill improvement when going from an averaging time of half an hour to an averaging time of one day, by processing the model output. Indeed, in the latter case, these variations of wind direction will be incorporated in the model (48 different wind directions can be thus taken in account).

One could also envision an improvement of the model, taking into account this wind variability (see §6.10).

No dependency of skill on the day of the week or on the month of the year has been found (Figure 79 and Figure 81). A remarkable overestimation is found in the morning hours, during rush hour (Figure 80). This could be due to three reasons:

- Traffic speed reduction at this location during the morning peak, which is not taken into account in the model (see §6.9.2 and §6.10).
- Overestimation of the emissions during the morning peak (see §6.9.1 and §6.10).

- Geometry: in the morning, most of the traffic is driving towards Brussels and thus farthest away from most of the measurement locations. However, this is not taken into account in the model, as for instance, both righternmost driving lanes (one towards Brussels, one towards Ghent) get the same time profile. However this effect does not seem to be dominant, as the difference in deviation from reality follows the same pattern in AF07 (close to the driving lanes towards Brussels) and in AF02 (close to the driving lanes towards Ghent).

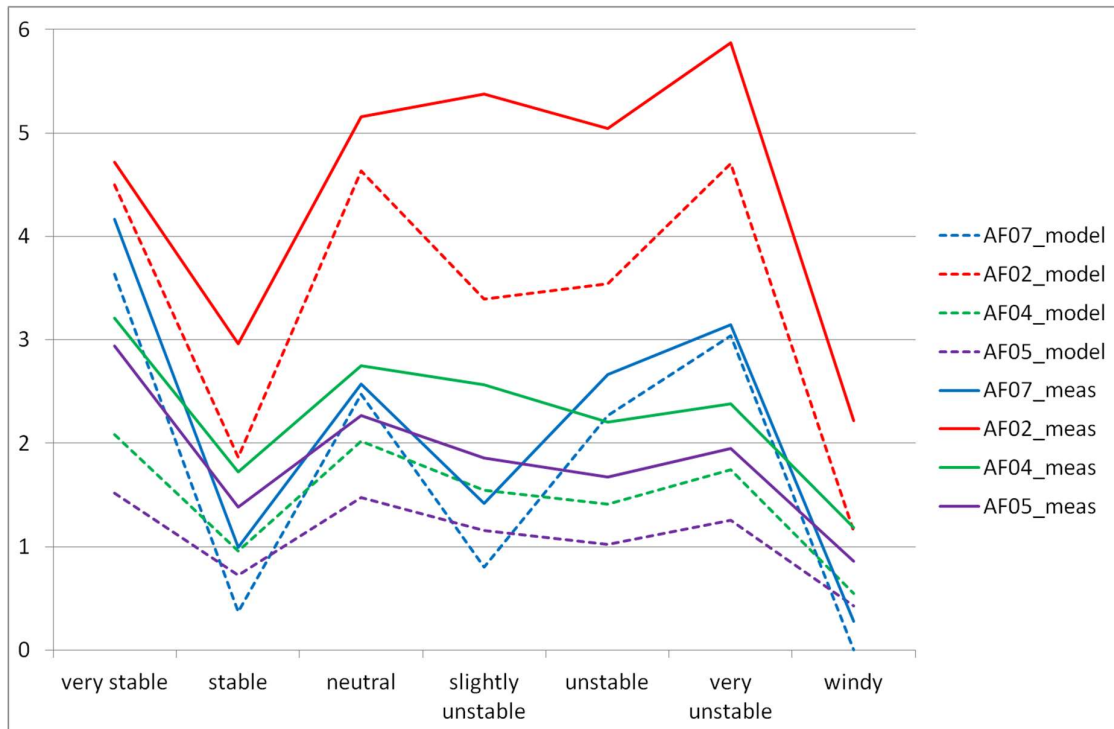


Figure 74 : Average BC concentration (Y-axis, in $\mu\text{g}/\text{m}^3$), per stability class (X-axis). Full lines: measurements. Dashed lines: Model values (without background). AF07 = blue; AF02 = red; AF04 = green; AF05 = purple.

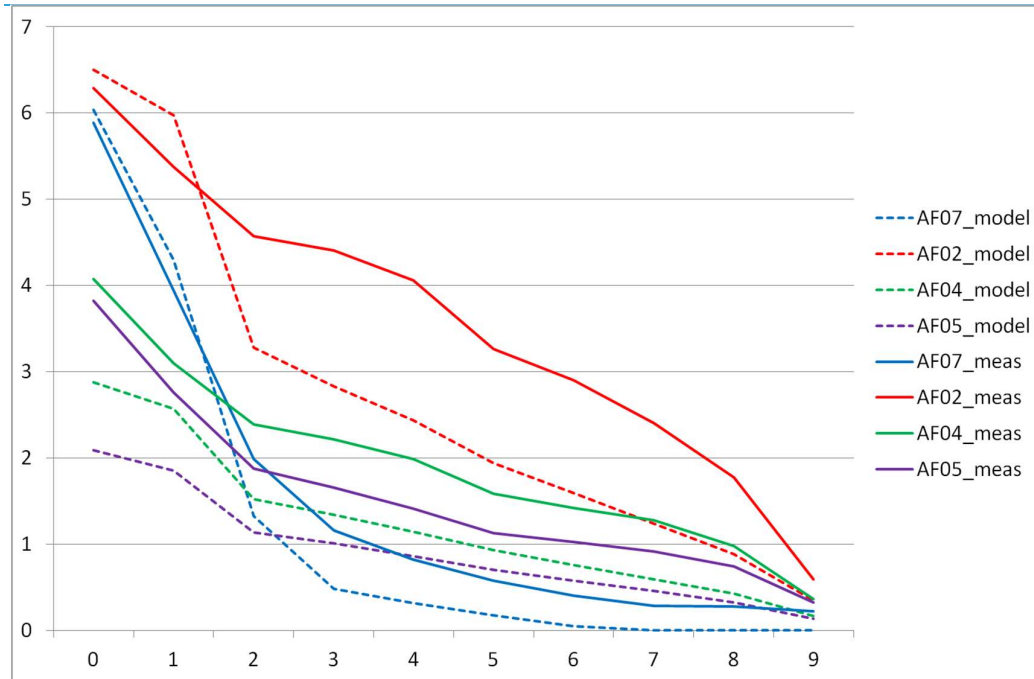


Figure 75 : Average BC concentration (Y-axis, in $\mu\text{g}/\text{m}^3$), per wind speed (X-axis, in m/s, rounded to the nearest integer). Full lines: measurements. Dashed lines: Model values (without background). AF07 = blue; AF02 = red; AF04 = green; AF05 = purple.

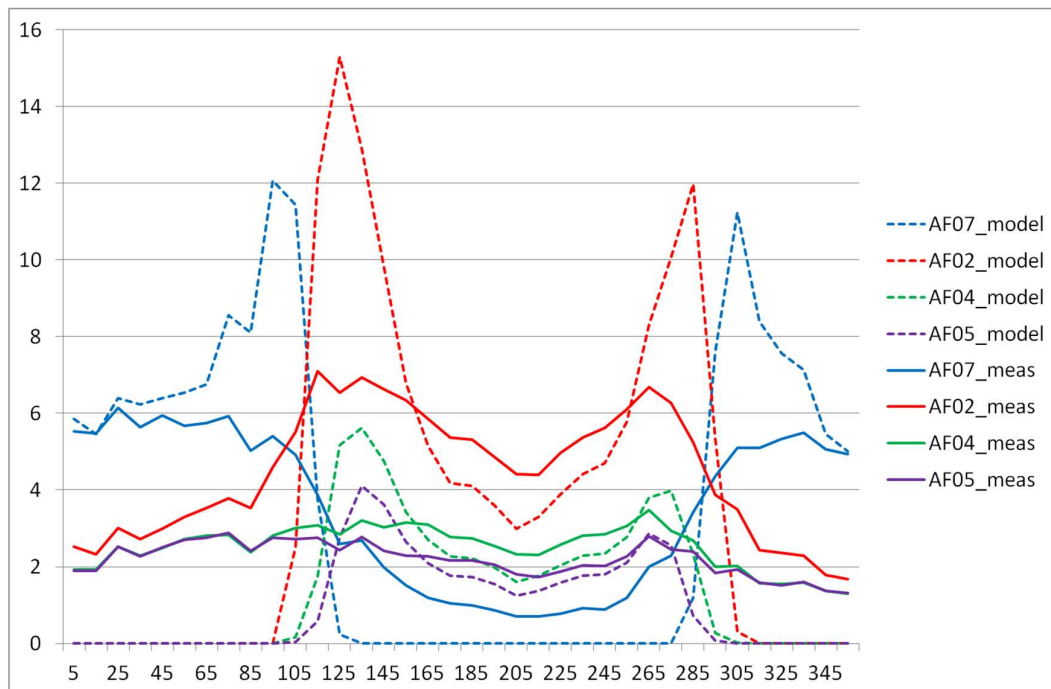


Figure 76 : Average BC concentration (Y-axis, in $\mu\text{g}/\text{m}^3$), per wind direction (X-axis, in 36 classes, for which the centre is given on the X-axis, in $^\circ$). Full lines: measurements. Dashed lines: Model values (without background). AF07 = blue; AF02 = red; AF04 = green; AF05 = purple.

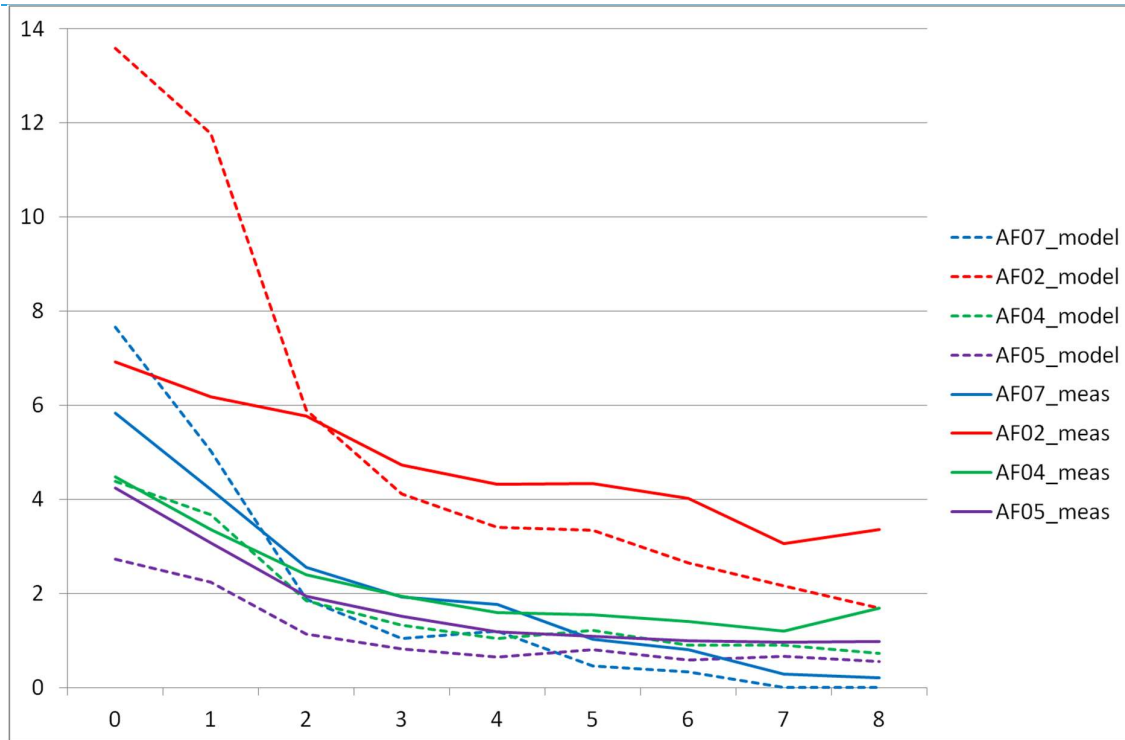


Figure 77 : Same as Figure 75, but only for wind directions quasi parallel ($\pm 20^\circ$) to the highway.

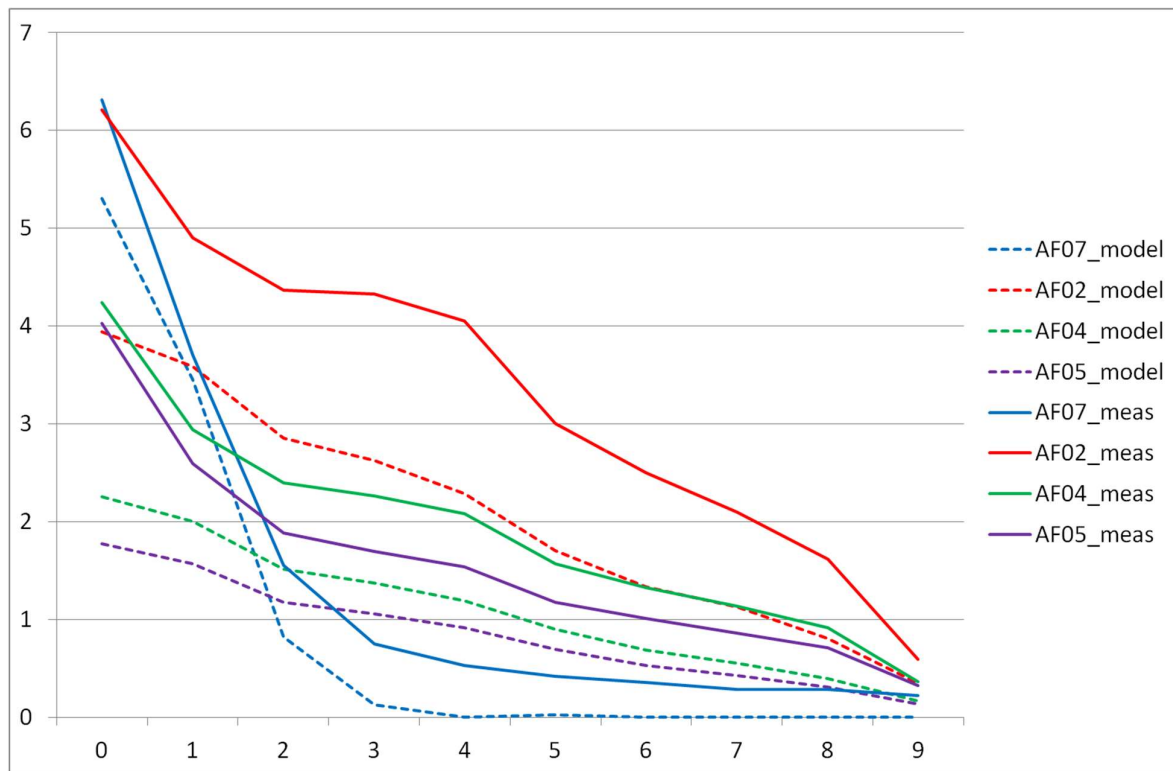


Figure 78 : Same as Figure 75, but only for wind directions quasi perpendicular ($\pm 20^\circ$) to the highway.

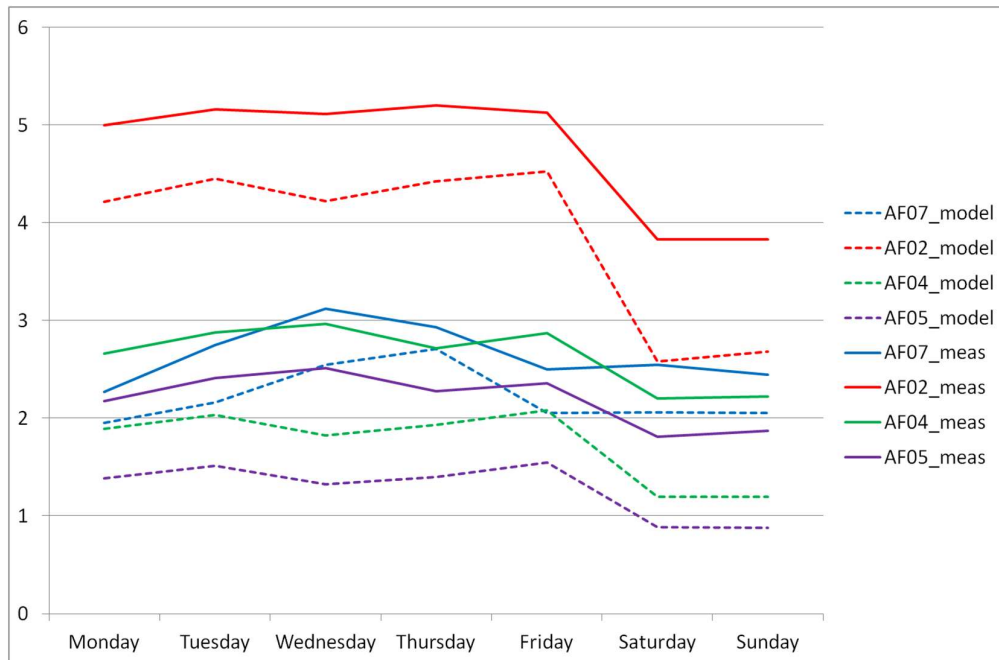


Figure 79 : Average BC concentration (Y-axis, in $\mu\text{g}/\text{m}^3$), per day of the week (X-axis). Full lines: measurements. Dashed lines: Model values (without background). AF07 = blue; AF02 = red; AF04 = green; AF05 = purple.

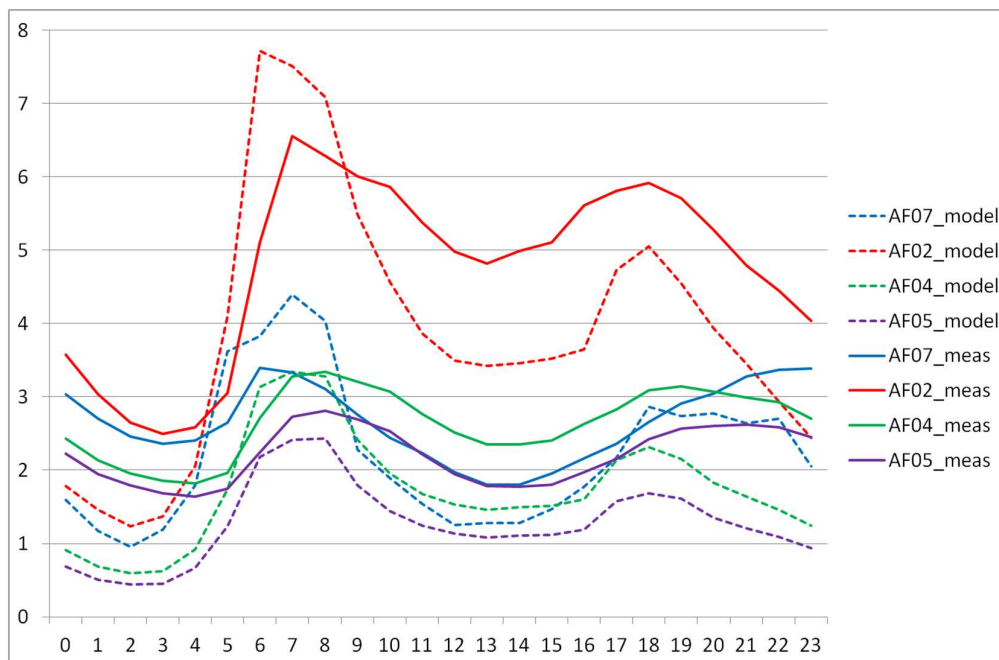


Figure 80 : Average BC concentration (Y-axis, in $\mu\text{g}/\text{m}^3$), per hour (X-axis, local time). Full lines: measurements. Dashed lines: Model values (without background). AF07 = blue; AF02 = red; AF04 = green; AF05 = purple.

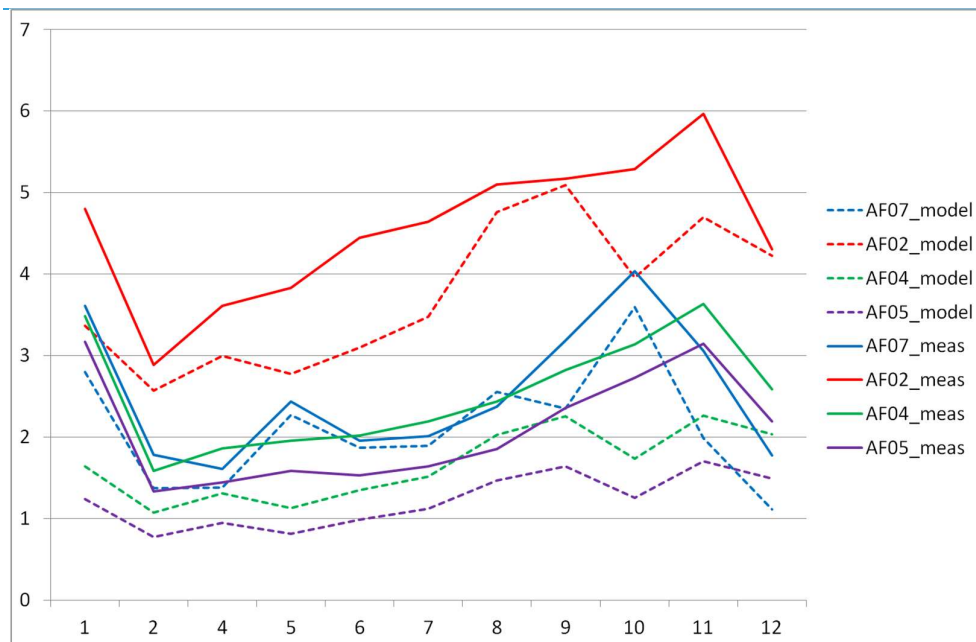


Figure 81 : Average BC concentration (Y-axis, in $\mu\text{g}/\text{m}^3$), per month (X-axis, 1=January 2013; 2 = February 2013; 4 = April 2012; 5 = May 2012; ... ; 12 = December 2012). Full lines: measurements. Dashed lines: Model values (without background). AF07 = blue; AF02 = red; AF04 = green; AF05 = purple.

6.6. PM_{10} AND $\text{PM}_{2.5}$

The skill in simulating PM_{10} and $\text{PM}_{2.5}$ around the highway is fairly low (Figure 82, Figure 83). This is due to a combination of several reasons. This is due to a combination of several reasons:

- The relative small influence of the highway on the PM-concentrations, and thus the relative higher measurement errors on this influence.
- The indication of another source which likely had an influence on the measurements at the locations furthest from the highway.

Furthermore, the pattern seen by BC (measurement at AF07 > measurement at AF05) is not seen by PM_{10} , nor $\text{PM}_{2.5}$. We also need to take into account the differences between methods used to determine the PM concentration, here a Leckel low volume sampler and a TEOM-FDMS monitor respectively. The differences between both these measurement methods will be further discussed in the VMM report of the highway campaign (VMM, 2013).

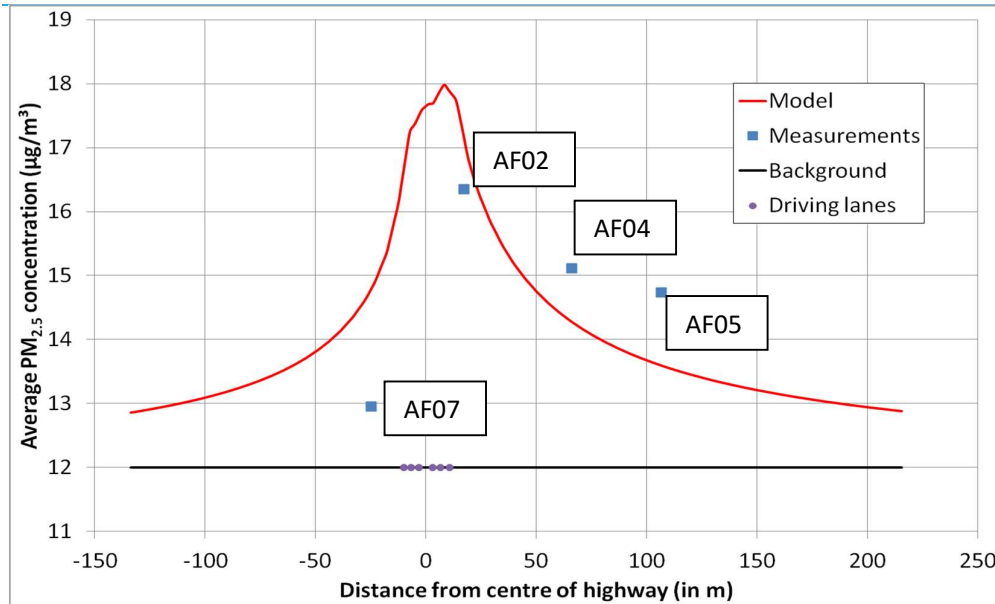


Figure 82 : PM_{2.5} Model values (red), measurements (blue squares) and background concentrations (black line) (PM_{2.5}, all in µg/m³) plotted by their distance to the centre of the highway. Purple dots represent the location (and thus not the concentrations) of the different driving lanes. A constant background concentration of 12 µg/m³ has been used to obtain best fit.

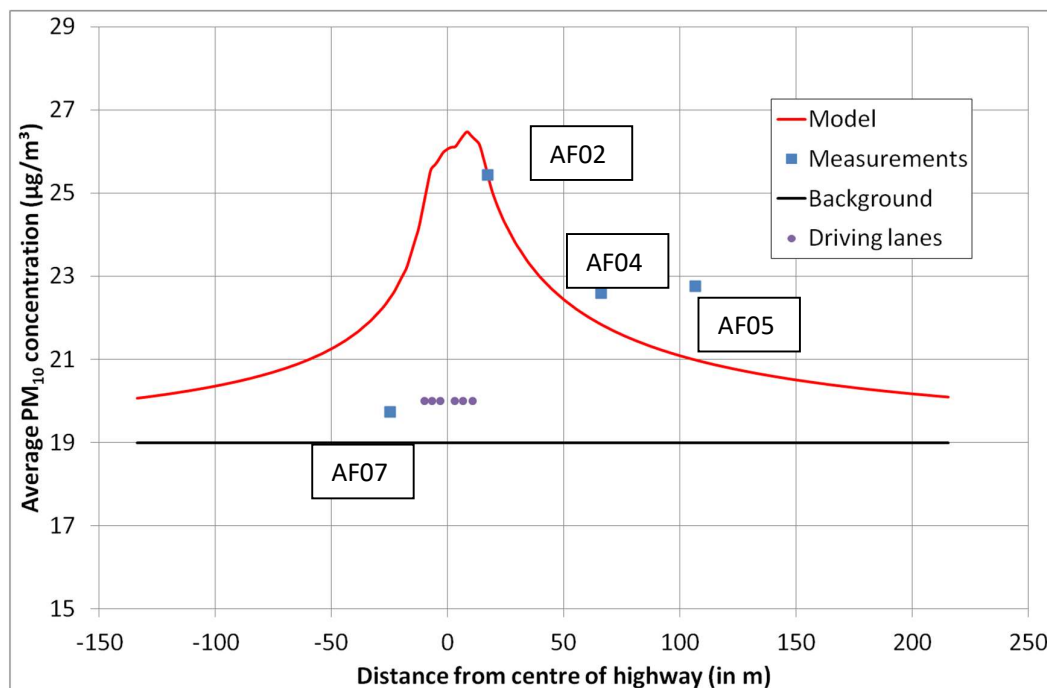


Figure 83 : PM₁₀ Model values (red), measurements (blue squares) and background concentrations (black line) (PM₁₀, all in µg/m³) plotted by their distance to the centre of the highway. Purple dots represent the location (and thus not the concentrations) of the different driving lanes. A constant background concentration of 19 µg/m³ has been used to obtain best fit.

6.7. NO_x

Halfhourly NO_x- and NO₂-measurements were performed at AF07. Comparison of the measurements and the model data (Figure 84-Figure 89) leads to the following conclusions:

- A similar wide scatter around the 1-1 line is reduced to a good model-measurement comparison at longer averaging times.
- The model overestimation at some half-hours is much less present for NO_x and NO₂ than for BC.
- The validation at a weekly averaging period is better for the half-hourly measurements than for the passive samplers (compare Figure 51 (all points) and Figure 89). The reason for this is not yet known. In VMM (2011a) some indications of (time-dependent?) necessities for calibration of daily samplers can be found. This could have an influence on this results.
- On average, a small negative bias for NO_x exists. The average modelled and measured values for NO₂ are very close to each other.

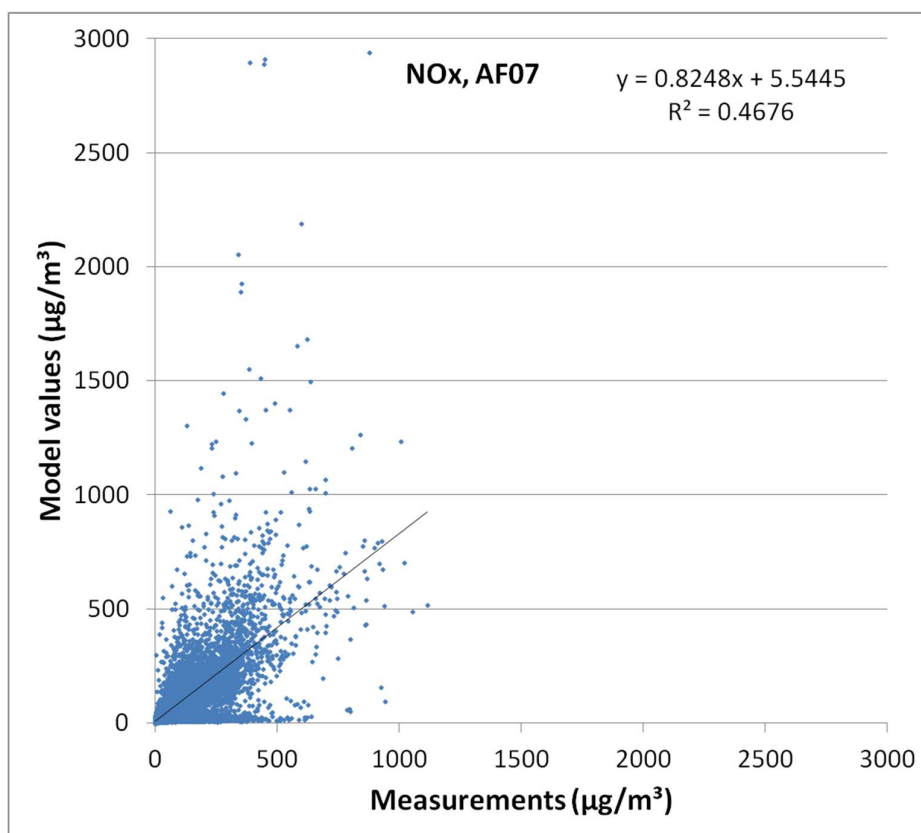


Figure 84 : Scatter plot of the modelled NO_x-concentration at AF07 on the measured concentration (both in µg/m³). Every symbol represents 30 minutes.

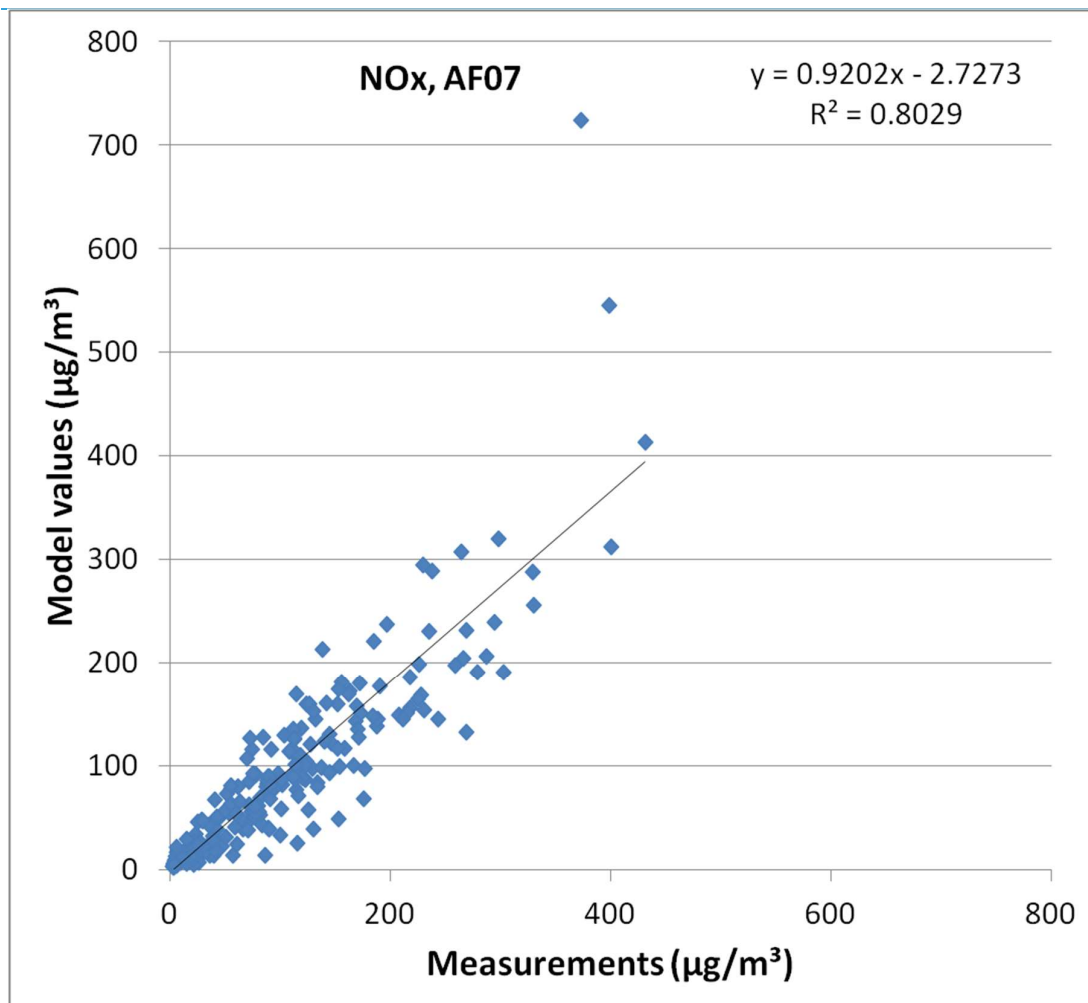


Figure 85 : Scatter plot of the modelled NO_x-concentration at AF07 on the measured concentration (both in $\mu\text{g}/\text{m}^3$). Every symbol represents one day.

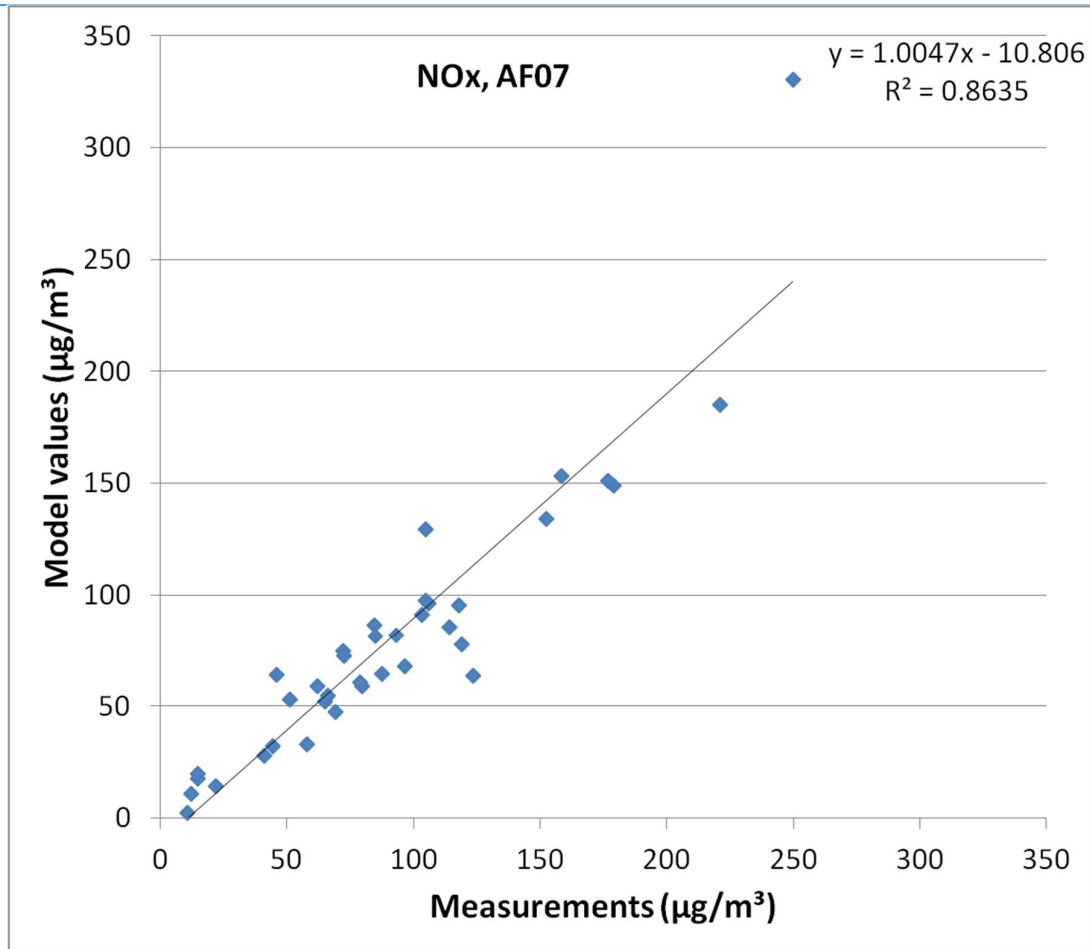


Figure 86 : Scatter plot of the modelled NO_x-concentration at AF07 on the measured concentration (both in $\mu\text{g}/\text{m}^3$). Every symbol represents one week.

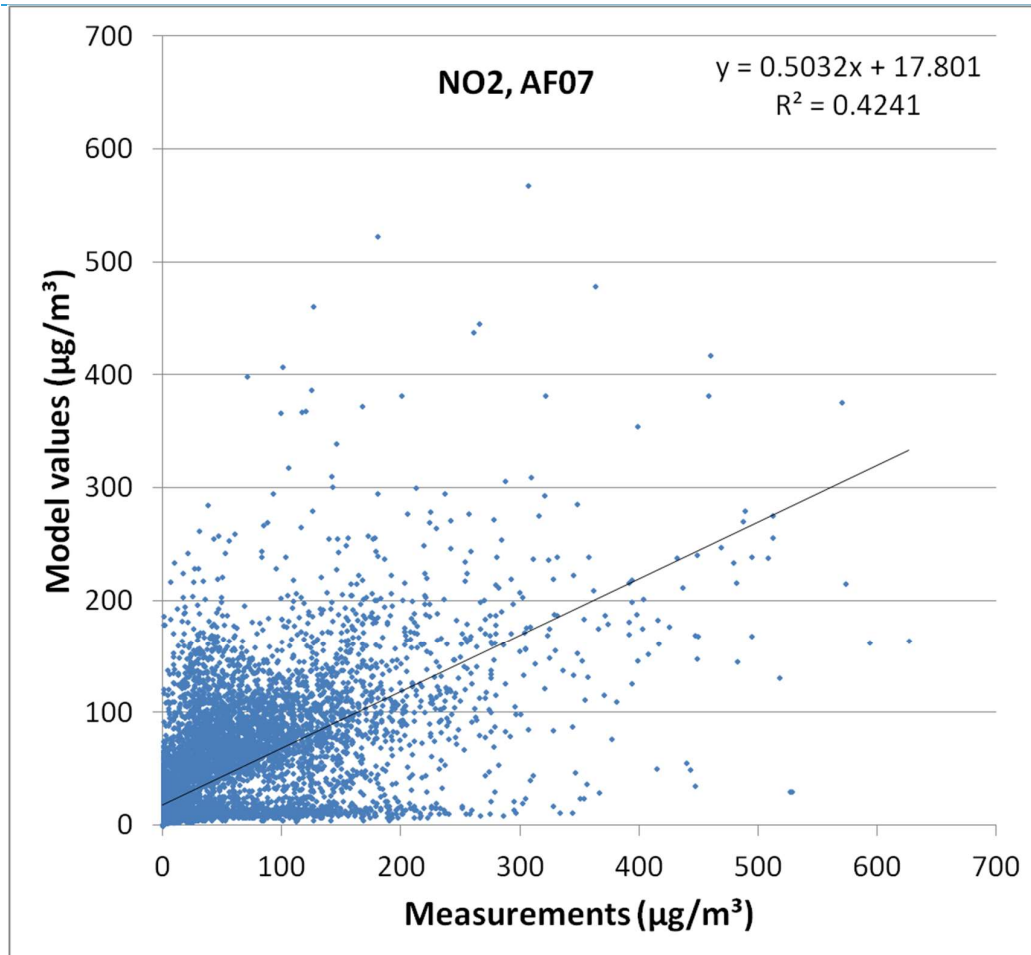


Figure 87 : Scatter plot of the modelled NO₂-concentration at AF07 on the measured concentration (both in $\mu\text{g}/\text{m}^3$). Every symbol represents 30 minutes.

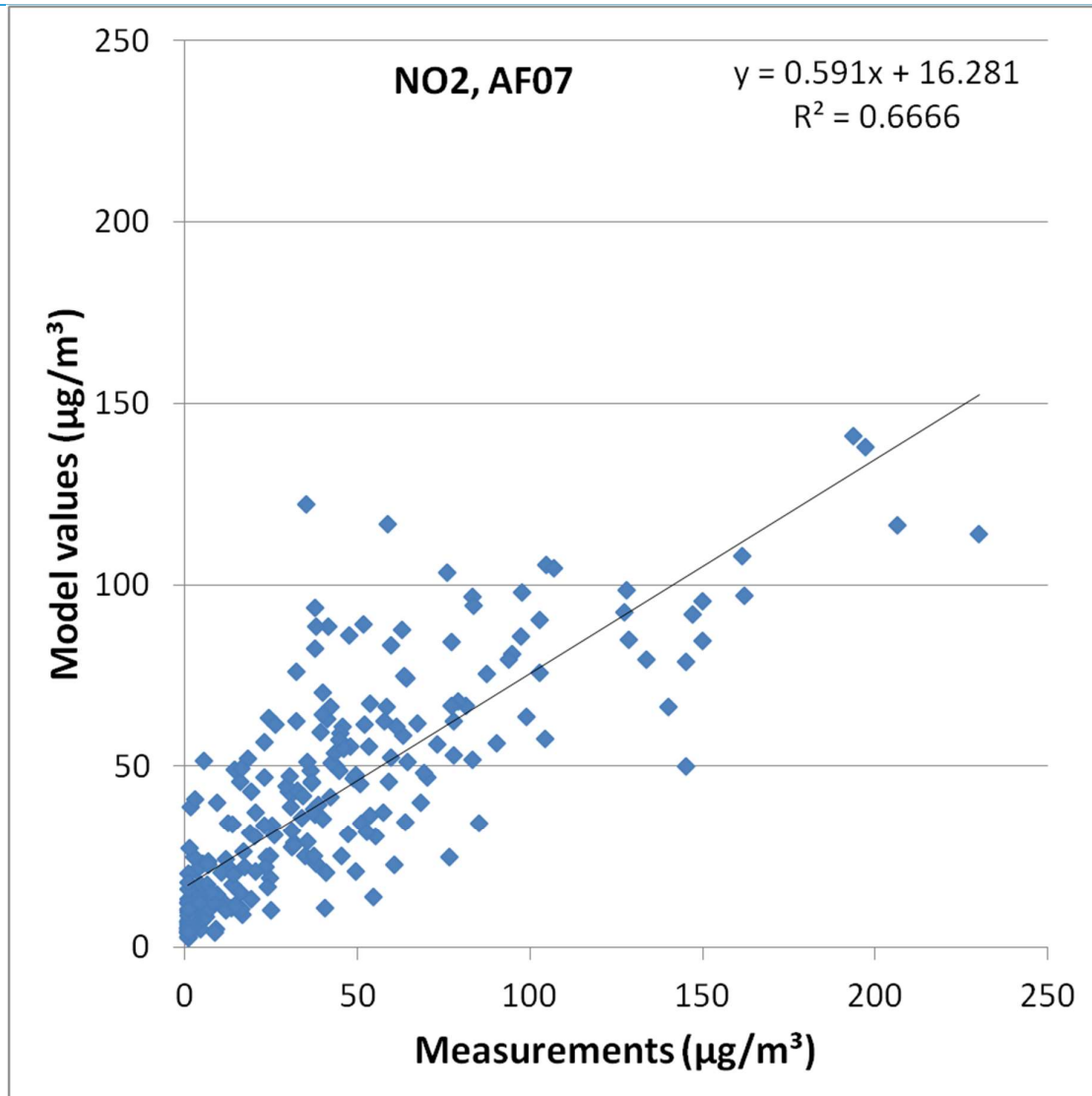


Figure 88 : Scatter plot of the modelled NO₂-concentration at AF07 on the measured concentration (both in $\mu\text{g}/\text{m}^3$). Every symbol represents one day.

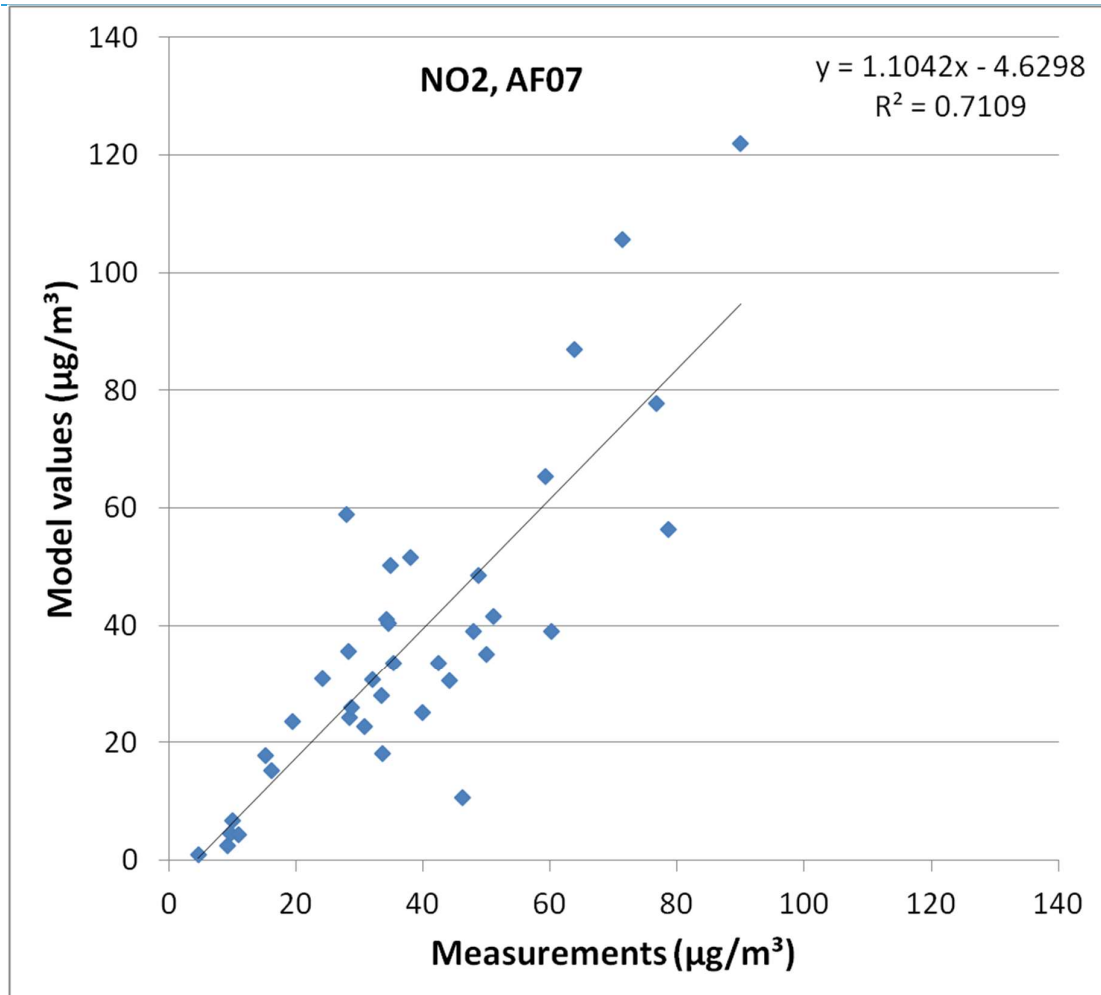


Figure 89 : Scatter plot of the modelled NO₂-concentration at AF07 on the measured concentration (both in $\mu\text{g}/\text{m}^3$). Every symbol represents one week.

6.8. SENSITIVITY TO THE URBAN PARAMETERIZATION

The same emission emitted just above ground level will lead to a larger increase in concentrations in regions with a low surface roughness (Op 't Eyndt et al., 2012). As a result, using the urban parameterization for the Affligem case leads to an underestimation of the concentrations close to the highway. This can be seen in Figure 90 (compare green lines with red lines). The effect on the concentrations is an underestimation of about 30% of the local contribution (not the total concentration).

These results are not completely in line with previous estimations by Kretzschmar et al. (1984), which state that the error which is made by not taking into account the surface roughness is small compared to the other errors.

Using meteorology from Luchtbal instead of local meteorology adds to the problem (Figure 91), probably due to a difference in wind speeds, related to the distance between the measurement location and the coast (Op 't Eyndt et al., 2012).

For regulatory purposes, this means that in the simulations for Flanders as a whole (which use the urban parameterization), a small underestimation of the concentrations close to highways located in open land is to be expected. As a result, the regions with exceedences close to the highways when the highway crosses an open area could be slightly underestimated in these studies.

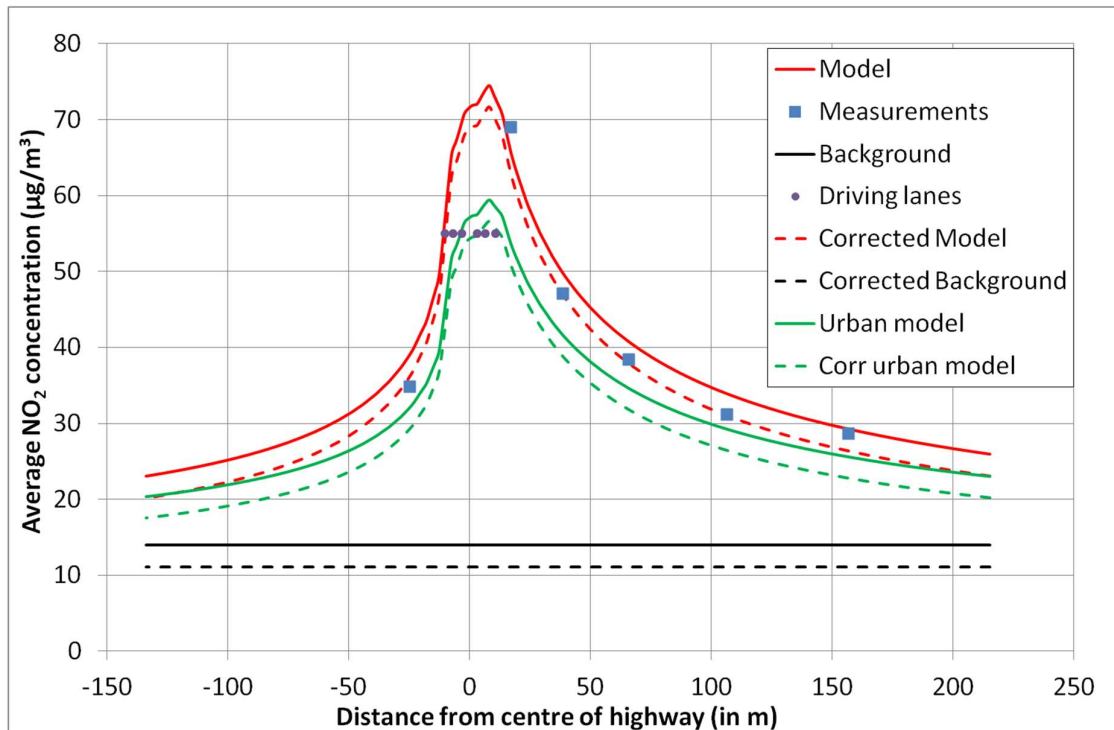


Figure 90 : Same as Figure 50, but with the urban parameterization added in green lines.

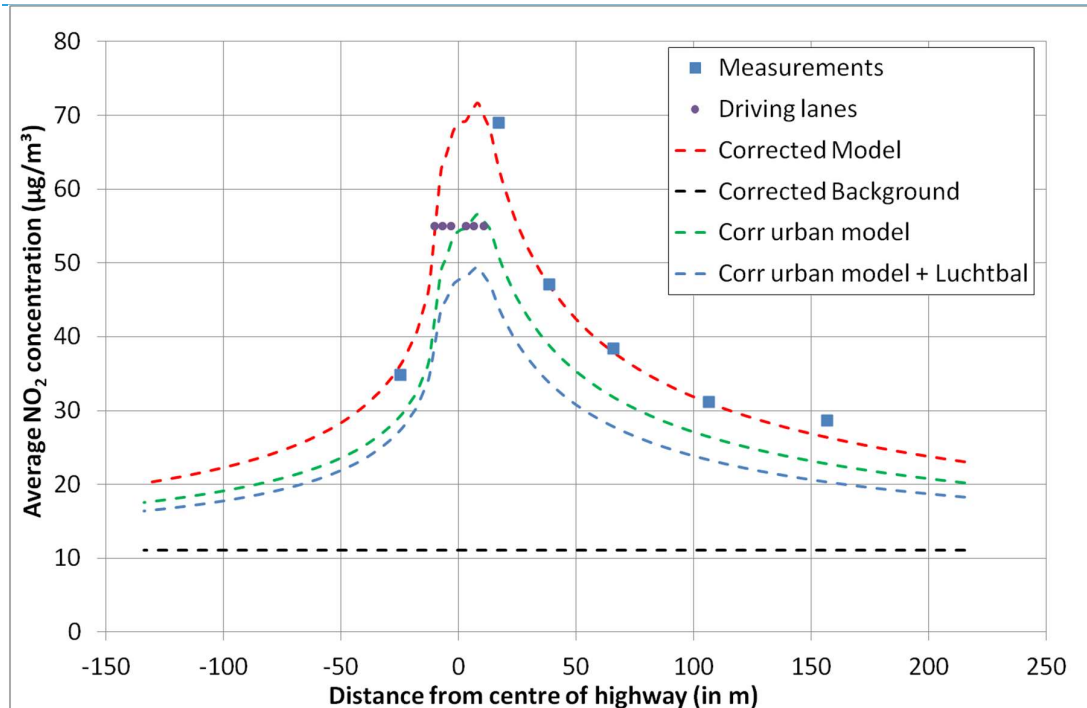


Figure 91 : Same as Figure 90, but only for the correct model values. The added blue dashed line is the simulation as with the green line but with meteorology from Luchtbal.

6.9. TRAFFIC COUNTS

Up till now, we have not taken into account the traffic counts made at this location. This was done on purpose, in order to show how the model behaves without this type of information. Indeed, most simulations made for clients (e.g. IFDM-traffic) cannot take into account this detailed type of information. However, for this location, this data is available, and we analyse it here so that hopefully some deviations of the model from reality can be explained. In this analysis, we use the data provided by the VCC on the highway at Affligem (counting locations 1913-1918).

Comparison of the total traffic simulated by the VVC and measured locally shows a very good agreement. As a result, if the distribution of the traffic over the day/week/months is also very good then the traffic input of the model will only deviate minimally from the reality. This distribution is studied in this section.

For taking into account the traffic counts, we make use of a parameter called PM_{2.5} emission equivalents. This value is equal to the number of passenger cars + 3.5 times the number of heavy duty vehicles. This last value is determined using the same methodology as in Beckx et al. (2013).

6.9.1. TIME FACTORS

The model uses time factors to spread the emissions over the day. These time factors can be checked against the traffic counts. The following conclusions can be made:

- The time factors describing the hour of the day are very good (R^2 of 0.985). There is a slight overestimation of the morning peak in Affligem and an underestimation in the hours before the morning peak.
- The time factors describing the hour of the day are much better on weekdays (R^2 of 0.957) than on weekend days (R^2 of 0.799).
- The time factors for the day of the week are also very good (R^2 of 0.987), with a light underestimation on weekdays and an overestimation on weekend days.
- The correlation between the model time factors for the month of the year and the counts is less good (R^2 of 0.556). However, the variation is quite small. As a result, this should not pose too much problems.

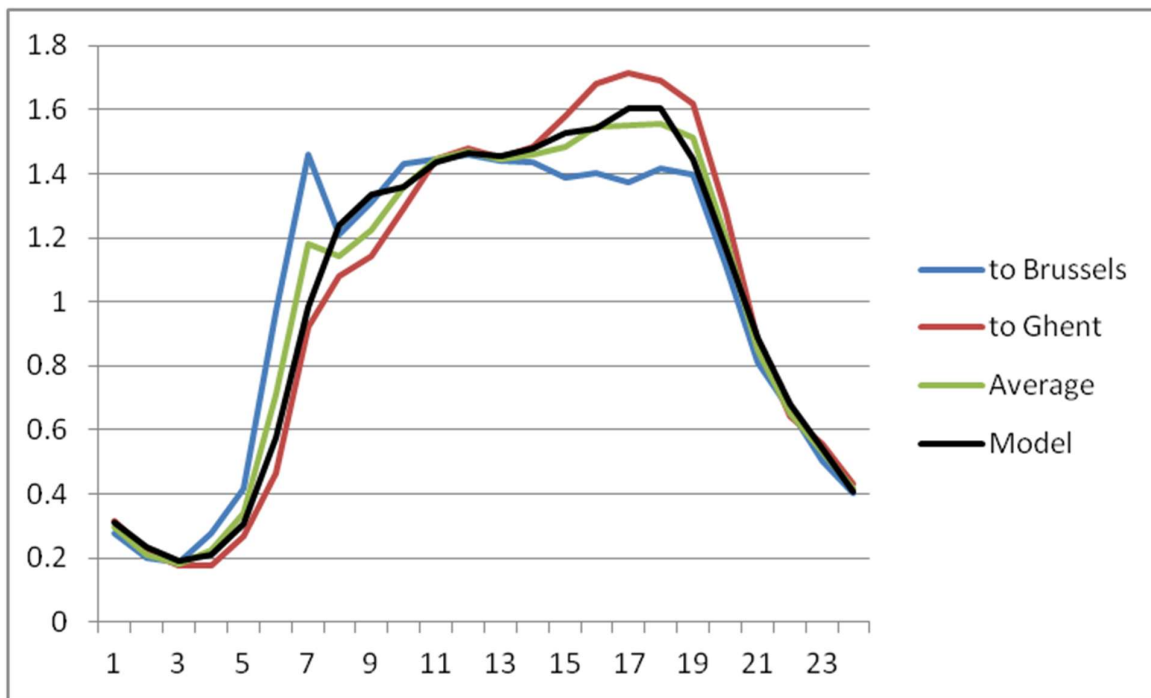


Figure 92 : Normalized PM_{2.5} emission equivalents per hour of day (X-axis). In blue: the sum of the driving lanes towards Brussels; in red: the sum of the driving lanes towards Ghent. In green: the weighted average of the blue and red line. In black: the time factors used in the model.

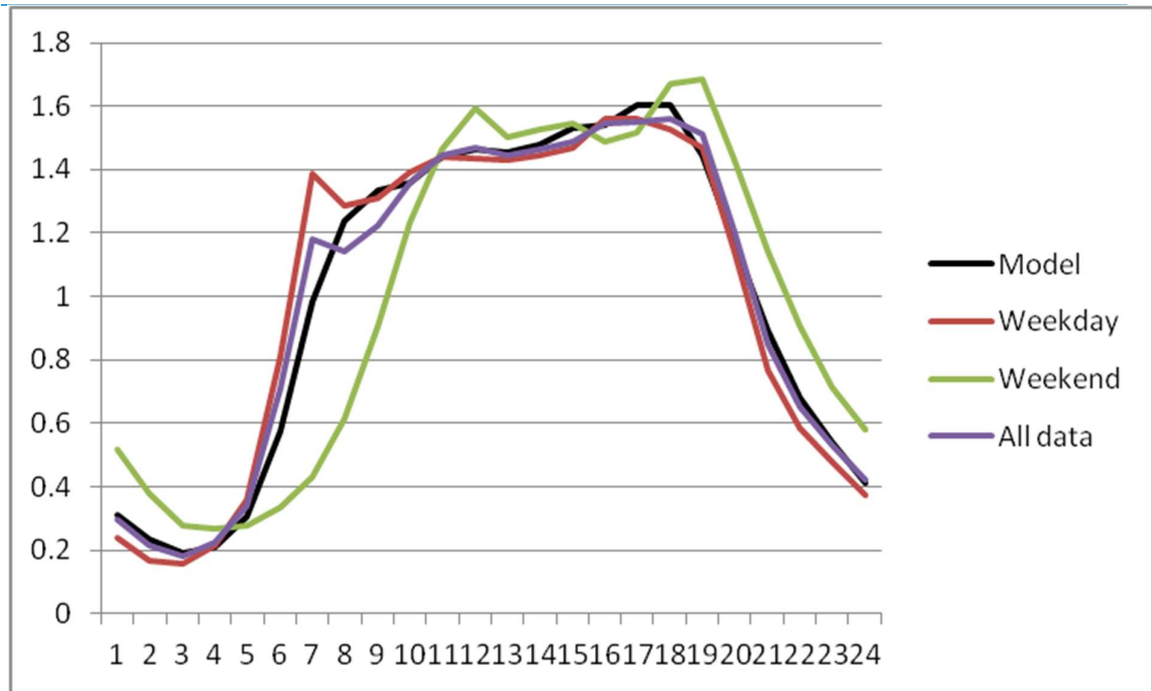


Figure 93 : Normalized PM_{2.5} emission equivalents per hour of day (X-axis). In red: average for a weekday. In green: average for a weekend day. In purple: the weighted average of the green and red line. In black: the time factors used in the model.

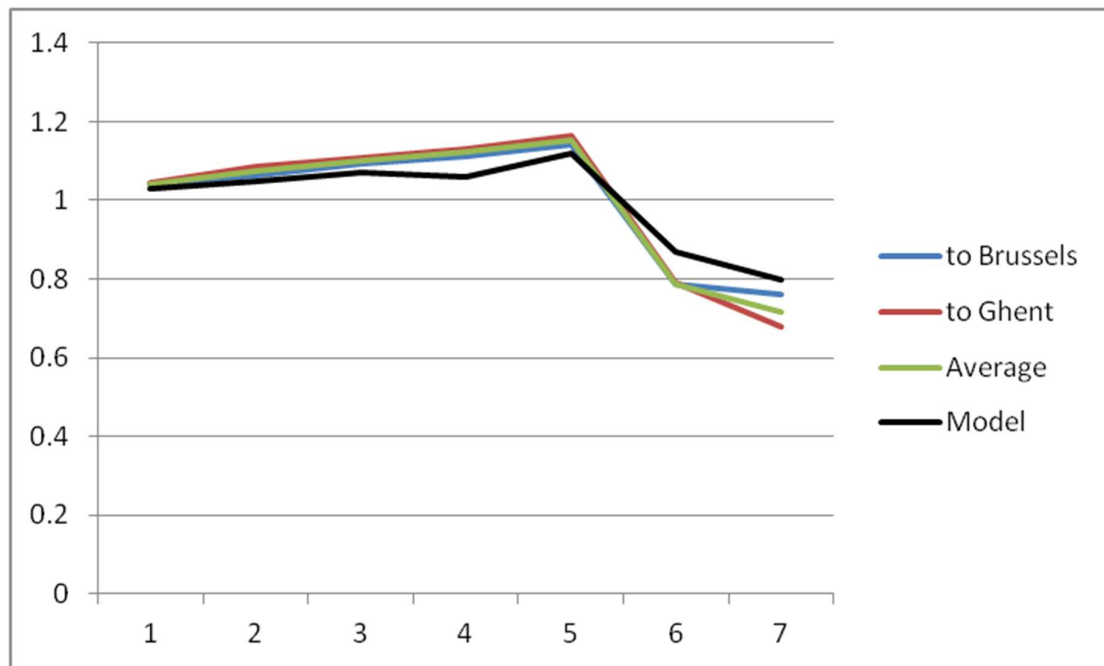


Figure 94 : Normalized PM_{2.5} emission equivalents per day of the week (X-axis). In blue: the sum of the driving lanes towards Brussels; in red: the sum of the driving lanes towards Ghent. In green: the weighted average of the blue and red line. In black: the time factors used in the model.

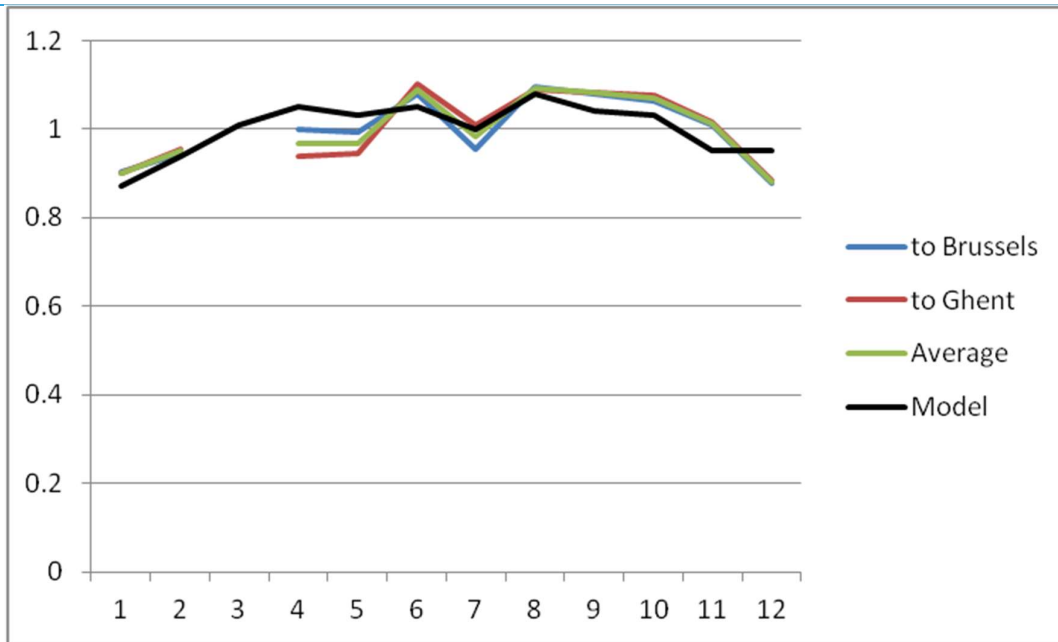


Figure 95 : Normalized PM_{2.5} emission equivalents per month of the year (X-axis). In blue: the sum of the driving lanes towards Brussels; in red: the sum of the driving lanes towards Ghent. In green: the weighted average of the blue and red line. In black: the time factors used in the model.

6.9.2. TRAFFIC SPEEDS

There is a lower passenger car traffic speed during morning rush hour in the direction of Brussels. This reduction in speed is not seen in the evening rush hour, nor in the direction of Brussels, nor in the direction of Ghent. This reduction speed will lead to lower emissions than if the speed would not be reduced and can thus explain a (large) part of the model overestimation in the morning hours.

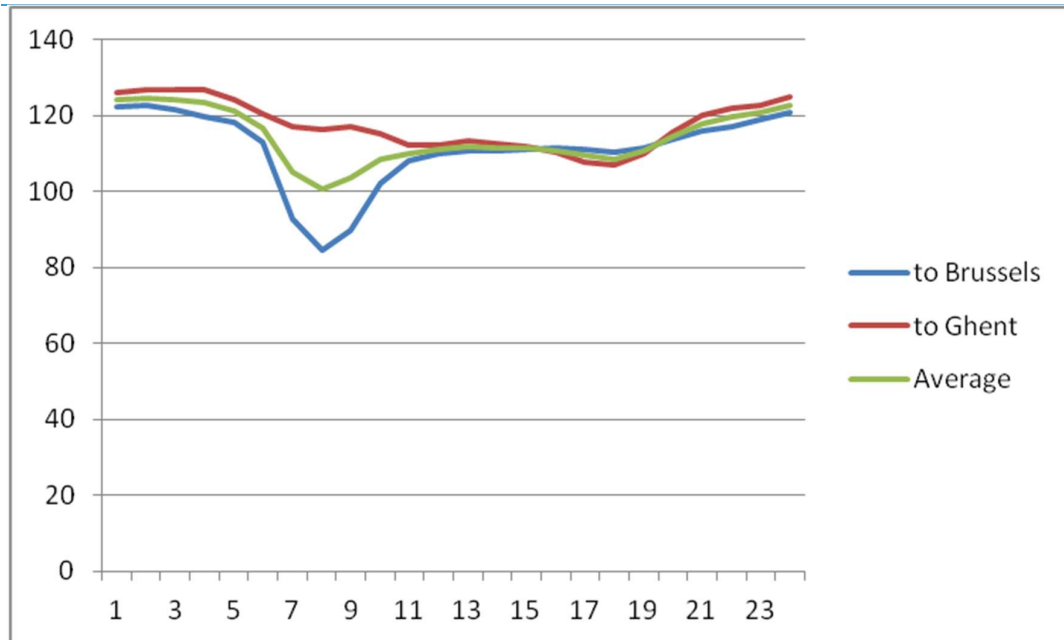


Figure 96 : Average speed (in km/h) of passenger cars per hour of the day (X-axis). In blue: the average of the driving lanes towards Brussels; in red: the average of the driving lanes towards Ghent. In green: the weighted average of the blue and red line.

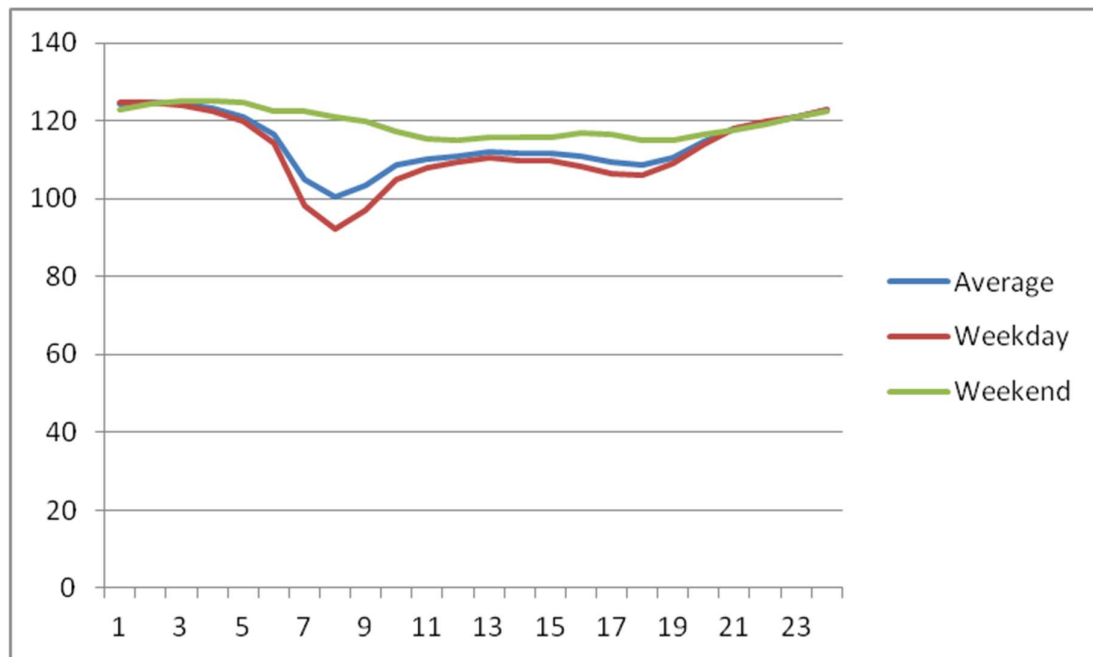


Figure 97 : Average speed (in km/h) of passenger cars per hour of the day (X-axis). In red: the average on weekdays.; in green: the average on weekend days. In blue: the weighted average of the green and red line.

6.9.3. DISTRIBUTION OVER THE TRAFFIC LANES

As said before, we have used an a priori distribution over the traffic lanes of 50, 30 and 20%. The traffic counts however point towards a distribution of 43, 37 and 20%. The difference between the model results with both cases would however be small.

6.10. MODEL ADAPTATIONS

In order to counter the problems seen in the previous chapters, the following adaptations to the model setup have been made:

- Adaptation of the emission distribution on the driving lanes to 43, 37 and 20% (§6.9.3).
- Adaptation on the emission factors of the intraweekly and intrayearly cycle to the data shown in Figure 94 and Figure 95 (green lines).
- Adaptation on the emission factors of the intradaily cycle based on the traffic counts. Therefore we start from the green line on Figure 92 (also green line on Figure 98). We adapt this line by the speeds driven by the passenger cars at the different moments (Figure 96) as follows:
 - Speed > 120 km/h: no change
 - Speed < 90 km/h: emission reduction of 30% (Lefebvre et al., 2011a).
 - Speed between 90 and 120 km/h: emission reduction between 0% (120 km/h) and 30 % (90 km/h) following a parabolic pattern.

This leads to the blue line on Figure 98.

- Wind-dependent traffic-induced dispersion of line sources. The traffic-induced dispersion of line sources is made linearly dependent on the inverse of the wind speed at source height. The traffic-induced dispersion at a wind speed of 2 m/s is kept constant.
- An increase in the horizontal plume spread to take into account the variable wind direction at low wind speeds. The system of NRC (1981) has been used with a correspondence between stability classes 1 (very stable), 2 (stable) and 3 (neutral) of Bultynck-Malet and stability classes G (extremely stable), F (stable) and D (neutral) of Pasquill. As a result, the σ_y is multiplied with a factor which can be found in Table 14.

Stability class	$u \leq 2 \text{ m/s}$	$2 \text{ m/s} < u < 6 \text{ m/s}$
1 (very stable)	6	$1+(6-u)/0.8$
2 (stable)	4	$1+(6-u)/1.33$
3 (neutral)	2	$1+(6-u)/4$

Table 14 : Correction factor to σ_y in case of neutral and stable conditions.

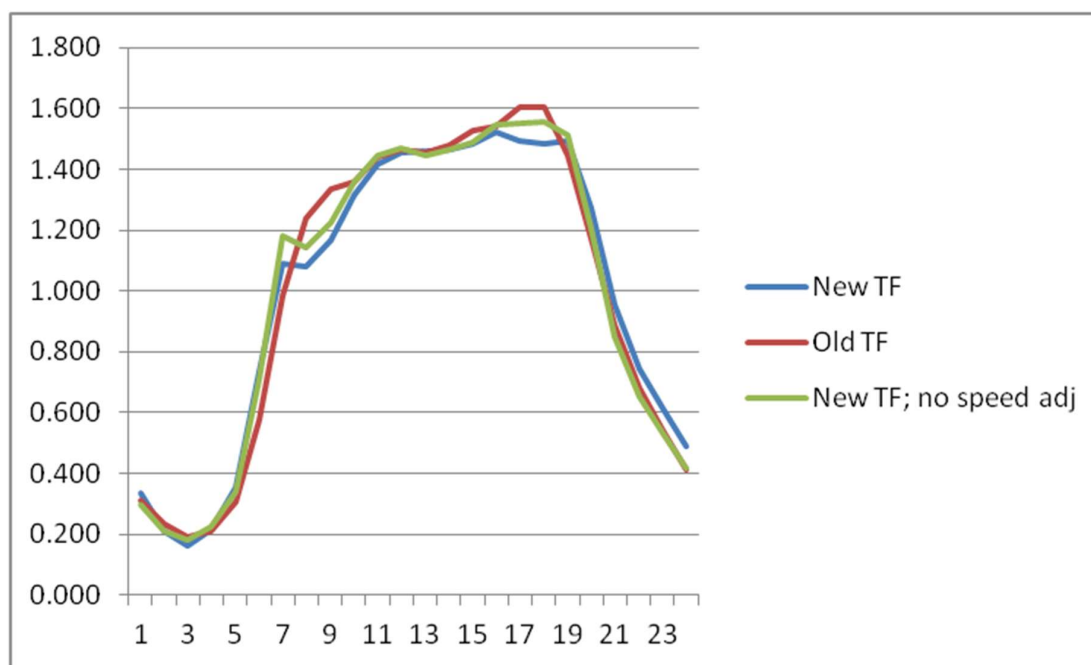


Figure 98 : Time profiles for the different hours of the day (on the X-axis). In red: old time factors; in blue: new time factors; in green: new time factors without the speed component.

6.11. RESULTS WITH MODEL ADAPTATIONS FOR BC

We can summarize the results as follows:

- The spatial validation does not change significantly.
- The halfhourly validation improves slightly, with less extreme outliers and an improved R^2 (see for instance Figure 99).
- No big changes in the daily nor in the weekly averaged model results.
- The overestimation during the morning peak is still present (Figure 100). The inconsistency between the high traffic counts in the early morning, the high stability in the early morning and the relative low concentrations at this time remains (6h-7h local time).
- The dependence on the wind speed is very similar then before (Figure 101). However, this is due to a compensation of two effects. The change in time factors has increased the emissions in the late night, where low wind speeds are present which increases the incompatibility between model and measurements (Figure 102). The model code adaptations annihilate this effect (compare Figure 75, Figure 101, Figure 102).
- The dependence on the wind direction has improved, albeit insufficiently (Figure 76, Figure 103).

- The changes in the traffic-induced dispersion have a relatively small effect, whereas the changes in the wind variability show a larger one (not shown).

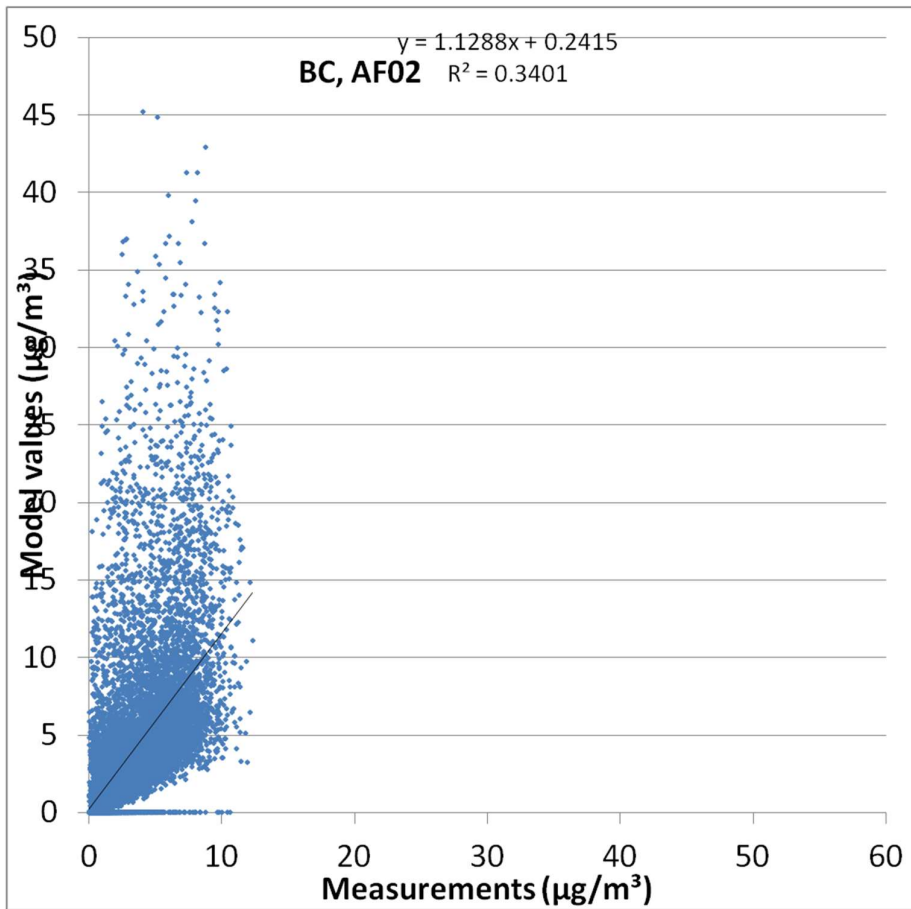


Figure 99 : Same as Figure 62, but after model adaptations.

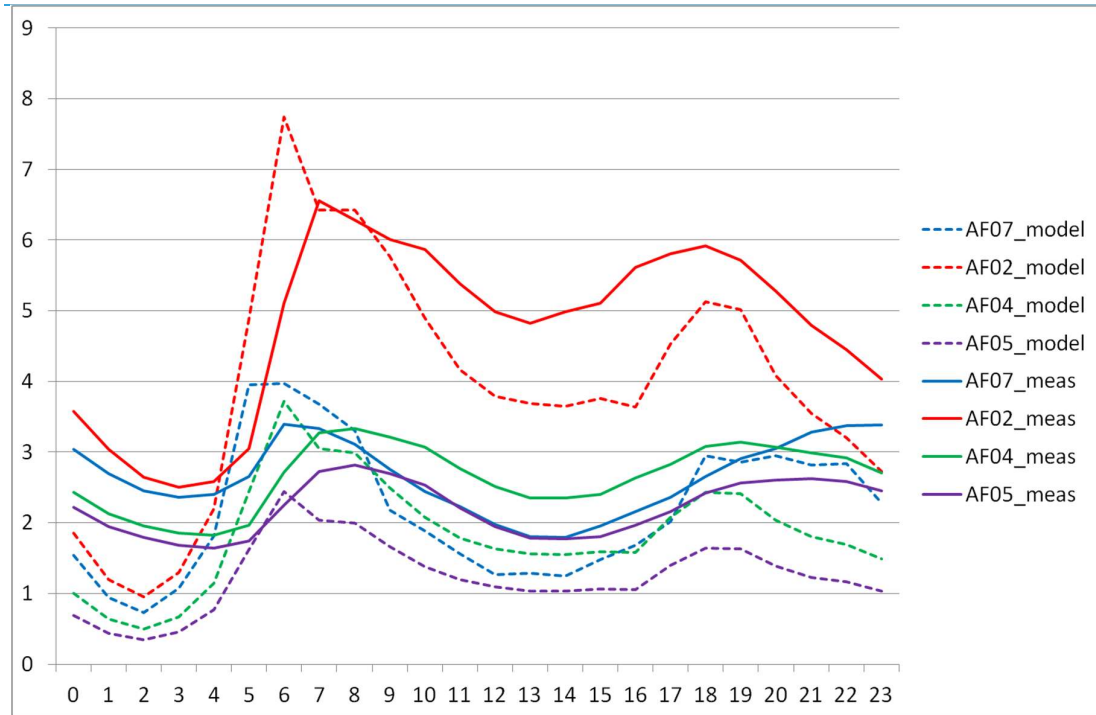


Figure 100 : Same as Figure 80, but after model adaptations.

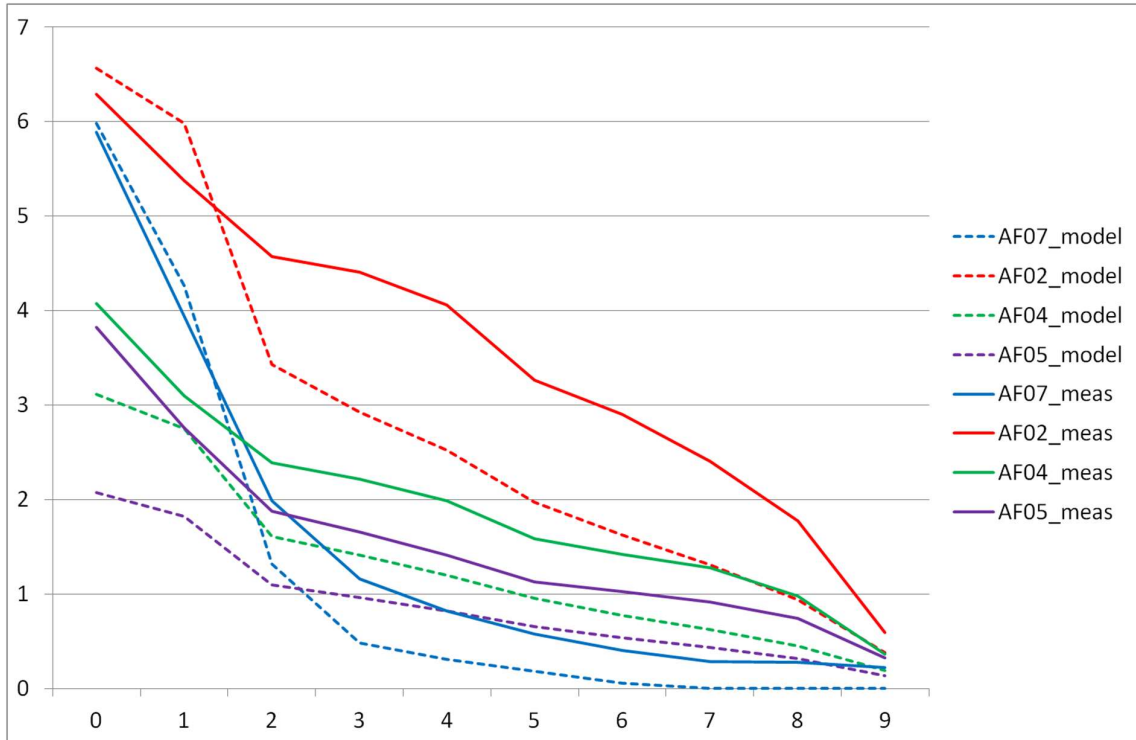


Figure 101 : Same as Figure 75, but after model adaptations.

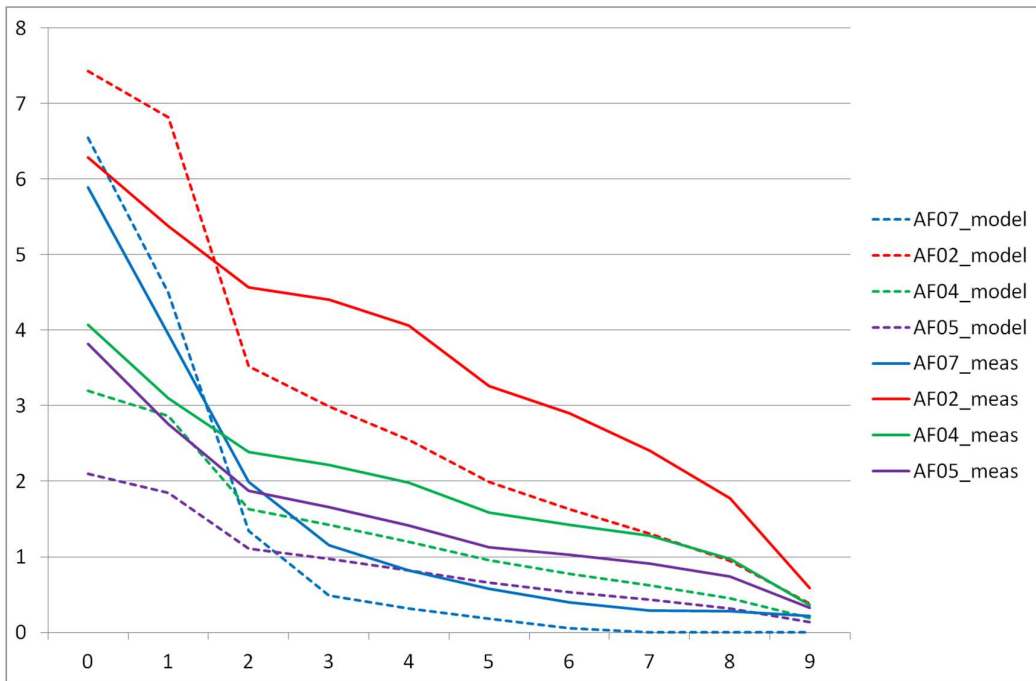


Figure 102 : Same as Figure 75, but with only adaptations to the emissions, not to the model.

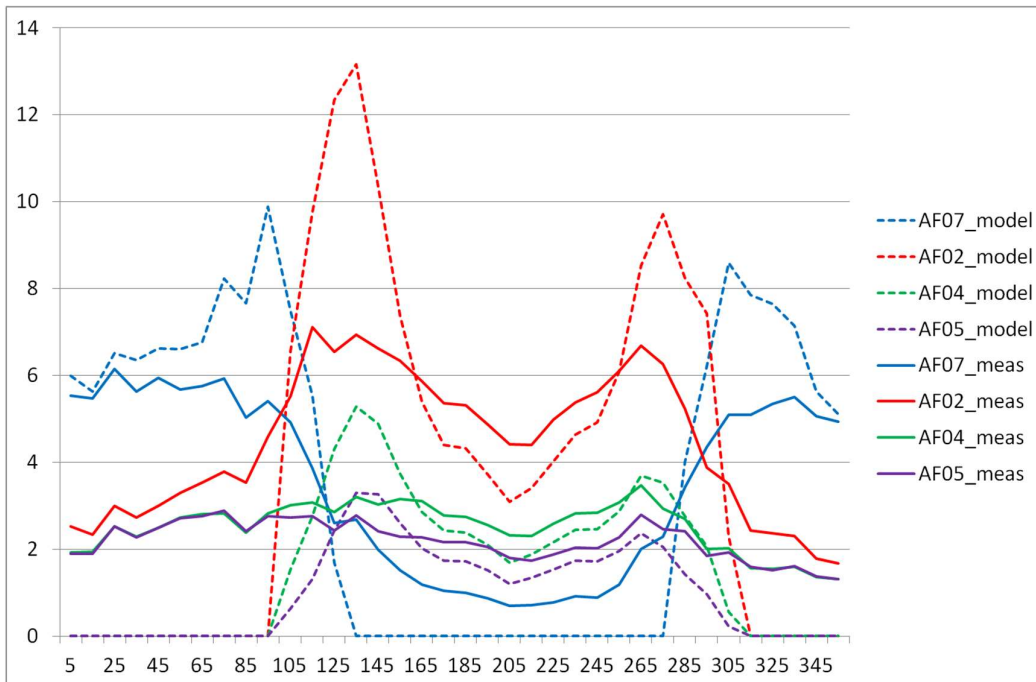


Figure 103: Same as Figure 76, but with model adaptations.

6.12. THE INFLUENCE OF RESULTS AGGREGATION TIME ON THE VALIDATION PARAMETERS

With the latest model adaptations (§6.10), the effect of the time aggregation of results on the validation parameters has been investigated. Therefore, the RMSE and the correlation between model results and measurements for the BC concentrations of the highway-campaign have been determined for different aggregation times (ranging from half an hour to one week). This has been shown in Figure 104 and Figure 105 respectively. An increase in aggregation time improves model validation. However, at about one day (48 half hours), the maximum seems to be reached for the correlation. Furthermore, the increases in RMSE for longer aggregation times are small. Another cut-off point seems to exist at about 3 hours (6 half hours, fourth point from left on the graphs), at which already a good deal of the gain due to aggregation is reached.

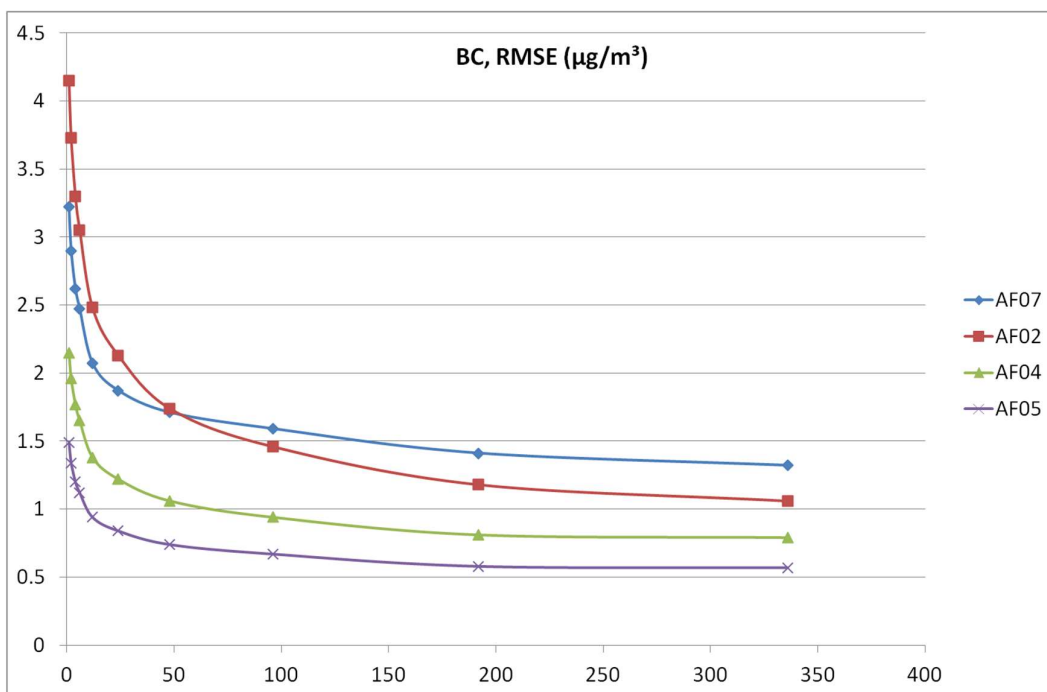


Figure 104 : The RMSE (Y-axis, in µg/m³) between measurements and model values at different locations (colors) for different aggregation times (X-axis, in periods of 30 minutes).

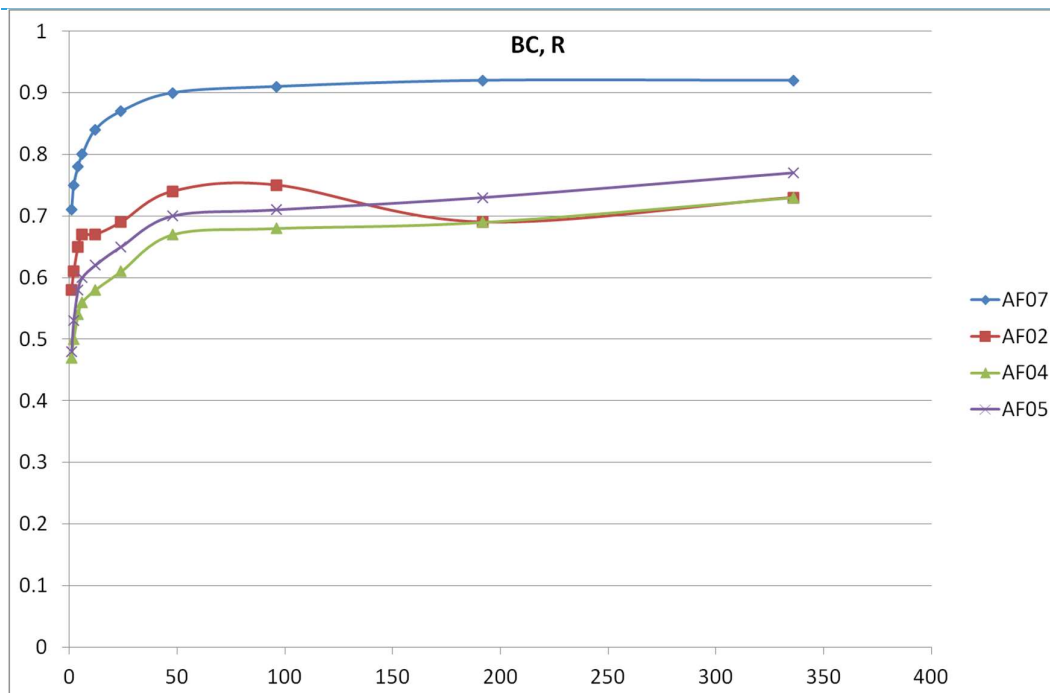


Figure 105 : The correlation (Y-axis) between measurements and model values at different locations (colors) for different aggregation times (X-axis, in periods of 30 minutes).

6.13. CONCLUSIONS AND SOME EXTRA REMARKS

The following conclusions have been reached in this section:

- The spatial validation for components with a large traffic contribution (NO_2 , BC) is very good for the measurements close to the highway. For the other components (PM_{10} , $\text{PM}_{2.5}$), the validation is mediocre, due to other sources not taken into account by the model.
- The temporal validation for the traffic components (BC, NO_2) is good, when aggregated at time scales of a day or longer. For halfhourly aggregations, the validation is less good. However, this poses no direct problem for regulatory purposes as the only hourly limit value with a high percentile value (i.e. a limit value which would be strongly affected by this problem) is the hourly limit of NO_2 . However, when this limit is reached, the yearly limit is also strongly exceeded. The number of hours exceeding this limit will be overestimated by the model.
- The model has problems with sources at low heights with low wind speeds (see also Van Renterghem, 1999), due to a lack in wind variability. However, this problem is mitigated when aggregating results over longer time scales. It has been shown in earlier studies that this does not pose a problem for higher stacks (less wind variability at height), and thus for industrial cases where hourly concentrations can be important. Adapting the model for this problem with a solution which is used in the USA alleviates but not solves the problem.

-
- The urban parameterization used in most IFDM-studies tends to underestimate the contribution of sources emitting at low altitudes in open areas.
 - There are some indications that the model is underestimating very high concentrations and overestimating very low concentrations at somewhat longer time scales (week), especially for NO₂. This is in agreement with other studies. However, these deviations are not important close to the annual limit value of 40 µg/m³.

CHAPTER 7 ATMOSYS CITY CAMPAIGN AND THE NO₂-MEASUREMENT CAMPAIGN USING PASSIVE SAMPLERS IN CITIES

Two more measurement campaigns are available for validation.

7.1. THE NO₂-MEASUREMENT CAMPAIGN USING PASSIVE SAMPLERS IN CITIES IN 2010

The measurement campaign is described in VMM (2011a). In 13 cities, measurements were made at three locations: an urban background location, a location close to major approach road to the city and a street canyon.

This campaign has been used to validate the background concentrations of CAR, IMMI-2 and IFDM-traffic (VMM, 2011b). This is however outside the scope of this report.

However, this campaign cannot be used for the moment (if the following problems were to be solved, a validation study with this campaign would become possible) to validate the IFDM model as:

- The exact location of the VVC-roads is not guaranteed. This is important for this campaign, due to the measurements close to the major roads, where slight differences in road locations could lead to large deviations in modeled values. For the studies discussed in chapters 2 and 3, this road location problems were also present (although partly corrected in the study mentioned in chapter 3), but due to the location of the measurements (in general, further away from the major roads), this was less of a problem.
- The error on the traffic volumes on urban VVC-roads is much higher than on highway roads, as the latter ones can be calibrated on continuous measurements. This is also the case for the studies in chapters 2 and 3. However, this was less of a problem, due to the location of the measurements (see above).
- The street geometry is not known for most of the cities (height of the buildings, width of the street canyon, ...), which would eliminate all the street canyon measurements for the purpose of the validation.

7.2. THE ATMOSYS CITY CAMPAIGN

This measurement campaign is described in Roet (2013). For the same reasons as stated above, this campaign cannot be used for the moment for validation of the IFDM-model. However, the results of this campaign point to interesting data about for instance resuspension, which has to be studied further. However, this is outside the scope of this report.

CHAPTER 8 VALIDATION OF THE ATMOSYS-RETROSPECTIVE SIMULATIONS FOR THE YEAR 2009

Within task 9.1 of the ATMOSYS-project, retrospective simulations for the year 2009 have been set up (Vranckx and Lefebvre, 2013). In this chapter, we will present shortly the main aspects of the simulation model and discuss the validation methodology and results. More information about the setup of the model can be found in Vranckx and Lefebvre (2013).

8.1. METHODOLOGY

The demonstrative retrospective simulation presented in this report has been conducted for the calendar year 2009; as this is the most recent year for which all the necessary input data were available at the start of the retrospective simulation. Pollutants of interest include NO₂, O₃, PM₁₀, PM_{2.5} and EC (elementary carbon). For each pollutant a high resolution concentration map of Belgium is produced for each hour of the year 2009, which offers the possibility to use yearly 'state-of-the-air quality' maps, occurrences of exceedances, complete time series from each model receptor point, etc. Further, the obtained model results are validated against the available hourly data from the measuring stations in Belgium for NO₂, O₃, PM₁₀ and PM_{2.5}. For EC, the daily data (six day interval) from the 2008-2009 CHEMKAR-II campaign of VMM (VMM, 2010) are used as validation material.

Recently, VITO has published a detailed report comparing the available models to create large scale annual concentration maps for PM₁₀, PM_{2.5}, NO₂ and O₃ (Maiheu et al., 2012). The analysis was based on annually averaged concentration maps for 2009. The different techniques taken into account were:

- (i) the most recent version of the RIO interpolation model for which a distinction was made between 'the standard RIO model' that uses trends based on long-term averages and 'the RIO-09 model' that only uses data for 2009
- (ii) (ii) the deterministic AURORA model with four different methods of calibration: simple classical bias correction, simple bias correction according to orthogonal regression, advanced bias correction based on 'Kalman Filtering' and 'Optimal Interpolation' data assimilation
- (iii) (iii) the VLOPS model with calibration for NO₂ (using different calibration functions) and PM₁₀.

The various techniques and maps were critically analyzed, validated and compared in order to identify the best possible large-scale concentration map for each pollutant / indicator. This comparison was in favour of the usage of the RIO interpolation model for large scale pollution concentration maps, as it combines high accuracies, and performed best compared to other

techniques for most pollutants and regions. An important remark here is that RIO can not be used in forecast mode as it uses intelligent interpolation of pollutant concentration measurements and thus per definition relies on available data. Further, RIO can not be used for EC as no measurement data are available for the year 2009.

The quality forecast developed within ATMOSYS (see Action 8) is thus relying on the regional model AURORA. For the retrospective simulations RIO is the preferred regional model because actual measurements are used as input.

In highly developed countries such as Belgium, it is recommended to simulate the air pollution for the complete region with sufficient detail to describe the large gradients along highways. It is insufficient to rely on a large scale interpolation of a deterministic model, as its output is not detailed enough. A bi-Gaussian plume model such as the IFDM model used at VITO can simulate pollutant dispersion at local scale. Coupling of a large scale regional model to IFDM enables one to cover both the regional scale trends in air pollution as well as the large gradients observed on the local scale. The model combination of choice for the retrospective simulations thus is:

- NO₂: RIO + IFDM
- O₃: RIO + IFDM
- PM₁₀: RIO + IFDM
- PM₂₅: RIO + IFDM
- EC: AURORA + IFDM

The three-hourly ECMWF meteo data are combined with the measurements of one meteo station (Antwerp, Luchtbal). The meteorological ECMWF model wind speed and temperature data are corrected by the measurements from this meteo station.

The MIMOSA model has been applied to estimate road traffic emissions based on hourly traffic information. These emissions are available for 2007 and are scaled to the available total traffic emissions per region for 2009. The emissions are calculated as described in §3.1 of (Maiheu, 2011) and §5 of (Maiheu & Lefebvre, 2011). The only difference is that the minimum requirement (for emissions) for inclusion of a road in the emission dataset was eliminated.

All model runs have been started for an irregular grid of 425.145 points. This irregular grid is an advanced line source following grid to capture the large gradients around highways. The amount of receptor points is an optimum between high resolution and a reasonable computation time. With the chosen grid and settings, a computation time of 816 CPU days is needed, leading to 1 terabyte of data.

Some examples of the resulting maps are given in Figure 106 and Figure 107.

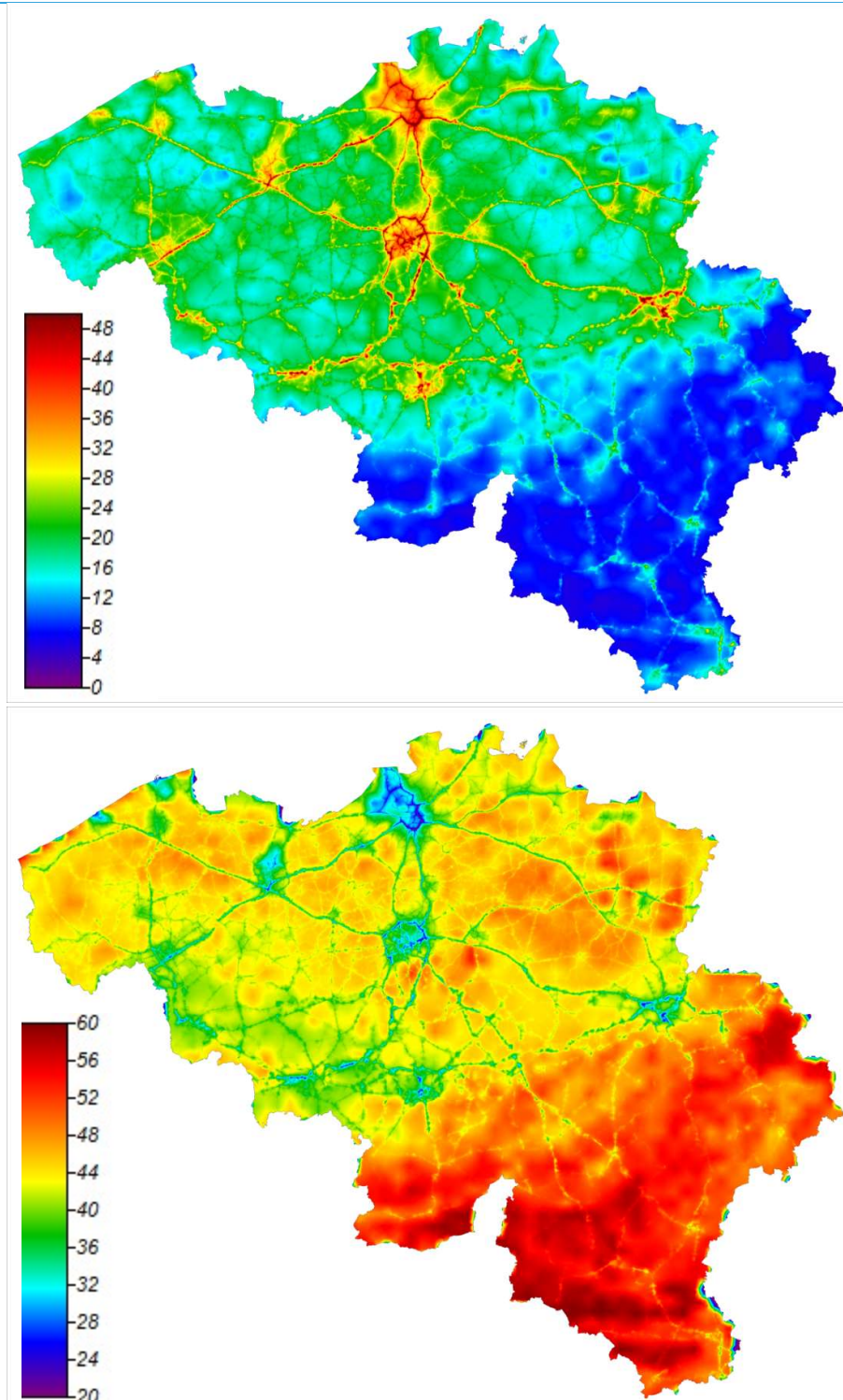


Figure 106: The time-averaged NO₂ (above) and O₃ (below) concentration maps of Belgium for the year 2009 as simulated by RIO-IFDM. Units: µg/m³.

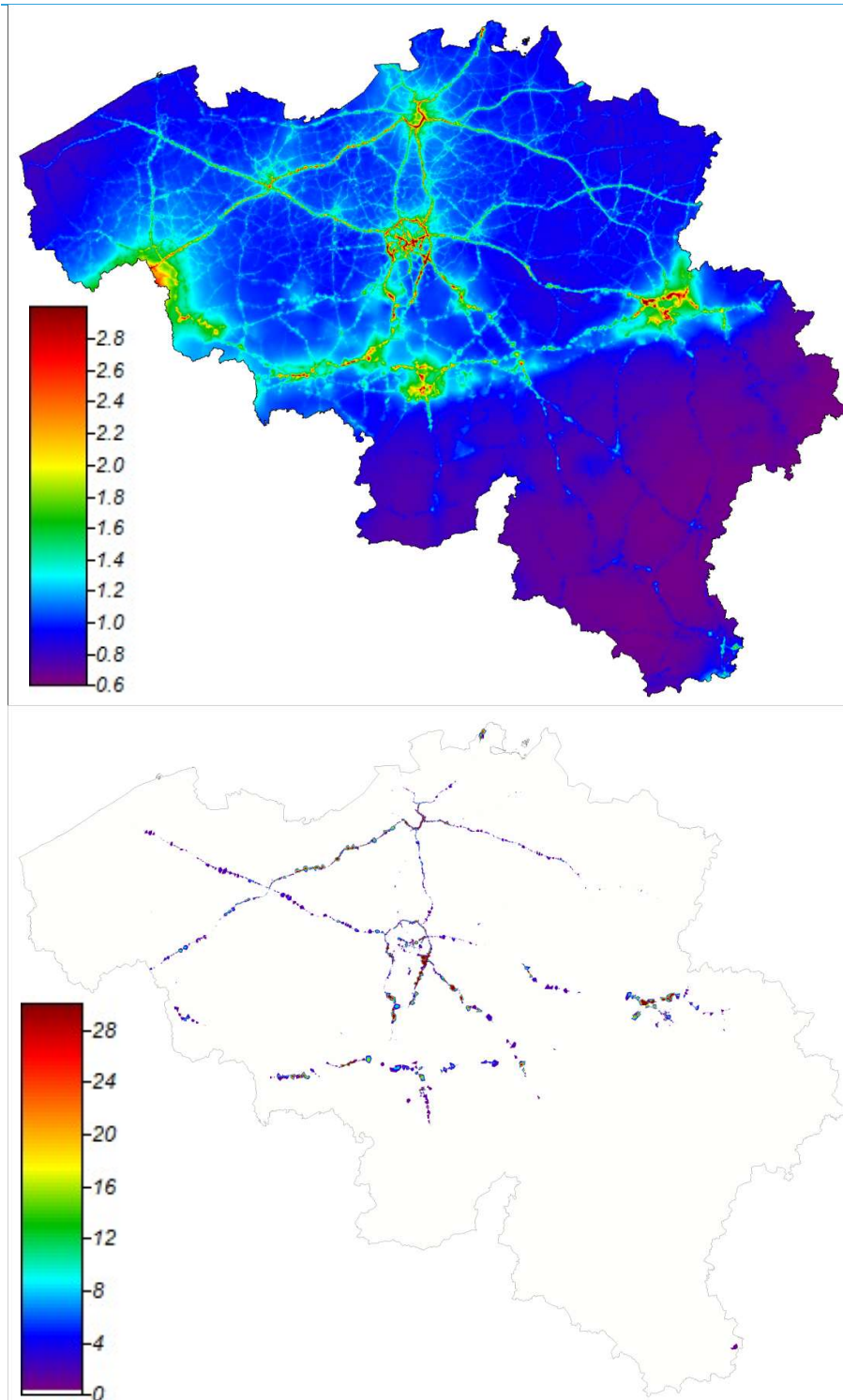


Figure 107 : Above: The time-averaged EC concentration map of Belgium for the year 2009 as simulated by AURORA-IFDM. Units: $\mu\text{g}/\text{m}^3$. Below: the number of hours exceeding an NO_2 concentration of $200 \mu\text{g}/\text{m}^3$ for the year 2009 as simulated by RIO-IFDM. Units: hours.

8.2. VALIDATION FOR NO₂, O₃, PM₁₀ AND PM_{2.5}

8.2.1. METHODOLOGY

Several air quality models have recently been validated in the frame of the ‘Determination of the best available large-scale concentration maps for air quality in Belgium’ (Maiheu et al., 2012). To validate the RIO-IFDM (NO₂, O₃, PM₁₀ and PM_{2.5}) model chain, the same approach has been followed and all scripts have been re-used. Validation has been performed against all available 2009 concentration data for the pollutants of interest from the Belgian measuring stations. For a fully detailed explanation of the validation approach, the interested reader is referred to MIRA-report (Maiheu et al., 2012). The latter study indicated that the RIO results, if available, can be considered state-of-the-art in most cases. One of the main questions can thus be if IFDM further improves the available RIO results.

As a first step, the new RIO-IFDM results can be added to the existing validation plots. A method to give a good visual representation of statistical values obtained during the validation is the use of *target plots*. Such a target plot is an XY diagram plotting 2 statistical indicators against each other, the ‘Centered RMSE (CRMSE)’ on the X-axis and the ‘BIAS’ on the Y-axis. Both quantities are normalized using the standard deviation of the observations. A model performs better for the investigated validation data set, the closer its target value is to the origin.

$$\frac{CRMSE}{\sigma_o} = \frac{\sqrt{\frac{1}{n} \sum_{i=1}^n \left([(M_i - \bar{M}) - (O_i - \bar{O})]^2 \right)}}{\sqrt{\frac{1}{n} \sum_{i=1}^n [(O_i - \bar{O})^2]}}$$

$$\frac{BIAS}{\sigma_o} = \frac{\frac{1}{n} \sum_{i=1}^n (M_i - O_i)}{\sqrt{\frac{1}{n} \sum_{i=1}^n [(O_i - \bar{O})^2]}}$$

with O_i the observed and M_i the modeled concentration.

As this is calculated for each measuring station, the values are averaged over all measuring stations to give a final indication of model performance. An example of such a plot is given in Figure 108 for PM_{2.5} for IFDM (starting from RIO background concentrations), RIO and other available models.

From Figure 108 one might conclude that IFDM does further improve the RIO concentration maps. This is not a fair comparison as the ‘leaving-one-out’ technique has been applied for the RIO and AURORA validations. This means that the measuring station for which a validation is done is left out in the RIO simulation; so RIO gives as value a smart interpolation based on the land use. For IFDM, the background concentrations are however the RIO values calculated using all stations (without leaving-one-out). The model improvement is therefore artificial.

Applying the leaving-one-out technique on the RIO-IFDM chain would be optimal. This is not realistic as this would imply running an extra simulation for each measuring station, each requesting about 816 CPU-days. Since applying the leaving-one-out to RIO-IFDM is computational too costly, RIO has been validated excluding the leaving-one-out to enable a fair comparison.

The target plot was initially devised for validation at different measurement locations. However, for model comparison, the resulting graph becomes quickly very crowded (Figure 108, left). Therefore, the average location for all stations is used for model comparison (Figure 108, right). This makes the graph much easier to interpret. However, the graph cannot be used to check if the model corresponds to the model validation criteria at every measurement location.

In the study of (Maiheu et al., 2012), the traffic stations (measuring stations close to roads with intense traffic) had been left out as they were not considered representative in the frame of that study. As one can expect to see the largest influence of using IFDM close to emission sources, where the largest gradients in concentrations are present, the traffic stations have to be included for this study.

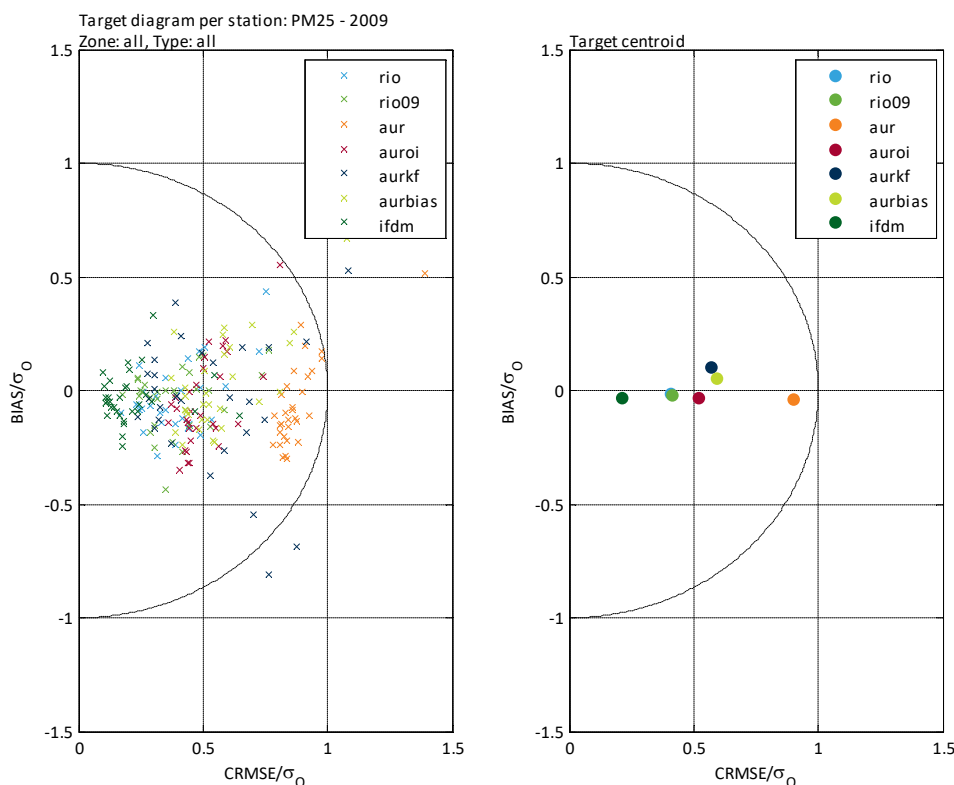


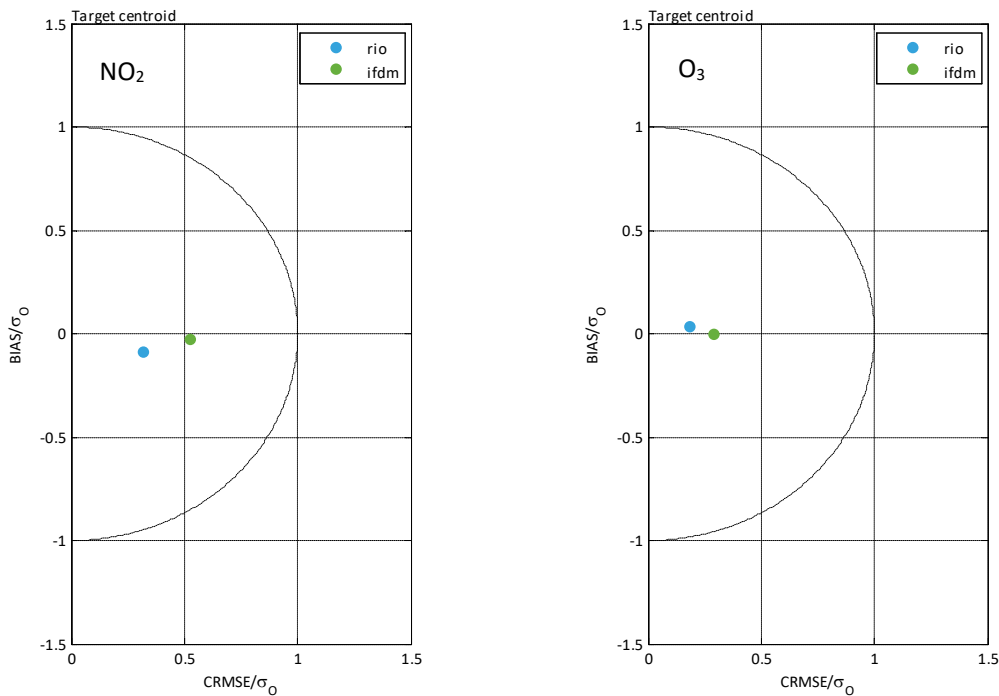
Figure 108: Target plot for PM_{2.5} for the year 2009 comparing the model performance of IFDM (starting from RIO background concentrations), RIO and other available models. The figure on the left gives a separate value per measuring station; on the right the average over all measuring stations is depicted. The comparison is made applying the ‘leaving one out’ technique for all models except IFDM.

Throughout this report, validation is thus performed:

- Excluding leaving-one-out for both RIO-IFDM and RIO
- Including all traffic stations

8.2.2. RIO-IFDM TEMPORAL VALIDATION

The target values for NO_2 , O_3 , PM_{10} and $\text{PM}_{2.5}$, averaged over all measuring stations, are plotted in Figure 109. From these plots it is directly evident that the improvement observed for RIO-IFDM in Figure 108 is indeed artificial due to the leaving-one-out technique not being applied to RIO-IFDM. Overall, RIO-IFDM appears to give a slight deterioration compared to RIO when validating temporally for the available measuring stations.



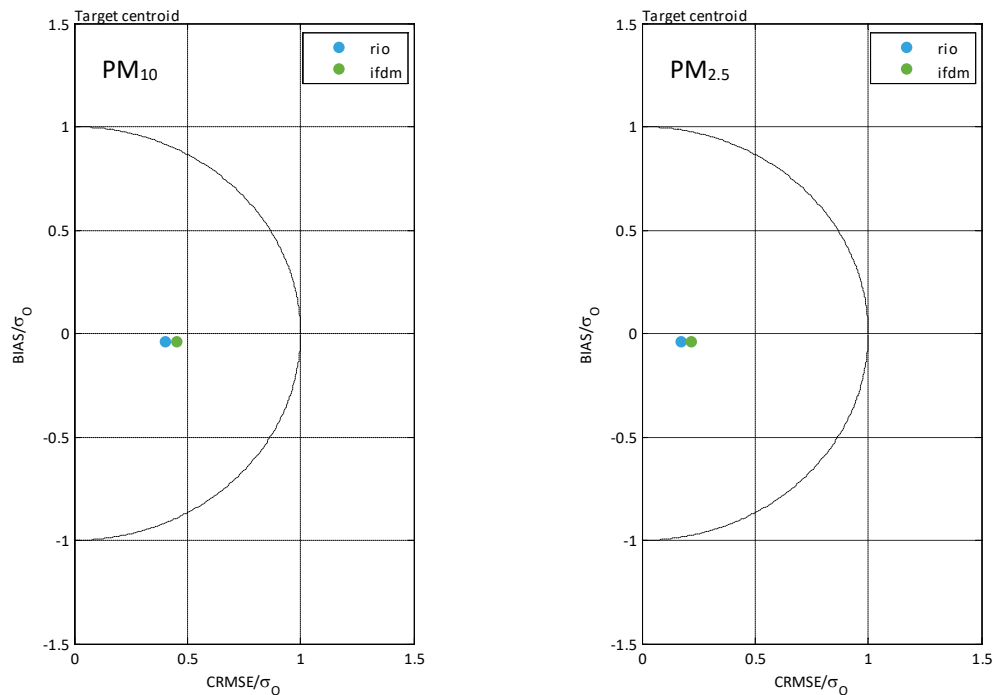


Figure 109: Target plots for NO₂, O₃, PM₁₀ and PM_{2.5}. Values are averaged over all available measuring stations including the traffic stations. Comparison of validation for RIO and RIO-IFDM.

A few remarks have to be made before drawing conclusion:

- Only 5 traffic stations are operational in Belgium. One station, Kunst-Wet (Brussels) did not report in 2009. Three stations measured NO₂; 3 stations measured PM₁₀, 2 stations measured O₃ and only 1 measured PM_{2.5}. Of these 4 stations which were operational in 2009, 3 are located in the Brussels-Capital region, the 4th in Diepenbeek (Limburg). The input data for IFDM for the Brussels region are less detailed as for other parts of Belgium.
- IFDM has to interpolate. The IFDM interpolation on top of the intelligent RIO-interpolation used for the background values can lead to a deterioration. This was especially observed here since measuring stations were also input for RIO.
- The quality of the IFDM results depends on the quality of the input data (emissions). RIO only relies on the pollutant concentrations from the monitoring network (which are the data against which we validate) and land use parameters for the interpolation. A more detailed emission inventory will thus further improve the IFDM results.

In the light of the remarks given, for the temporal validation, one can indeed observe a deterioration of target values of RIO-IFDM for NO₂ and O₃. Hardly any change is seen for PM. For PM the gradients in concentration in Belgium are smaller and therefore the effect of the interpolation has less influence.

To illustrate the importance of detailed input data, separate target plots have been made per region in Belgium. An illustration is given in Figure 110, which shows the target plots for PM₁₀ for Flanders and Wallonia. Here, a negative influence of IFDM is observed for Wallonia. No change, is however observed for Flanders, for which more detailed input data were available for this study (see above). This type of comparison has been made for each pollutant and each Belgian region (Brussels, Flanders and Wallonia).

The added value of IFDM will be highest close to emission sources where high gradients in the concentrations are presented and the increased resolution proves most valuable. The current validation can not show this added value due to the lack in relevant data; the current telemetric measuring network works here in favour of RIO. Further, the differences observed in validation between RIO and RIO-IFDM remain small. One can even question the significance of these differences given the uncertainties on the measurements, simulations, RMSE and BIAS.

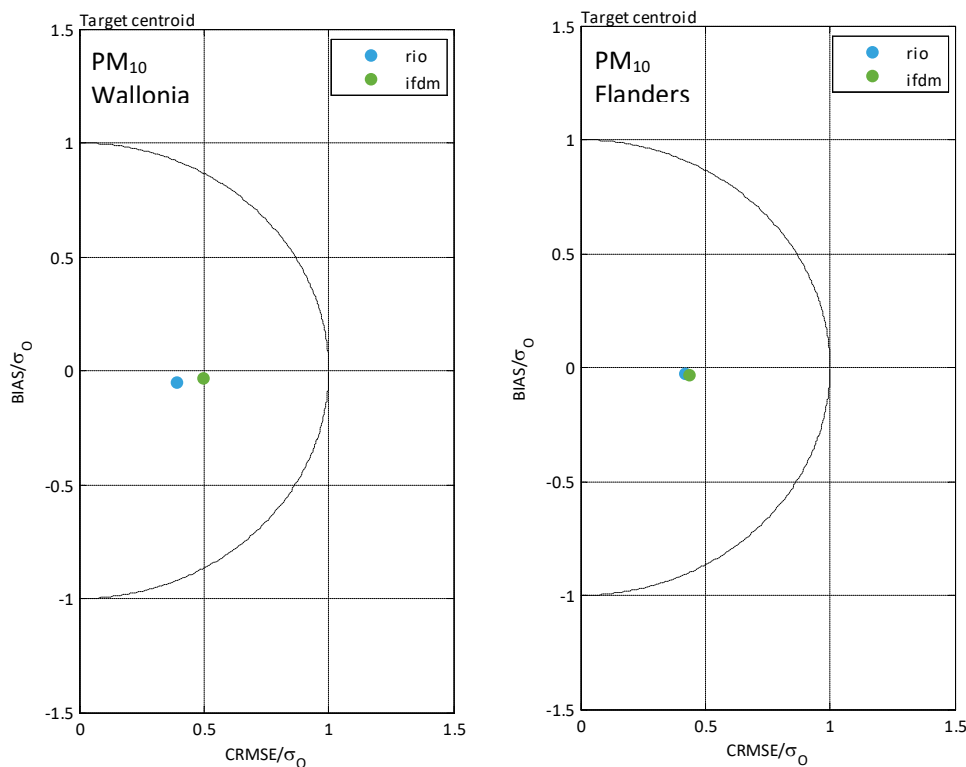


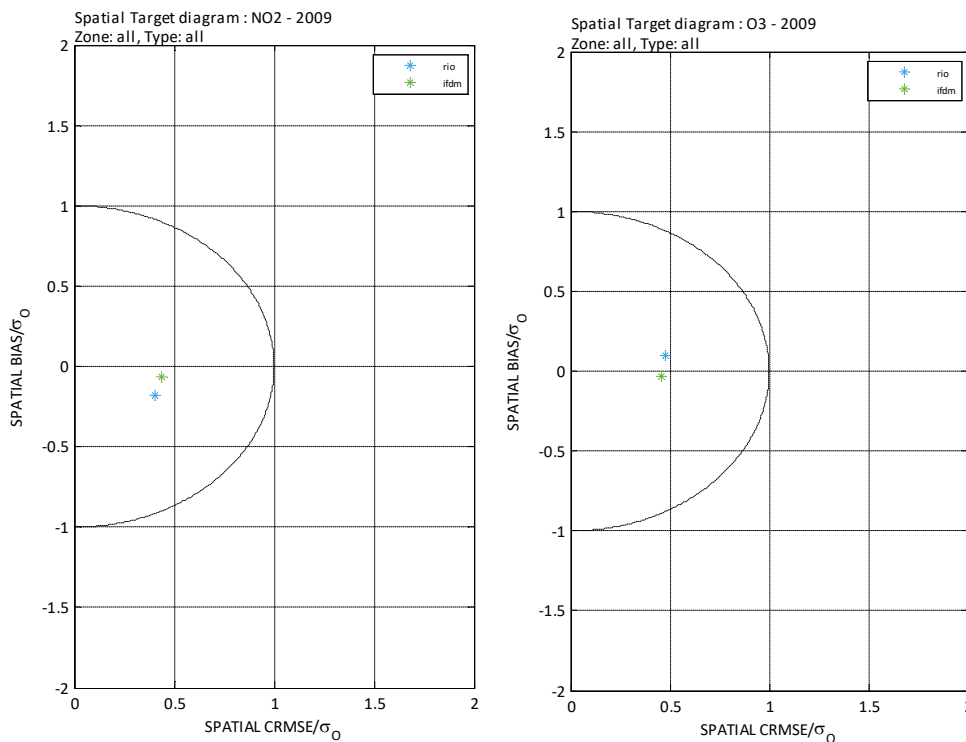
Figure 110: Target plots for PM₁₀ split up per region in Belgium. Values are averaged over all available measuring stations. Validation is performed for RIO and RIO-IFDM.

8.2.3. RIO-IFDM SPATIAL VALIDATION

The model results can be spatially validated through comparison of the 2009-average measured concentrations with the 2009-average simulated concentrations for each measuring station. Full details of the spatial validation approach can be found in (Maiheu et al., 2012). A first indicator of the quality of the spatial validation can again be given through target plots. Figure 111 depicts the target values. While a slight deterioration is observed for the temporal validation, coupling IFDM to RIO leads to no significant effect on the spatial validation for the total of Belgium.

As target plots are only a measure of the RMSE and BIAS, simple scatter plots of the modelled annual average concentrations of the models versus the measurements are well suited to represent the spatial correlation. The spatial correlation appears to improve slightly for both NO₂ and O₃, as shown in Figure 112, despite barely no changes in the target plot (Figure 111). Again, hardly any change is observed for PM, possibly due to the larger influence of the background concentrations compared to local contributions.

These scatter plots are well suited to illustrate the importance of the input data on which the simulations rely and the need for a wide range of validation targets. Figure 113 shows the scatter plots split up per region for NO₂. A better validation is obtained for Flanders, where a range of measuring station is in place and the highest quality of input data was available for this study.



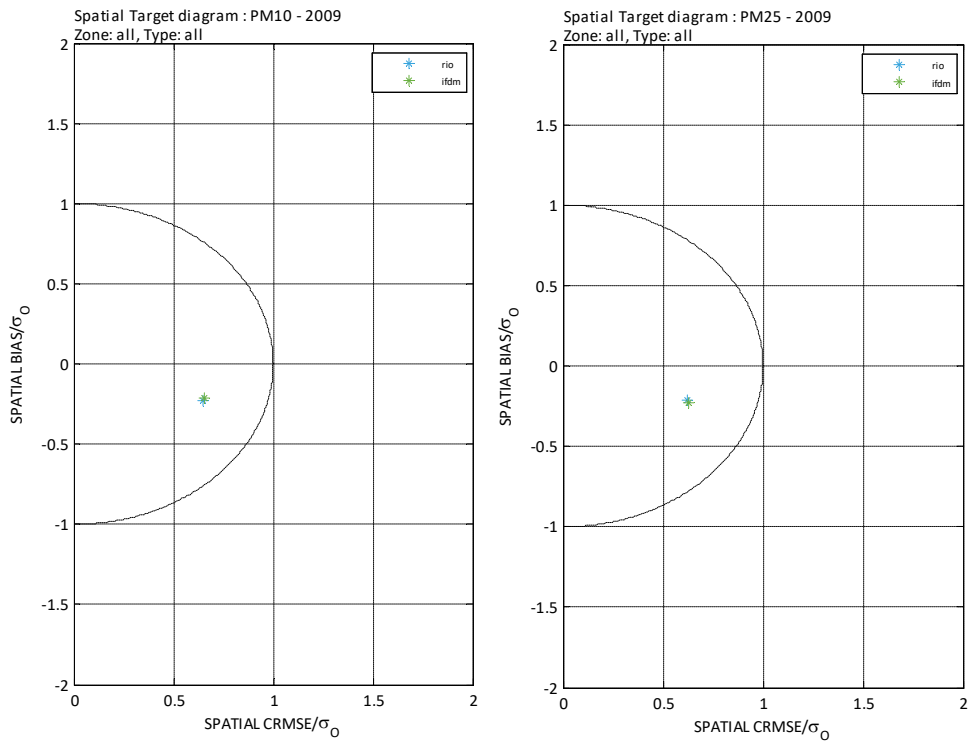
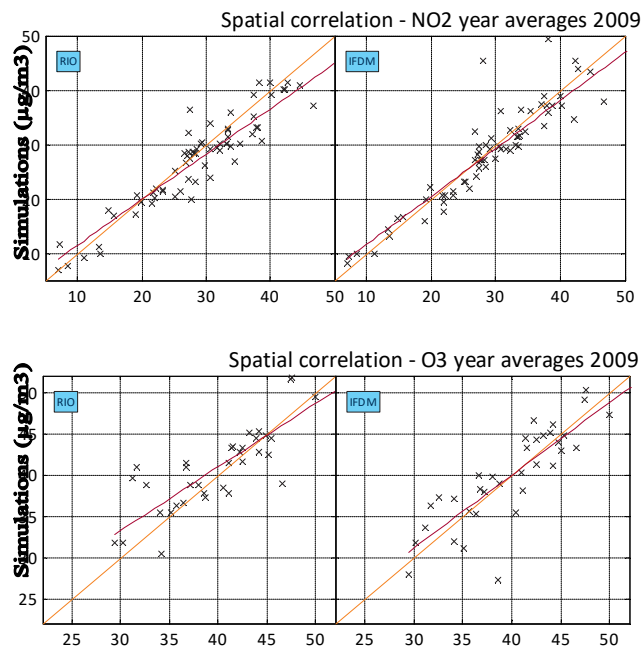


Figure 111: Target plots spatial validation NO₂, O₃, PM₁₀ and PM_{2.5} for RIO and RIO-IFDM



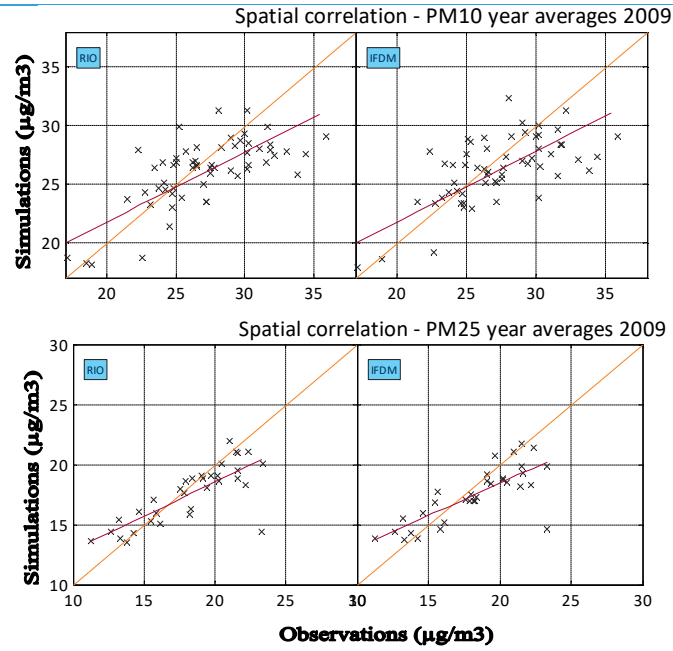
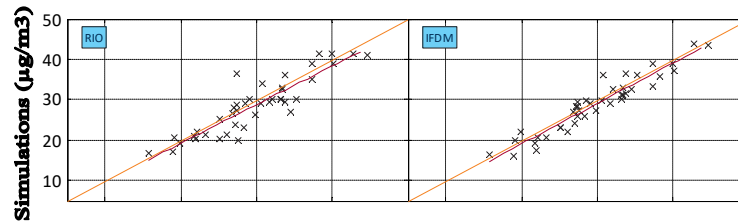


Figure 112: Scatter plots of the year average concentrations, simulations vs. measurements, for NO_2 , O_3 , PM_{10} and $\text{PM}_{2.5}$ per measuring station. The linear regression line is plotted in red, the orange line represents ideal correlation.



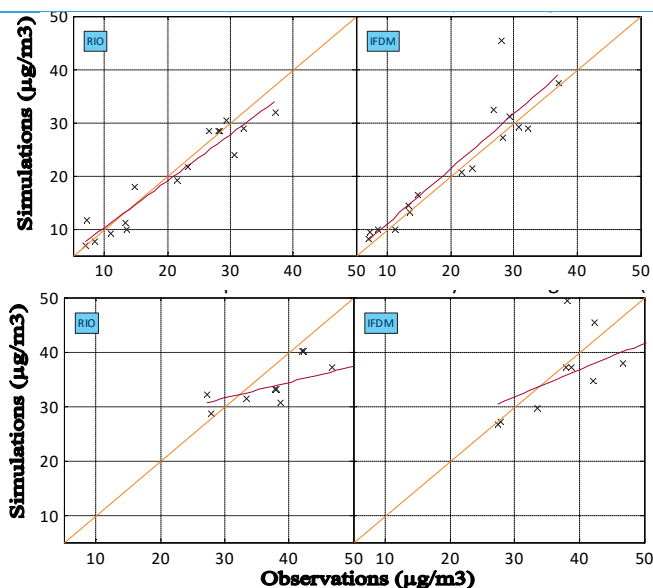


Figure 113: NO₂ scatter plots of year-average simulation vs. measurement concentrations split up per region in Belgium. Top plot: Flanders; middle plot: Wallonia; bottom plot: Brussels.

8.3. EC-VALIDATION

As stated before, for EC, the daily data (six day interval) from the 2008-2009 CHEMKAR-II campaign of VMM (VMM, 2010) are used as validation material. In this campaign nine stations were operational. Three of these stations, Aarschot, Moerkerke and Retie, can be considered background stations, while the other six, Borgerhout, Zwijndrecht, Evergem, Oostrozebeke, Roeselare and Zwevegem are selected as hotspots with increased concentrations and significant urban, industrial or traffic influences. The model chain for EC simulations consists of IFDM coupled to AURORA background concentration maps for Belgium, as RIO is not available for EC due to the lack in measurements.

As a first indication of the quality of the simulations, the daily averages of the simulations (6 day interval) have been plotted against the available experimental data in Figure 114, Figure 115 and Figure 116. The model simulations show overall the correct trends of lower concentrations for the background stations and increased EC levels for the selected hotspots. The temporal trends in the EC concentrations are largely reproduced by the model simulations, the quality varies between the stations however. EC concentrations can be heavily affected by local contributions with an atypical temporal behavior, such as the combustion of wood and other organic material.

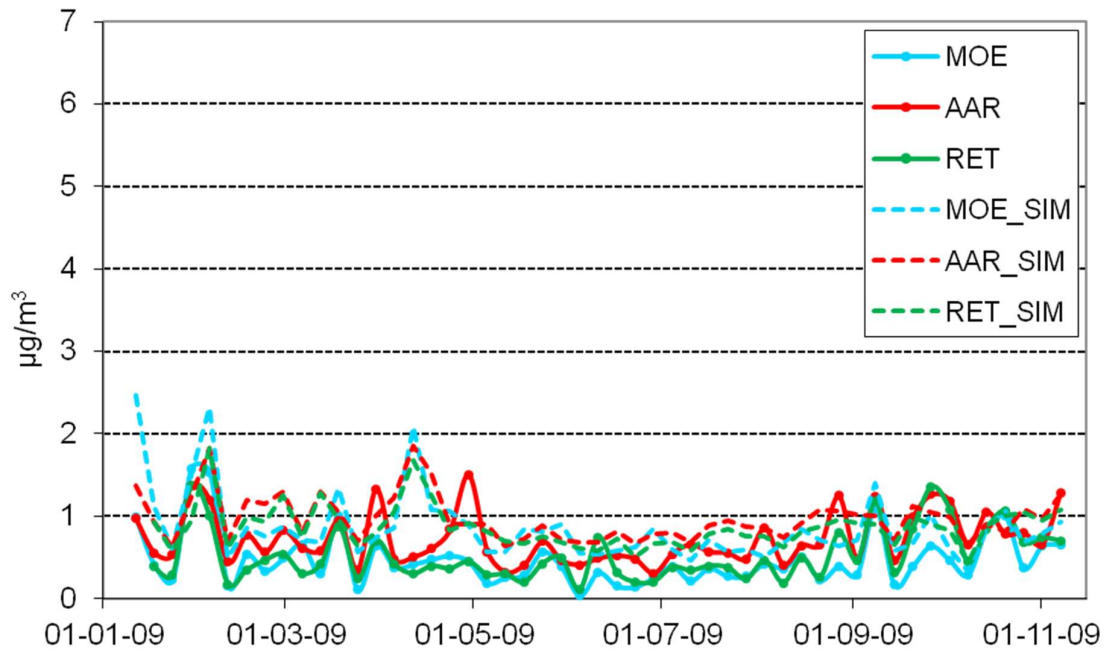


Figure 114: Daily average EC concentrations ($\mu\text{g}/\text{m}^3$) of the AURORA-IFDM simulations (dashed lines) vs. the experimental data (VMM) for the background stations Aarschot, Moerkerke and Retie.

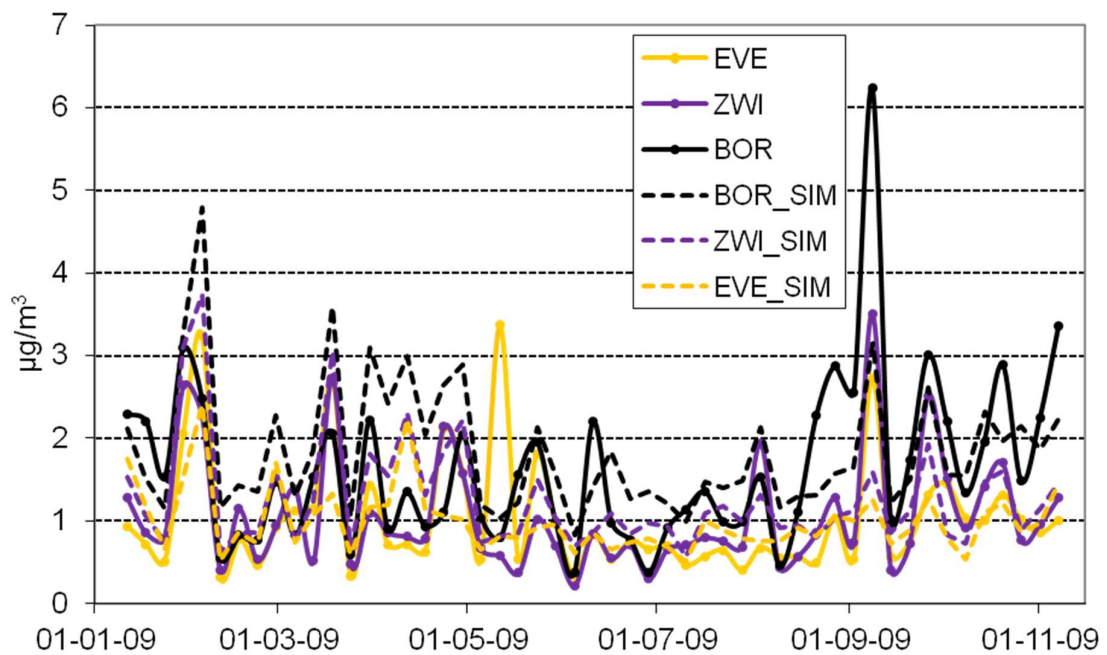


Figure 115: Daily average EC concentrations ($\mu\text{g}/\text{m}^3$) of the AURORA-IFDM simulations (dashed lines) vs. the experimental data (VMM) for the hotspot stations Borgerhout, Evergem and Zwijndrecht.

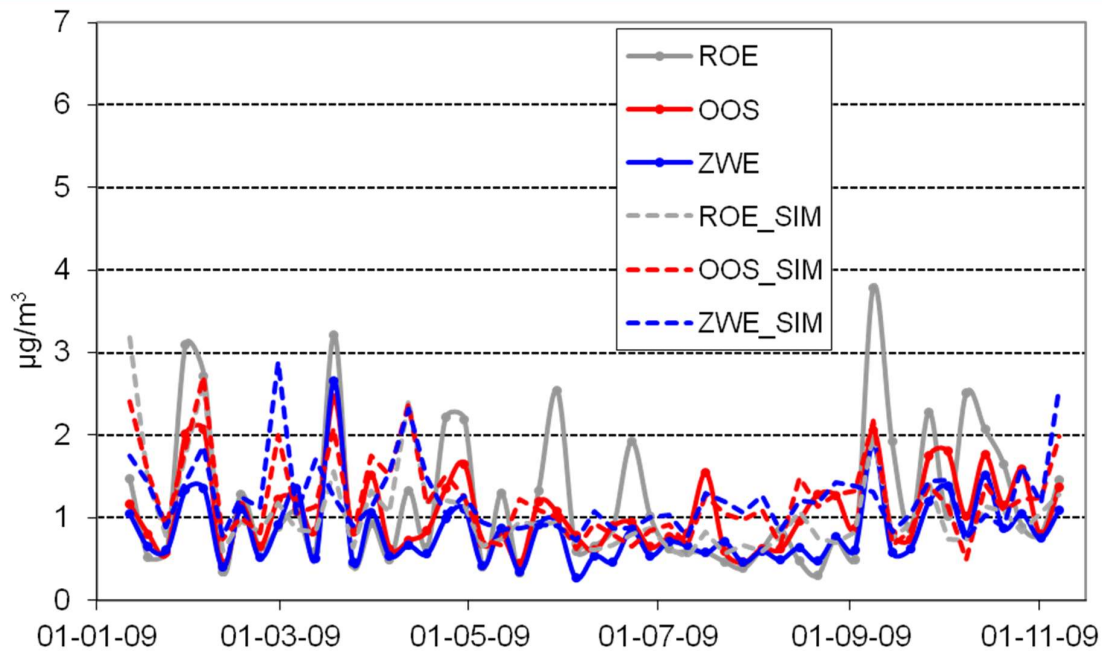
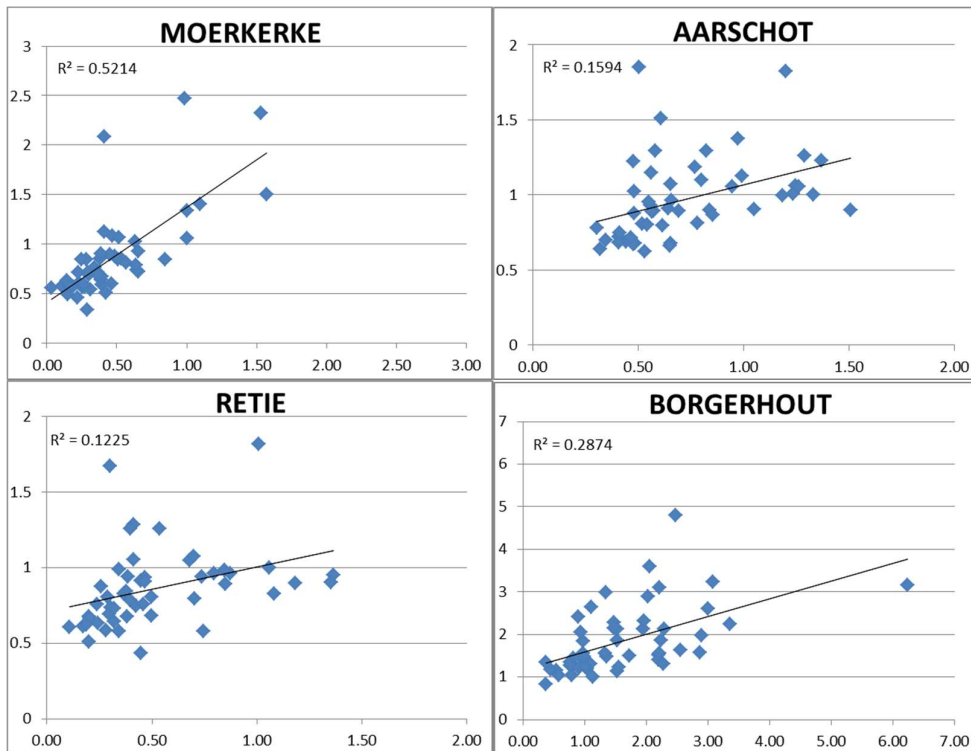


Figure 116: Daily average EC concentrations ($\mu\text{g}/\text{m}^3$) of the AURORA-IFDM simulations (dashed lines) vs. the experimental data (VMM) for the hotspot stations Roeselare, Zwevegem and Oostrozebeke



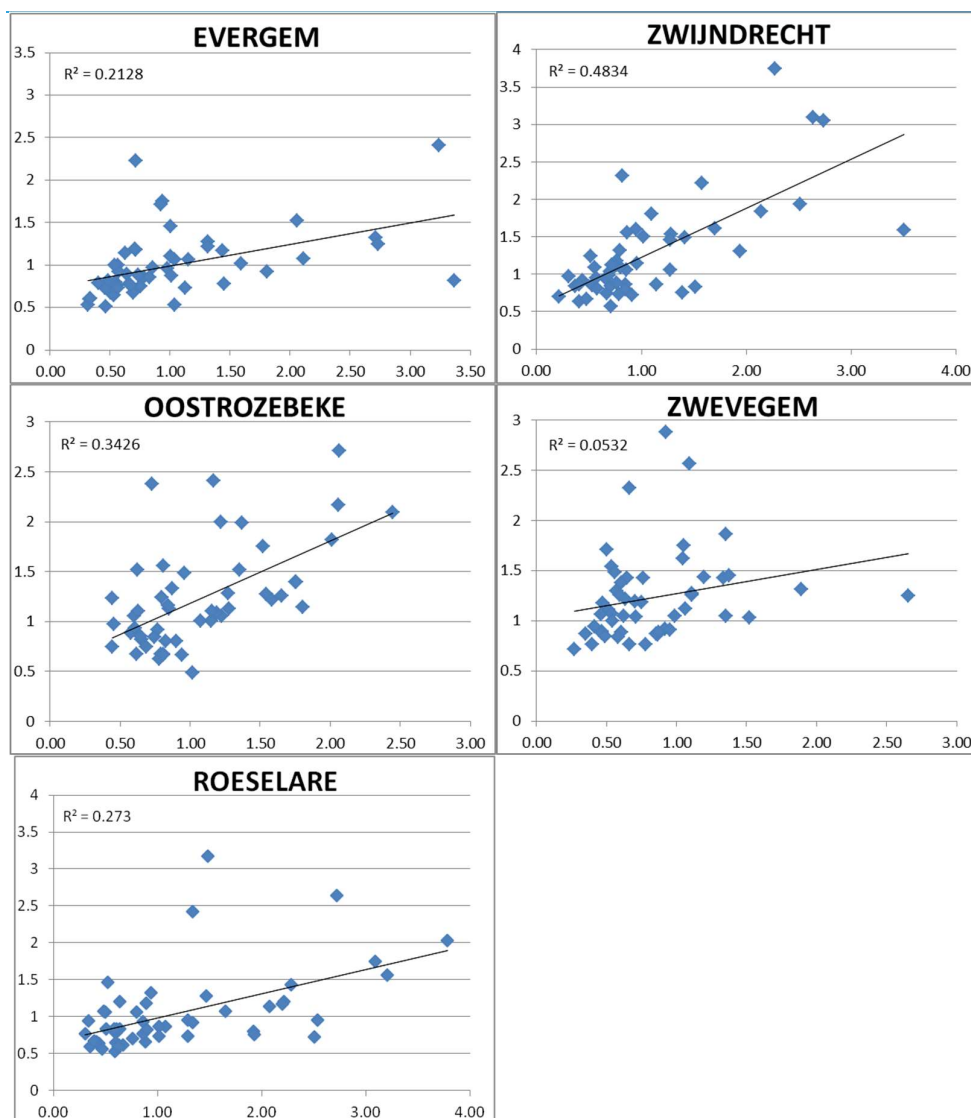


Figure 117: Scatter plots of the EC simulated daily –average concentrations (Y-axis) vs. the measured concentrations (X-axis) per station. Units: $\mu\text{g}/\text{m}^3$

The temporal validation (on a daily basis) is further completed by creating scatter plots per station of the simulations versus the measurements, shown in Figure 117. Simple linear regression yields the coefficients of determination, indicating the degree of correlation between the model simulations and the measurements. The correlations prove to be at best reasonable and relatively poor for a few stations.

To investigate which effects cause the relatively low correlations between EC data and simulations, the correlation between NO_2 and EC, both pollutants with a significant traffic contribution, has been checked. The degree of correlation between EC and NO_2 proves to be high for both the measurements and the simulations, see Figure 118. Since the simulations for NO_2 have been

successfully validated, this is a strong indication that the AURORA-IFDM simulations for EC well capture the traffic component of the EC concentration. The observed differences between AURORA-IFDM simulations and available measurements from the CHEMKAR hotspot campaign on a temporal scale can be explained by the strong effect local sources can have. Even a small EC source can have a relatively large effect if it is within a close distance upwind of the measuring station. Further, the background concentrations from AURORA do not have enough detail for this application. The domestic combustion of organic material typically has a highly heterogeneous spatial and temporal pattern which cannot be captured in the emission input for the model chain.

Finally, no point sources were added to IFDM (thus, their effect is only taken into account via the AURORA background). However, for some of the measurement locations, the effect of point sources is probably important.

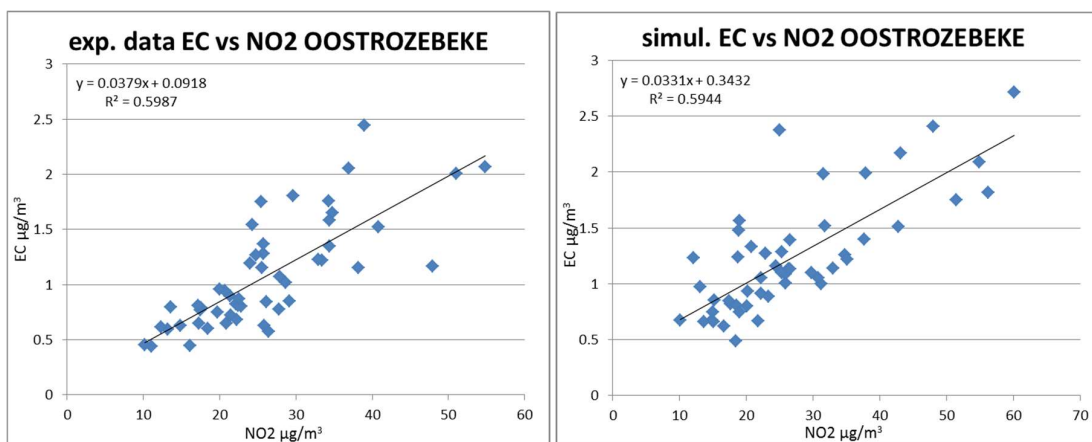


Figure 118: Correlation between EC and NO₂ measurements (left) and simulations (right) for the station Oostrozebeke. Units: µg/m³

The spatial validation yields better results for the AURORA-IFDM EC simulations. For the spatial validation, annual average concentrations for the simulations and measurements are compared, shown in Figure 119. Simple linear regression of this scatter plot shows good correlation with a high coefficient of determination. The intercept of the regression line shows the lowest concentrations to be overestimated. The heterogeneous temporal character of EC emissions averages well, when looking at annual averages. The heterogeneous spatial character remains an issue. If the total EC emissions for Belgium are well known, the distribution of these emissions over the country proves problematic.

Only nine measuring stations in Flanders have been used in the CHEMKAR campaign, no validation could thus be performed for Brussels or Wallonia. The current validation is therefore only a limited description of the skills of AURORA-IFDM for EC modeling.

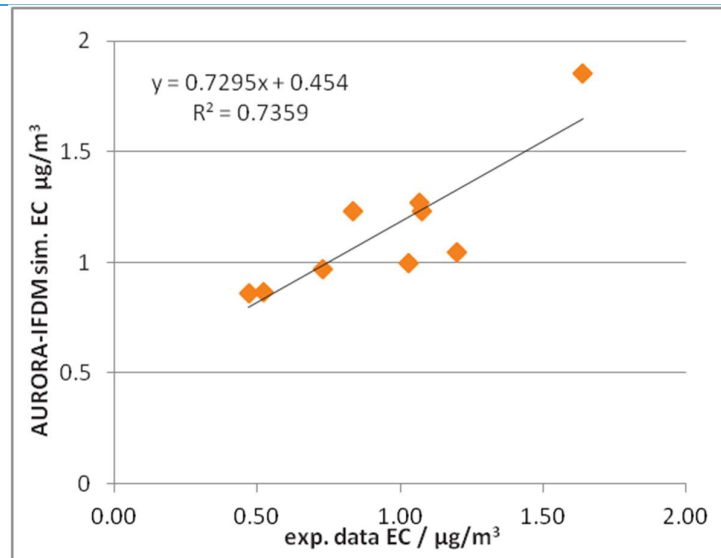


Figure 119: Scatter plot annual average EC concentration AURORA-IFDM simulation vs. measured data (VMM) per station.

8.4. CONCLUSIONS

The main conclusions for the validation of the IFDM-RIO model chain can be summarized as:

- A fair comparison of IFDM-RIO and RIO request extra measurement data from locations where the added skill of IFDM could be shown, as the current telemetric network is not dense enough for this application close to major roads.
- The validation of IFDM-RIO is heavily affected by the detail of the input data, in particular the emissions.
- Only minor differences in validation between IFDM-RIO and RIO are observed (slight negative influence possible for the temporal validation due to the effect of the difference in interpolation).
- The temporal validation for the AURORA-IFDM combination is at best reasonable and relatively poor for a few stations. The spatial validation shows good correlation. However, the difference between the locations is too small in the model. However, we have to take into account the limited possibilities for the validation of the EC-results, compared to the other pollutants, with measurements at only 9 locations, one day out of every six.

The strength of coupling IFDM to RIO or AURORA has been shown earlier , e.g. in the validation using of the highway campaign of the VMM (see CHAPTER 6). Within the framework of this validation, it proofs difficult to highlight the strength of the addition of IFDM to the model chain given the shortage in validation data near strong pollutant sources where high concentration gradients could be and the absence of independent validation data. .

CHAPTER 9 CONCLUSION

This report presents the results from a series of validation studies that have been performed with IFDM. All these validation studies discuss the use of IFDM at an urban/regional scale, where the major pollution sources is in general road traffic. In some cases IFDM was coupled to a regional model (RIO/AURORA), in some cases IFDM was coupled to a street box model (OSPM). The following studies are presented:

- Case 1: Spatial validation of the EC-concentration in Flanders simulated by the AURORA-IFDM model and the measurements during the ChemKar-campaign (Lefebvre et al., 2011b).
- Case 2: Comparisons of the RIO-IFDM model chain over Flanders and Brussels with the measurements of the telemetric measurement network (Lefebvre et al., 2013a).
- Case 3: Spatial validation of the RIO-IFDM-OSPM model chain over Antwerp for NO₂ and measurements with passive samplers (Lefebvre et al., 2013b).
- Case 4: Sensitivity study of the RIO-IFDM-OSPM model chain over Antwerp for NO₂ (not previously published).
- Case 5: Spatial and temporal validation of the IFDM-model against measurements close to the E40 at Affligem (ATMOSYS highway campaign, not previously published).
- Case 6: Spatial and temporal validation of the RIO-IFDM model chain over Belgium with measurements of the telemetric measurement network (ATMOSYS action 9, not previously published).

A summary is given in Table 4.

Taking into account all this different validation campaigns, we try to answer a series of questions.

1. Does IFDM have an added value over to the RIO- and AURORA-model in an urban region?

Despite difficulties to show the added value of IFDM to RIO on a Belgian/Flemish scale using the correct telemetric network for NO₂, O₃, PM₁₀ and PM_{2.5}, there is ample evidence that IFDM does improve on the background concentrations provided to it for pollutants strongly influenced by traffic:

- For the EC study in Flanders (Case 1), there is a significant increase in R² between AURORA (columns AUR07 and AUR10 in Table 7) and AURORA-IFDM (column Combined in Table 7), without strong changes in the bias and the RMSE.

- For the NO₂-study in Antwerp (Case 3), there is a significant increase in model performance between RIO and RIO-IFDM-OSPM (Figure 32, Figure 33).
- In the simulations of the ATMOSYS highway campaign (Case 5), close to the E40, considerable skill is shown by IFDM, both at the spatial (Figure 50) and at the temporal (Figure 51) scale. None of these local effects would be visible in RIO/AURORA.

For pollutants for which the effect of the sources included in IFDM is small compared to the background concentrations, the improvement of IFDM over RIO is insignificant (Figure 105).

Nevertheless, IFDM also takes resources to run. It is thus important, despite its added value compared to RIO/AURORA, to estimate for each purpose if the addition of IFDM is worthwhile.

2. Is the IFDM model fit for use for regulatory purposes?

In order to answer this question we have to define the air quality regulations that are important at an urban scale. We'll discuss them one by one:

- The yearly limit value of NO₂ is 40 µg/m³. In order to test for this value, the spatial validation of the model is paramount. As shown for instance in Figure 33 and Figure 50, the spatial validation is excellent. On top of this, the deviation of the regression line in Figure 33 of the measurements onto the model value crosses the 1:1 line close to the limit value of 40 µg/m³ showing only small deviations between measurements and model values close to this critical limit. The deviations may be larger further away from the limit value (overestimations for low concentrations, underestimations for high concentrations), but this will not play a role in determining the adherence to this limit value.
- The hourly limit value for NO₂ of 200 µg/m³ may be exceeded only 18 times per year. It has been shown that, although the model in general is reasonable well in simulating the (half)hourly values, there is a possible model overestimation for low sources and low wind speeds close to the source (Figure 62). As a result, this would lead to an overestimation of the extent of exceedance of this limit value. However, the extent in which the model estimates this limit value to be exceeded is very small and is completely included in the region with yearly average values much larger than the annual limit value. As a result, the inability of the IFDM model in determining the exact extent of exceedance of this limit value is not very important. Furthermore, there is no official Belgian measurement location where this limit value is exceeded at this moment.
- The yearly limit value of PM₁₀ is 40 µg/m³. As with the yearly limit value of NO₂, the spatial validation will be the most important. As it is shown before, for cases for which the emissions and background concentrations are well known, IFDM simulations are very close to the reality. Therefore, the model will be fit for regulatory purposes provided that the

input data is of sufficient quality. The coupling of the IFDM model to RIO shows good skill in determining these concentrations (Table 8).

- The daily limit value of PM₁₀ of 50 µg/m³ may be exceeded only 35 times per year. It has been shown that the model validation at a daily resolution is good (Figure 66, which shows half-hourly values for BC, however, similar results can be assumed for PM₁₀, Table 8). Of course, the same caveat concerning the input data applies.
- The yearly limit value of PM_{2.5} is 25 µg/m³ combined with a three-yearly averaged limit value of PM_{2.5} at urban background locations (different limit values for different regions). As for the yearly limit value for PM₁₀, the spatial validation is the most important, which has been shown to be very good. Therefore, the model will be fit for regulatory purposes provided that the input data is of sufficient quality. The coupling of the IFDM model to RIO shows good skill in determining these concentrations (Figure 105).
- The other existing limit values are less important at an urban scale. It is nevertheless possible that new regulations important at an urban scale will be put into place. Based on the experience with the limit values described above, we can state that they would be probably well represented by the IFDM-model, provided good input for emissions and background concentrations. A possible exception would be limit values for certain pollutants that can only be exceeded during a small number of hours per year, as the temporal validation for traffic sources at an hourly scale is only reasonable. However, this problem will be important only near line sources (due to accumulation effects) and only near those, which are found just above the ground. This has to be taken into account if at certain moment such a new regulation is put in place.

3. Is the IFDM model fit for use for determining exposure?

For exposure estimations, there is a large difference in what is needed from a model depending if one determines static or dynamic exposure.

- **Static exposure:** In this case, only the spatial validation of the model is important. This validation is previously shown to be very good (Figure 33, Figure 50, Figure 5, Table 7, Table 8), certainly when coupled to a regional model such as RIO or AURORA. The improved spatial resolution due to IFDM will increase the accuracy of the exposure estimations.
- **Dynamic exposure:** In this case, both the spatial validation and the temporal validation of the model is important. As has been seen before, aggregated to daily and weekly averages, the temporal validation of the model is good; however, larger discrepancies between the model and the measurements exist at lower frequencies. However, for dynamic exposure, the presence of the typical cycles (within the day, within the week and within the year) is very important as individual over- and underestimations at an hourly scale will cancel out, but problems with typical cycles will not. The presence of these cycles in the RIO-IFDM model is shown in Figure 22 to be very good, for NO₂, O₃ and PM₁₀. For EC, the capability of the model to reproduce these cycles is not yet proven.

Finally, the feasibility of doing so has to be demonstrated. This has been done within the SBO-Mase project, where dynamic exposure of the Flemish population was determined.

4. How can modelling using IFDM be further improved for the urban to local scale?

There are several points where the IFDM modelling can be improved. The following list gives an overview of the points that should be addressed in order to improve the IFDM-model.

- The model shows a tendency to overestimate low concentrations and underestimate high concentrations (e.g. Figure 33). More research is needed to find the source of this deviation. This is probably due in part due to the detail of the input data (both emissions and meteorology) which entail a certain degree of averaging.
- The model does not take into account differences in roughness lengths in its simulations.
- Increased wind direction variation at low wind speeds is not modelled yet. An improved model scheme has been presented in this work. However, some deviations between the measurements and the modelling remain.
- The treatment of traffic-induced dispersion should be made wind-dependent, although this is shown to have only a small effect.

However, next to these changes, it is shown that the quality of the input data provided to the model is very important. First of all, the quality of the emission inputs is of paramount importance. The lack of even a small source close to a measurement location can make the model results deteriorating significantly. In addition, small changes in the time profiles of emissions can also have large influences. Finally, the quality of the meteorology measurements has an important influence on the model results.

The uncertainty on the emissions is probably, in many cases, larger than the model uncertainty itself. This should, however, not stop us to further strive to improve the IFDM model.

Conclusion

It has been shown that the IFDM model does provide an added value over RIO and AURORA and that it is fit for use both for regulatory and for determination of exposure. It is our goal to continue to update, refine and improve the IFDM-model in the future.

LIST OF LITERATURE

Arentze, T.A., Timmermans, H.J.P., 2004. A learning-based transportation oriented simulation system. *Transportation Research Part B-Methodological* 38(7): 613-633.

Arentze, T., Hofman, F., Timmermans, H., 2003. Reinduction of Albatross decision rules with pooled activity-travel diary data and an extended set of land use and cost-related condition states. *Transportation Research Record: Journal of the Transportation Research Board*, No. 1831, Transportation Research Board of the National Academies, Washington, D.C., 2003, pp. 230-239, doi:10.3141/1831-26

Assael, M.J., Delaki M., Kakosimos, K.E., 2008. Applying the OSPM model to the calculation of PM₁₀ concentration levels in the historical centre of the city of Thessaloniki, *Atm. Env.*, 42, 65-77, doi:10.1016/j.atmosenv.2007.09.029.

Beckx, C., Int Panis, L., Arentze, T., Janssens, D., Torfs, R., Broekx, S., Wets, G., 2008. A dynamic activity-based population modelling approach to evaluate exposure to air pollution: methods and application to a Dutch urban area. *Environmental Impact Assessment Review*, 29(3), 179-185. DOI: 10.1016/j.eiar.2008.10.001

Beckx, C., Int Panis, L., Van de Vel, K., Arentze T., Lefebvre W., Janssens D. and Wets G., 2009. The contribution of activity-based transport models to air quality modelling: A validation of the ALBATROSS-AURORA model chain, *Science of the Total Environment*, 407, 3814-3822.

Beckx C., Int Panis L., Arentze T., Janssens D., Wets G., 2009a. Disaggregation of nation-wide dynamic population exposure estimates in the Netherlands: applications of activity-based transport models. *Atmospheric Environment*. Volume 43(34), pages 5454-5462
doi:10.1016/j.atmosenv.2009.07.035

Beckx, C., Arentze, T., Int Panis, L., Janssens, D., Vankerkom, J., Wets, G., 2009b. An integrated activity-based modelling framework to assess vehicle emissions: approach and application. *Environment and Planning B: Planning and Design*. volume 36(6), pages 1086-1102
doi:10.1068/b35044

Beckx, C., Lefebvre W., Degraeuwe B., Vanhulsel M., Kochan B., Bellemans T., Dhondt S., Int Panis L., 2013. Assessing the environmental impact associated with different trip purposes. *Transportation Research Part D*, 18, 110-116.

Bellemans, T., Kochan, B., Janssens, D., Wets, G., Arentze, T., Timmermans, H., 2010. Implementation Framework and Development Trajectory of FEATHERS Activity-Based Simulation Platform. *Transportation Research Record*(2175): 111-119.

Berkowicz, R., Hertel, O., Larsen, S.E., Sørensen, N.N., Nielsen, M., 1997. Modelling traffic pollution in streets (report in PDF format, 850 kB), link on http://www.dmu.dk/en/air/models/ospm/ospm_description/

Berkowicz R., Ketzler M., Solvang Jensen S., Hvidberg M., Raaschou-Nielsen O., 2008. Evaluation and application of OSPM for traffic pollution assessment for a large number of street locations, *Env. Mod. & Soft.*, 23, 296-303.

Birch, E., 2003. Diesel Particulate Matter 5040, NIOSH, <http://www.cdc.gov/niosh/docs/2003-154/pdfs/5040.pdf>.

Blocken, B., Gualtieri, C., 2012. Ten iterative steps for model development and evaluation applied to Computational Fluid Dynamics for Environmental Fluid Mechanics, *Env. Mod. Soft.*, 33, 1-22, doi:10.1016/j.envsoft.2012.02.001

Böhner, J., McCloy, K.R., Strobl, J. [Eds.], 2006. SAGA – Analysis and Modelling Applications. Göttinger Geographische Abhandlungen, Vol.115, 130pp.

Borrego, C., Tchepel, O., Costa, A.M., Martins, H., Ferreira, J., and Miranda, A.I., 2006. Traffic-related particulate air pollution exposure in urban areas. *Atmospheric Environment* 40: 7205-7214.

Brunekreef, B., Beelen, R., Hoek, G., Schouten, L., Bausch-Goldbohm, S., Fischer, P., Armstrong, B., Hughes, E., Jerrett, M., van den Brandt, P., 2009. Effects of Long-Term Exposure to Traffic-Related Air Pollution on Respiratory and Cardiovascular Mortality in the Netherlands: The NLCS-Air Study, Health Effects Institute, 139, 2009.

Buekers J., Stassen K., Int Panis L., Hendrickx K., Torfs R., 2011. Ten years of research and policy on particulate matter air pollution in hotspot Flanders. *Environmental Science and Policy*, Volume 14, Issue 3, May 2011, Pages 347-355, <http://dx.doi:10.1016/j.envsci.2010.10.012>

Bultynck H. and Malet L. M., 1972. Evaluation of atmospheric dilution factors for effluents diffused from an elevated continuous point source, *Tellus*, 24, 453-471.

COPERT 4, 2007. Emission Inventory Guidebook, Chapter Road Transport, Activities 070100 - 070500, version 6.0 of 23 August 2007, Aristotle University Thessaloniki, Greece

Cosemans G., Kretzschmar J., De Baere G. and Vandervee J., 1981. Large scale validation of a bi-gaussian dispersion model in a multiple source urban and industrial area, *Air Pollution Modelling and Its Application II*, Edited by C. De Wispelaere, NATO, Plenum Press, ISBN 0-306-41115-6, pg. 709-728.

Cosemans G., Lefebvre W., Mensink C., 2012. Calculation scheme for a Gaussian parameterization of the Thompson 1991 wind tunnel building downwash dataset, *Atm. Env.*, 59, 355-365, doi:10.1016/j.atmosenv.2012.05.017

da Silva, A. S., Cardoso, M. R., Meliefste, K., & Brunekreef, B., 2006. Use of passive diffusion sampling method for defining NO₂ concentrations gradient in São Paulo, Brazil. *Environmental health : a global access science source*, 5(2), 19. doi:10.1186/1476-069X-5-19

Decoene, 2013, EC/PM Emission Maps, ATMOSYS, Action 6 Deliverable

Dennis, R., Fox, T., Fuentes, M., Gilliland, A., Hanna, S., Hogrefe, C., Irwin, J., Rao, S.T., Scheffe, R., Schere, K., Steyn, D., and Venkatram, A.: A framework for evaluating regional scale numerical photochemical modelling systems, *Environ. Fluid Mech.*, 10, 471-489, 15 doi:10.1007/s10652-009-9163-2, 2010.

De Ridder K. and Mensink C., 2002. Improved algorithms for advection and vertical diffusion in AURORA. In: Borrego and Schayes (eds.), *Air pollution modelling and its Application XV*, Kluwer Academic/Plenum Publishers, New York, 395-401.

De Ridder, K., Lefebvre, F., Adriaensen, S., Arnold, U., Beckroege, W., Bronner, C., Damsgaard, O., Dostal, I., Dufek, J., Hirsch, J., Int Panis, L., Kotek, Z., Ramadier, T., Thierry, A., Vermoote, S., Wania, A., Weber, C., 2008a. Simulating the impact of urban sprawl on air quality and population exposure in the German Ruhr area. Part I: Reproducing the base state. *Atmospheric Environment* 42, 7059–7069

De Ridder, K., Lefebvre, F., Adriaensen, S., Arnold, U., Beckroege, W., Bronner, C., Damsgaard, O., Dostal, I., Dufek, J., Hirsch, J., Int Panis, L., Kotek, Z., Ramadier, T., Thierry, A., Vermoote, S., Wania, A., Weber, C., 2008b. Simulating the impact of urban sprawl on air quality and population exposure in the German Ruhr area. Part II: Development and evaluation of an urban growth scenario. *Atmospheric Environment* 42, 7070–7077

De Vlieger I. and 10 co-authors, 2011. LIMOBEL: Long-run impacts of policy packages on mobility in Belgium, Annex I: E-motion model. Belgian Science Policy Office, 2011.

Deutsch F., Mensink C., Vankerkom J. and Janssen L., 2008a. Application and validation of a comprehensive model for PM₁₀ and PM_{2.5} concentrations in Belgium and Europe, *Applied Mathematical Modelling*, 32, 1501-1510.

Deutsch F., Janssen L., Vankerkom J., Lefebvre F., Mensink C., Fierens F., Dumont G., Roekens E., 2008b. Modelling changes of aerosol compositions over Belgium and Europe, *Int. J. of Environment and Pollution*, 32, 162-173.

Deutsch F., Viaene P., Janssen S., Maes J., Vankerkom J., Janssen L., Vliegen J., Peelaerts W., Mensink C., 2009. Validation of the completely renewed BeEUROS model, Final report for project by order of the Flemish Environment Agency (in Dutch).

Dhondt S., Beckx, C., Degraeuwe, B., Lefebvre, W., Kochan, B., Bellemans, T., Int Panis, L., Macharis, C., Putman, K., 2012a. Health impact assessment of air pollution using a dynamic exposure profile: Implications for exposure and health impact estimates, *Environmental Impact Assessment Review*, Volume 36, Pages 42–51 , doi: 10.1016/j.eiar/2012.03.004

Dhondt, S., Beckx, C., Degraeuwe, B., Lefebvre, W., Kochan, B., Bellemans, T., Int Panis, L., Macharis, C., Putman, K., 2012b. Integration of population mobility in the evaluation of air quality measures on local and regional scale, *Atm. Env.*, 59, 67-74, doi: 10.1016/j.atmosenv.2012.04.055.

Dijkema M.B.A., van der Zee S.C., Brunekreef B., van Strien RT, 2008. Air quality effects of an urban highway speed limit reduction, *Atmospheric Environment*, 42, 9098-9105, doi:10.1016/j.atmosenv.2008.09.039.

Dons, E., Int Panis, L., Van Poppel, M., Theunis, J., Willems, H., Torfs, R., Wets, G., 2011a. Impact of time-activity patterns on personal exposure to black carbon. *Atmospheric Environment*, Volume 45, Issue 21, July 2011, Pages 3594-3602.

Dons, E., Beckx, C., Arentze, T., Wets, G., Int Panis, L., 2011b. Using an activity-based framework to determine effects of a policy measure on population exposure to nitrogen dioxide, *Transportation Research Record: Journal of the Transportation Research Board*, No., 2233, Transportation Research Board of the National Academies, Washington, D.C., 2011, pp. 72-79, doi:10.3141/2233-09.

Dons E., Int Panis L., Van Poppel M., Theunis J., Wets G., 2012. Personal exposure to Black Carbon in transport microenvironments, *Atm. Env.*, 55, 392-398, doi: 10.1016/j.atmosenv.2012.03.020.

Ferm, M., Svanberg, P.-A., 1998. Cost-efficient techniques for urban- and background measurements of SO₂ and NO₂. *Atmospheric Environment*, 32, 1377-1381.

Gauderman W.J. and 10 co-authors, 2007. Effect of exposure to traffic on lung development from 10 to 18 years of age: a cohort study. *Lancet*. 369:571–577.

Gkatzoflias, D., Kouridis, C., Ntziachristos, L., Samaras, Z., 2012. 'COPERT IV: Computer Programme to calculate emissions from road transport', user manual (version 9.0). Available from: http://www.emisia.com/docs/COPERT4v9_manual.pdf

Gery, M.W., Whitten G.Z., Killius J.P. and Dodge M.C., 1989. A Photochemical Kinetics Mechanism for Urban and Regional Scale Computer Modelling. *J. Geophys. Res.*, **94**, 925-956.

Hao, J.Y., Hatzopoulou, M., Miller, E.J., 2010. Integrating an activity-based travel demand model with dynamic traffic assignment and emission models: An implementation in the Greater Toronto Area. *Transportation Research Record: Journal of the Transportation Research Board*, No. 2176, Transportation Research Board of the National Academies, Washington, D.C, p. 1-13.

Hatzopoulou M., Miller, E.J., 2010. Linking an activity-based travel demand model with traffic emission and dispersion models: Transport's contribution to air pollution in Toronto. *Transportation Research Part D*, 15, 315-325.

Hatzopoulou, M., Hao J.Y., Miller E., 2011. Simulating the impacts of household travel on greenhouse gas emissions, urban air quality, and population exposure. *Transportation* 38: 871-887.

Hirtl M., Baumann-Stanzer K., 2007. Evaluation of two dispersion models (ADMS-Roads and LASAT) applied to street canyons in Stockholm, London and Berlin. *Atm. Env.*, 41, 5959-5971, doi:10.1016/j.atmosenv.2007.03.026.

Hitzenberger R., Petzold A., Bauer H., Ctyroky, P., Pouresmaeil P., Laskus L. and Puxbaum H. (2006), Intercomparison of Thermal and Optical Measurement Methods for Elemental Carbon and Black Carbon at an Urban Location, *Environ. Sci. Technol.*, 40, 6377-6383.

Hoek G., Brunekreef B., Goldbohm S., Fischer P. and van den Brandt PA, 2002. Association between mortality and indicators of traffic-related air pollution in the Netherlands: a cohort study, *the Lancet*, 360, 1203-1209.

Holmes, N.S. and Morawska L., 2006. A review of dispersion modelling and its application to the dispersion of particles: an overview of different dispersion models available, *Atm. Env.*, 40, 5902-5928, doi:10.1016/j.atmosenv.2006.06.003

Hooyberghs, J., Mensink, C., Dumont, G., Fierens F., 2006. Spatial interpolation of ambient ozone concentrations from sparse monitoring points in Belgium, *Journal of Environmental Monitoring*, 8, 1129-1135, doi: 10.1039/b612607n.

Int Panis, L., Broekx, S., Liu R. 2006. Modelling instantaneous traffic emission and the influence of traffic speed limits. *Science of the Total Environment* 371 (2006) 270–285

Jakeman, A.J., Letcher, R.A., Norton, J.P., 2006. Ten iterative steps in development and evaluation of environmental models, *Environmental Software and Modelling* 21, 602-614, doi:10.1016/j.envsoft.2006.01.004.

Janssen, S., Dumont, G., Fierens, F., Mensink, C., 2008. Spatial interpolation of air pollution measurements using CORINE land cover data, *Atm. Env.*, 42, 20, 4884-4903, doi: 10.1016/j.atmosenv.2008.02.043.

Janssen, S., Dumont, G., Fierens, F., Deutsch, F., Maiheu, B., Celis, D., Trimpeneers, E., Mensink, C., 2012. Land use to characterize spatial representativeness of air quality monitoring stations and its relevance for model validation. *Atmospheric Environment*, 59, 492–500. doi:10.1016/j.atmosenv.2012.05.028

Jensen S.S., Berkowicz, R., Hansen, H.S., Hertel, O., 2001. A Danish decision-support GIS tool for management of urban air quality and human exposures. *Transportation Research Part D: Transport and Environment* 6 (4), 229-241.

Joly, M., Peuch, V.-H., 2011. Objective classification of air quality monitoring sites over Europe. *Atmospheric Environment* 47, 111-123

Kochan, B., Bellemans, T., Janssens, D., Wets, G., 2012. Validation of an activity-based traffic demand model for Flanders. 2012. Forthcoming in *Computational Intelligence for Traffic and Mobility*. Edited by Wuhong Wang, Geert Wets, Atlantis Press, Springer.

Kretzschmar J.G., Mertens I. and Vanderborght B., 1984. Sensitivity, applicability and validation of bi-Gaussian off- and on-line Models for the Evaluation of the Consequences of Accidental Releases in Nuclear Facilities, Final Report Task 2: Development and evaluation of the possibilities of in-line dispersion models for use in an emergency plan of a nuclear installation, March 1984, SCK/CEN.

Lefebvre F., Lefebvre W., Op 't Eyndt T., Smeets N., Van Looy S., 2010a. IFDM-Traffic: Handleiding, 2010/RMA/R/239, September 2010.

Lefebvre F., Lefebvre W., Op 't Eyndt T., Schepens J., Smeets N., Vankerkom J., Van Looy S., 2010b. IFDM-traffic, eindrapport, Studie uitgevoerd in opdracht van LNE, 2010/RMA/R/238, september 2010.

Lefebvre W., Van de Vel K., De Ridder K., Maes J., Mensink C., Mijling B., van der A. R., Veldeman N., Viaene P. and Vliegen J., 2010, 2.11 AMFIC: Air Quality Modelling and Forecasting in China, in D.G. Steyn and S. T. Rao (eds.), *Air Pollution Modelling and Its Application XX*, pg. 167-174, doi: 10.1007/978-90-481-3812-8, Springer Science + Business Media B.V.

Lefebvre W., Janssen S., Schrooten L., Deutsch F., Vankerkom J., Degraeuwe B., Veldeman N., Peelaerts W., Van Looy S., Lodewijks P., Meynaerts E., De Vlieger I., Op 't Eyndt T., Schepens J., Lefebvre F., Blyth L., 2010b. Luchtkwaliteit langs snelwegen en belangrijke gewestwegen in Vlaanderen. Eindrapport, 2010/RMA/R/255.

Lefebvre, W., Fierens, F., Trimpeneers, E., Janssen, S., Van de Vel, K., Deutsch, F., Viaene, P., Vankerkom, J., Dumont, G., Vanpoucke, C., Mensink, C., Peelaerts, W., Vliegen, J., 2011a. Modelling the effects of a speed limit reduction on traffic-related elemental carbon (EC) concentrations and population exposure to EC, *Atmospheric Environment*, 45, 197-207, doi: 10.1016/j.atmosenv.2010.09.026

Lefebvre, W., Vercauteren, J., Schrooten, L., Janssen, S., Degraeuwe, B., Maenhaut, W., de Vlieger, I., Vankerkom, J., Cosemans, G., Mensink, C., Veldeman, N., Deutsch, F., Van Looy, S., Peelaerts, W., Lefebvre, F., 2011b. Validation of the MIMOSA-AURORA-IFDM model chain for policy support: modelling concentrations of elemental carbon in Flanders, *Atm. Env.*, 45/37, 6705-6713., doi: 10.1016/j.atmosenv.2011.08.033

Lefebvre W., Janssen S., Degraeuwe B., Lodewijks P., Deutsch F., Veldeman N., Vankerkom J., Schrooten L., Cochez E., Meynaerts E., Maiheu B., Van Looy S., Peelaerts W., Schepens J., Nikolova I., de Vlioger I., Lefebvre F., 2011c. Modelling van de concentraties aan en bronnentoe wijzing van NO₂, PM₁₀ en PM_{2.5} in de Vlaamse luchtkwaliteitszones Gent, Antwerpen en Haven Antwerpen in het kader van de richtlijn luchtkwaliteit 2008/50/EG, Report for the administration 'Leefmilieu, Natuur en Energie' of the Flemish Government, 2011/RMA/R/45.

Lefebvre W., Schillemans L. Op 't Eyndt T., Vandersickel M., Poncelet P., Neuteleers C., Dumez J., Janssen S., Vankerkom J., Maiheu B., Janssen L., Buekers J., Mayeres, I., 2011d. Voorstel van maatregelen om de luchtkwaliteit te verbeteren en de geluidshinder te beheersen in de stad Antwerpen, 2011/RMA/R/29.

Lefebvre W., Degraeuwe B., Beckx C., Vanhulsel M., Kochan B., Bellemans T., Janssens D., Wets G., Janssen S., de Vlioger I., Int Panis L., Dhondt S., 2013a. Presentation and evaluation of an integrated model chain to respond to traffic- and health-related policy questions, *Env. Mod. & Soft.*, 40, 160-170, doi: 10.1016/j.envsoft.2012.09.003

Lefebvre W., 2012. Het aspect luchtkwaliteit bij herinrichting Dampoort, 2012/RMA/R/240, November 2012.

Lefebvre W., Van Poppel M., Maiheu B., Janssen S., Dons E., 2013b. Evaluation of the RIO-IFDM-street canyon model chain, *Atm. Env.*, 77, 325-337, doi:10.1016/j.atmosenv.2013.05.026.

Lodewijks, P., Meynaerts, E., 2007. The environmental costing model: a tool to advise policy makers in Flanders on issues of cost efficiency, Urban Air Quality 2007 conference, March 2007.

Maes J., Vliegen J., Van de Vel K., Janssen S., Deutsch F., De Ridder K., Mensink C., 2009. Spatial surrogates for the disaggregation of CORINAIR emission inventories, *Atmospheric Environment*, 43, 1246-1254.

Maiheu B., Veldeman N., Viaene P., De Ridder K., Lauwaet D., Deutsch F., Janssen S., 2012. Bepaling van de best beschikbare grootschalige concentratiekaarten luchtkwaliteit voor België, MIRA/2013/01, December 2012.

Maiheu B. (2011). Ontwikkeling interpolatiemodel voor PM_{2.5} – Koppeling RIO-IFDM, 2011/RMA/R/30, Januari 2011.

Maiheu B. and Lefebvre W. (2011). Monte Carlo Analyse van de RIO onzekerheden, 2011/RMA/R/343, November 2011.

Marshall, J.D., Granvold, P.W., Hoats, A.S., Mckone, T.E., Deakin, E., Nazaroff, W.W., 2006. Inhalation intake of ambient air pollution in California's South Coast Air Basin. *Atmospheric Environment*, 40, 4381-4392.

Mensink C., De Vlieger I., Nys J., 2000. An urban transport emission model for the Antwerp area, *Atmospheric Environment*, 34, 4595-4602.

Mensink C., De Ridder K., Lewyckij N., Delobbe L., Janssen L., Van Haver P., 2001. Computational aspects of air quality modelling in urban regions using an optimal resolution approach (AURORA). *Large-scale scientific computing – lecture notes in computer science*, **2179**, 299-308.

Mensink, C., Cosemans, G., 2008. From traffic flow simulations to pollutant concentrations in street canyons and backyards, *Env. Mod. Soft.*, 23, 288-295, doi:10.1016/j.envsoft.2007.06.005.

Mills NL and 10 co-authors, 2007. Ischemic and Thrombotic Effects of Dilute Diesel-Exhaust Inhalation in Men with Coronary Heart Disease, *N Engl J Med* 357:1075-82.

Mues, A., Manders, A., Schaap, M., Kerschbaumer, A., Stern, R., Builtjes P., 2012. Impact of the extreme meteorological conditions during the summer 2003 in Europe on particulate matter concentrations, *Atm. Env.*, in press: doi:10.1016/j.atmosenv.2012.03.002

Nenes A, Pandis SN, Pilinis C, 1998. ISORROPIA: A new thermodynamic equilibrium model for multiphase multicomponent inorganic aerosols, *Aquat.Geoch.*, **4**, 123-152

NRC, 1981. Technical Basis for Regulatory Guide 1.145, "Atmospheric Dispersion Models for Potential Accident Consequence Assessments at Nuclear Power Plants, NUREG/CR-2260, NUS-3854, RB, R6, <http://pbadupws.nrc.gov/docs/ML1204/ML12045A197.pdf>

Olesen, H.R., 1995. The model validation exercise at Mol: overview of results. *Int. J. Environment and Pollution*, 5, 761-784.

Op 't Eyndt T., Lefebvre W., Verhees L., Erbrink H., 2012. IMPACT: functionele analyse, RMA/N78G9/2012-003.

Parra, M. a., Santiago, J. L., Martín, F., Martilli, a. and Santamaría, J. M.: A methodology to urban air quality assessment during large time periods of winter using computational fluid dynamic models, *Atmospheric Environment*, 44(17), 2089–2097, doi:10.1016/j.atmosenv.2010.03.009

Patel M.M., Chillrud S.N., Correa J.C., Feinberg M., Hazi Y., Deepti K.C., Prakash S., Ross J.M., Levy D., Kinney P.L., 2009. Spatial and temporal variations in traffic-related particulate matter at New York City high schools, *Atm. Env.*, 43, 4975-4981.

Piuleac, C.G., Rodrigo, M.A., Cañizares, P., Curteanu, S., Sáez, C., 2010. Ten steps modelling of electrolysis processes by using neural networks, *Env. Mod. Soft.*, 25, 74-81, doi:10.1016/j.envsoft.2009.07.012

Pope, C.A. III, Ezzati, M., Dockery, D.W., 2009. Fine-Particulate Air Pollution and

Life Expectancy in the United States. The New England Journal of Medicine, 360, 376-386.

PROMOTE, 2009a. GMES service element Promote 2; C6 Validation Report, Chapter 9: Local air quality forecast service, Version 3, http://validation.aeronomie.be/Documents/C6_2009/C6-09_AQ-LocForecast_v3.pdf

PROMOTE, 2009b. GMES service element Promote 2; C6 Validation Report, Chapter 10: Urban and Regional Air Quality Assessment Service, Version 3, http://validation.aeronomie.be/Documents/C6_2009/C6-10_AQ-Assessment_v3.pdf

Putaud J.-P and 38 co-authors (2010), A European aerosol phenomenology – 3: Physical and chemical characteristics of particulate matter from 60 rural, urban and kerbside sites across Europe, *Atmospheric Environment*, 44, 1308-1320, doi:10.1016/j.atmosenv.2009.12.011.

Quincey P., Butterfield D., Green D., Colyle M. and Cape J.N. (2009), An evaluation of measurement methods for organic, elemental and black carbon in ambient air monitoring sites, *Atm. Env.*, 43, 5085-5091.

Recker, W.W., Parimi, A, 1999. Development of a microscopic activity-based framework for analyzing the potential impacts of transportation control measures on vehicle emissions. *Transportation Research Part D*: 4: 357-378.

Righi S., Lucialli P., Pollini E., 2009. Statistical and diagnostic evaluation of the ADMS-Urban model compared with an urban air quality monitoring network, *Atm. Env.*, 43, 3850-3857, doi:10.1016/j.atmosenv.2009.05.016.

Robson, B.J., Hamilton, D.P., Webster, I.T., Chan, T., 2008. Ten steps applied to development and evaluation of process-based biogeochemical models of estuaries, *Env. Mod. Soft.*, 23, 369-384, doi: 10.1016/j.envsoft.2007.05.019

Roet, 2013. ATMOSYS, Action 5: Measurements Database

Schaap M., Denier Van der Gon H.A.C, Dentener F.J., Visschedijk A.J.H., Van Loon M., ten Brink H.M., Putaud J.-P., Guillaume B., Liousse C. and Builtjes P.J.H., 2004. Anthropogenic black carbon and fine aerosol distributions over Europe, *J. Geophys. Res.* 109, D18207, doi:10.1029/2003JD004330.

Schatzmann, M., & Leitl, B. (2011). Issues with validation of urban flow and dispersion CFD models. *Journal of Wind Engineering and Industrial Aerodynamics*, 99(4), 169–186. doi:10.1016/j.jweia.2011.01.005

Schrooten, L., De Vlieger, I., Lefebvre, F., Torfs, R., 2006. Costs and benefits of an enhanced reduction policy of particulate matter exhaust emissions from road

traffic in Flanders. *Atmospheric Environment*, 40, 904–912.

Setton, E., Marshall, J.D., Brauer, M., Lundquist, K.R., Hystad, P., Keller, P., Cloutier-Fisher, D., 2011. The impact of mobility on exposure to traffic-related air pollution and health effect estimates. *Journal of Exposure Science and Environmental Epidemiology* 21(1).

SGS Belgium NV, Wölfel, Geo-IT, 2010. Strategische geluidsbelastingskaarten agglomeratie Antwerpen, Rapport in opdracht van Stad Antwerpen, 090357-2-v1, Februari 2010.

Shiftan, Y., Suhrbier, J., 2002. The analysis of travel and emission impacts of travel demand management strategies using activity-based models. *Transportation*, 29, 145-168.

Shiftan, Y., 2000. The Advantage of Activity-based Modelling for Air-quality Purposes: Theory vs Practice and Future Needs. *Innovation*, 13, 95-110.

Solazzo E., Vardoulakis S., Cai X., 2011. A novel methodology for interpreting air quality measurements from urban streets using CFD modelling, *Atm. Env.*, 45, 5230-5239, doi:10.1016/j.atmosenv.2011.05.022.

Spangl, W., Schneider, J., Moosmann, L., Nagl, C., 2007. Final report, representativeness and classification of air quality monitoring stations. In: Umweltbundesamt GmbH (Ed.), Report REP-0121, Vienna

Thompson T.M., Selin N.E., 2012. Influence of air quality model resolution on uncertainty associated with health impacts, *Atmos. Chem. Phys.*, 12, 9753-9762, www.atmos-chem-phys.net/12/9753/2012, doi:10.5194/acp-12-9753-2012.

Thornburg, J., Rodes, C. E., Lawless, P. A., Williams, R., 2009. Spatial and temporal variability of outdoor coarse particulate matter mass concentrations measured with a new coarse particle sampler during the Detroit Exposure and Aerosol Research Study. *Atmospheric Environment*, 43(28), 4251–4258. doi:10.1016/j.atmosenv.2009.06.026

Thunis P., Triacchini G., White L., Maffei G. and Volta M., 2009. Air pollution and emission reductions over the Po-valley; Air quality modelling and integrated assessment. In Anderssen, R.S., R.D. Braddock and L.T.H. Newham (eds) 18th World IMACS Congress and MODSIM09 International Congress on Modelling and Simulation. Modelling and Simulation Society of Australia and New Zealand and International Association for Mathematics and Computers in Simulation, July 2009. ISBN: 978-0-9758400-7-8. <http://www.mssanz.org.au/modsim09/F10/thunis.pdf>

Van de Vel K. and 10 co-authors, 2010. Air-quality modelling in the Lake Baikal region, *Environ Monit Assess*, **165**, 665-674.

Vankerkom, J., De Vlieger, I., Schrooten, L., Vliegen, J., Styns, K., 2009. Beleidsondersteunend onderzoek: Aanpassingen aan het emissiemodel voor wegtransport MIMOSA. Studie uitgevoerd in opdracht van VMM - MIRA, 2009/TEM/R/084.

Van Poppel M., Dons E., Peters J., Brabers R., Damen E., Daems J., Van Laer J., Berghmans P., Int Panis L., 2012. Metingen van ultrafijn stof in Vlaanderen op hotspot(s) voor de blootstelling aan verkeerspolluenten. Final report for VMM. 2011/MRG/R/286. 175pp (in Dutch)

Van Renterghem T., 1999. Atmosferische dispersiemodellering bij inversie, lage windsnelheden en lage bronhoogtes, Ingenieurs-thesis, Universiteit Gent.

Vardoulakis, S., Fisher B.E.A., Pericleous K., Gonzalez-Flesca N., 2003. Modelling air quality in street canyons : a review, *Atm. Env.*, 37, 155-182.

Vardoulakis, S., Solazzo, E., Lumberras, J., 2011. Intra-urban and street scale variability of BTEX, NO₂ and O₃ in Birmingham, UK: Implications for exposure assessment. *Atmospheric Environment*, 45(29), 5069–5078. doi:10.1016/j.atmosenv.2011.06.038

Venkatachari P., Zhou L., Hopke P.K., Schwab J.J., Demerjian K.L., Weimer S., Hogrefe O., Felton D. and Rattigan O. (2006), An Intercomparison of Measurement Methods for Carbonaceous Aerosol in the Ambient Air in New York City, *Aerosol Science and Technology*, 40: 788-795.

Venkatram A. and Horst T.W., 2006. Approximating dispersion from a finite line source, *Atmospheric Environment*, 40, 2401-2408.

Vercauteren J., Matheeußen C., Wauters E., Roekens, E., van Grieken R., Krata A., Makarovska, Y., Maenhaut W., Chi, X., Geypens B., 2011. Chemkar PM₁₀: An extensive look at the local differences in chemical composition of PM₁₀ in Flanders, Belgium, *Atmospheric Environment*, 45, 108-116, doi:10.1016/j.atmosenv.2010.09.040

VMM (2009), Chemkar PM₁₀: Chemische karakterisatie van fijn stof in Vlaanderen, 2006-2007, http://www.vmm.be/publicaties/2009/CK_PM10_TW.pdf/view .

VMM (2010), Chemkar PM₁₀ 'hotspots': Chemische karakterisatie van fijn stof in Vlaanderen, 2008-2009, <http://www.vmm.be/pub/rapport-chemkar-pm10/view> .

VMM, 2011a. NO₂-meetcampagne met passieve samplers in steden in 2010.

VMM, 2011b. Validatieverslag CAR-Vlaanderen II.

VMM, 2013. Life+ ATMOSYS: snelwegcampagne.

Vranckx S. and Lefebvre W., 2013. ATMOSYS, Action 9.1: Retrospective simulations with AURORA.

Vos, P. E. J., Maiheu, B., Vankerkom, J., Janssen, S. (2013). Improving local air quality in cities: to tree or not to tree? *Environmental Pollution*, to appear. doi:10.1016/j.envpol.2012.10.021

Walcek, C.J., 2000. Minor flux adjustment near mixing ratio extremes for simplified yet highly accurate monotonic calculation of tracer advection. *Journal of Geophysical Research*, **105**, 9335-9348.

Wang T. and Xie S., 2009. Assessment of traffic-related air pollution in the urban streets before and during the 2008 Beijing Olympic Games traffic control period, *Atm. Env.*, **43**, 5682-5690, doi:10.1016/j.atmosenv.2009.07.034.

Welsh, W.D., (2008). Water balance modelling in Bowen, Queensland and the ten iterative steps in model development and evaluation, *Env. Mod. Soft.*, **23**, 195-205, doi:10.1016/j.envsoft.2007.05.014

Wilson, J. G., Kingham, S., Pearce, J., Sturman, A. P., 2005. A review of intraurban variations in particulate air pollution: Implications for epidemiological research. *Atmospheric Environment*, **39**(34), 6444–6462. doi:10.1016/j.atmosenv.2005.07.030

Xue, M., Droegemeier K.K., and Wong V., 2000. The Advanced Regional Prediction System (ARPS) – A multiscale non-hydrostatic atmospheric simulation and prediction tool. Part I: Model dynamics and verification. *Meteor. Atmos. Physics*, **75**, 161-193.

Xue, M., Droegemeier K.K., Wong V., Shapiro A., Brewster K., Carr F., Weber D., Liu Y., and Wang D.-H., 2001. The Advanced Regional Prediction System (ARPS) – A multiscale non-hydrostatic atmospheric simulation and prediction tool. Part II: Model physics and applications. *Meteor. Atmos. Physics*, **76**, 134-165.